The Electrochemical Kinetics of the

Evolution of Isotopically Enriched Gases

and the

Mechanism of the Oxygen Evolution Reaction

by

Christine Ruth Churchill

A thesis submitted for the degree of

Doctor of Philosophy

Bedford College, University of London

1984

ProQuest Number: 10098480

All rights reserved

INFORMATION TO ALL USERS
The quality of this reproduction is dependent upon the quality of the copy submitted.

In the unlikely event that the author did not send a complete manuscript
and there are missing pages, these will be noted. Also, if material had to be removed,
a note will indicate the deletion.

ProQuest 10098480

Published by ProQuest LLC(2016). Copyright of the Dissertation is held by the Author.

Abstract

This work describes a method which follows, by mass spectrometry, the kinetics of gas evolution from an isotopically enriched electrode surface. The mechanisms of both $^{18}O^{16}O$ and $^{4}D_2$ evolution were investigated by this technique. $^{34}O_2$ evolution was studied on platinum, $NiCo_2O_4$ and lithiated Co_3O_4 electrodes in alkaline electrolyte, and additionally on platinum electrodes in acid electrolyte. The kinetics were found to be consistent with a mechanism of oxygen evolution which involved successive oxidations on a single site or reaction via a bridge structure. It was found, in all cases, that the total number of sites responsible for oxygen evolution were less than the total number of sites at the surface. Additionally, on $NiCo_2O_4$ electrodes the number of sites which showed enrichment decreased with aging of the electrode, in agreement with evidence from its cyclic voltammogram. Tafel slopes and cyclic voltammograms are reported for each electrode. On each substrate the amount of enrichment detected was less than would have been expected from the degree of enrichment of the electrolyte. This is most readily explained on consideration of the proposed mechanism of oxygen evolution, where the first step involving oxide formation is rate determining on platinum and $NiCo_2O_4$ (high overpotential). The intermediate oxide species formed being rapidly removed as oxygen was evolved. On materials in which the metal was initially in a trivalent state, a mechanism involving a bridge structure between this trivalent site and a second site is postulated; its formation being rate determining at low overpotential on $NiCo_2O_4$.

This method was extended to follow the mechanism of hydrogen evolution on both platinum and platinised hydrogen tungsten bronze

electrodes. The kinetics of the removal of an adsorbed deuteron were consistent with a second order recombination and found to be fast ($k = 0.02 \pm 0.02$ s^{-1} at $25^{\circ}C$ on platinum). Experiments on platinised hydrogen tungsten bronze electrodes confirmed the existence of a synergistic effect in this system.

4

Table of Contents

List of Tables

List of Illustrations

13

Acknowledgements

I would like to express my thanks to my supervisor, Dr Brynn Hibbert, for his help and guidance on my project during my years at Bedford College.

I would like to acknowledge the help of the technical staff at Bedford College, particularly their assistance in providing a service on the atomic absorption spectrometer and X-ray diffractometer.

I am grateful to both the S.E.R.C. and British Gas for the provision of a Case award.

I must also convey my thanks to Toby Jarvis for his careful and critical reading of this manuscript.

Finally I would like to thank my typist, Veronica Brown, for her excellent work in typing this thesis and for bearing with me during the months it has taken.

Abbreviations

b	Tafel slope parameter
e	electronic charge
F	Faraday constant
h	Planck's constant
I_a	anodic current
I_c	cathodic current
i	current density
i_o	exchange current density
L	Avogadro's number
M	relative molecular mass
n	number of electrons transferred
Q	amount of charge
R	gas constant
T	temperature
V	voltage
z	charge
β	symmetry factor
λ	wavelength
η	overpotential
ρ	density

PART 1

INTRODUCTION AND THEORY OF THE OXYGEN EVOLUTION

REACTION AND ISOTOPIC EXPERIMENTS

CHAPTER I

Introduction

1.1   It is well known that the equilibrium potential of the oxygen

electrode with the electrochemical reaction

$$2H_2O \ \rightleftharpoons \ O_2 + 4H^+ + 4e \tag{1}$$
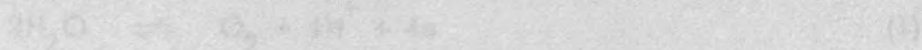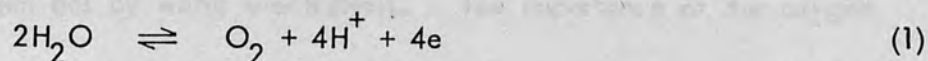
in acid electrolyte, and

$$4OH^- \ \rightleftharpoons \ O_2 + 2H_2O + 4e \tag{2}$$
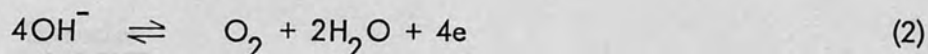
in alkaline electrolyte, is rarely achieved in practice. With the cathodic process

$$H^+ + e \ \rightleftharpoons \ \tfrac{1}{2}H_2 \tag{3}$$
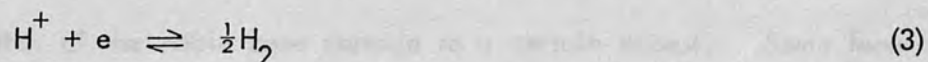
the overall galvanic cell reaction requiring the transfer of four electrons is

$$O_2 + 2H_2 \ \rightleftharpoons \ 2H_2O \tag{4}$$

the standard potential of the hydrogen-oxygen cell being 1.229V[1].

The kinetics of electrolytic hydrogen and oxygen generation were

the first problems in the sphere of electrochemistry to attract interest as a

result of their practical importance.   Both processes are extremely complex

and strongly influenced by particular conditions which has led to a delay in

the detailed elucidation of their mechanisms.   Consequently our knowledge

of the oxygen evolution reaction and understanding of the hydrogen evolution

reaction are far from complete, despite important progress having been made.

It is quite natural to compare the hydrogen and oxygen electrodes

both from a technological viewpoint as regards their relative performance

when used in energy conversion devices, and from a theoretical viewpoint

as the hydrogen electrode has been by far the most widely studied of

electrochemical processes that can be termed electrocatalytic, that is

involving a rate-determining step with adsorbed intermediates.

The kinetics of anodic oxygen evolution is the most important among

anodic processes. Interest in the oxygen evolution reaction continues due to its relevance in areas such as corrosion, fuel cells, metal-air battery systems and in recent years the possibility of large scale production of hydrogen gas by water electrolysis. The importance of the oxygen electrode to these four topics will now be considered in more detail.

1.1i Corrosion

The problems of corrosion are immense, as all metals with the exception of the noble ones corrode to a certain extent. Some form oxide layers on their surface, protecting them from further attack. Corrosion can occur by either direct oxidation of the metal by air or oxygen, forming metal oxides which are, as a rule, more thermodynamically stable than the metal and oxygen in their elementary states; or by an electrochemical route, with two electrode reactions taking place on the surface of the corroding metal. A greater understanding of the mechanism of oxide formation may lead to the development of methods to overcome this problem.

1.1ii Fuel Cells

During the past two centuries the world has had access to an abundant supply of carbon-based fuels. First coal, followed by oil and natural gas, have been widely used in energy consuming devices which were developed to use the fuels or their derivatives, in the most convenient way. Thus now we experience the problem of trying to change the way in which energy is made available; the question being whether we should be trying to synthesize similar carbon-based fuels which would be compatible for use with the existing engineering technology, or should we start again to develop new technology to be used with the new energy forms.

In the short term, we must work to supplement existing fuels with a similar type, but long term plans need the development of new devices to use both nuclear and solar energy as directly as possible.

In the immediate viewpoint, fuel cells have long been considered as a future means of electricity generation. Today man obtains the bulk of the energy he uses by burning oil; this is undesirable both from the point of view that this is a low efficiency heat conversion method which is intrinsically limited by Carnot's theorem, and from the environmental aspects of air pollution. The solution to this problem is to burn the fuel electrochemically, as is the method of fuel cells.

The most likely role visualised for these devices is their use in transportation, in this respect their noiseless production of power would have a great effect upon our cities. However, following a great surge of interest in the potential of fuel cells during the 1960's, their rate of progress has not been so impressive during the last decade. Present economic calculations do not even match those of conventional systems. For low temperature fuel cells, it is required to use inexpensive electrode materials for the oxidation of cheap fuels, but the major problem here has been in trying to increase the exchange current density sufficiently to make the process viable. Conversely in high temperature fuel cells the temperature alone ensures that the energy output is adequate without the use of expensive catalysts, but such conditions generate material stability problems. The theoretical oxygen electrode potential has rarely been established and then only at open circuit and under strict laboratory conditions. Therefore in the case of the hydrogen-oxygen fuel cell at zero current or low current density, the difference between the theoretical

and observed potential arises for the most part from polarisation losses at the oxygen electrode, and therefore any improvement in performance of the oxygen electrode implies improved performance in fuel cells also.

1.1iii Metal-air battery systems

Oxygen of the air is the most universal oxidant for all chemical reactions involving the production of energy both in nature and technological processes. However, chemical power sources are, it would seem, the only energy-producing units which make use of expensive low capacity solid oxidants instead of freely available oxygen. Development work on cells utilizing oxygen from the air is now under way, so that one of the most efficient ways of energy conservation, electrochemical conversion, does not have to rely on the use of inefficient and expensive reactants. The advantages of air cells are due mainly to the practically unlimited availability of free air, and the decrease in mass and cost of cells owing to the elimination of heavy oxide oxidants. Pure oxygen has a higher activity than air but due to storage and transportation problems it is rarely used. Today a variety of high performance air and oxygen electrodes have been developed for use in concentrated alkaline solution but progress in acid and salt solutions has been slower.

1.1iv Water electrolysers

During the early years of the seventies, a dramatic rise of interest occurred in a concept termed the 'hydrogen economy', which was concerned with the ultimate replacement of the conventional fossil fuel system with a synthetic fuel. It was proposed that hydrogen produced electrochemically from water by nuclear or solar energy would take the role of oil, gas and

coal in our present energy system.

The constraints relevant to the concept of a completely synthetic fuel are fundamentally that it must be capable of being made from materials which are in abundant supply and that it can be burned in air without forming noxious byproducts. These two conditions limit the choice to hydrogen and oxygen.

Hydrogen is unique in being very simple to make and also pollution free in use; it is electrochemically active at ambient temperatures, can be used in fuel cells without pretreatment and has a high energy to weight ratio. However, it has the drawback of wide combustion units and a low ignition energy. It is difficult to store in a compact form except at high pressure or as a cryogenic liquid.

The electrolysis of water is attractive in that it yields complete separation of its products, hydrogen and oxygen, but its use of electrical energy for their production is undesirable. Since electrolysis of water performs the reverse chemical reaction to the combustion of hydrogen, the electrolyser must be supplied with as much energy to produce the hydrogen as is released when the hydrogen is ultimately burned. Only the free energy change of the reaction can be interchanged with the electrical energy. The difference between the free energy change and the total energy change is balanced by the entropy change for the process. The entropy change cannot be converted to electricity, but must be liberated or supplied as heat. The enthalpy change for hydrogen at $25^{\circ}C$ in a water electrolysis cell is calculated to correspond to a potential of $1.47V^2$ while the cell voltage equivalent to the free energy change only is $1.23V$. This variation is important as it is a factor which works to the favour of

water electrolysis and against fuel cells. Forming hydrogen and oxygen at 1.23V, the cell would absorb heat from its surroundings. Thus the electrical energy required is only 83.7% of the combustion energy of the hydrogen produced, the extra 16.3% having been supplied as heat. Hence the water electrolyser can have a theoretical 'electrical' efficiency of up to 120% as the heat energy absorbed is also included in this figure. The primary cause for the lack of use of this method is due to the high cost involved in manufacturing as the electrolysis uses expensive electrical energy. For this to play an integral part in energy technologies there is the need for the development of low-cost, high efficiency water electrolysers.

1.2   The oxygen evolution mechanism

The oxygen evolution reaction occurs along a number of consecutive steps, any of which may be the rate determining step. In general the overall rate of reaction is affected for each of these steps by a different and specific property of the electrode material; for example electronic properties such as work function and d-band character, physical properties such as geometric arrangement of atoms on the surface, the adsorption energy of reaction intermediates and possibly the concentration of some surface defects. A wide variety of direct ion neutralisation products are possible, oxygen atoms and hydroxyl radicals, for example, are strongly adsorbed or chemisorbed on all electrodes and form a wide variety of activated complexes, the natures of which depend on potential, even on a given metal. The path of the overall reaction on different electrode materials must be determined, and it is essential to determine the rate-controlling step in each, so that the factors affecting the rate of reaction

and the role of these factors to the catalysis mechanism may be analysed. Thus in a systematic catalytic study of the reaction at a given electro-catalyst, the first step must be a detailed analysis of the mechanism involved.

1.3   The Electrified Interface

A chemical reaction occurs when electrons are exchanged between reacting chemical species at a reaction site. However, in an electro-chemical reaction the oxidation and reduction processes occur at different sites remote from each other. This is accomplished physically by separating the sites by means of an electrolyte. The electrodes collect the charge and current is transported through the electrolyte by ions. The charge is transferred from the particle to solution and across the electrical double layer to the electrode, or from a particle chemisorbed on the conducting layer to the electrode. A double layer of charge builds up at all phase boundaries because the activity of an ion common to both phases is different in each phase. Thermodynamics tells us that the resulting free energy difference causes ions to drift from the more concentrated to the less concentrated phase with a resulting separation of charge. The final steady state is only reached when the driving force of the concentration gradient across the phase boundary equals the electro-static force of the charge separation.

In electrochemical systems most interest is shown in the solid-liquid boundary. All the charge exists on the electrode surface as the dielectric constant of the metal is near enough infinite. But in solution there is a distribution of charge, ranging from the phase boundary into the bulk of

solution. A linear drop in potential occurs in the region 40-50nm from the metal surface and it is here that much of the charge is distributed. This is known as the Helmholtz double layer region. Charge is transferred across this region during the course of an electrochemical reaction and thus the potential across this part of the double layer influences the rate of the reaction.

We require the Galvani potential difference across the interface, φ, which is the sum of the outer (Volta) and surface potentials at the interface and defined as the work done to bring a unit test charge from infinity, across the charged surface covered with a dipole layer to a point inside the phase. Thus

$$\varphi = \psi + \chi \qquad (5)$$

where ψ is the outer or volta potential, defined as the work done to transport a test charge from infinity to a point outside the charged phase and χ represents the surface potential in being the work done in taking the charge through the surface dipole layers. The Galvani potential cannot be measured or calculated, as it is impossible to measure the absolute potential difference across an interface, the very fact of using a measuring instrument supplies at least a second interface. However, the Volta potential difference can be measured experimentally.

It is of little use to measure cell potential changes as a function of the various parameters of the system as the cell potential is only the algebraic sum of the individual electrode potentials. Electrochemical measurements require a three electrode system, comprising a working electrode, a secondary or counter electrode to sustain the current, and a calibrated

reference electrode, to which the potential of the working electrode can be measured.

The fundamental equation used in electrochemistry relates the net current density of the electrochemical reaction to the overpotential, and was derived by Butler[3,4] and Volmer.

$$i = i_0 \left[\exp \left(\frac{-\beta F \eta}{RT} \right) - \exp \left(\overline{1 - \beta} \; \frac{F \eta}{RT} \right) \right] \qquad (6)$$

The high field approximation to this equation yields the Tafel relationship. These equations are commonly used as a means to elucidate reaction mechanisms and rate determining steps. If an electrode reaction were truly reversible the overvoltage would be zero and an activation energy barrier would not exist. When the Tafel slope is extrapolated to the point of zero overvoltage, the current density is equal to the exchange current density.

1.4   Reasons for the lack of knowledge of the oxygen electrode reaction

The oxygen evolution reaction lacks the necessary background to give the information required for a rational approach to the search for a better electrocatalyst as few studies have as yet been made with the aim of establishing the factors affecting the catalysis of the reaction. The main reasons for this may be stated as follows:

i)   The standard electrode potential for the oxygen evolution reaction

$$O_2 + 4H^+ + 4e \rightleftharpoons 2H_2O \qquad (1)$$
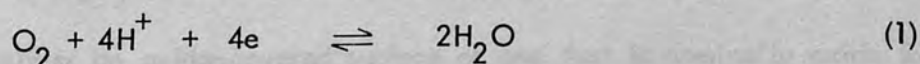
is 1.23V on the standard hydrogen scale[1], and thus it falls above the standard potential of almost all of the solid elements. Therefore the choice of suitable materials for this reaction is limited. Among the

metallic elements (excluding the noble metals) all substances except gold
are thermodynamically unstable with respect to water in this high potential
range.   In acidic solutions those metals which do not spontaneously
dissolve will at least be covered by an oxide film or adsorbed oxygen
derived from the oxidation of water, below 1.1V.   Thus only the noble
metals and gold can be considered as possible substrates amongst the metals,
although in many cases these have high surface coverages of oxygen above
0.8V.   Stable semiconductors are an alternative possibility as catalysts
in acidic solution, for instance insoluble oxides and certain organic
materials.   The situation is more favourable in alkaline solution, as the
oxygen evolution potential is 0.8-0.85V more negative, effectively due
to the pH difference.   In addition the choice of oxides is much wider
as the majority of metal oxides are stable in alkali.   However, it must
be remembered that even substances which are supposedly unstable thermo-
dynamically often show so slow a transformation that they can be considered
stable from a practical point of view.

ii)   It has only recently been realised that in the potential region at
which oxygen dissolution occurs, the electrode surface may be either
comparatively bare or covered by an 'oxide' film.   No meaningful
conclusion as to the path of catalysis should be deduced unless the surface
of the electrocatalyst is defined.   Once an oxide has been formed the
process is highly irreversible and thus subsequent reduction of oxygen may
be on either an oxide-covered surface or one that is nominally oxide free.
The oxygen evolution mechanism on phase oxide-covered surfaces is quite
different in both mechanistic and kinetic character from that on a reduced
surface, which is only accessible in the cathodic direction.

iii)   A large number of reaction intermediates and hence possible

mechanisms and rate determining steps may occur for the oxygen electrode.

The electrode potential and coverage being responsible for the energy of

adsorption.   Some of these intermediates may be sufficiently stable under

certain conditions, to be end products of the reaction.   The reduction

of oxygen may occur via a two-electron process to peroxide, or proceed

fully to form water by the four-electron process.   In the former case the

potential of the oxygen electrode will be far below that predicted for

the overall four-electron reduction process.   In energy conversion devices

it is imperative that the highest possible thermodynamic efficiency is

attained for an economically feasible operation, hence reduction to water

must take place as the overall process.

iv)   In considering the behaviour of noble metals as electrocatalysts for

both the hydrogen and oxygen evolution reactions, the most striking point

is the very large difference in rate between the two systems.   Typically

the exchange current density for the oxygen electrode is about 10^{-10}

A cm^{-2} on platinum in normal acid electrolyte[5] at room temperature.

This is many orders of magnitude less than the exchange current density for

the hydrogen electrode, a value of 10^{-5} A cm^{-2} being quoted on platinum

in acid electrolyte[6].   With such a low exchange current density other

electrode reactions may become potential controlling, particularly at low

current densities.

v)   As with the   hydrogen electrode, the oxygen electrode is

seriously affected by impurities.   Pre-electrolysis usually suffices to remove

impurities from solution for the hydrogen evolution reaction;   but this

technique must be used carefully in the case of the oxygen electrode especially if platinum electrodes are employed since under certain conditions anodic pre-electrolysis in the working electrode compartment can seriously contaminate the electrolyte with platinum and introduce errors. Similarly platinum counter electrodes are best avoided.

There is some doubt as to whether the mechanism is the same in acid and alkaline solution. Although this will be discussed in greater detail in the following chapter, the general view at present seems to be that the same mechanism holds across the pH range, but that the rates of consecutive steps in a given reaction path may be different functions of the potential and consequently the rate determining step could change with potential.

1.5 Aim of Project

One aim of this project is to establish an isotopic technique to contribute to the elucidation of the mechanism of oxygen evolution which studies the incorporation of oxygen as an oxide on the electrode surface. Rosenthal and Veselovski[7] used the stable isotope ^{18}O as a tracer in the oxygen evolution reaction to determine the participation of the surface oxide on platinum. Their results showed that ^{18}O was detected in the evolved gas in excess over that due solely to background.

This idea has been extended extensively in this project to the point where the total number of surface sites available for the oxygen evolution reaction, the extent of higher oxide formation and the general mechanism have been determined from kinetic interpretations. This method has not only been applied to platinum electrodes in acid and alkaline electrolyte,

but also to the new species of oxygen evolution electrocatalysts, namely mixed metal oxide spinels.   Additionally these systems have also been studied by basic electrochemical techniques, such as cyclic voltammetry and Tafel slope measurements.

Finally, this basic isotopic technique has been adapted to follow the kinetics of the hydrogen evolution reaction, using a deuterium tracer; thus indicating the diversity of the method.

CHAPTER II

Theory of oxygen evolution

II.1   It has already been stated that the theoretical reversible potential

of $1.229V^1$ for the reaction

$$O_2 + 4H + 4e \rightleftharpoons 2H_2O \tag{1}$$
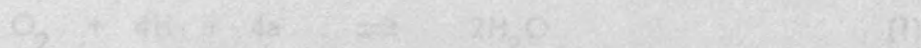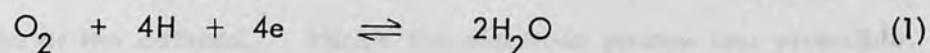
at standard conditions of $25°C$, 760mm Hg pressure and pH = 0 is rarely

achieved in practice.   Many early workers found that potentials usually

established at a platinum electrode were between 100-300 mV lower.

Hoar[8], studying the kinetics of the dissolution and deposition of oxygen

at several so-called 'inert' electrodes was the first to demonstrate the

existence of this theoretical potential by extrapolating anodic and cathodic

Tafel lines to the low current density region, giving a potential value of

$1.20 \pm 0.3V$ at the interception point.   From open circuit voltage

measurements, Bockris and Huq[9] observed this potential at zero current

density for a platinum electrode in acid solution.   From observations of its

dependence on the partial pressure of oxygen, they proved that this was in

fact the reversible oxygen potential.

The electrolysis of water was first reported by Deimann and Paets

van Troastwyk in Haarlem, Netherlands in 1789.   The first chemical

power source, or 'galvanic battery' appeared in March 1800 and was the

Volta pile.   Volta described his battery as being the "..... construction

of an apparatus ..... of unfailing charge, of perpetual power".   The

chemical effects of an electric current were discovered within a

few months of this achievement;   Nicholson and Carlisle illustrating the

decomposition of water to its gaseous components in May 1800.

Grove[10], as the pioneer of fuel cell research, was the first person

to use an oxygen electrode.   Combining this with a hydrogen electrode in the same solution he showed that a current could be drawn from this combination.   Conversely he also demonstrated that if current was supplied to the system, oxygen would be evolved at the anode and hydrogen at the cathode.   Hence the electrode process was reversible.

Since it has now been realised that noble metals are not inert to oxygen saturated electrolytes, electrochemists have been trying to explain why such irreversibility for the oxygen electrode is observed and why the data relating to this is very irreproducible.   Most of the research work has been carried out on the platinum-oxygen system, and this is the system mainly considered in the following review.

Early values obtained for the open circuit voltage of the Grove cell were lower than the theoretical reversible oxygen electrode potential, around 0.98-1.12V.   Without special preparation of electrodes, such potentials are still recorded today.   This corresponds to a mixed potential set up between cathodic oxygen reduction and spurious anodic processes, usually the oxidation of impurities or adsorbed oxygen formation on platinum, as follows,

$$\frac{n}{4} \left[O_2 + 4H^+ + 4e \right] \longrightarrow \frac{n}{2} H_2O \qquad (2)$$

$$PtO_{(x - \frac{n}{2})} + \frac{n}{2} H_2O \longrightarrow PtO_x + nH^+ + ne \qquad (3)$$
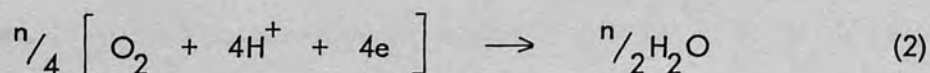
In some instances in alkaline solution a reversible O_2/H_2O_2 potential is set up.   In acid, the potential found at platinum in oxygenated H_2O_2 solution is independent of oxygen partial pressure and controlled by decomposition mechanisms[11].

The significance of this low rest potential has been discussed by

many authors[8,12-16]; its importance lies in the fact that for zero currents it would be the highest potential obtained at an oxygen electrode in most energy convertors and storers. The loss of power of a system being measured as the difference between this value and that of the reversible oxygen electrode potential.

On a platinum electrode initially in a clean, phase-oxide-free state, a rest potential of about 1V is frequently observed at an oxygen partial pressure of 1 atmos. even in solutions which have been extensively pre-purified. Such electrodes display a high log p_{O_2} dependence of RT/F after short times at rest, which fall to lower values after long periods at the rest potential. Bockris and Huq[9] argue that the very low oxygen electrode exchange current density is generally several orders of magnitude less than impurity limiting currents, and consequently a mixed rest potential lower than the reversible oxygen potential will inevitably occur in practice.

It has been shown that under open-circuit conditions the amount of adsorbed oxygen changes with time of exposure to oxygen[17] and that the rest potential is a linear function of coverage. This never exceeds 30% at a steady state rest potential of 1.06V for both bright and platinised platinum.

The kinetics and overvoltage of the oxygen evolution reaction are highly dependent on the nature of the metal; that is on the state of the surface and the nature of the adsorbed oxygen or oxide layer. During anodic oxygen evolution, a layer of adsorbed oxygen atoms or hydroxyl radicals is formed even on the surface of noble metals. Thus on metals with passivating oxide layers, the kinetics of oxygen evolution is governed directly by the properties of the film, and not by those of the bare metal surface.

It was first shown by Bowden[18] that oxide layers on noble metals are only formed above a certain potential. Experiments to support this were reported by Butler et al[19,20] which demonstrated that a single layer of adsorbed oxygen atoms was formed on anodically polarising platinum electrodes.

In IM H_2SO_4, Hoare[21] identified the different types of platinum-oxygen species as a function of potential. He detected no sorbed oxygen below 800 mV. As the potential was raised, oxygen was adsorbed, and becomes dermasorbed (i.e. the oxygen adsorption sites are located at the first one or two atomic layers of the platinum surface) at potentials above 1V.

Early in the 1960's it was clearly demonstrated[22] that thin surface oxide films anodically formed at noble metal catalysts profoundly affect not only the catalytic activity of a given reaction, but also the mechanism. This came at a time when many electrochemists were favouring the adsorption theory rather than the phase oxide theory for anodic film formation on platinum.

It is now generally accepted that the film consists of a platinum oxide phase whose stoichiometry varies with potential. X-ray diffraction experiments failed to show a pattern for anodised platinum which leads to the conclusion that either the films have crystallites that are smaller than 50Å in diameter, or that they are essentially amorphous[23].

Conway et al[24] have shown the existence of three anodic current peaks in the current-potential profile before a monolayer of hydroxyl species has been completed in acid solution. These peaks do not arise because of polycrystallinity since a similar structure is observed at a single crystal

surface. They conclude that this phenomenon must be attributed to successive states of occupation of the surface lattice in three significantly different sub-lattices. Sublattices are the first two types of structures below the hydroxyl monolayer, and are respectively 'just not nearest neighbours Pt_4OH' or 'just diagonal nearest neighbours Pt_2OH'. The formulae are simply surface site occupancy ratios and not stoichiometric species. After completing the arrangement 'Pt_4OH', it is evident that the next hydroxyl species to be deposited must occupy a new kind of lattice position amongst neighbouring hydroxyl species. Further deposition of hydroxyl will continue similarly until beyond 'Pt_2OH' a third type of site will be occupied to form a monolayer. Beyond this stage, "PtO" must arise in further oxidation.

Vetter and Schultze[25] working on galvanostatic and potentiostatic techniques for the formation and reduction of platinum oxides in 0.5M H_2SO_4 pointed out that the oxide layer properties depend on its formation conditions, such as growth rate and layer aging, and the method of obtaining a surface coverage, either by anodic oxidation or by the reduction of thicker oxides. They proposed the following model to explain the kinetics of layer formation, according to the equilibrium reaction

$$H_2O \text{ (aq)} \rightleftharpoons O^{2-} \text{ (aq)} + 2H^+ \text{ (aq)} \qquad (4)$$
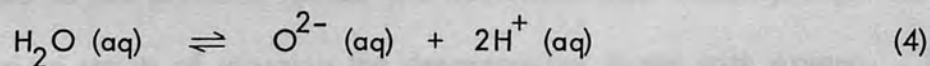
Oxygen ions are chemisorbed from the electrolyte solution, the coverage at the electrode surface not exceeding 10%. A site exchange process then takes place between the adsorbed oxygen ions and platinum ions from the first atomic layers. This is the rate determining step and is independent of field strength taking place in the inner Helmholtz layer. Thicker oxide

layers ($\vartheta = 1$-2.5) are formed by a similar process at the metal/oxide and oxide/electrolyte interfaces, followed by a migration of the platinum and oxygen ions over vacancies and interstitial sites in an high electric field. The oxide is reduced by the same mechanism, though only at the edges of 'oxide islands'. The interchange mechanism is discussed by Lanyon and Trapnell[26].

Ruetschi and Delahay[27] have correlated Hickling and Hill's[28] oxygen evolution results to give what appears initially to be an excellent confirmation of variation in potential compatible to changes in M-OH bond energy. However, Hickling and Hill's results differ from those of other workers in many respects as they were obtained by using a clean electrode at each current density. Thus the oxide film thicknesses were not constant throughout the plots and the results were obtained at potentials where very thick oxide films occur.

The appearance of more than one arrest in the oxygen adsorption region of the charging curves on platinum has been offered as proof for the existence of at least two platinum oxides, PtO and PtO_2[29]. They used a very low charging current (1 . $\mu A \ cm^{-2}$) so that approximately one hour was required for charging. Under these conditions however, oxygen could be dissolved in the platinum lattice and deviations from linearity might reflect the various stages of charging the dermasorption layers with oxygen. When a high current density was used, such deviations were not observed, because insufficient time had elapsed for the oxygen to be sorbed in the dermasorption layer.

Anson and Lingane[30] oxidised platinum for periods of time under a variety of conditions, after which the 'oxides' were stripped chemically by

a solution of 0.2M hydrochoric acid and 0.1M sodium chloride .

From results of the spectrophotometric analysis of the solution for $PtCl_4^{2-}$

and $PtCl_6^{2-}$ they concluded that both PtO and PtO_2 exist on the adsorbed

anodic film in a ratio of 6:1.   No matter how strong the oxidising

conditions were, the ratio of $PtO:PtO_2$ had a constant value of 6:1.

This is in contrast to the expectation that the amount of PtO_2 in the film

would increase at the expense of PtO when the potential was made more

anodic.   They also noted that only part of the adsorbed film could be

stripped, which is in agreement with the theory that oxygen dissolved in

the dermasorbed layers of the metal is protected from chemical attack by

the stripping solution.

Breiter and Weininger[31] conducted experiments on the open-circuit

decay and potential sweep techniques on platinum in a solution containing

0.2M hydrochloric acid and 0.1M sodium chloride and concluded that Anson

and Lingane's results could be equally well interpreted in terms of a mixed

potential mechanism, in which the local cathodic current arises from

reduction of the Pt-O film as follows:

$$Pt - O + 2H^+ + 2e \rightarrow Pt + H_2O \qquad Ic \qquad (5)$$
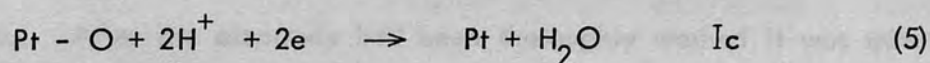
with the anodic reactions

$$Pt + 4Cl^- \rightarrow PtCl_4^{2-} + 2e \qquad Ia \qquad (6)$$

$$Pt + 6Cl^- \rightarrow PtCl_6^{2-} + 4e \qquad Ia' \qquad (7)$$
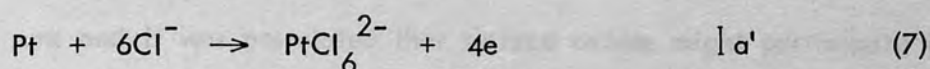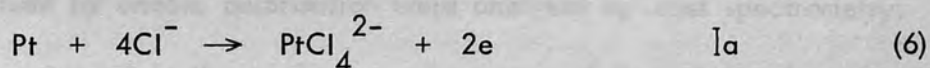
Following this scheme, the platinum in solution comes from the metal

and not from the platinum oxide layer.   In a local cell, no external current

flows and thus,

$$I_c = I_a + I_{a'} \tag{8}$$

If $I_a/I_{a'}$ remains constant over the range of experimental conditions studied, a constant value of Pt^{2+}/Pt^{4+} in solution would be expected for all degrees of oxidation of the platinum surface.

According to Pourbaix[32] the limits of the domains of relative stability of the solid platinum-oxides are given by,

$$Pt + H_2O \rightleftharpoons PtO + 2H^+ + 2e \qquad E_o = 0.98 - 0.0591 pH \tag{9}$$

$$PtO + H_2O \rightleftharpoons PtO_2 + 2H^+ + 2e \qquad E_o = 1.045 - 0.0591 pH \tag{10}$$

$$PtO_2 + H_2O \rightleftharpoons PtO_3 + 2H^+ + 2e \qquad E_o = 2.00 - 0.0591 pH \tag{11}$$
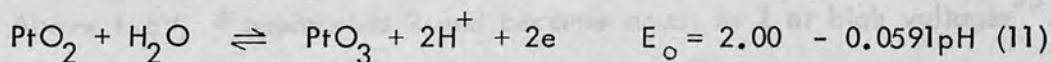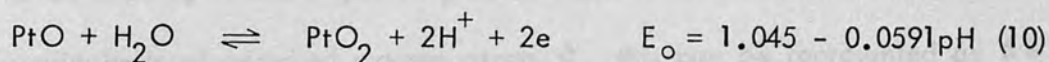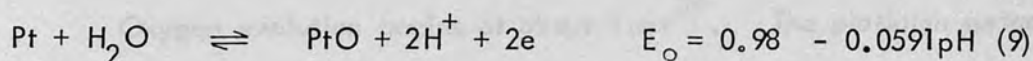
Thus platinum (IV) oxide appears to be the form of platinum thermodynamically stable in the presence of oxygen at $25^{\circ}C$ and atmospheric pressure.

Rosenthal and Veselovski[7] used the stable isotope ^{18}O as a tracer in the oxygen evolution reaction to determine the participation of the surface oxide at platinum. A large platinised platinum electrode was initially polarised at a set potential in an electrolyte which was ^{18}O enriched. After the electrode had been thoroughly washed it was transferred to a cell containing the same electrolyte but unenriched. Volumes of the gas evolved by anodic polarisation were analysed by mass spectrometry. ^{18}O was detected in the evolved gas in excess of that obtained on standardisation runs and it was postulated that surface oxides might participate in the oxygen evolution reaction according to

$$Pt.PtO [O^*] + H_2O \rightarrow Pt.PtO + OO^* + 2H^+ + 2e \tag{12}$$
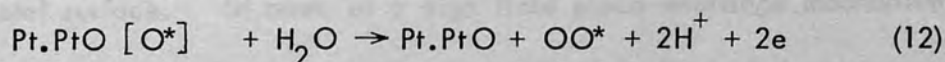
where O^* represents an oxygen atom which is enriched.

Factors against this idea include the fact that the percentage of ^{18}O observed in the evolved oxygen was lower than would have been expected by a factor of six. Secondly, Vetter[33] considered that it was possible for ^{18}O on the surface oxide to exchange with ^{16}O in a water molecule in the immediate vicinity of the electrode surface before the molecule entered the evolution process, in which case an enrichment of ^{18}O would also be detected in the initial samples of evolved gas.

Oxygen evolution begins at about $1.6V$[34]. The platinum surface is covered by a monolayer of platinum oxide, in terms of monolayer equivalents of adsorbed oxygen atoms ϑ, this can be represented as $\vartheta = 1$. Above $1.6V$, ϑ approaches 2 and becomes equal to 2 at high voltages[35]. This has been interpreted by Thacker and Hoare[36] to mean that above $1.6V$, platinum (II) oxide sites are converted to platinum (IV) oxide sites approximately one monolayer thick. Such a layer must have considerable electronic conductivity as it does not grow under moderate oxidising conditions.

It has been assumed in the analysis of the kinetics of the oxygen evolution reaction that such anodic oxide films are electronically conducting[9,21]. However, from the mechanism of growth of the anodic oxide field on platinum it has been found that the films can easily sustain high electric fields during growth, indicating poor conduction characteristics. The model presented by Vetter and Schultze[25] suggests that the potential drop across this platinum (II) oxide layer causes the Pt^{2+} ions to migrate outwards from the metal surface. In terms of a high field place-exchange mechanism the linear variation of charge with potential above $1V$ and the exponential decrease in oxide formation current with coverage under potentiostatic

conditions may be explained in terms of the film acting increasingly as a barrier to charge transfer.

The potential difference across the film, with respect to a suitable reference such as the reversible oxygen potential is the sum of the potential difference across the oxide film ΔV_{of} and that across the double layer ΔV_{dl}

$$\Delta V = \Delta V_{of} + \Delta V_{dl} \tag{13}$$

In the steady state, when the current for oxide growth is negligible, and the thickness of the oxide film remains nearly constant, ΔV_{of} and ΔV_{dl} for the same ΔV adjust themselves such that[37]

$$i_{obs} = i_{dl} = i_{of} = Ka_{H^+}^{-p} \exp\left(\alpha \cdot \frac{F \cdot \Delta V}{RT}\right) \tag{14}$$

where p is the negative of the reaction order for H^+.

The rates of growth of anodic oxide films at platinum in acid and alkaline solution have been studied by Damjanovic, Yeh and Wolf[38]. They found the rate of growth to be pH independent in acid, but affected by pH in alkaline solution; the exchange current density increasing one decade as the pH increased one unit. This dependence of exchange current density on pH is not expected according to the usual model of high-field assisted formation of films with either the step at the metal/ oxide film interface or a step within the film as rate determining. They suggest that a process at the oxide film/solution interface is rate determining with hydroxyl ion as the reacting species. This step is similarly rate determining in acid solution, but with H_2O as the reacting species.

Although the oxide film undoubtedly has a major effect on the kinetics of the oxygen evolution reaction, the manner in which this influence

is exerted is still uncertain. If the oxide film is assumed to be poorly conducting, it is necessary to postulate tunnelling of electrons through the surface layer[9]. It should be remembered that in general an oxide film formed anodically on metals will be semi-conducting. If the film is only a few angstroms thick the effect of the gap-width term (in the absence of a degenerate surface) will not be significant as electron tunnelling from the surface of the metal will be possible as stated. As the thickness increases, the electronic properties of the film itself will become apparent. In semi-conducting films with non-degenerate surfaces little potential fluctuation with overpotential will be expected in the Helmholtz double layer, assuming that the film thickness is less than the Debye length. Thus for thick films with non-degenerate surfaces the hole current will have an approximate Tafel slope of RT/F in a primary discharge anodic process, the electron current will be independent of overpotential and a low overall current will be measured because of the gap-width term. Thus films with non-degenerate surfaces also show the possibility of tunnelling from the metal. They will therefore show large currents of more metallic character and will exhibit the normal $2RT/F$ primary discharge anodic Tafel slope since the potential drop in the space charge region will be quite small. However they are expected to show currents at a given overpotential that are appreciably lower than those on a metal with the same adsorption properties, because of the effect of the tunnelling probability term. This effect is not expected on films with degenerate surfaces. Assuming then that the platinum-oxide films are semi-conducting with non-degenerate surfaces it is possible to explain the observation that the current for oxygen evolution falls with increasing anodisation because of tunnelling effects. Alternatively, it is

possible with mixed oxide species, that increasing the oxygen co-ordination
of cations in the surface film can affect the rate of reaction at the oxide/
solution interface.

At high current density ($\sim$ 100mA cm^{-2}) potential-time plots for
the oxidation behaviour at platinum anodes show a maximum although the
thickness of the surface film continues to increase.   During this process,
current-time plots also show a maximum.   In both cases the catalytic
activity increases with increasing thickness of the oxide film.   The
evidence suggests the presence of two oxide phases, with the second phase
being a good conductor, changing both the mechanism of the reaction and
the catalytic activity[39].

Bockris et al[40] have shown by ellipsometrical work, in particular the
determination of the optical constant and the thickness of the anodic films
formed from ellipsometric data alone, that by potentiostatic polarisation of
the platinum electrode a film is formed above 1.1V that must be described
as a definite oxide phase.   The film thickness was shown to increase with
the polarisation potential for a fixed time of polarisation, suggesting that
the oxygen evolution reaction occurs only on a platinum electrode when it
is covered with a relatively thin film of an oxide phase.   Thus the
properties of the metal are not so much responsible for the catalysis but
rather the process is controlled by the nature of the oxide films, such as
their semiconductor properties and their thickness.

Many investigators have found that in general using slow charging
techniques the number of coulombs required to form an adsorbed oxygen layer
during the anodisation process Q_A, is larger than the number required to
remove it during the cathodic process Q_C.[19,41,42,43]   Often the ratio

Q_A/Q_C was found to approach 2. However, those that used rapid charging techniques tended to find that the two values were equal[44,45]. Initially it was postulated that the reduction step might lead to H_2O_2, but the work of Johnson et al[46] using a rotating platinum ring disc electrode has shown that the adsorbed oxygen layer on preanodised platinum is reduced directly to water without going through the peroxide intermediate.

The most feasible explanation is based on the concept of dissolved oxygen in the platinum lattice. During the anodic charging pulse, not only is the platinum surface covered by a layer of platinum (II) oxide but the platinum metal is also charged with dermasorbed oxygen. This is more easily dissolved in platinum than removed[45] and it has also previously been mentioned in the work of Anson and Lingane[30] that part of the adsorbed layer could not be removed by chemical stripping. Thus if the derma-sorbed oxygen is not removed during the cathodic pulse we would expect that $Q_A > Q_C$. During fast anodic charging, there is not enough time for the oxygen to be dermasorbed and hence Q_A is equal to Q_C. On repeated cycling of this procedure, the platinum eventually becomes saturated with dermasorbed oxygen and hence Q_A/Q_C tends to unity as is observed experimentally.

As the dermasorbed oxygen is bound more tightly to the surface than surface adsorbed oxygen, the arrest in the cathodic trace for its removal should occur at higher overvoltages than that for adsorbed oxygen. In fact, the dermasorbed oxygen is so strongly held that its arrest coincides with that for hydrogen deposition. Above a potential of 1V the amount of dermasorbed oxygen increases directly with the potential of preanodisation[47] as well as with the time of preanodisation at a given potential[36].

Three types of sorbed oxygen can now be defined as present on the surface. Surface adsorbed oxygen which reaches a limiting coverage equivalent to a monolayer of platinum (IV) oxide stoichiometry is the most weakly bound and is removed at low overvoltage, around 0.7V. More strongly bound dermasorbed oxygen, which is dissolved in the first two to three atomic layers of the platinum lattice is removed at higher over-potentials, around 0.3V. Oxygen which has penetrated more deeply into the platinum lattice will be referred to as absorbed oxygen. After oxygen has been stripped from the surface and dermasorbed layers of platinum by a cathodic pulse, the dermasorbed layers are filled relatively quickly with absorbed oxygen diffusing from deeper layers in the platinum lattice causing the open circuit voltage to return to high noble values around 1V. This can be stripped similarly with a second cathodic pulse[36].

It has been found[48,49] that significant amounts of oxygen may be dissolved in platinum which has been strongly anodised. After such treatment, attainment of potentials approaching the reversible oxygen electrode potential are more easily achieved. Similar effects are noted on treating platinum with concentrated nitric acid; not only is a complete passivating layer of adsorbed oxygen formed on the surface, but large amounts of oxygen are dissolved in the bulk metal to form a platinum-oxide alloy[50].

II.2   Oxygen Evolution Reaction Mechanism

The possible reaction mechanisms on the platinum-oxygen electrode and the resulting kinetic parameters have been reviewed by Bockris[51] and Damjanovic, Dey and Bockris[5]. Bockris[51] considered five different pathways for the electrolytic evolution of oxygen, and obtained limiting

expressions for the dependence of the current density (or rate) of the reaction upon electrode potential when one of a consecutive series of reactions had a rate constant much smaller than those of the other reactions in the series.   By considering all possible reaction intermediates that could occur during the oxygen evolution reaction, Millner[52] has recently pointed out that a very large number of reaction paths are then possible.

As an initial consideration of the oxygen evolution mechanism, the adsorption isotherms, either Langmuir or Tempkin type, must be distinguished. The Langmuir isotherm is valid when the coverage of the surface by intermediates is very low or close to unity.   In cases when the adsorption energy is not constant, but varies approximately linearly with coverage, a Tempkin type adsorption isotherm must be used.   This is the situation when an electrode has medium coverage by adsorbed intermediates.

II.3   Mechanism of oxygen evolution on platinum electrodes in acid solution

In acidic solution, an anodic Tafel slope of 2RT/F has been determined by many workers, notably Bockris and Huq[9], Damjanovic, Dey and Bockris[5], Hoar[8], Hickling and Hill[53] and Bowden[54].   A stoichiometric number of four was determined by Bockris and Huq[9].

Many workers agree that the rate limiting step is an electron transfer reaction and most likely to be the first discharge of water molecules in acidic solution,

$$PtO_2 + H_2O \rightarrow PtO_2 \cdot OH + H^+ + e \qquad (15)$$
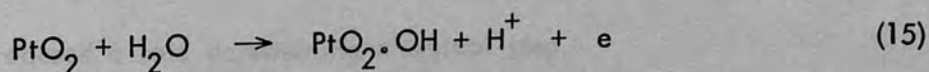
occurring on a platinum-oxide substrate.

The observed Tafel slope varying between 0.1 and 0.13 experimentally agrees with Bockris's calculation[51].

The next step could either involve a fast combination of hydroxyl radicals,

$$(OH)_{ads} + (OH)_{ads} \rightarrow (O)_{ads} + H_2O \qquad (16)$$
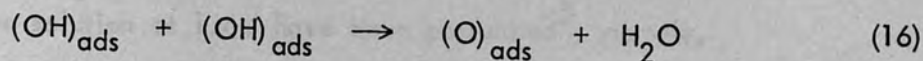
or the discharge of hydroxyl radicals,

$$(OH)_{ads} \rightarrow (O)_{ads} + H^+ + e \qquad (17)$$
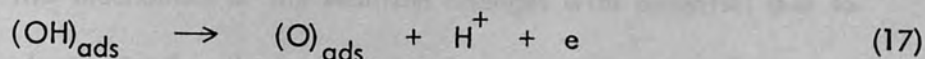
to produce adsorbed oxygen atoms.

Oxygen is finally evolved via the processes,

$$(O)_{ads} + (O)_{ads} \rightarrow (O_2)_{ads} \qquad (18)$$

$$(O_2)_{ads} \rightarrow O_2 \qquad (19)$$
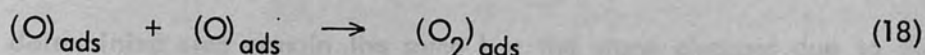
It must be remembered that this process occurs on a surface which is covered by an oxide layer[21].

II.4 Mechanism of oxygen evolution on platinum electrodes in alkaline solution

Many authors conclude that the situation differs in alkaline solution[55,56]. The anodic Tafel line shows a distinct change of slope at about 1.6V[5]. At lower potentials a slope of RT/F is found, whilst it is equal to 2RT/F at higher potentials. An exchange current density of 10^{-11} A cm^{-2} and a stoichiometric number of two have been determined[55] in contrast to the stoichiometric number of four found in acidic solution[9].

From results of a study of oxygen overpotential on platinum in 0.1M NaOH, Hoar[55] concluded that the mechanism differed in acid solution and proposed a rate determining chemical step,

$$(OH)_{ads} + OH^- \rightarrow (H_2O_2^-)_{ads} \qquad (20)$$
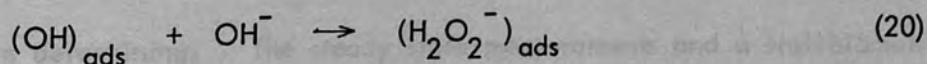
as none of Bockris's mechanisms[51] were consistent with his measured kinetic

parameters. This was unacceptable as peroxides could not be detected[57].

Four possibilities to explain the abrupt change of anodic slope in alkaline solution at 1.6V have been postulated[5], namely,

1. the reaction changes path at this potential;

2. the mechanism of the reaction changes with potential due to change in the electrode surface;

3. the rate controlling step in the same path changes at this potential;

4. conditions are created at the electrode such that the path and rate determining step remain the same but the slope changes due to the change in surface coverage by intermediates.

Damjanovic, Dey and Bockris[5] concluded that the change of slope was most likely to be interpreted as a change in rate determining step and not a change in mechanism.

The activation energy in alkaline solution decreases with increasing overpotential. The activation energy at the reversible potential has been calculated to be 22.5 kcal mol^{-1}.[54]   A step cannot be rate controlling if its activation energy is less than this value at the reversible potential. However, if the activation energy for this step decreases more slowly with increasing potential than does the activation energy for the rate determining step, then a change in the rate controlling step will occur.

Bockris and Huq[9] concluded from analysis of overpotential time plots that the electrochemical radical-ion discharge step,

$$(OH)_{ads} + OH^- \rightarrow (O)_{ads} + H_2O + e \tag{21}$$
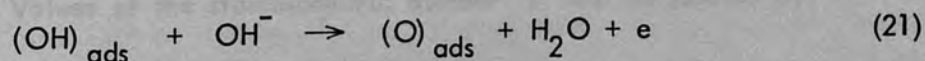
was rate determining. The steady state measurements and a stoichiometric number of four imply the step,

$$OH^- \longrightarrow (OH)_{ads} + e \qquad (22)$$
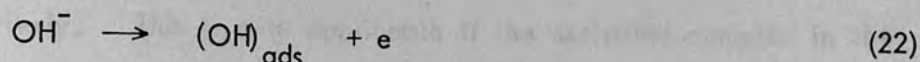
to be rate determining[51].

Riddiford[58] objected to the idea of a change in mechanism occurring with pH, and suggested that the electrochemical oxide path determined the kinetics in acid and alkaline solution.

Rates of consecutive steps in a given reaction path may be different functions of the potential and consequently the rate determining step could change with potential. Thus Krasil'shchikov[59] suggested that the mechanism is the same in acid and alkaline solution with the primary discharge step,

$$OH^- \longrightarrow (OH)_{ads} + e \qquad (22)$$
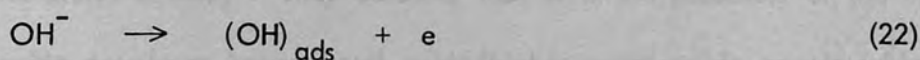
as rate determining at high current density. The following step being rate controlling at low current density,

$$(OH)_{ads} + OH^- \longrightarrow (O)_{ads} + H_2O + e \qquad (21)$$
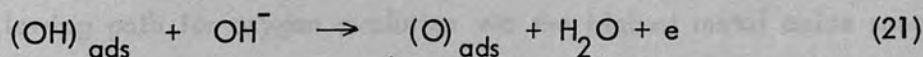
concluding with the mechanism as in acid solution,

$$(O)_{ads} + (O)_{ads} \longrightarrow (O_2)_{ads} \qquad (18)$$

$$(O_2)_{ads} \longrightarrow O_2 \qquad (19)$$
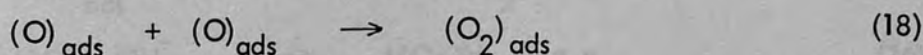
It is thought that the specific adsorption of hydroxyl ions in alkaline solution may be the chief reason for the change of rate determining step with decreasing overpotential as the surface coverage of the anode with adsorbed hydrogen is a function of potential[5].

Values of the stoichiometric number v are calculated by[60]

$$v = \cfrac{1}{\cfrac{RT}{nF} \left(\cfrac{1}{b_a} - \cfrac{1}{b_c} \right)} \qquad (23)$$

where b_a and b_c represent the values of the anodic and cathodic Tafel slopes

respectively. This is only applicable if the activated complex in the rate determining reactions is the same for both the oxidation and reduction processes. This seems improbable in the case of the oxygen evolution reaction as during the evolution process electron transfer occurs between the electrode and a singly bonded oxygen species, $(OH)_{ads}$, whilst for the reduction process it is between the electrode and a double bonded oxygen species $(O_2)_{ads}$.

Tseung and Jasem[61] have recently proposed a mechanism for the oxygen evolution reaction in alkaline solution which proceeds via transitions to higher metal oxides. They consider that it is the potential of the metal/metal oxide couple or lower metal oxide/higher metal oxide couple which is important, as unless the anodic potential is higher than that of these couples oxygen evolution cannot proceed efficiently. They postulated the following path for oxygen evolution via the highest metal oxide species,

$$M + OH^- \longrightarrow MOH_{ads} + e \tag{24}$$

$$MOH_{ads} + OH^- \longrightarrow MO + H_2O + e \tag{25}$$

$$\rightarrow MO + OH^- \longrightarrow MOOH_{ads} + e \tag{26}$$

$$MOOH_{ads} + OH^- \longrightarrow MOO + H_2O + e \tag{27}$$

$$MOO + OH^- \longrightarrow MOOOH_{ads} + e \tag{28}$$

$$MOOOH_{ads} + OH^- \longrightarrow MO + O_2 + H_2O + e \tag{29}$$
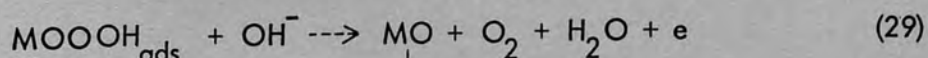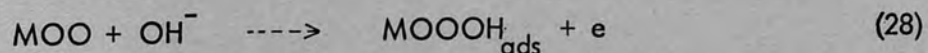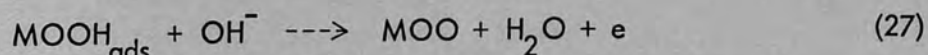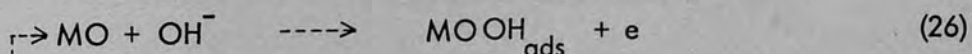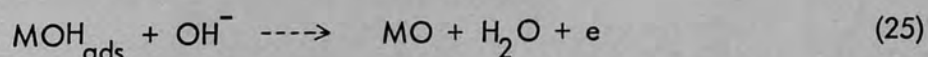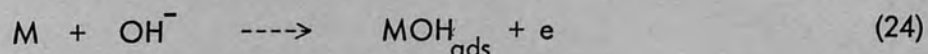
the MO species being regenerated in the final step, and thus the process continuing from step (26).

They suggest that by use of the isotope $H_2{}^{18}O$ in alkaline electrolyte, the formation of ${}^{16}O{}^{18}O$ may be detected by mass spectrometry, which can be presumed to have come from the breakdown of a higher metal oxide species, $MO.{}^{18}O{}^{16}O$, if the evolution process is subsequently performed in normal electrolyte.

Metal Oxide Electrocatalysts

III.1   Introduction

At present the evidence points to the need for the formation of the highest oxide on an electrode prior to oxygen evolution, which in many cases occurs at high overpotentials; hence the displacement from the equilibrium potential for this reaction is great.   With this knowledge it is possible to choose electrocatalyst materials which form their highest oxide species at potentials close to 1.23V, but if they are to be considered as potential oxygen evolution catalysts they must also conform to the requirements of high electrical conductivity, corrosion resistance and other general catalytic properties.   The theories of oxygen evolution have been reviewed in the preceding chapter.   In the case of platinum, the need for

CHAPTER III

the electrode to be anodically polarised beyond the potential of the PtO/ PtO$_2$ couple prior to oxygen evolution was first demonstrated by Hoare[ ]. This argument can be extended to other metals such that unless the electrode potential exceeds that of the metal/metal oxide couple, or lower metal oxide/ higher metal oxide couple if more than one oxide is formed, oxygen evolution cannot occur[ ].   Data for the potentials of oxide formation can be obtained from Pourbaix diagrams[ ].

III.2   Mixed oxide species

Many oxides possess conductivity similar to metals.   Among them, transition metal dioxides with the rutile structure (e.g. TiO$_2$) have found wide applications in electrochemistry.

Most oxides which contain two or more different types of cations occur in three basic structural types, perovskite, spinel and ilmenite

Metal Oxide Electrocatalysts

III.1 Introduction

At present the evidence points to the need for the formation of the

highest oxide on an electrode prior to oxygen evolution, which in many

cases occurs at high overpotential; hence the displacement from the

equilibrium potential for this reaction is great.   With this knowledge it

is possible to choose electrocatalyst materials which form their highest

oxide species at potentials close to 1.23V, but if they are to be considered

as potential oxygen evolution catalysts they must also conform to the

requirements of high electrical conductivity, corrosion resistance and other

general catalytic properties.   The theories of oxygen evolution have been

reviewed in the preceding chapter.   In the case of platinum, the need for

the electrode to be anodically polarised beyond the potential of the $PtO/$

PtO_2 couple prior to oxygen evolution was first demonstrated by Hoare[21].

This argument can be extended to other metals such that unless the electrode

potential exceeds that of the metal/metal oxide couple or lower metal oxide/

higher metal oxide couple if more than one oxide is formed, oxygen

evolution cannot occur[61].   Data for the potentials of oxide formation can

be obtained from Pourbaix diagrams[32].

III.2 Mixed oxide species

Many oxides possess conductivity similar to metals.   Among them,

transition metal dioxides with the rutile structure (e.g. TiO_2) have found

wide applications in electrochemistry.

Most oxides which contain two or more different types of cations,

occur in three basic structural types, perovskite, spinel and ilmenite

structures.   Only the first two categories are relevant to the field of electrochemistry.

III.2i   Perovskite structure

In the perovskite structure, symbolised ABO_3, oxide ions and the larger cation A form a close packed array, with the smaller cation B occupying those octahedral holes formed exclusively by oxide ions; the structure often being slightly distorted.   This structure is adopted by numerous ABO_3 oxides in which one cation is comparable in size to the O^{2-} ion, with the other much smaller; with the cations possessing variable charge so long as their sum is equal to six.

III.2ii   Spinel structure

The spinel structure, symbolised AB_2O_4, is also a close packed cubic arrangement of oxide ions, in which one half of the octahedral interstices and one eighth of the tetrahedral interstices are occupied by positive ions, with the A cations in tetrahedral sites and the B cations in octahedral sites, as shown in Fig. 1.   Each unit cell contains eight formula units, thus thirty two O^{2-} anions form a densely packed face centred cubic cell of the spinel.   A lattice parameter of 0.8nm is achieved with closest packing; this in practice varies between 0.80 and 0.89 nm.

Tseung and Jasem[62] have considered possible materials for oxygen evolution electrocatalysts, these are listed with their properties in Table I. They suggest mixed oxides of nickel and cobalt as likely candidates.   The unit cell parameters of CoO and NiO being sufficiently similar (4.26 and 4.18 Å respectively) to permit the formation of solid solutions throughout the whole composition range[63].   In particular, further experiments have shown that the spinel $NiCo_2O_4$ is exceptionally active for this reaction[64].   This is

Fig 1: The unit cell of a spinel oxide, AB_2O_4 [137]

Filled circles are tetrahedrally co-ordinated cations (A)

Small hatched circles are octahedrally co-ordinated cations (B)

Large unfilled circles are oxygen anions (O)
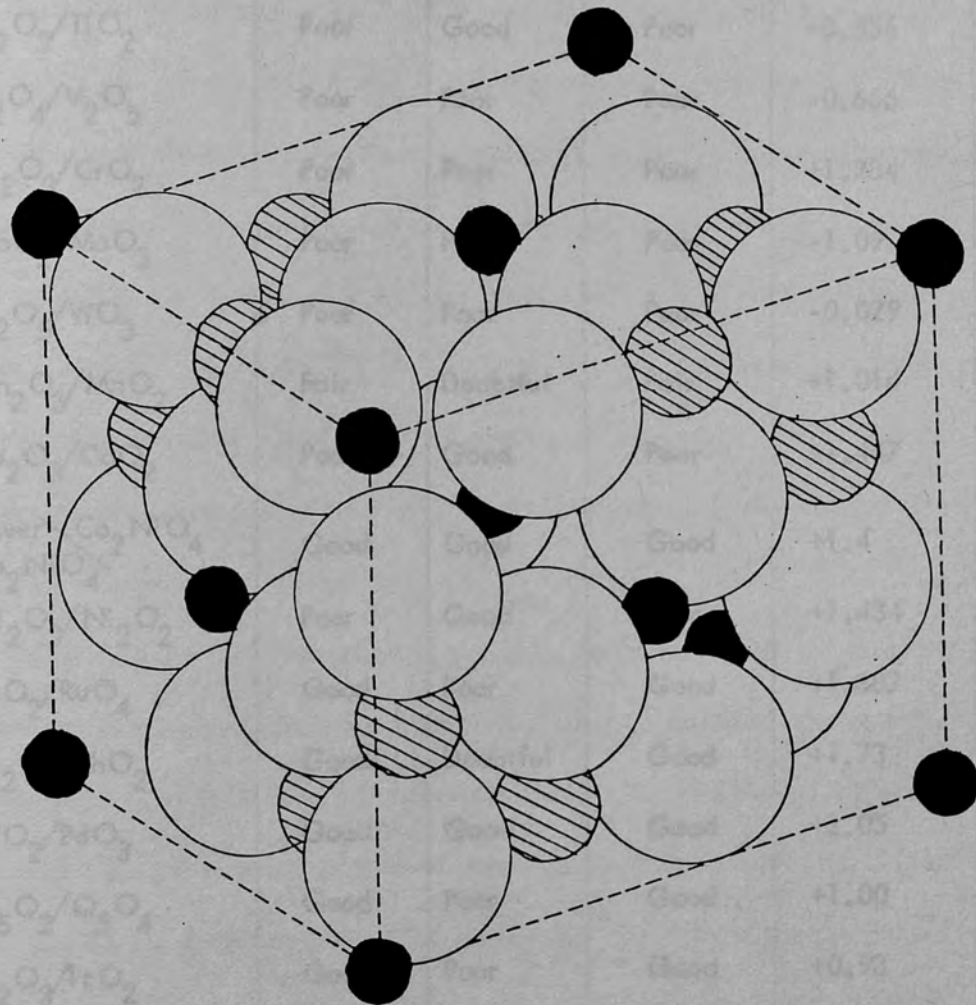
TABLE I: Properties of semiconducting oxides[62]

Oxide	Electrical Conductivity	Corrosion Resistance at pH=14	Oxygen Reduction	Potential VS NHE Volts
La/La$_2$O$_3$	Poor	Good	Poor	-2.069
Ti$_2$O$_3$/TiO$_2$	Poor	Good	Poor	-0.556
V$_2$O$_4$/V$_2$O$_5$	Poor	Poor	Poor	-0.666
Cr$_2$O$_3$/CrO$_2$	Poor	Poor	Poor	+1.284
MoO$_2$/MoO$_3$	Poor	Poor	Poor	-1.09
W$_2$O$_5$/WO$_3$	Poor	Poor	Poor	-0.029
Mn$_2$O$_3$/MnO$_2$	Fair	Doubtful	Fair	+1.014
Co$_2$O$_3$/CoO$_2$	Poor	Good	Poor	+1.447
lower Co$_2$NiO$_4$ / Co$_2$NiO$_4$	Good	Good	Good	+1.4
Ni$_2$O$_3$/Ni$_2$O$_2$	Poor	Good	Poor	+1.434
RuO$_2$/RuO$_4$	Good	Poor	Good	+1.387
Rh$_2$O$_3$/RhO$_2$	Good	Doubtful	Good	+1.73
PdO$_2$/PdO$_3$	Good	Good	Good	+2.05
O$_5$O$_2$/O$_5$O$_4$	Good	Poor	Good	+1.00
Ir$_2$O$_3$/IrO$_2$	Good	Poor	Good	+0.93
PtO/PtO$_2$	Good	Good	Good	+1.7
Cu$_2$O/CuO	Poor	Doubtful	Poor	+0.667
AgO/Ag$_2$O$_3$	Good	Poor	Good	+1.57
Au$_2$O$_3$/AuO$_2$	Good	Doubtful	Poor	+2.63

based on the spinel Co_3O_4 and is readily formed provided that the nickel content does not exceed one third[65].

The main factors in favour of spinels are their high activity, cheapness, availability and that they show satisfactory thermodynamic stability. However, they are mainly limited to alkaline solution and often have low specific surface areas. One particular feature of the crystalline structure of all spinels is that the crystallographically equivalent places in the lattice are occupied by cations of different valencies between which electronic transitions may take place without perceptible energy.

Co_3O_4 has been shown to be a normal 2-3 spinel with a charge distribution $Co^{2+}\left[Co^{3+} Co^{3+}\right] O_4^{2-}$, such that all the trivalent cobalt ions are in octahedral holes[66]. The doping of this species with lithium to increase its conductivity has been postulated as giving rise to the following charge distribution, $Li_{\frac{1}{3}x} Co^{2+}_{1-\frac{2}{3}x} \frac{1}{2}Co^{3+}_{x/3} \left[2Co^{3+}\right] O_4^{2-}$ [67] It is interesting to note that upon prolonged anodic polarisation, ordering in the lattice structure of the parent species Co_3O_4 is reported to occur, leading to a film containing an excess of oxygen. This is not thought to have arisen by penetration of oxygen ions into lattice interstitials, but rather to be due to the formation of cation vacancies[68]. These cation vacancies, B, are located in octahedral positions, and in order to preserve electro-neutrality some of the trivalent cobalt ions in octahedral interstices are oxidised to the tetravalent species, thus $Co^{2+}\left[Co^{3+}_{2-x} Co^{4+}_{3x/4} B_{x/4}\right]O_4$. The number of such cation vacancies, and accordingly the amount of excess oxygen are related to the conditions under which the oxide layer was formed, mainly temperature effects. The excess oxygen is gradually removed when the films are heated to $850^{\circ}C$. The stoichiometric relation between

components in the oxide is attained at this temperature, and a weight loss in the film shown by differential thermal analysis. The elimination of oxygen on heating and its absorption upon cooling are processes which affect not only the surface, but also the interior of the crystallites. The rate of this process at relatively low temperatures ($300^{\circ}C$) is high and thus equilibrium state is attained quite rapidly. The rates of electrode processes which have been studied in detail have been shown to increase with the number of cationic vacancies in the oxide. In particular the oxygen evolution reaction has been shown to be accelerated under these conditions.

In the formation of the spinel $NiCo_2O_4$, the nickel cations substitute for B site cobalt ions, due to their high preference for octahedral co-ordination in oxides[69]. The substitution of Ni^{2+} for Co^{3+} in Co_3O_4 partly weakens the bonding of the oxide ions to approximately O^-, while the residual charge imbalance is taken up by the oxidation of Ni^{2+} to Ni^{3+}. This loosening effect is expected to occur mainly at the surface where the co-ordination shell of the oxide is incomplete and thus the stability of the material is in turn dependent on surface areas.

The point of instability in the preparation is reached when one third of the cobalt cations have been substituted by nickel cations, which corresponds to a surface layer of $[O^-]$. This is feasible at surface areas in the region of $30m^2g^{-1}$. The catalyst is active since if surface $[O^-]$ or O_2 is electrochemically reduced, the rate of chemisorption of the replacement would be encouraged by the 'strained' lattice.

King and Tseung[60] have suggested that the distribution of nickel, cobalt and oxygen ions in the $NiCo_2O_4$ lattice is given by,

$$Co^{2+}_{0.9} \quad Co^{3+}_{0.1} \left[Ni^{2+}_{0.9} \quad Ni^{3+}_{0.1} \quad Co^{3+} \right] O^{2-}_{3.2} \quad O^{-}_{0.8}$$
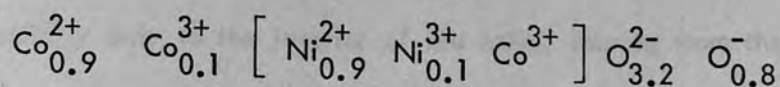
on the basis of crystallographic and electronic considerations of the spinel structure as well as thermogravimetric analysis results. The internal stability of $NiCo_2O_4$ is postulated as arising from the 'spare electron' or unplaced positive charge. If the O^{2-} ion in the lattice can be replaced by a hydroxyl ion, charge compensation will result. The ionic radius of the hydroxide ion is 1.53Å which is less than ten per cent larger than that of the oxide ion (of radius 1.40Å), and thus will fit in the lattice as has been proved to be the case in some spinels.

On passing the breaking point of 450°C the surface area decreases and oxygen is removed, the spinel form breaking down to the cubic $NiCo_2O_3$. This is thought to be a reflection of the loosely-bound oxygen, as the parent compound Co_3O_4 is stable to 900°C.

III.3 Conductivity

The initial question must be whether the measured conductivity arises only as a surface phenomenon or whether it is a property of the bulk of the solid. Materials of high surface area contain a significant proportion of ions at the surface of the solid where they are subject to anomalous conditions which occur at interfaces. The cations here may exist in oxidation states or electronic spin states which are unimaginable in the bulk of the solid, by the adsorption of atmospheric constituents or by a change in crystal field energy caused by incomplete co-ordination. Additionally these states may not be electrochemically stable. Whereas catalytic activity applies only to surface states, many analytical procedures measure a mixed surface/bulk value, and moreover theoretical considerations

apply strictly only to the interior of the solid, remote from the surface.

In general most spinels are poor conductors, but metallic or semi-conducting properties may appear if one type of metal ion is present in different valency states. In $NiCo_2O_4$ the low resistivity is due to almost unrestricted interchange of electrons between cations on the B sites. It has been demonstrated that for high conductivity, two types of cations are required on octahedral sites which differ in formal charge by one[71]. In $NiCo_2O_4$, this spare electron is introduced by the substitution of Ni^{2+} for Co^{3+}. The high conductivity of this species is explained by 'electron hopping' between Ni^{2+} and Ni^{3+} ions on octahedral sites, and the observed p-type conductivity is accounted for if the Ni^{3+} ions are in the minority. In general, a p-type semiconductor displays a decrease in resistance on contact with oxygen, since the adsorption of oxygen accompanied by the capture of an electron of the oxide, facilitates the formations of electron defects, that is the basic charge carriers.

The resistivity of Co_3O_4 is found to be 4×10^3 Ω.cm, and the mechanism of its conductance is,

$$Co^{n+} \rightleftharpoons Co^{(n-1)+} + D^+ \tag{1}$$
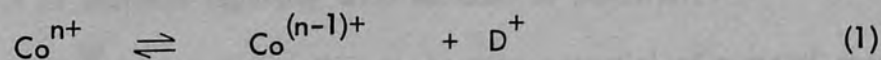
where D^+ represents a hole. However, this can be reduced by doping with lithium. The electrical conductivity of the lithium doped oxide is thought to be by electron hopping between the Co^{2+}/Co^{3+} transition in the tetrahedral sites.

III.4 Magnetic effects

Assuming the theory that ferromagnetic surfaces enhance the breaking of the O-O bond in oxygen reduction reactions is valid, then such a surface

should also act in the reverse sense to facilitate the combination of

adsorbed oxide ions.   The magnetic data shows that ferromagnetism occurs

whenever cobalt and nickel coexist[64].   As CoO and NiO are antiferro-

magnetic, and Co_3O_4 is paramagnetic, this ferromagnetism must arise from

the mixed cobalt nickel oxide spinel.   It can be explained by a strong

negative super exchange interaction between tetrahedral site cobalt and

octahedral site nickel.

III.5   Corrosion resistance

Information concerning the stability of the oxide materials under

the proposed experimental conditions is necessary.   The available source

of information are Pourbaix diagrams[32] as other detailed experimental data is

not readily available.

When a cobalt oxide electrode is immersed in an electrolyte, the

potential in the absence of an external current is displaced towards more

positive values and the accumulation of dissolved cobalt in the electrolyte

indicates simultaneous dissolution of the oxide[72].   The rate of dissolution

was found to decrease regularly with increase of potential.

Vetter[33] proposed that the steady state potential of a metal oxide

electrode in aqueous solution which does not contain depolarising agents

was determined by redox reactions of the following type, taking place at

the boundary of the electrolyte,

$$v MO_n + H_2O \rightleftharpoons v MO_{n + 1/v} + 2H^+ + 2e \qquad (2)$$
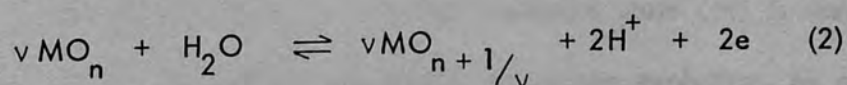
Thus dissolution of the oxide occurs via,

$$Co_3O_4 + 2H^+ \rightleftharpoons Co_2O_3 + Co^{2+} + H_2O \qquad (3)$$
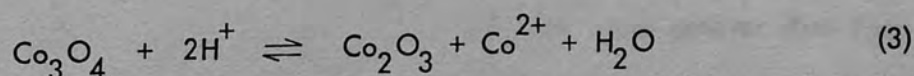
This leads to the formation of a surface layer of non-stoichiometric oxide, the composition of which differs from the bulk.

In the voltage range of 1.2-1.7V, the dependence of the rate of dissolution of the electrode with potential under potentiostatic conditions, consists of three regions, characterised as follows:

1. $V < 1.35 - 1.4V$:   retardation of process until displacement of potential towards more positive values.

2. $1.35 < V < 1.55$:   ratio of dissolution is independent of potential.

3. $V > 1.5-1.55$:   increase in rate of process with further increase in potential.

On anodic polarisation, an increase in the rate of dissolution is observed after the attainment of potentials at which the formation of the unstable higher oxide CoO_2 becomes thermodynamically possible:

$$Co_2O_3 + H_2O \rightleftharpoons 2CoO_2 + 2H^+ + 2e \qquad V \backsim 1.48V \qquad (4)$$
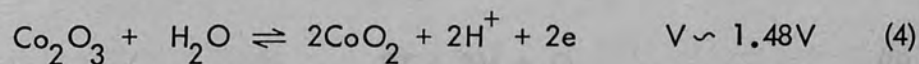
The dissolution of this oxide,

$$CoO_2 + 2H_2O \rightleftharpoons Co^{2+} + 2O_2 + 4H^+ + 6e \qquad\qquad (5)$$
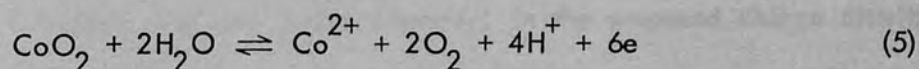
is accompanied by oxygen evolution, but the contribution of this process to the overall current at the potential region in question does not exceed 1-2%, so that oxygen is chiefly liberated by the discharge of water.

III.6   Mechanism of oxygen evolution

In the species $NiCo_2O_4$, the highest oxidation state (+4) is reached by the nickel and cobalt cation sites active for oxygen evolution, by a maximum of two electron transfer steps.   Further electron transfer steps are not possible as they would lead to an oxidation state greater than four; this assumes that oxygen evolution occurs chemically by the step,

$$2MO \quad \longrightarrow \quad 2M + O_2 \qquad (6)$$
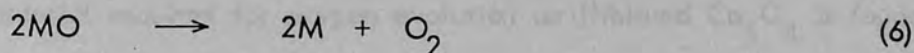
This idea is also only applicable if initially the cation is in the divalent state, M representing the metal oxide species in its stable state.

However if the first electron transfer step should occur on a trivalent site, the second electron transfer step cannot be the same as that suggested which initiates on a divalent site, as the maximum oxidation state would already be achieved. An alternative route then involves the interaction with another site, represented as M, either di- or tri-valent to form a bridged species,

$$TOH + M + {}^-OH \rightleftharpoons \begin{array}{c} T \diagdown \\ \diagup O \\ M \end{array} + H_2O + e \qquad (7)$$
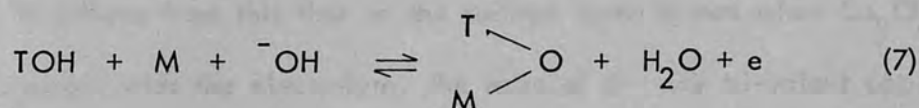
where T represents a trivalent site. Oxygen evolution can subsequently occur by,

$$2 \begin{array}{c} T \diagdown \\ \diagup O \\ M \end{array} \rightleftharpoons 2T + 2M + O_2 \qquad (8)$$
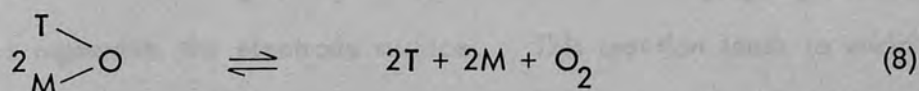
Trivalent sites are in the minority; in the proposed charge distribution only two fifths of the cations are trivalent. To evolve oxygen by this mechanism they also have to be at sufficient proximity to form a bridged species. It has been suggested that this route for oxygen evolution occurs at low overvoltage[73] and that the oxygen is evolved at a slightly lower potential than by the divalent route. However, the limitations imposed prevent this method interfering with the kinetics of oxygen evolution at higher potentials. This would be expected to be revealed in Tafel slope measurements and indeed is found to be the case, with a change in gradient at low overpotential.

This argument may be extended to cover oxygen evolution on lithiated Co_3O_4 in which over two thirds of the cobalt ions are in trivalent sites.

The potential required for oxygen evolution on lithiated Co_3O_4 is found to be lower than that required on $NiCo_2O_4$ and the electrode performance is found to increase with lithium doping[67]. This increase in the level of dopant does not only improve the electrical conductivity of the electro-catalyst, but additionally serves to increase the number of trivalent cobalt ions present. The steady state potential of a Co_3O_4 electrode in one molar perchloric acid is appreciably higher than the standard potential according to

$$2Co_3O_4 + H_2O \rightleftharpoons 3Co_2O_3 + 2H^+ + 2e \qquad (9)$$
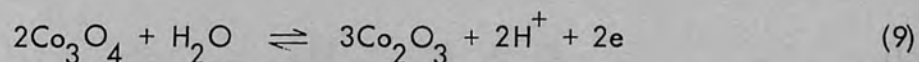
It follows from this that in the surface layer formed when Co_3O_4 makes contact with the electrolyte, the ratio of di- and tri-valent cations may be greater than in the original oxide[72]. . On the surface,

$$(2 \left[Co^{2+} \right] O^{2-})_s + 2D^+_s + H_2O \rightarrow (\left[Co^{3+} \right]_2 O_3^{2-})_s + 2H^+ \qquad (10)$$
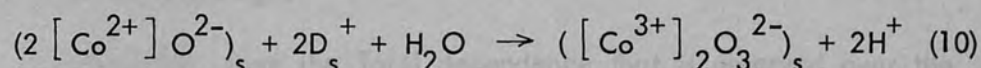
where s represents the electrode surface. This reaction leads to enrichment on the surface of Co^{3+}, which creates favourable conditions for the discharge of water, the state of which is controlled by the surface concentration of holes.

$$(Co_2O_4)_s + 4D^+_s + 2H_2O \rightarrow (Co_3O_4)_s + 4H^+ + O_2 \qquad (11)$$
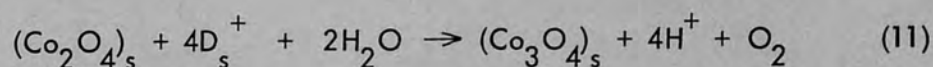
Thus the behaviour of the Co_3O_4 electrode is controlled by redox and corrosion properties taking place on the surface, and also by its semi-conducting properties.

A proposed mechanism of oxygen evolution on lithiated Co_3O_4 follows[73]

$$T + \bar{O}H \rightleftharpoons TOH + e \qquad (12)$$

Since the oxidation state of T in TOH is four, the site cannot undergo further oxidation state transitions. Kinetic interpretations suggest a subsequent rate determining step as,

$$TOH + {}^-OH \rightleftharpoons TO^- + H_2O \tag{13}$$
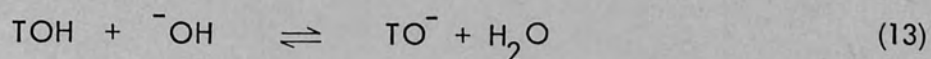
of the type suggested by Krasil'shchikov[59] at low coverage.

The tetravalent species TO^- undergoes a second electron transfer step involving a neighbouring di- or tri-valent site M, to form a bridged species

$$TO^- + M \rightleftharpoons \begin{array}{c} T \\ \diagdown \\ \diagup \\ M \end{array} O + e \tag{14}$$

Subsequent oxygen evolution occurs by,

$$2 \begin{array}{c} T \\ \diagdown \\ \diagup \\ M \end{array} O \rightleftharpoons 2T + 2M + O_2 \tag{15}$$
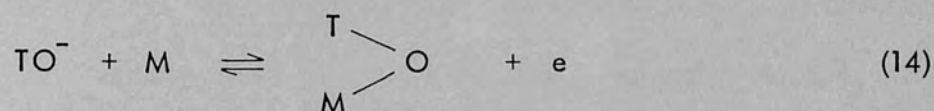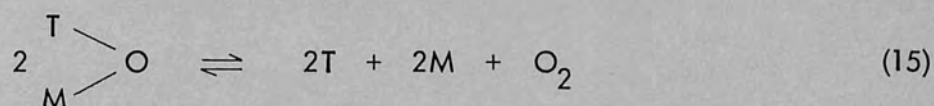
This mechanism for oxygen evolution involves four sites whose proximity to each other is of great importance, this assumption being justifiable at low coverage.

The deviation from the Tafel dependence that is observed over the narrow potential range of 1.45-1.6V is possibly due to limitations in the supply of carriers to the surface, that is ohmic losses in the oxide which decrease with increasing imperfections of the films.

CHAPTER IV

Theory of Isotopic Experiments

IV.1 Introduction

The evidence for oxide formation on an anodically polarised electrode, preceding oxygen evolution, has been discussed in the previous chapters.   One of the aims of my work has been to develop an isotopic technique to ascertain what role this oxide surface plays in the oxygen evolution reaction, and whether it is directly involved in the reaction mechanism.   The work of Hibbert[74] gave a preliminary insight into the scope of this idea and suggested that further research would be profitable.

Basically the technique involved evolving oxygen on an electrode in electrolyte which is ^{18}O enriched for a set period of time.   After a thorough washing procedure it was transferred to a cell containing normal electrolyte, and the subsequent oxygen evolved on passage of current analysed by mass spectrometry, detecting the m/e 34 ($^{18}O^{16}O$) peak. Detection of m/e 34 greater than the background amount indicated enrichment and suggested that an enriched higher oxide species was active in the oxygen evolution mechanism.

This chapter describes the theoretical basis of the method, considering the formation of both one and two higher oxide species in turn.   The equations have been derived to relate the signal m/e 34 seen at the mass spectrometer to the total number of sites on the surface active for oxygen evolution.

IV.2.i   Fraction of ^{18}O in evolved gas at electrode surface

A simple mechanism for oxygen evolution on a metal in oxidation state N, M^N via higher oxidation states M^{N+1}, M^{N+2} is:
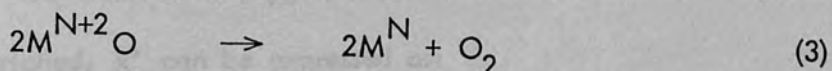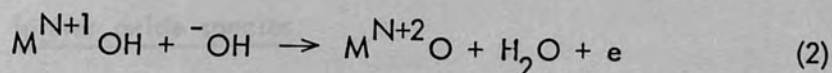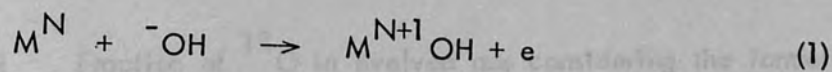
$$M^N + {}^-OH \rightarrow M^{N+1}OH + e \qquad (1)$$

$$M^{N+1}OH + {}^-OH \rightarrow M^{N+2}O + H_2O + e \qquad (2)$$

$$2M^{N+2}O \rightarrow 2M^N + O_2 \qquad (3)$$

for reactions in alkaline media, and

$$M^N + H_2O \rightarrow M^{N+1}OH + H^+ + e \qquad (1a)$$

$$M^{N+1}OH + H_2O \rightarrow M^{N+2}O + H_3O^+ + e \qquad (2a)$$

$$2M^{N+2}O \rightarrow 2M^N + O_2 \qquad (3a)$$
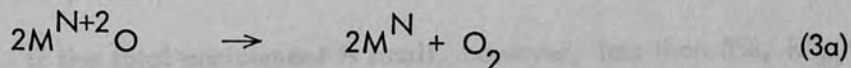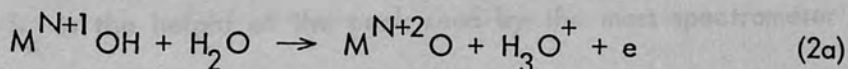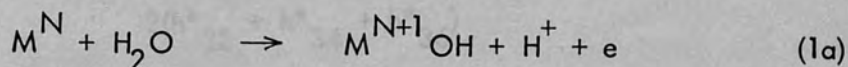
for reactions in acid media.

The initial oxidation state of the metal (N) may refer to a large metal surface (N=O) or to an oxide covered surface (N > O). For example, on platinum, PtO_2 (i.e. N=4) is the stable oxide on which oxygen is evolved.

If an electrode is "enriched" by evolution of oxygen in an electrolyte containing a certain percentage of ^{18}O which is greater than the background level, the subsequent evolution of oxygen on this electrode in electrolyte having a normal ^{18}O content will lead to the appearance of $^{18}O^{16}O$ in the gas phase by reactions such as:

$$M^{18}O + M^{16}O \longrightarrow 2M + {}^{18}O{}^{16}O \tag{4}$$

$$M^{18}O + M^{18}O \longrightarrow 2M + {}^{18}O{}^{18}O \tag{5}$$
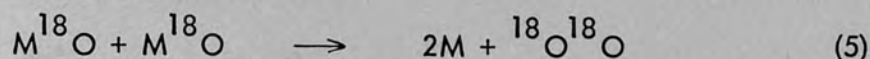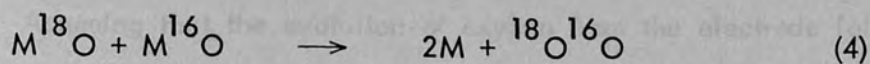
IV.2.ii Fraction of ^{18}O in evolved gas considering the formation of one higher oxide species

The fraction of oxygen atoms which are evolved at the oxide and are enriched, x^* can be expressed as:

$$x^* = \frac{h^*_{34} + 2h^*_{36}}{2(h^*_{32} + h^*_{34} + h^*_{36})} \tag{6}$$

where h_a is the height of the peak seen by the mass spectrometer at $m/e = a$, and the superscript $*$ denotes oxygen evolved from the electrode.

If the total enrichment is small, however, less than 5%, $h^*_{32} \gg h^*_{34} \gg h^*_{36}$ and therefore to a reasonable approximation (6) may be reduced to

$$x^* = \frac{h^*_{34}}{2h^*_{32}} \tag{7}$$

where $h^*_{32} = h_{32} - \dfrac{h^o_{32}}{h^o_{28}} h_{28} = h_{32} - y^o h_{28}$ \hfill (8)

and $h^*_{34} = h_{34} - \dfrac{h^o_{34}}{2h^o_{32}} \dfrac{h^o_{32}}{h^o_{28}} 2h_{28} = h_{34} - 2x^o y^o h_{28}$ \hfill (9)

where h_a^o is the peak height of $m/e = a$ in air. Therefore values of x^* being observed to be greater than x^o (which is 0.204×10^{-2}) will indicate enrichment of the electrode.

Assuming that the evolution of oxygen from the electrode follows first order kinetics, then

$$\frac{dx^*}{dt} = K(x^* - x^o) \tag{10}$$

where K is a first order rate constant for the process. If the initial enrichment of the electrode is expressed by x^*_o, then integration of (10) leads to

$$x^* = x^o + (x^*_o - x^o) \exp(-Kt) \tag{11}$$

A plot of $\log(x^* - x^o)$ versus time for each electrode should then take the form as shown in Fig. 1. The left-hand side axis measuring the fraction of enrichment, the usual decay curve being obtained. The $\log(x^* - x^o)$ plot axis visible on the right hand side. The intercept, $\log(x^*_o - x^o)$ being dependent on the initial enrichment of the electrode. The first order rate constant, K, may be determined from the gradient, which should be similar for each electrode. A change in the initial enrichment being demonstrated by parallel slopes.

From this graphically determined value of K, an estimate of the number of surface sites active for this reaction can be obtained. Faraday's Law predicts the number of gram atoms of oxygen produced each second to be equal to $iL/2F$ atoms s^{-1}. If n^* represent the number of ^{18}O atoms formed at the electrode and n_T is the total number of exchangeable atoms then,

$$\frac{-dn^*}{dt} = \frac{iL}{2F}(x^* - x^o) \tag{12}$$

However, as $x^* = n^*/n_T$, we have

Fig. 1: Schematic diagram of expected results obtained from the V.G. Micromass 12 mass spectrometer assuming only one higher oxide is formed.
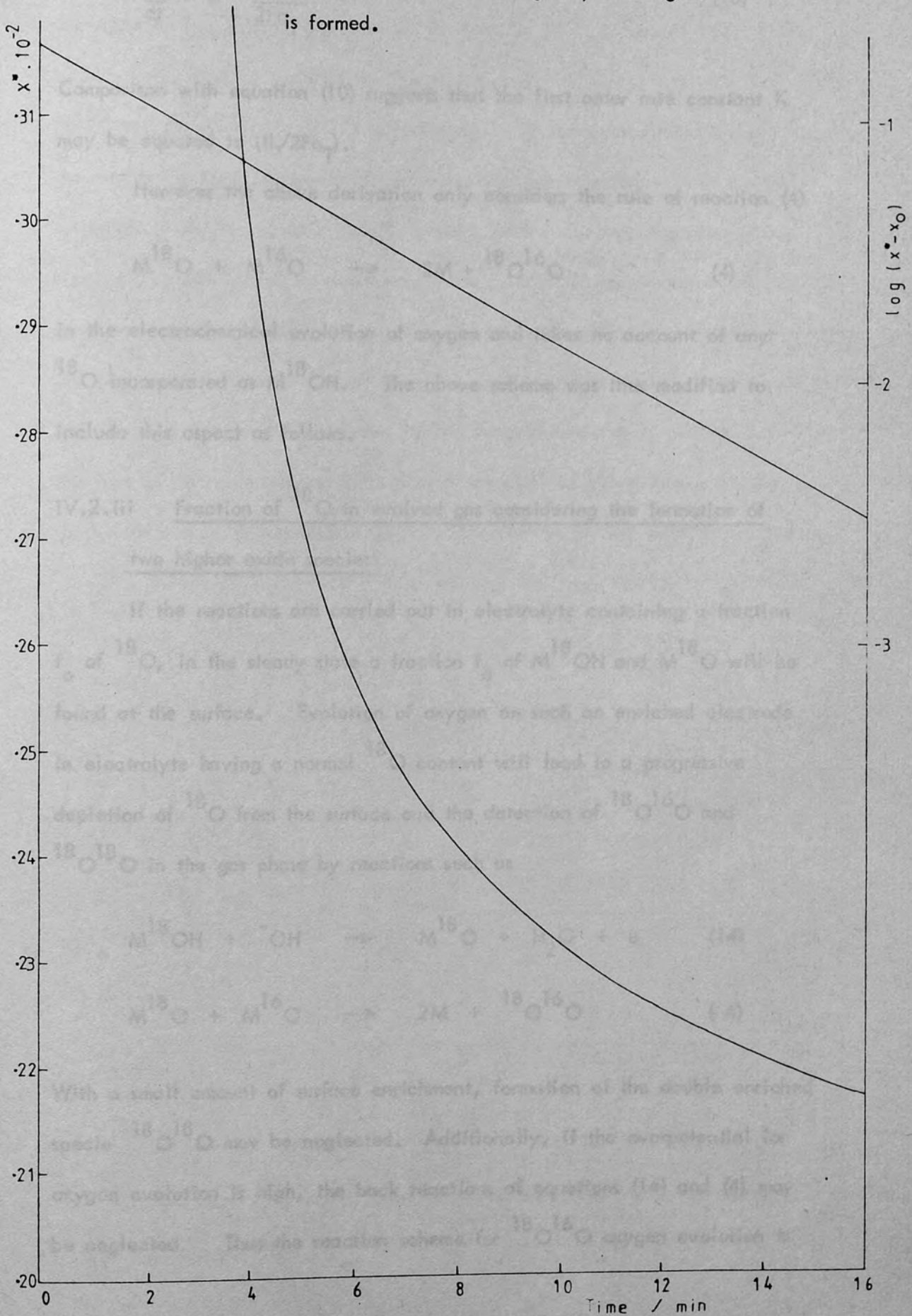
$$-\frac{dx^*}{dt} = \frac{iL}{2Fn_T} (x^* - x^o) \tag{13}$$

Comparison with equation (10) suggests that the first order rate constant K may be equated to $(iL/2Fn_T)$.

However the above derivation only considers the role of reaction (4)

$$M^{18}O + M^{16}O \rightarrow 2M + {}^{18}O^{16}O \tag{4}$$
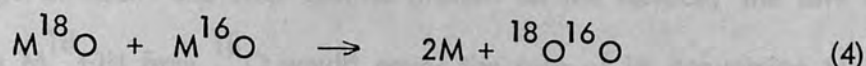
in the electrochemical evolution of oxygen and takes no account of any ^{18}O incorporated as $M^{18}OH$. The above scheme was thus modified to include this aspect as follows.

IV.2.iii   Fraction of ^{18}O in evolved gas considering the formation of
    two higher oxide species

If the reactions are carried out in electrolyte containing a fraction f_o of ^{18}O, in the steady state a fraction f_o of $M^{18}OH$ and $M^{18}O$ will be found at the surface. Evolution of oxygen on such an enriched electrode in electrolyte having a normal ^{18}O content will lead to a progressive depletion of ^{18}O from the surface and the detection of $^{18}O^{16}O$ and $^{18}O^{18}O$ in the gas phase by reactions such as

$$M^{18}OH + {}^-OH \rightarrow M^{18}O + H_2O + e \tag{14}$$

$$M^{18}O + M^{16}O \rightarrow 2M + {}^{18}O^{16}O \tag{4}$$
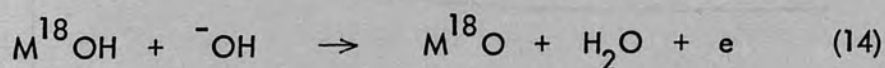
With a small amount of surface enrichment, formation of the double enriched specie $^{18}O^{18}O$ may be neglected. Additionally, if the overpotential for oxygen evolution is high, the back reactions of equations (14) and (4) may be neglected. Thus the reaction scheme for $^{18}O^{16}O$ oxygen evolution is

one of consecutive first order processes.   Let a and b be the initial

enrichment of ^{18}O in the surface oxide layer as $M^{18}OH$ and $M^{18}O$

respectively, and x, y and z be the enrichment of ^{18}O at time t as

$M^{18}OH$, $M^{18}O$ and $^{18}O^{16}O$ respectively.   If the surface oxides on

the electrode were not enriched, when equilibrium is achieved and a steady

coverage of MOH and MO species present on the surface, the rate of

forming $M^{18}OH$ from ^{18}O would equal the rate of its conversion to $M^{18}O$,

and therefore the overall rate would be zero.   However, in the case of

an 'enriched' electrode, the initial value of $M^{18}OH$ is high, comparatively,

and thus the decay of this species by the forward reaction is greater than

the rate of its replenishment from normal electrolyte;   therefore a decrease

in the amount of this species with time is observed, in the form shown below:
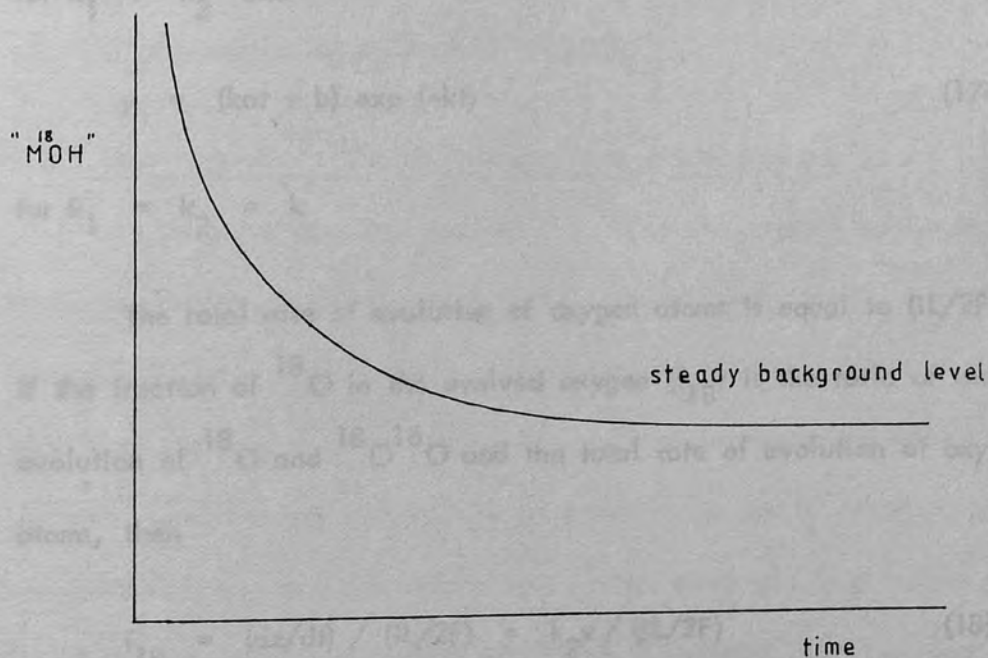
Thus the quantities x, y and z refer to excess enrichment over the normal

background levels.

The kinetic equations are thus:

$$\frac{dx}{dt} = -k_1 x, \quad \frac{dy}{dt} = k_1 x - k_2 y, \quad \frac{dz}{dt} = k_2 y \tag{15}$$

where k_1 and k_2 are first order rate constants for the reactions removing the two higher oxide species, given by equations (14) and (4) respectively. In this derivation no account is taken of kinetic isotope effects and single values of k_1 and k_2 are assumed.

Solution of the above equations (15) gives:

$$x = a \exp(-k_1 t) \tag{16}$$

$$y = \exp(-k_2 t) \left[\frac{k_1 a}{k_2 - k_1} \right] \left\{ \left[\exp(k_2 - k_1)t - 1 \right] + b \right\} \tag{17}$$

for $k_1 \neq k_2$ and

$$y = (kat + b) \exp(-kt) \tag{17a}$$

for $k_1 = k_2 = k$

The total rate of evolution of oxygen atoms is equal to $(iL/2F)$ atom s^{-1}. If the fraction of ^{18}O in the evolved oxygen (f_{18}) is the ratio of the rate of evolution of ^{18}O and $^{18}O^{16}O$ and the total rate of evolution of oxygen atoms, then

$$f_{18} = (dz/dt) / (iL/2F) = k_2 y / (iL/2F) \tag{18}$$

The rate constants k_1 and k_2 are dependent on the current flowing and the total number of sites at the electrode surface. The rate of reaction (14) for all oxygen atoms must be $(iL/2F)$ atom s^{-1} and therefore the rate of reaction of $M^{18}OH$ is $(iL/2F)(f_{MOH})$, where f_{MOH} is the fraction of MOH which is $M^{18}OH$. In terms of $M^{18}OH$ (x) and the total MOH (x_T) the rate is $(iL/2F)(x/x_T)$. Thus,

$$dx/dt = -iLx/(2Fx_T) \tag{19}$$

Comparison with the above shows that $k_1 = iL/(2Fx_T)$. If y_T represents the total MO, then by similar reasoning it can be shown that $k_2 = iL/(2Fy_T)$. Substituting this for k_2 into equation (18) gives

$$f_{18} = y/y_T \tag{20}$$

where y is given by equations (17) or (17a).

IV.3 Fraction of ^{18}O in evolved gas at mass spectrometer

In an experiment the fraction of ^{18}O in the evolved gas cannot be measured directly at the electrode surface, but some distance away where it is diluted by a purging gas. Allowance was made for this in the kinetic equations and an expression derived from the experimental m/e 34 signal. Consider the evolved oxygen and a purge gas to expand into a volume which may accommodate n moles of an ideal gas at a total rate v mols s^{-1}. The rate at which all ^{18}O is introduced into the volume is k_2y (equation 4) plus a background component v_b. The natural abundance of ^{18}O is 2.04×10^{-3}, and so $v_b = (iL/2F) \times 2.04.10^{-3}$ atom s^{-1}.

The rate at which ^{18}O is removed from the volume is the rate at which all gas flows through (v) multiplied by the fraction of ^{18}O in the volume, which is n_{18}/n, if n_{18} is the total ^{18}O in the volume.

Thus,

$$dn_{18}/dt = k_2 y + v_b - (n_{18}/n)v \tag{21}$$

v/n is a first order rate constant which determines the rate at which the mass spectrometer 'sees' changes in ^{18}O at the electrode surface, and will be called k_n.   Solution of equation (21) using the expression (17) for y gives

$$n_{18} = (v_b/k_n)(1 - e^{-k_n t}) + \left[\frac{ak_1 k_2}{k_2 - k_1}\right]\left[\frac{e^{-k_1 t} - e^{-k_n t}}{k_n - k_1}\right] \tag{22}$$

$$+ \frac{k_2}{k_n - k_2}\left[b - \frac{ak_1}{k_2 - k_1}\right]\left[e^{-k_2 t} - e^{-k_n t}\right]$$

for $k_1 \neq k_2$, and

$$n_{18} = (v_b/k_n)(1 - e^{-k_n t}) + \frac{k}{k_n - k} e^{-kt}\left(akt - \frac{ka}{k_n - k} + b\right)$$

$$+ \left[\frac{k}{k_n - k}\right](e^{-k_n t})\left[\frac{ka}{k_n - k} - b\right] \tag{22a}$$

for $k_1 = k_2 = k$

The first term is the same in each of the two above expressions (22 and 22a) as it is only a function of the background fraction of ^{18}O. By solution of a similar expression,

$$dn^b_{18} / dt = v_b - k_n n^b_{18} \qquad (23)$$

where n^b_{18} is the total background amount of ^{18}O, we obtain,

$$n^b_{18} = (v_b / k_n) (1 - e^{-k_n t}) \qquad (24)$$

The mass spectrometer signal of m/e 34 (S) is proportional to the fraction of ^{18}O in the volume at constant pressure.

$$S = K (n_{18}/n) \qquad (25)$$

where K is the constant of proportionality.

PART 2

EXPERIMENTAL   METHODS

CHAPTER V

Preparation of Catalysts and Electrodes

V.1   Introduction

Catalysis may be defined as the maximisation of a chemical reaction rate to obtain the desired product.   It is achieved by using high surface area materials that may have specific features such as preferred reaction sites.   Such high surface area electrocatalysts are generally supported on a substrate which must be both chemically stable and electronically conducting. Often the preparation of catalysts has been considered as an art rather than a science, but for any large scale industrial use reproducibility must be achieved.

The methods of catalyst preparation used in this work fall broadly into two groups, namely those which involve the direct formation of the electrocatalyst on the electrode substrate, i.e. electrochemical decomposition and thermal decomposition, and those in which the electrocatalyst is first individually prepared, e.g. by freeze drying or slurry co-precipitation procedures, prior to being adhered to the substrate by means of a Teflon binder.

V.2   Materials

Platinum foil, mesh and wire were supplied by Engelhard.   The mesh was 80 gauge of diameter 0.076 mm, the wire was of diameter 0.5 mm.

Nickel foil, mesh and wire were supplied by Goodfellow Metals. The mesh was 40 gauge, and the wire 1.0 mm in diameter.

All chemicals used were of Analar grade, without further purification.

V.3   Methods of Preparation

V.3.i   Electrochemical Decomposition

This method was used for the formation of high surface area platinum black electrodes.

The electrode substrate was made by spot welding a length of platinum wire onto the platinum foil, or onto a piece of platinum mesh reinforced at the welding point by a strip of platinum foil.

Such an electrode was first cleaned by immersion in a solution of aqua regia which is a solution containing concentrated hydrochloric and nitric acids in the ratio 3:1 by volume.   It was then introduced as the cathode in a cell containing a 2% solution of platinum chloride, the auxiliary electrode being a piece of platinum foil.   Current of magnitude 10mA cm^{-2} was passed through the cell until the shiny platinum surface was covered with a deposit of black platinum.

Such an electrode owes its high surface area to the very finely divided surface layer of platinum deposited by electrolysis.

V.3.ii   Thermal Decomposition

Non-noble metal oxide electrodes were prepared by this method which involves the direct decomposition of a metal salt solution onto the electrode substrate by heat treatment.

Mixed nickel cobalt oxide electrodes with a Ni:Co ratio of 1:2 were prepared from a solution containing 0.5 mol dm^{-3} $Ni(NO_3)_2.6H_2O$ and 1 mol dm^{-3} $Co(NO_3)_2.6H_2O$. A nickel mesh electrode formed by the spot welding technique described above was immersed in the mixed salt solution, removed and placed in a preheated oven at 300°C for 10 minutes.

This procedure was repeated about 5 times, or until a catalyst loading of about 10 mg cm^{-2} had been achieved. The resulting electrode was finally cured in air at 400°C for 10 hours.

The spinel structure of $NiCo_2O_4$ has been shown to be the electrochemically active species[64], this breaks down to the cubic form above 450°C, but it has been found experimentally that maximum activity will be achieved if the catalyst is cured as near to this limiting temperature as possible.

Lithiated cobalt oxide electrodes were prepared similarly, by the decomposition of a solution containing $Li(NO_3)3H_2O$ and $Co(NO_3)_2.6H_2O$[75] the concentration of each dependent upon the final value of lithium content required. Curing was performed at 350°C for one hour in air.

V.3.iii   Freeze drying

This cryochemical method is an excellent way to achieve high surface area catalysts as the substances produced do not require high temperature calcining, to achieve inter-diffusion of ions, which obviously plays a large part in reducing surface area.[76]

A homogeneous mixed salt solution containing the elements to be present in the final product is frozen instantaneously; thus allowing the freezing process to occur without fractional crystallisation and enabling the ions to keep their random liquid configuration under vacuum allowing the final dry product to retain the same state of division.

To prepare $NiCo_2O_4$ by this method, 12.4g $Co(NO_3)_2.6H_2O$ and 6.16g $Ni(NO_3)_2.6H_2O$ were dissolved in 40 cm^3 hot acetic acid.[77] This solution was sprayed into a crystallising dish containing liquid nitrogen.

The solid sample was then placed in a 250 cm^3 round bottomed flask and connected to the vacuum system comprising of a rotary oil pump and mercury diffusion pump as shown in Figure 1.. The solvent was sublimed under vacuum (0.05 Torr), during which time the pressure in the system rises slightly, a final drop in pressure indicating that the process is complete. The use of an I.R. lamp directly on the sample reduced the drying time without causing melting.[78]

The catalyst was decomposed under vacuum for one hour at 250°C, and finally cured in air at 400°C for 10 hours.

This preparation technique was also used to form platinized tungstic oxides for use in the deuterium isotope experiments. Initially, the volume of solvent required to just wet a specified weight of WO_3 was determined experimentally. A chloroplatinic acid solution of the correct concentration to give a 1% Pt in WO_3 sample was made in this volume and mixed with the WO_3 powder in a round bottomed flask. This mixture was rapidly frozen by immersion in a vessel containing liquid nitrogen; the flask attached to the vacuum system whilst still surrounded by liquid nitrogen, and the solvent sublimed as before.

The product was reduced by passing a stream of hydrogen over the sample at 50°C, until all the yellow powder had turned black. This method produces a large dispersion of platinum on the tungsten trioxide substrate. Other loadings, of less than 1% Pt, were obtained by mechanically mixing tungsten trioxide with the stock sample.[79]

V.3.iv   Slurry Precipitation

This method[80] has been shown to produce powders with electro-

Fig 1: Freeze drying apparatus

sample

liq. N₂ trap
& rotary oil pump

dewar containing
liq. N₂
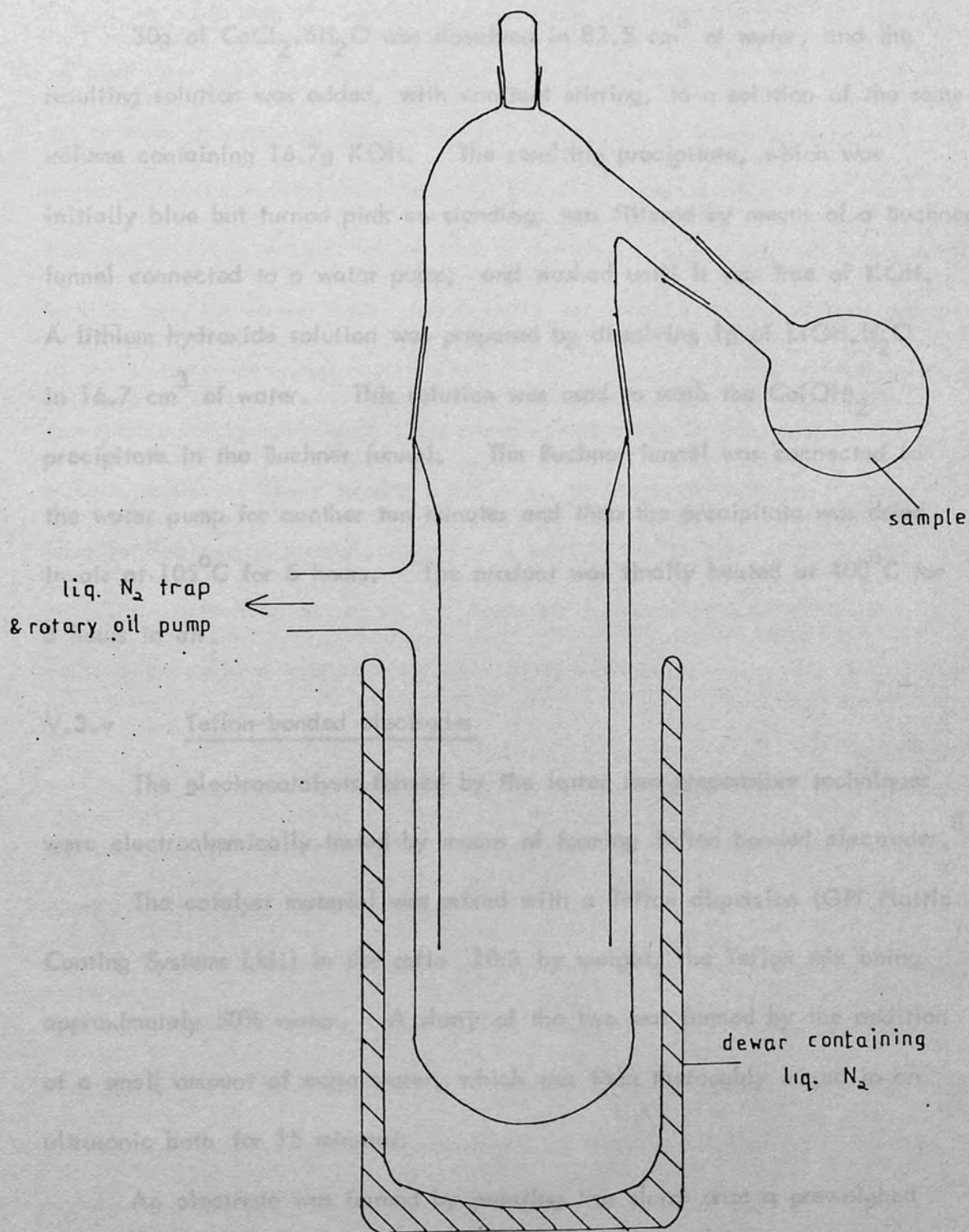
catalytic properties comparable to those prepared by freeze drying, but with the advantage that by this route the products can be prepared by heating at lower temperatures and for shorter times than those necessary to form the optimum product by means of the freeze drying technique.

30g of $CoCl_2.6H_2O$ was dissolved in 82.5 cm^3 of water, and the resulting solution was added, with constant stirring, to a solution of the same volume containing 16.7g KOH. The resulting precipitate, which was initially blue but turned pink on standing, was filtered by means of a Buchner funnel connected to a water pump; and washed until it was free of KOH. A lithium hydroxide solution was prepared by dissolving 1g of $LiOH.H_2O$ in 16.7 cm^3 of water. This solution was used to wash the $Co(OH)_2$ precipitate in the Buchner funnel. The Buchner funnel was connected to the water pump for another ten minutes and then the precipitate was dried in air at 105°C for 5 hours. The product was finally heated at 400°C for 5 hours in air.

V.3.v   Teflon-bonded electrodes

The electrocatalysts formed by the latter two preparative techniques were electrochemically tested by means of forming Teflon bonded electrodes.[81]

The catalyst material was mixed with a Teflon dispersion (GPI Plastic Coating Systems Ltd.) in the ratio 10:3 by weight, the Teflon mix being approximately 50% water. A slurry of the two was formed by the addition of a small amount of extra water, which was then thoroughly mixed in an ultrasonic bath for 15 minutes.

An electrode was formed by painting this slurry onto a preweighed nickel mesh, drying each application thoroughly and finally curing at 300°C

for 10 hours. Generally, electrocatalysts loadings were in the region of 10-15 mg cm^{-2}.

V.4 Discussion

In each case the decision as to which method of preparation should be used must take into account the use of the final product and often is a compromise between the advantages and disadvantages of each particular route. In the thermal decomposition method, a balance has to be reached between utilizing a high temperature to achieve maximum inter-diffusion of ions to form the mixed metal species, with the lowering of the surface area as the sintering temperature is raised. The advantage of this method over the freeze drying technique is the comparative speed of preparation of a sample, albeit of lower surface area. In the range of temperatures used here for the curing process, sintering is most likely to take place by the migration of lattice ions along the outermost surface layers of the solid causing the surface irregularities and cracks between neighbouring crystallites to be filled up.[82]

The technique of freeze drying gives the highest surface area powders but the time involved to produce such powders and in comparatively small quantities is a major disadvantage.[64]

In gas evolution reactions the formation of gas bubbles on the surface of the electrode tends to consume surface area, thereby blocking significant amounts of the surface which could otherwise have participated in the reaction. The amount of this blockage is dependent on the current density. At low current densities the small quantities of gas produced are able to dissolve in the electrolyte and diffuse out of the pore without the formation of bubbles.

However, the rate of diffusion of the gas through the electrolyte cannot occur quickly enough to be comparable to the rate of gas evolution as the current density is raised, and hence bubbles are formed. The bubbles inside the pores of porous electrodes push the electrolytes out of the pores as they escape, significantly reducing the amount of surface available for the electrochemical reaction.

In theory the use of a Teflon binder provides a suitable means of attaching the electrocatalyst to the electrode. Work by Tseung and Vassie[83] on Teflon bonded platinum black electrodes showed that more of the platinum surface was utilized during the evolution of hydrogen, compared to conventional porous platinum black electrodes, due to the ease of escape for the gas bubbles through the dry Teflon channels.

The electrode structure consists of two porous phases, criss-crossing one another. The electrolyte can fill the porous catalyst phase whilst the hydrophobic Teflon phase remains dry. With close mixing of these two phases, as soon as the gas bubbles reach the surface of the catalyst aggregate, during oxygen evolution, they are able to escape through the dry Teflon network.

In practice, however, especially in the case of oxygen evolution, it was found that very large bubbles tended to adhere quite strongly to the surface of the electrode, which was especially undesirable in the isotopic experiments where the method relies strongly on the fast transfer of the evolved gas from the electrode surface to the probe of the mass spectrometer.

It has been suggested[84] that this problem can be overcome at least in part, by coating the outside of the electrode with a hydrophilic layer of pure catalyst, whence smaller gas bubbles are generated and removed with comparative ease. Even this modification was not found to be sufficient to

increase the rate of removal of gas bubbles significantly.

In general the performance of these electrodes is dependent upon a number of independent variables such as catalyst:Teflon ratio, surface area of catalyst, pore size distribution, aggregate size of catalyst. Many of the variables and their effects on the electrode properties have been studied in detail[83,85,86] and the optimised conditions and compositions utilized in this work.

CHAPTER VI

Characterisation of electrode materials and electrochemical techniques

VI.1   Introduction

The initial problem in electrochemistry is the inability to measure

the exact potential of a single electrode reaction as the absolute potential

difference across a single electrified interface cannot be measured.   The

minimum number of interfaces in any electrical circuit is two.   This

fundamental difficulty is overcome by relating the potential of the specified

reaction to a standard system.   The standard reference system universally

used is based on the hydrogen evolution reaction

$$H^+ + e^- \rightleftharpoons \tfrac{1}{2} H_2 \tag{1}$$
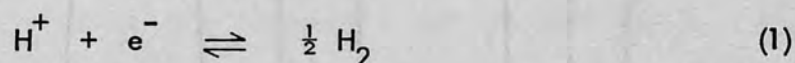
defined under standard conditions of 298K and in 1 Molar electrolyte as

being equal to 0V.

For the study of electrode kinetics three electrodes are required.

The working electrode being the one at which the electrochemical reaction

of interest is taking place.   Its potential is measured relative to a reference

electrode whose sole purpose is as in its name, to act as a reference system.

The cell is completed by a counter electrode, the overall cell reaction

being the sum of the reactions taking place at the working and counter

electrodes.

A basic cell design is shown in figure 1.   A glass frit separates the

working and counter electrode compartments to prevent mixing of any gases

that might be evolved during the reaction.   A capillary joins the reference

to the working compartment.   As current flows through the cell there is a

further potential difference which must be considered, arising from the

Fig. 1:. The electrochemical cell.

gas inlet

Fig. 1:. The electrochemical cell.
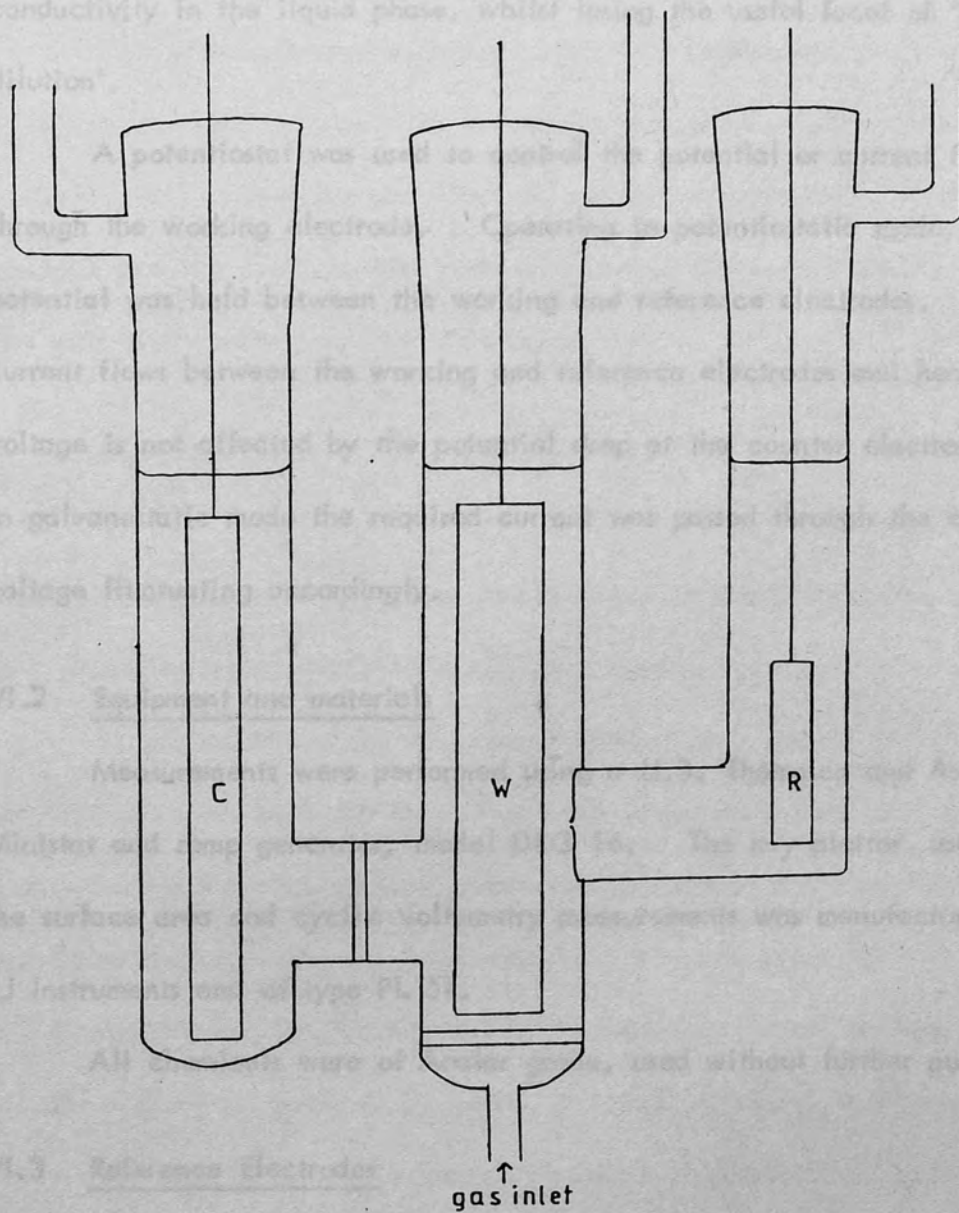
resistance of the electrolyte. The use of a Luggin capillary in voltage measurements can reduce this resistance, present in the iR term, in solution to 0.1-0.2 Ω. This voltage drop can be calculated as a function of the distance between working and reference electrodes and the current passing, voltage measurements then being corrected for this term.[86] Generally, concentrated solutions are favoured as electrolytes, thus increasing the conductivity in the liquid phase, whilst losing the useful facet of 'infinite dilution'.

A potentiostat was used to control the potential or current flowing through the working electrode. Operating in potentiostatic mode, a set potential was held between the working and reference electrodes. No current flows between the working and reference electrodes and hence the voltage is not affected by the potential drop at the counter electrode. In galvanostatic mode the required current was passed through the cell, the voltage fluctuating accordingly.

VI.2 Equipment and materials

Measurements were performed using a H.B. Thompson and Associates Ministat and ramp generator, model DRG 16. The x-y plotter used for the surface area and cyclic voltametry measurements was manufactured by JJ Instruments and of type PL 51.

All chemicals were of Analar grade, used without further purification.

VI.3 Reference Electrodes

Generally in both acid and alkaline electrolytes a dynamic hydrogen electrode[87] was used as the reference system, though for some experiments

in alkaline solution a Hg/HgO reference electrode[88] was used.   Both

were calibrated by means of a standard bubbling hydrogen electrode[88]

prior to use.   In normal activity solutions the convention is to take the

potential of the standard hydrogen electrode as zero and measure all

potentials relative to it.

VI.3.i   Dynamic Hydrogen Electrode

This electrode may be regarded as an oxidation-reduction electrode

at which equilibrium is reached between electrons in a noble metal,

hydrogen ions in solution and dissolved molecular hydrogen.   It is generally

thought that the platinum electrode must adsorb hydrogen atoms to assume

the potential obtained by the equilibrium,

$$H_2 \text{ (aq. soln.)} \;\rightleftharpoons\; 2H \text{ (adsorbed on metal)} \rightleftharpoons 2H^+ \text{ (aq. soln.)} + 2e$$

$$(2)$$
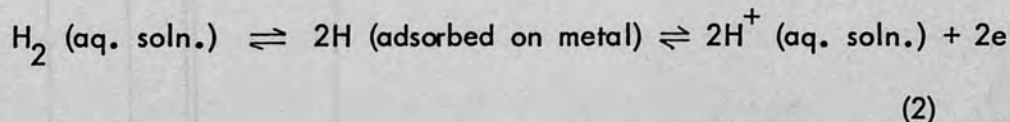
This can be assumed to represent the hydrogen evolution reaction, with all

four processes taking place to a sufficient extent.

In this electrode the hydrogen is generated by means of a secondary

circuit, as shown in figure 2.   Two small (0.25 cm^2) platinised platinum

electrodes were sealed into an open-ended glass tube and connected to the

circuit as shown.   The resistors were R.S. wire-wound variable resistors of

$1 \text{ k}\Omega$ and $10 \text{ k}\Omega$ magnitude, a 9V PP3 battery was used to supply the

current which was measured by means of a R.S. 0-10 mA ammeter.

This electrode was calibrated against a standard bubbling hydrogen

electrode to obtain the dependence of the overpotential on the current in

this circuit.

Fig. 2: Circuit diagram for dynamic hydrogen electrode reference system.
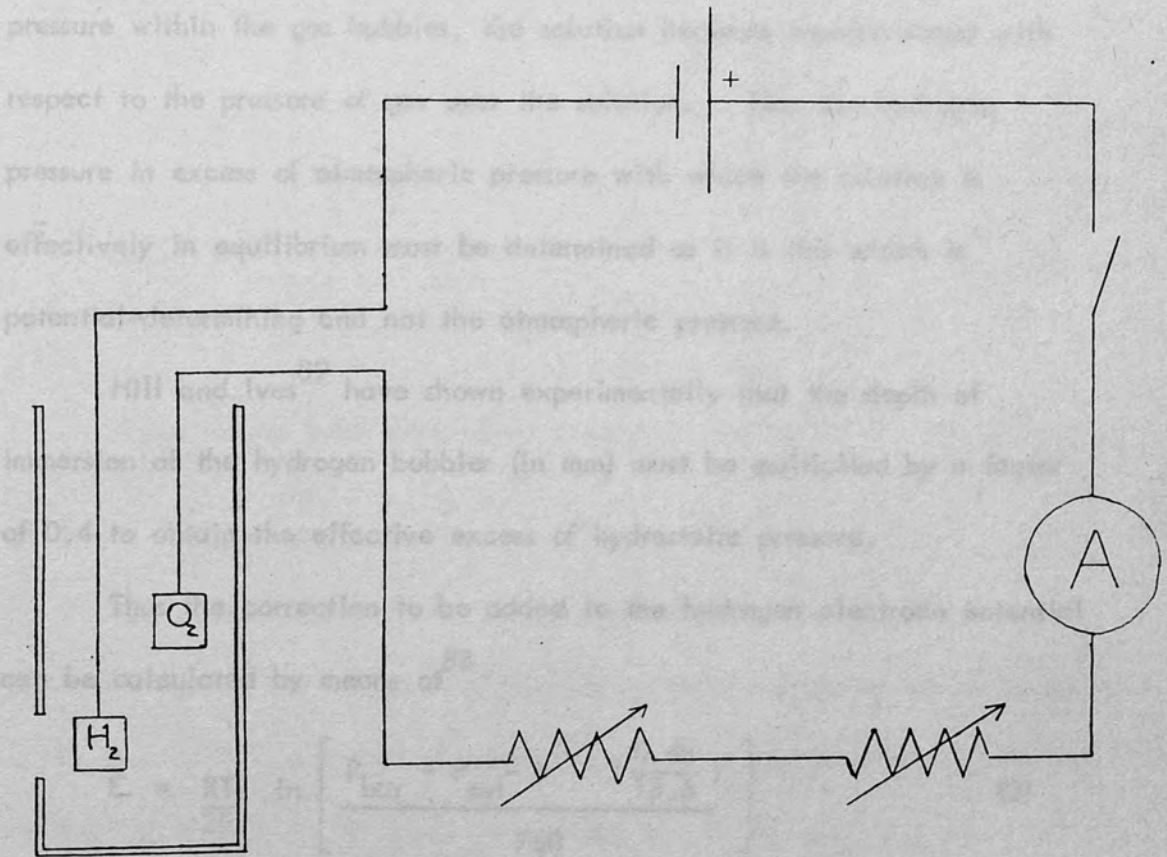
The potential of a standard bubbling hydrogen electrode is not a function of its depth of immersion below the surface of the electrolyte as a reasonable bubbling rate ensures sufficient stirring to make the solution homogeneous with respect to the dissolved hydrogen. The potential of the electrode is, however, dependent upon the depth at which bubbles are delivered to the solution; because of the additional hydrostatic pressure within the gas bubbles, the solution becomes supersaturated with respect to the pressure of gas over the solution. Thus the hydrogen pressure in excess of atmospheric pressure with which the solution is effectively in equilibrium must be determined as it is this which is potential-determining and not the atmospheric pressure.

Hill and Ives[89] have shown experimentally that the depth of immersion of the hydrogen bubbler (in mm) must be multiplied by a factor of 0.4 to obtain the effective excess of hydrostatic pressure.

Thus the correction to be added to the hydrogen electrode potential can be calculated by means of[88]

$$E = \frac{RT}{2F} \ln \left[\frac{P_{bar} - P_{sol} + \left(\frac{0.4h}{13.6} \right)}{760} \right] \tag{3}$$

where P_{bar} is the barometer pressure, and P_{sol} the vapour pressure which can be identified with that of pure water at the same temperature for most aqueous solutions. This can be calculated as a function of temperature using an expression of the form

$$\log_{10} P_{sol} \text{ (mm)} = a - b \log_{10} T - c/T \tag{4}$$

where $a = 20.96$, $b = 4.08$ and $c = 2825$.

For the calibration, the temperature at which readings were taken was 294.66K, thus giving P_{sol} as 19.957 mm Hg. The measured barometric pressure 733.1 mm Hg, and with the bubbler at a depth of 20 mm leads to the voltage correction of 0.808 mV.

DHE voltage correction

Current through cell/mA	Corrected potential/mV
2	25.59
4	32.59
6	37.39
8	41.49
10	44.79

These values were determined throughout the period of the experiments.

VI.3.ii   Hg/HgO electrode

Any electrode in which the metal phase is in the reduced form of the redox equilibrium system must vary in potential according to the state of the metal, this in turn must depend upon its purity, and its thermal and mechanical history. However, as mercury can be brought to a reproducible state, those difficulties encountered with hard metals are overcome. Mercury is free from the effects caused by variable valency of the oxide as mercury (I) oxide does not exist, and precipitation reactions which might form it or mercury (I) hydroxide give only a mixture of the metal and mercury (II) oxide[90]. Mercury (II) oxide exists in two forms, red and yellow, which have different solubilities and it is likely that their difference is due to particle size.

Lewis and Randall calculated the standard electrode potential and found it to be 0.9265V at 25°C[91]. This was confirmed by Brönsted for the cell[92]

$$H_2, Pt \mid KOH \text{ (aq)} \mid HgO \mid Hg$$
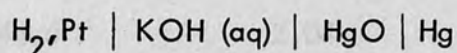
which he found to have an emf independent of the concentration of the electrolyte, except for very small differences which were attributed to varying water activity. Donnan and Allman found the electrode to be stable over several days,[93] reproducible to better than $\pm$ 0.1 mV and independent of the form of mercury (II) oxide used.

No special precautions were necessary in the preparation of this electrode, apart from the use of components of reasonable purity.

VI.4 <u>X-ray diffraction</u>

X-ray analysis of the electrocatalysts was carried out to determine the crystal structures. For instance in the case of nickel cobalt oxide it was used to confirm that the spinel form had been prepared by the thermal decomposition preparative technique, and not the cubic form. A Philips PW 1010 generator and PW 1050/25 difractometer were used for the analysis, utilising Cu Kα radiation of wavelength 1.542Å.

The major lines present in the X-ray diffraction pattern for the NiCo$_2$O$_4$ sample are listed below, alongside data from the National Bureau of Standards for the spinel form of the compound. The compatibility between these two sets of data confirms the formation of the spinel structure.

X-ray diffraction data for $NiCo_2O_4$ sample

	2ϑ	$d = \dfrac{\lambda}{2\sin\vartheta}$	Nat. Bur. St. data
	31.05	2.88	2.86
major line	36.7	2.45	2.44
	44.5	2.04	2.03
	59.15	1.56	1.56
	65.0	1.43	1.44

Similarly data is presented for a lithiated Co_3O_4 sample which contained approximately 10% lithium.

X-ray diffraction data for lithiated Co_3O_4 sample

	2ϑ	$d = \dfrac{\lambda}{2\sin\vartheta}$	Nat. Bur. St. data
	19.1	4.65	4.67
	31.35	2.85	2.86
major line	36.95	2.43	2.44
	45.0	2.01	2.02
	59.6	1.55	1.56
	65.4	1.43	1.43

The following table lists the major lines seen in the X-ray diffraction pattern obtained for a sample of platinised tungsten trioxide.

X-ray diffraction data for 1% Pt in WO_3 sample

2ϑ	$d = \dfrac{\lambda}{2\sin\vartheta}$
23.7	3.755
24.4	3.648
28.2	3.165
34.2	2.62
36.9	2.436
41.8	2.16
48.4	1.881
50.0	1.824
54.3	1.689
55.9	1.644

VI.5   Surface Area Determination

Three methods have been used as a means for the determination of the surface areas of the electrocatalysts; one by gravimetric means and two by electrochemical techniques.

VI.5.i   BET method

The gravimetric method uses the basic BET equation with nitrogen gas as the absorbate at $77K$[94]. The surface area of the powdered material is measured by determining the quantity of gas necessary to form a single layer of gas molecules on the sample. Testing is carried out using nitrogen gas at the temperature of liquid nitrogen because under these conditions the gas molecules are strongly adsorbed on the surface of the solid. Additionally the space occupied by each adsorbed molecule is known within relatively narrow limits under this condition. The instrument used was a surface area analyser made by Coulter Electronics Ltd.

VI.5.ii   Electrochemical oxygen charging methods

An electrochemical method for the measurement of surface areas was devised to be applicable to electrode materials such as platinum which can undergo reduction as well as oxidation of surface species without damaging or changing the absolute nature of the species.

The method consists of reducing all surface species present on the electrode, commonly by cathodic polarisation until eventually hydrogen is evolved. The current is switched off and the cell strongly purged with nitrogen gas. An anodic current pulse of known magnitude was applied to the test electrode after a set time interval, and the potential-time

transient followed by means of a Y-T plotter. A typical trace is shown in figure 3. The initial rise in potential is due to the stripping of adsorbed hydrogen from the surface; during the following steep rise in potential no process is predominant but this region is usually ascribed to the charging of the double layer. From a potential in the region of 0.8V, a more gently sloping region emerges which can be ascribed to oxygen atom adsorption. Bowden[18] demonstrated that if a roughness factor is considered the number of coulombs determined from the length of the oxygen adsorption region corresponds to a monolayer of adsorbed oxygen atoms. Hoare[95] concludes that PtO_2 is not present at potentials below 1.55V in the presence of metallic platinum on platinum anodes; and thus it can be assumed that any oxygen adsorbed in this region is in the form Pt-O or $Pt(OH)_2$. Butler[96] confirmed that one atom of adsorbed oxygen is associated with one surface atom of platinum and since the amount of adsorbed oxygen may be determined from the charging curve, a measure of the true surface is obtained. Above 1.6V the curve flattens out and oxygen evolution commences.

Thus the region of oxygen atom adsorption is the area of interest for the determination of surface areas. The product of the transition time of this region and the applied current pulse gives the number of coulombs necessary for this process. A correction to this value must be applied for the charging of the double layer, but in most cases, this is small enough to be neglected. The surface area can be calculated from the charge passed by the use of Faraday's Laws and knowledge of the cross-sectional area of one platinum atom, which is 8.9×10^{-16} cm^2.[97] An alternative calculation is to divide the number of coulombs required by the charge

Fig. 3: Voltage-time trace on platinum electrode as a means of determining surface area.
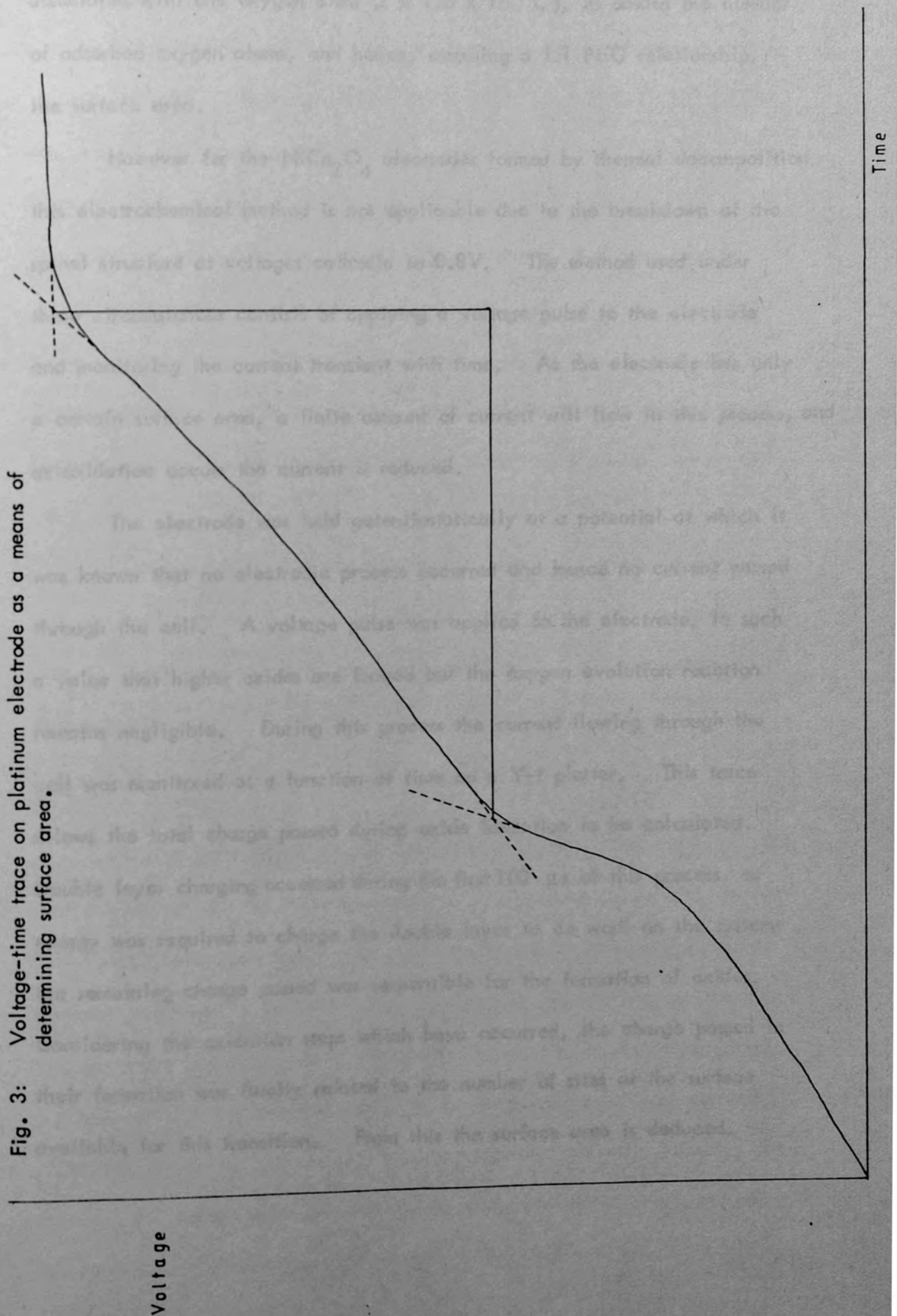
associated with one oxygen atom ($2 \times 1.6 \times 10^{-19}$C), to obtain the number

of adsorbed oxygen atoms, and hence, assuming a 1:1 Pt:O relationship,

the surface area.

However for the $NiCo_2O_4$ electrodes formed by thermal decomposition

this electrochemical method is not applicable due to the breakdown of the

spinel structure at voltages cathodic to 0.8V.   The method used under

these circumstances consists of applying a voltage pulse to the electrode

and monitoring the current transient with time.   As the electrode has only

a certain surface area, a finite amount of current will flow in this process, and

as oxidation occurs the current is reduced.

The electrode was held potentiostatically at a potential at which it

was known that no electrodic process occurred and hence no current passed

through the cell.   A voltage pulse was applied to the electrode, to such

a value that higher oxides are formed but the oxygen evolution reaction

remains negligible.   During this process the current flowing through the

cell was monitored as a function of time on a Y-t plotter.   This trace

allows the total charge passed during oxide formation to be calculated.

Double layer charging occurred during the first 100 μs of this process, as

energy was required to charge the double layer to do work on the system;

the remaining charge passed was responsible for the formation of oxides.

Considering the oxidation steps which have occurred, the charge passed in

their formation was finally related to the number of sites at the surface

available for this transition.   From this the surface area is deduced.

VI.6   Tafel slopes

The Butler-Volmer equation gives the dependence of current density

on overpotential.   If the overpotential is large, such that $|\eta| \gg RT/zF$

and one of the partial currents becomes much greater than its reverse, the

Butler-Volmer equation reduces to the form $\eta = a + b \log i$. Here a

is a constant related to the exchange current density and characteristic

of the electrode material and its surface state, and b is called the 'Tafel

slope', a parameter indicative of the reaction mechanism.   This equation

derives its name from its originator, Tafel, who empirically determined the

linear dependence of overpotential on the logarithm of current density in

1905.

Experimental Tafel slopes are commonly used as a means to help in

the elucidation of reaction mechanisms to determine the rate-controlling

step by comparison of the experimental values with those calculated

theoretically.[51]

VI.6.i   Method

Anodic Tafel slopes on platinum, $NiCo_2O_4$ and lithiated Co_3O_4

were determined by the following method.   The electrode in question was

first cycled potentiostatically throughout the range of voltages for which

measurements were to be taken so as to obtain a reproducible surface state.

The electrode was then held galvanostatically at the highest current until

a steady voltage was reached, prior to the stepwise decrease of current

at regular intervals, with voltage readings recorded at each current.   On

reaching the lowest value of current, the route was retraced by increasing

the current in a similar stepwise manner.   It was found that if cyclisation

of the potential was not performed before readings were taken, large
discrepancies were obtained in readings taken during the initial and
reverse sweeps.   Oxide film growth occurring during measurements tends
to give no meaningful results for the voltage-log i relationship, but if
readings commence from the highest voltage the film growth is effectively
stopped and data is all obtained on the same surface;   the slopes obtained
being a function of the film thickness.[98]

VI.6.ii   Platinum electrodes

On platinum in acid and alkaline electrolyte, a Tafel region is
observed in the anodic oxygen evolution curve between the current density
range of 10^{-6} - 10^{-3} A cm^{-2}, with a slope of 0.122 mV in acid electrolyte
(figure 4) and 0.114 mV in alkaline electrolyte (figure 5).   Downward
deviations at low current densities are due to depolarisation caused by
trace impurities and this practicable current density range could only be
extended to lower current densities with further solution purification by
anodic pre-electrolysis of electrolyte.   On the first run of these polarisation
curves, steady state points were not obtained and a curve without a Tafel
region was observed.   This was likely to be due to the continual build-up
of an adsorbed oxygen layer with anodic polarisation.   This showed the
importance of the pre-cyclisation of the electrode, to bring it to a
reproducible state as quickly as possible.   A gradient of around 0.115 mV
corresponds to a slope of 2RT/F.   The values reported here agree well with
those of other workers.[5]

Fig. 4: Anodic Tafel slope on a platinised platinum electrode in 0.5M H_2SO_4
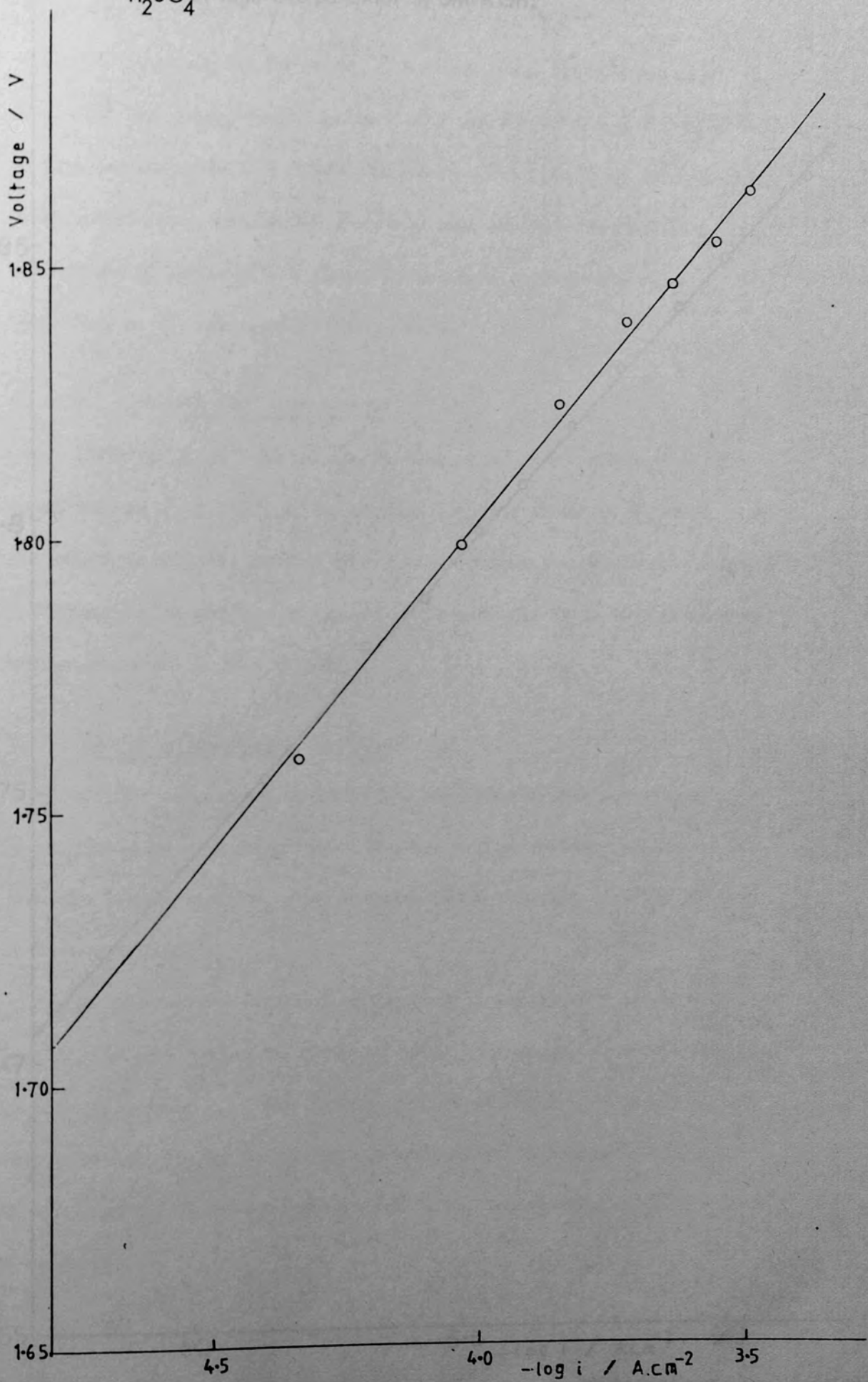
Fig. 5: Anodic Tafel slope on a platinised platinum electrode at high overpotential in 5M KOH.
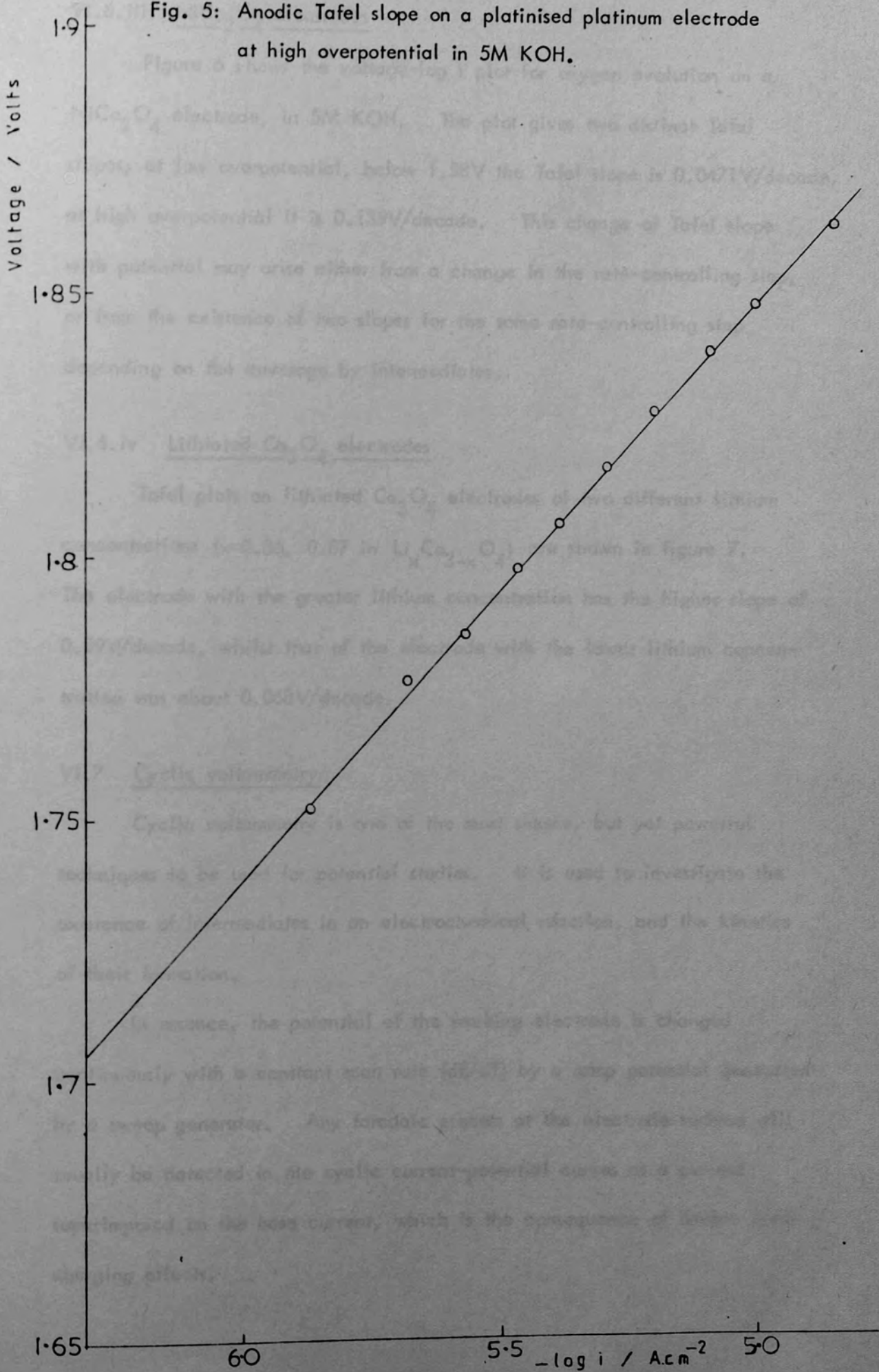
VI.6.iii <u>$NiCo_2O_4$ electrodes</u>

Figure 6 shows the voltage-log i plot for oxygen evolution on a

$NiCo_2O_4$ electrode, in 5M KOH. The plot gives two distinct Tafel

slopes; at low overpotential, below 1.58V the Tafel slope is 0.0471V/decade,

at high overpotential it is 0.139V/decade. This change of Tafel slope

with potential may arise either from a change in the rate-controlling step,

or from the existence of two slopes for the same rate-controlling step

depending on the coverage by intermediates.

VI.6.iv <u>Lithiated Co_3O_4 electrodes</u>

Tafel plots on lithiated Co_3O_4 electrodes of two different lithium

concentrations (x=0.36, 0.07 in $Li_xCo_{3-x}O_4$) are shown in figure 7.

The electrode with the greater lithium concentration has the higher slope of

0.09V/decade, whilst that of the electrode with the lower lithium concen-

tration was about 0.068V/decade.

VI.7 <u>Cyclic voltammetry</u>

Cyclic voltammetry is one of the most simple, but yet powerful

techniques to be used for potential studies. It is used to investigate the

existence of intermediates in an electrochemical reaction, and the kinetics

of their formation.

In essence, the potential of the working electrode is changed

continuously with a constant scan rate (dE/dT) by a ramp potential generated

by a sweep generator. Any faradaic process at the electrode surface will

usually be detected in the cyclic current-potential curves as a current

superimposed on the base current, which is the consequence of double layer

charging effects.

Fig. 6: Anodic Tafel slope on a $NiCo_2O_4$ electrode in 5M KOH.

110
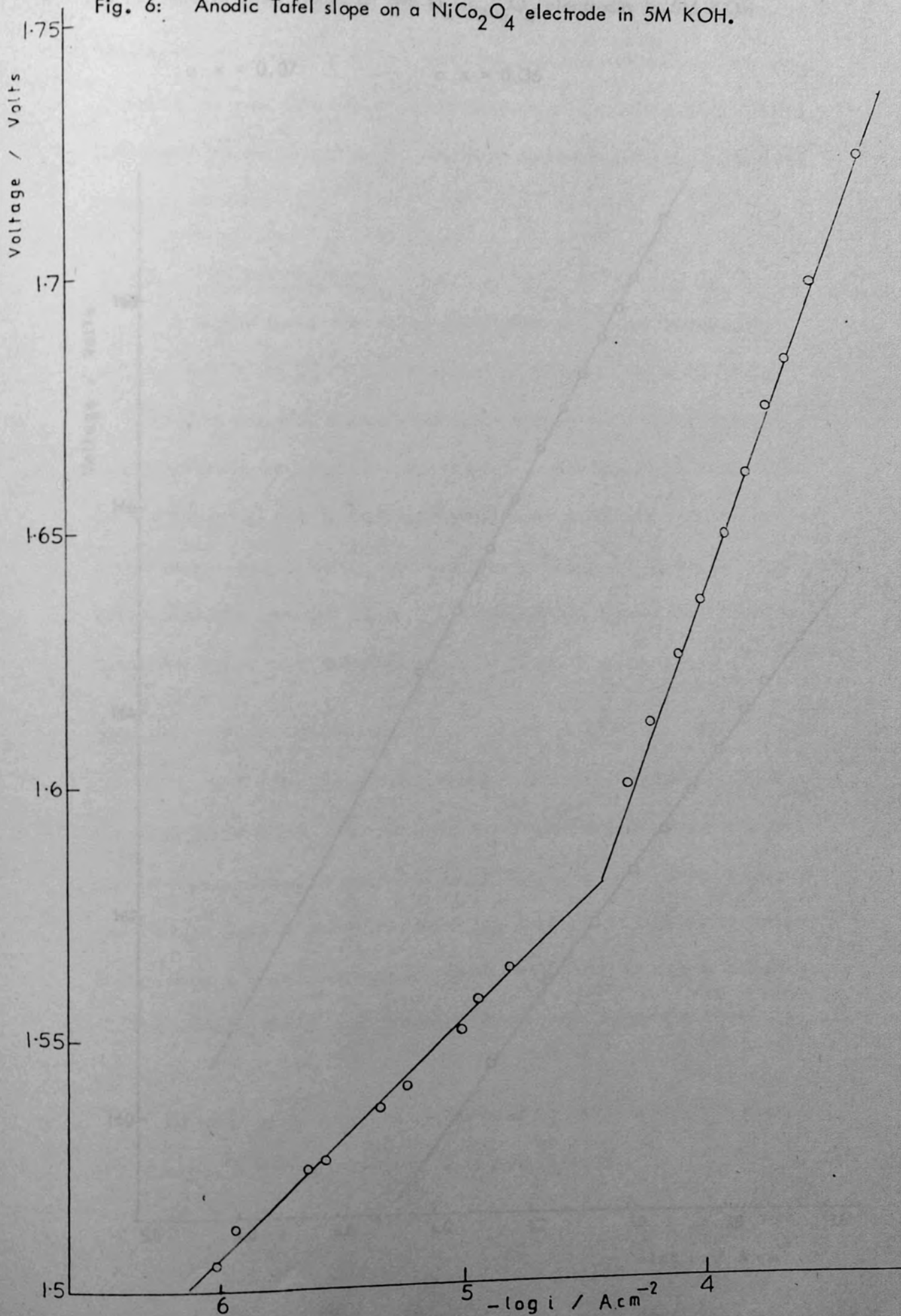
Fig 7: Anodic Tafel slopes on two $Li_xCo_{3-x}O_4$ electrodes in 5M KOH

□ x = 0.07   o x = 0.36
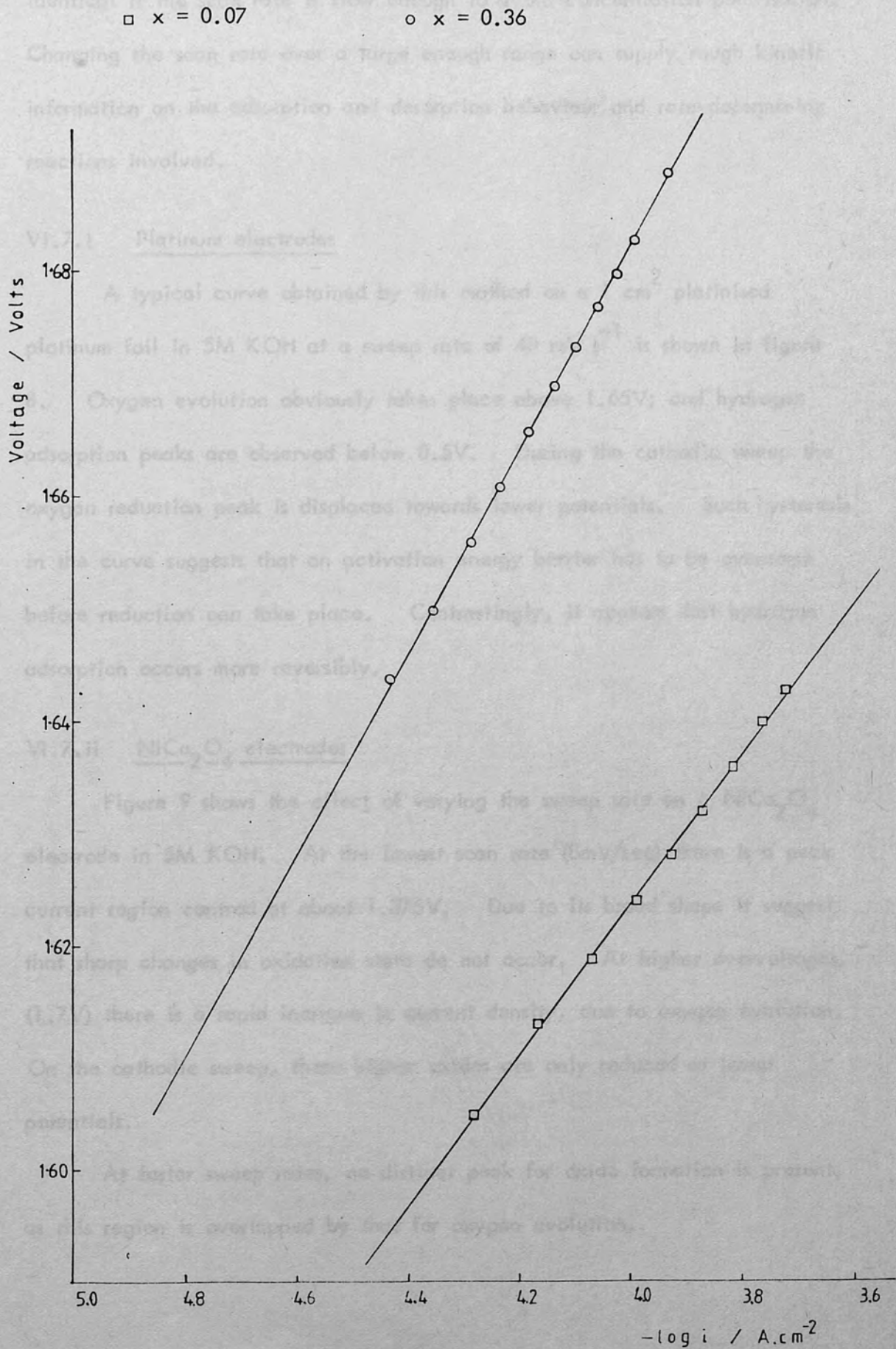
For reversible adsorption, the anodic and cathodic scans are normally identical if the scan rate is slow enough to avoid concentration polarisation. Changing the scan rate over a large enough range can supply rough kinetic information on the adsorption and desorption behaviour and rate-determining reactions involved.

VI.7.i   Platinum electrodes

A typical curve obtained by this method on a 1 cm^2 platinised platinum foil in 5M KOH at a sweep rate of 40 mV s^{-1} is shown in figure 8.   Oxygen evolution obviously takes place above 1.65V, and hydrogen adsorption peaks are observed below 0.5V.   During the cathodic sweep the oxygen reduction peak is displaced towards lower potentials.   Such hysteresis in the curve suggests that an activation energy barrier has to be overcome before reduction can take place.   Contrastingly, it appears that hydrogen adsorption occurs more reversibly.

VI.7.ii $NiCo_2O_4$ electrodes

Figure 9 shows the effect of varying the sweep rate on a $NiCo_2O_4$ electrode in 5M KOH.   At the lowest scan rate (8mV/sec) there is a peak current region centred at about 1.375V.   Due to its broad shape it suggests that sharp changes in oxidation state do not occur.   At higher overvoltages, (1.7V) there is a rapid increase in current density, due to oxygen evolution. On the cathodic sweep, these higher oxides are only reduced at lower potentials.

At faster sweep rates, no distinct peak for oxide formation is present, as this region is overlapped by that for oxygen evolution.

Fig. 8: Cyclic voltammogram on a platinised platinum electrode in 5M KOH at a sweep rate of 40 mV sec^{-1}.
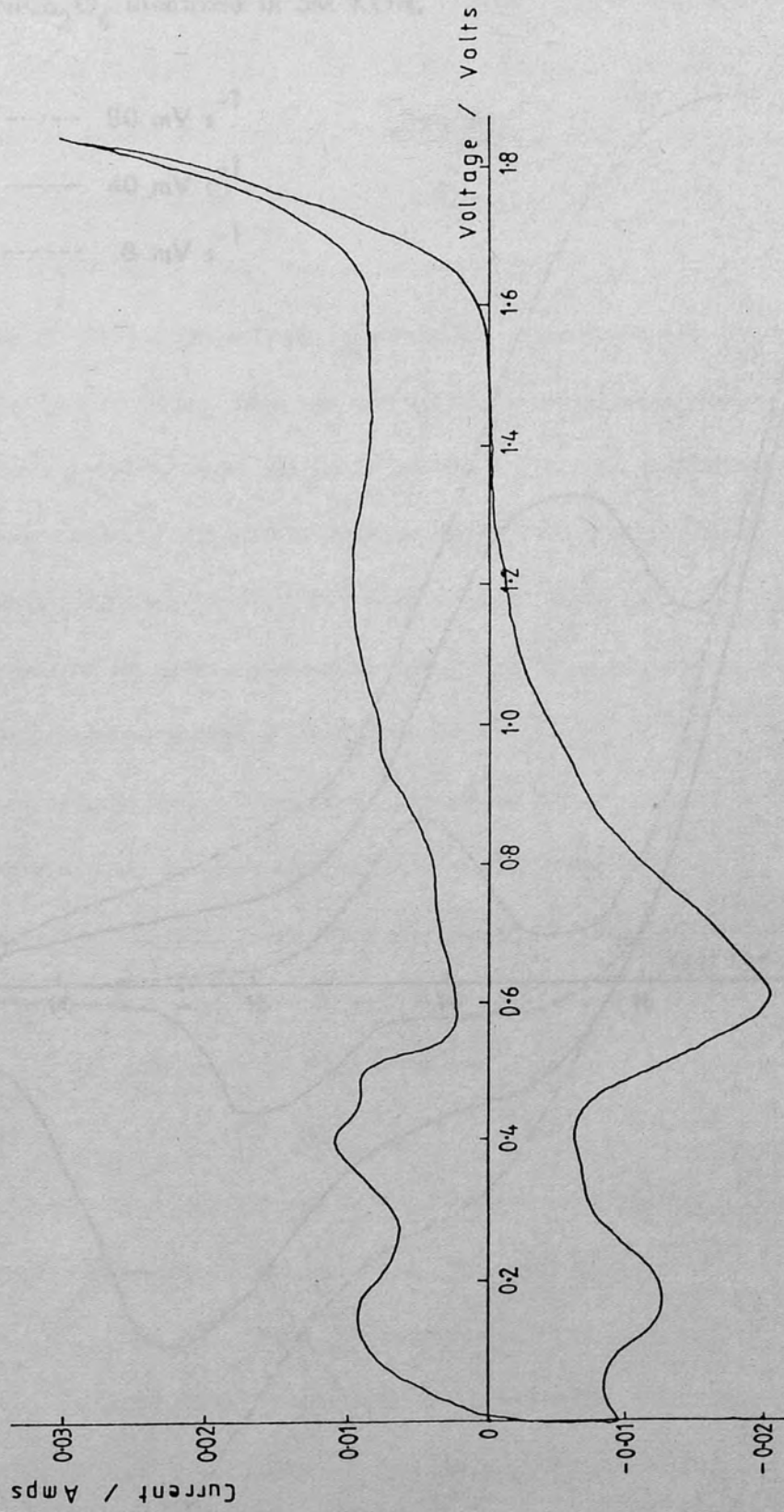
Fig. 9: Cyclic voltammograms at various scan speeds on a
$NiCo_2O_4$ electrode in 5M KOH.
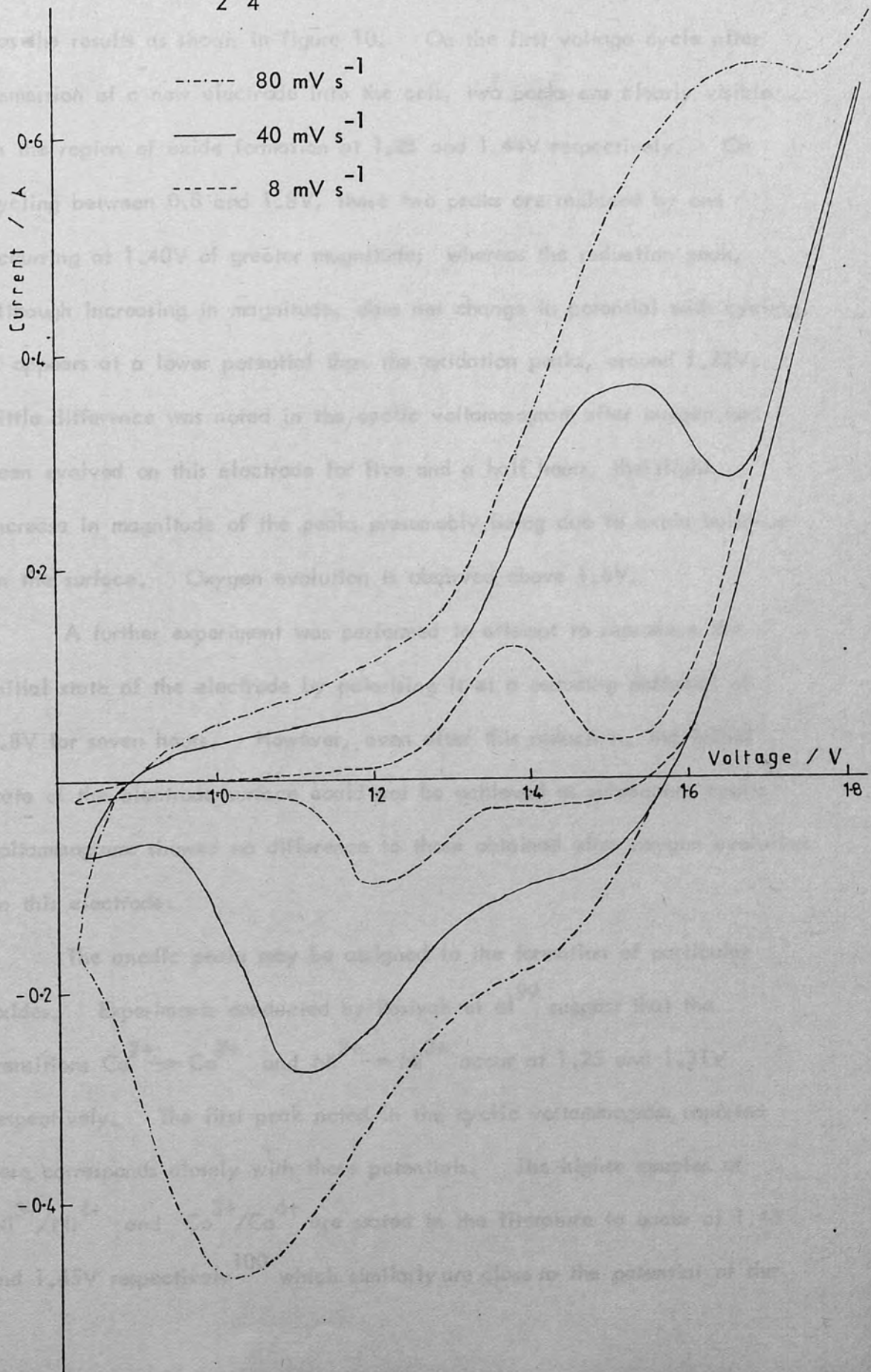
The effect of aging of $NiCo_2O_4$ electrode by cyclic voltammetry is of greater interest. An experiment performed in nitrogen purged 5M KOH has the results as shown in figure 10. On the first voltage cycle after immersion of a new electrode into the cell, two peaks are clearly visible in the region of oxide formation at 1.28 and 1.44V respectively. On cycling between 0.8 and 1.8V, these two peaks are replaced by one occurring at 1.40V of greater magnitude; whereas the reduction peak, although increasing in magnitude, does not change in potential with cycling. It appears at a lower potential than the oxidation peaks, around 1.22V. Little difference was noted in the cyclic voltammogram after oxygen had been evolved on this electrode for five and a half hours, the slight increase in magnitude of the peaks presumably being due to oxide build-up on the surface. Oxygen evolution is observed above 1.6V.

A further experiment was performed to attempt to reproduce the initial state of the electrode by polarising it at a reducing potential of 0.8V for seven hours. However, even after this reduction, the initial state of the electrode surface could not be achieved as subsequent cyclic voltammograms showed no difference to those obtained after oxygen evolution on this electrode.

The anodic peaks may be assigned to the formation of particular oxides. Experiments conducted by Rasiyah et al[99] suggest that the transitions $Co^{2+} \rightarrow Co^{3+}$ and $Ni^{2+} \rightarrow Ni^{3+}$ occur at 1.25 and 1.31V respectively. The first peak noted in the cyclic voltammogram, reported here, corresponds closely with these potentials. The higher couples of Ni^{3+}/Ni^{4+} and Co^{3+}/Co^{4+} are stated in the literature to occur at 1.43 and 1.45V respectively[100] which similarly are close to the potential of the

Fig. 10: Cyclic voltammograms of a NiCo₂O₄ electrode in 5M KOH
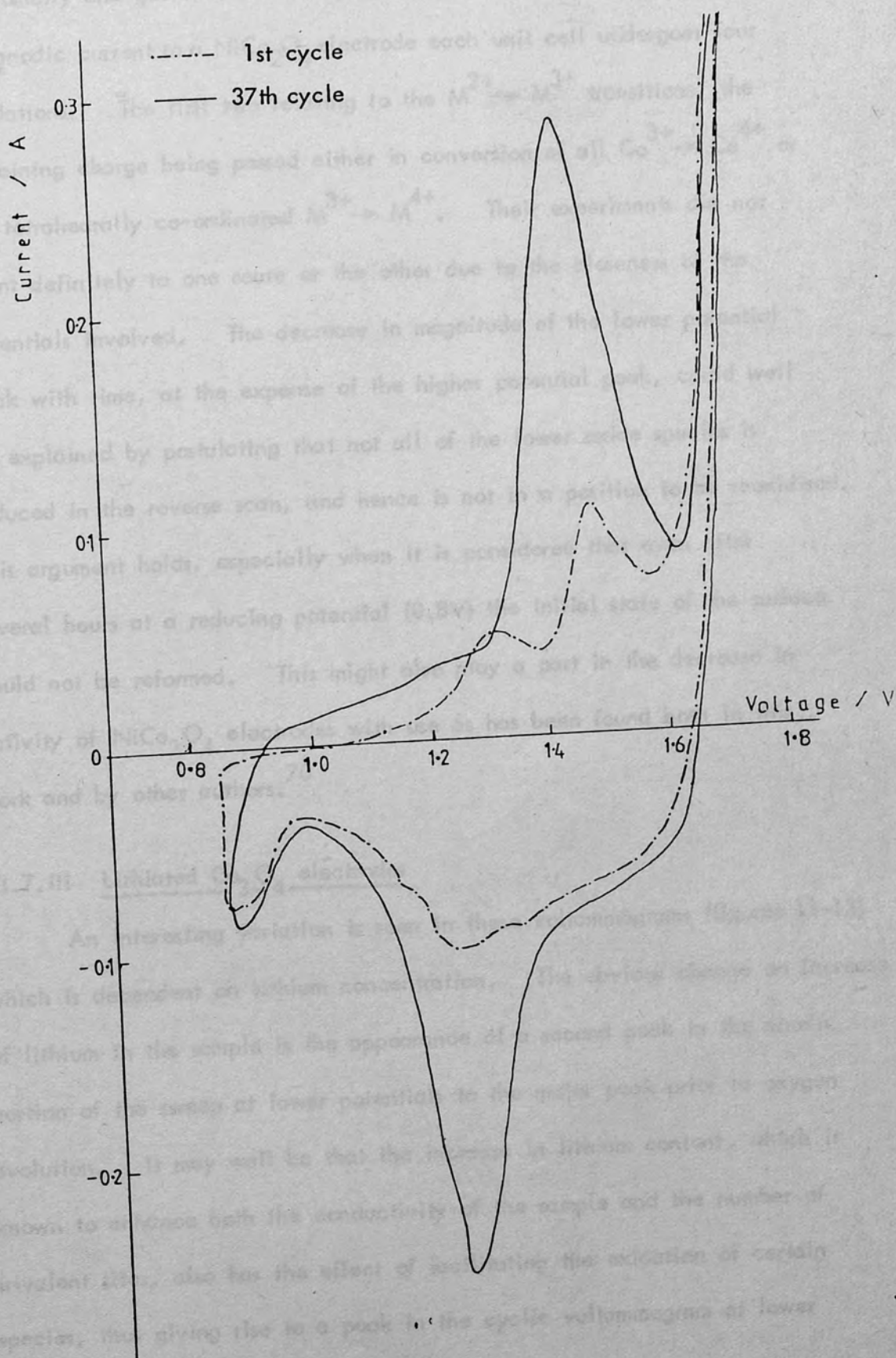
second peak determined here. Rasiyah et al[99] using controlled potential coulometry and galvanostatic charging curves showed that on application of an anodic current to a $NiCo_2O_4$ electrode each unit cell undergoes four oxidations. The first two relating to the $M^{2+} \rightarrow M^{3+}$ transitions, the remaining charge being passed either in conversion of all $Co^{3+} \rightarrow Co^{4+}$ or all tetrahedrally co-ordinated $M^{3+} \rightarrow M^{4+}$. Their experiments did not point definitely to one route or the other due to the closeness of the potentials involved. The decrease in magnitude of the lower potential peak with time, at the expense of the higher potential peak, could well be explained by postulating that not all of the lower oxide species is reduced in the reverse scan, and hence is not in a position to be reoxidised. This argument holds, especially when it is considered that even after several hours at a reducing potential (0.8V) the initial state of the surface could not be reformed. This might also play a part in the decrease in activity of $NiCo_2O_4$ electrodes with use as has been found both in this work and by other authors.[70]

VI.7.iii Lithiated Co_3O_4 electrodes

An interesting variation is seen in these voltammograms (figures 11-13) which is dependent on lithium concentration. The obvious change on increase of lithium in the sample is the appearance of a second peak in the anodic portion of the sweep at lower potentials to the major peak prior to oxygen evolution. It may well be that the increase in lithium content, which is known to enhance both the conductivity of the sample and the number of trivalent sites, also has the effect of facilitating the oxidation of certain species, thus giving rise to a peak in the cyclic voltammogram at lower potentials.

Fig 11: Cyclic voltammogram of a $Li_{0.07}Co_{2.93}O_4$ electrode in 5M KOH at a scan rate of 40 mV/sec
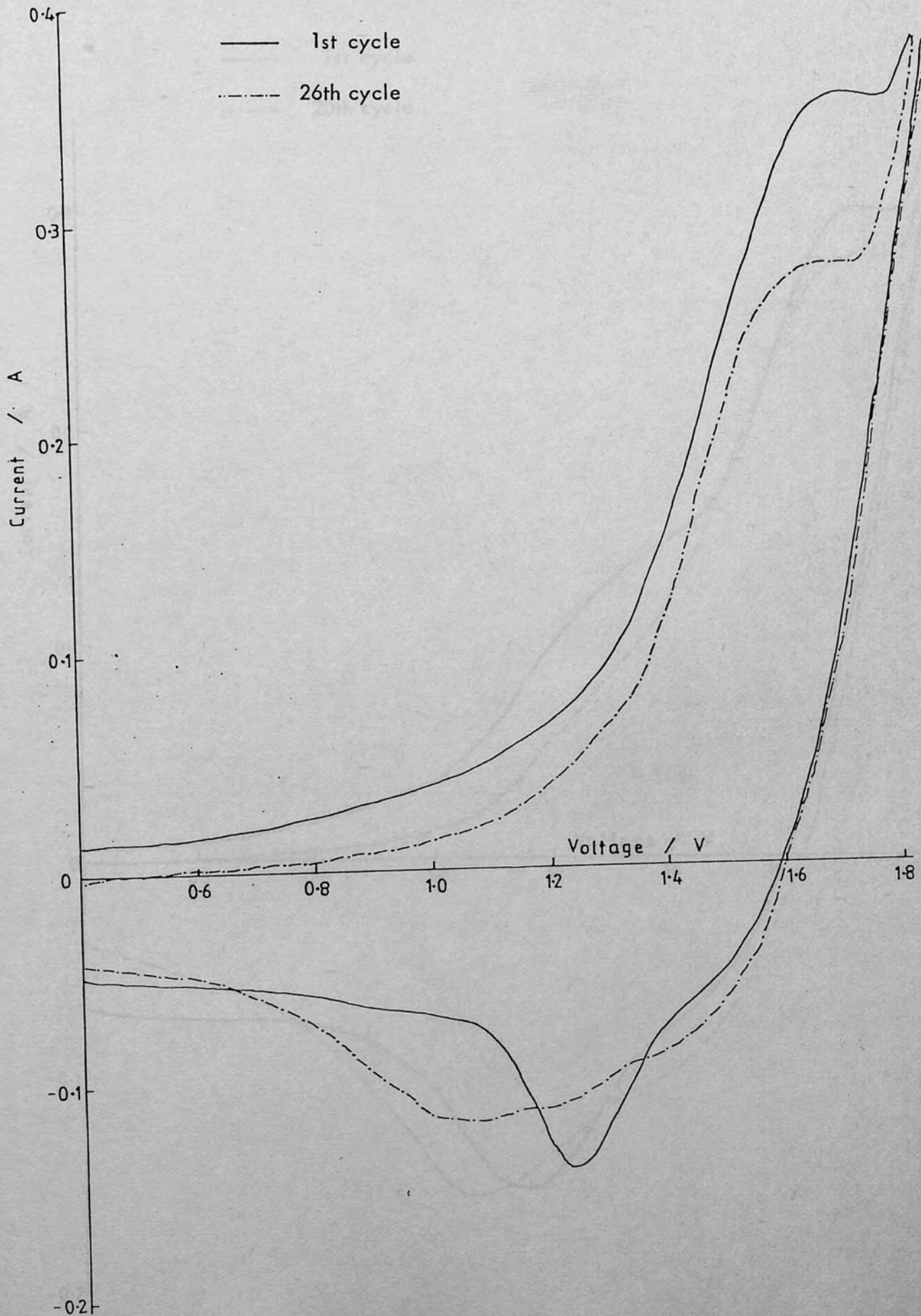
Fig 12: Cyclic voltammogram of a $Li_{0.18}Co_{2.82}O_4$ electrode
in 5M KOH at a scan rate of 40 mV/sec

1st cycle

20th cycle
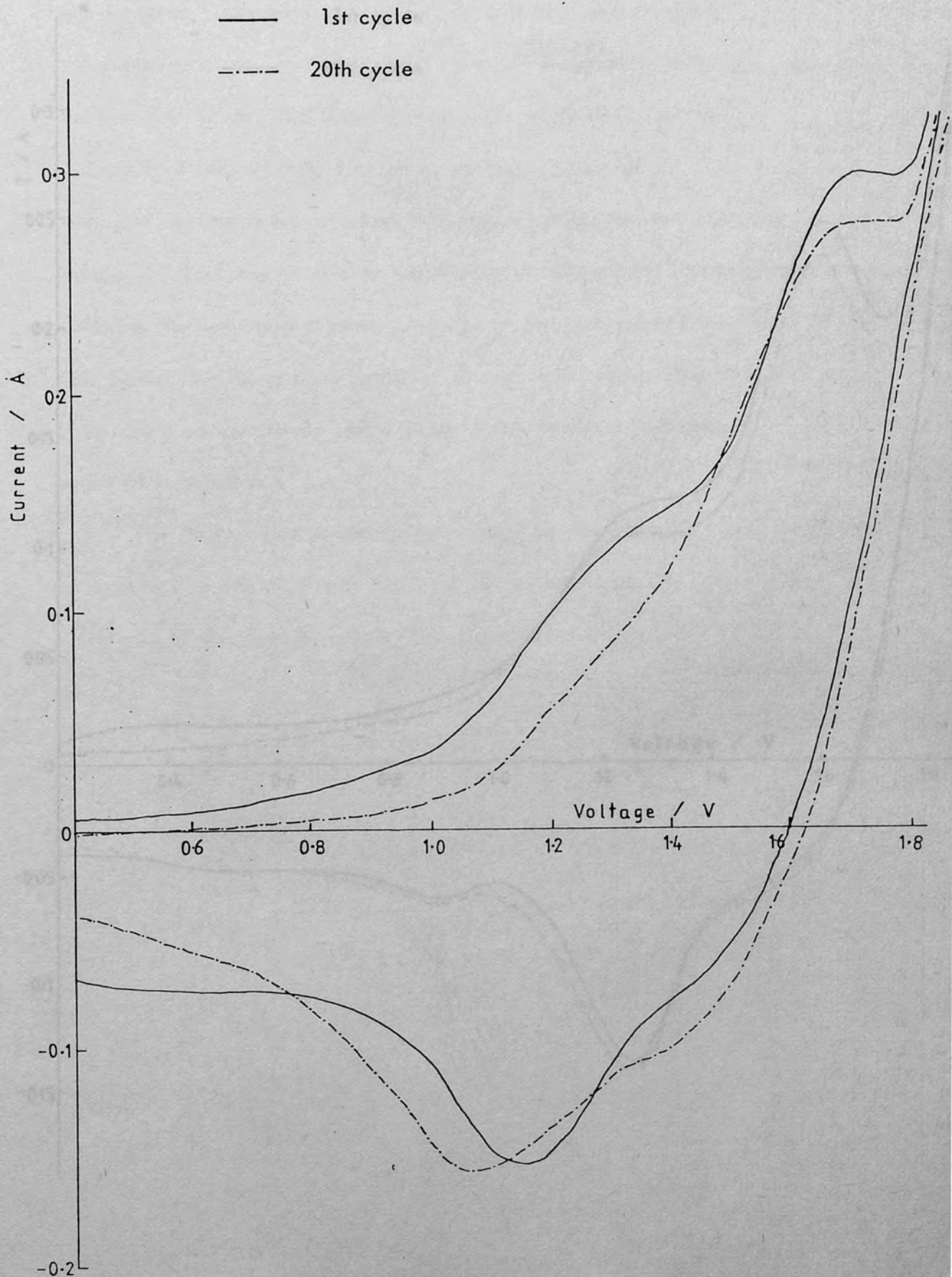
Fig 13: Cyclic voltammogram of a $Li_{0.36}Co_{2.64}O_4$ electrode in 5M KOH at a scan rate of 40 mV/sec
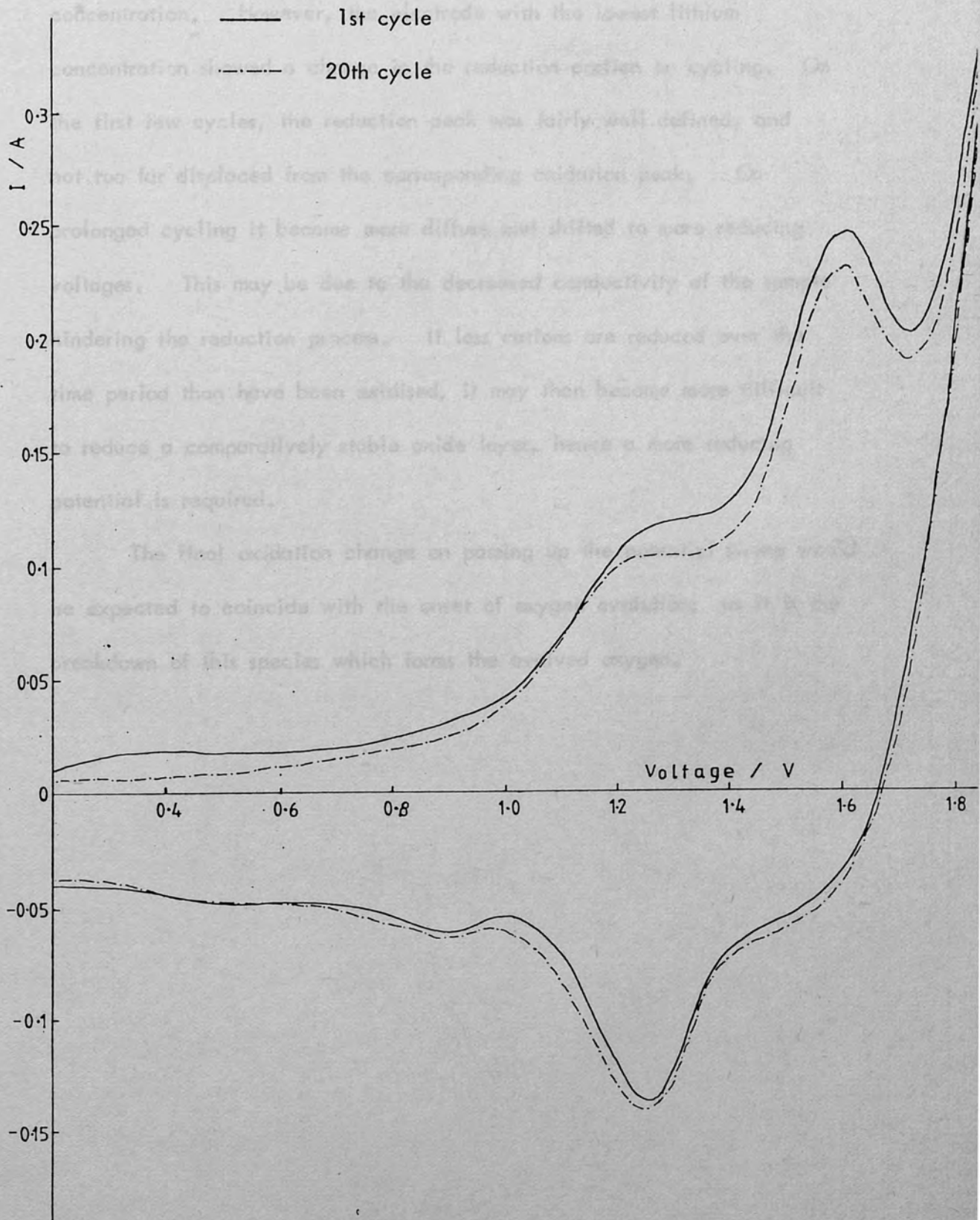
The reduction portion of the sweep did not change on cycling in the cyclic voltammograms of the two electrodes of higher lithium concentration. However, the electrode with the lowest lithium concentration showed a change in the reduction portion on cycling. On the first few cycles, the reduction peak was fairly well defined, and not too far displaced from the corresponding oxidation peak. On prolonged cycling it became more diffuse and shifted to more reducing voltages. This may be due to the decreased conductivity of the sample hindering the reduction process. If less cations are reduced over the time period than have been oxidised, it may then become more difficult to reduce a comparatively stable oxide layer, hence a more reducing potential is required.

The final oxidation change on passing up the potential sweep would be expected to coincide with the onset of oxygen evolution; as it is the breakdown of this species which forms the evolved oxygen.

Experimental Methods used in Isotopic Experiments

VII.1   Introduction

Throughout the time period during which these experiments were performed it was continually necessary to adapt and operate existing methods and techniques as the variable factors and their consequences emerged. The rate of detection of the enriched oxygen species $[^{34}O_2]$ was found to depend primarily on the purge gas flow rate and evolution current, and only to a minor extent on the operating pressure of the mass spectrometer. This latter variable was a much more influential criterion in the magnitude of the $^{34}O_2$ peak, as would be expected.

The underlying problem throughout was the difficulty of transferring the enriched gas from the electrolyte solution to the probe of the mass spectrometer at a detectable concentration with sufficient speed. As demonstrated below the limit of detection of suitable accuracy has presently been reached on the present system.

CHAPTER VII

VII.2   Electrolytic Cell

The electrolytic cell used for oxygen evolution in aethonic electrolyte is shown in Figure I. It is of the usual three-compartment type, with the facility to monitor the potential of the working electrode (W) via the reference electrode (R) in the third compartment which is attached by a Luggin capillary. A purge gas can be introduced into the cell via the glass frit of the base of the working electrode (T).

This cell was designed to have as little dead space as possible. For this reason the probe to the mass spectrometer (P) was placed in the path of

Experimental Methods used in Isotopic Experiments

VII.1   Introduction

Throughout the time period during which these experiments were
performed it was continually necessary to adapt and update existing methods
and techniques as the variable factors and their consequences emerged.   The
rate of detection of the enriched oxygen species ($^{34}O_2$) was found to depend
primarily on the purge gas flow rate and evolution current, and only to a
minor extent on the operating pressure of the mass spectrometer.   This
latter variable was a much more influential criterion in the magnitude of
the $^{34}O_2$ peak, as would be expected.

The underlying problem throughout was the difficulty of transporting the
enriched gas from the electrode surface to the probe of the mass spectrometer
at a detectable concentration with sufficient speed.   As demonstrated below
the limit of detection of suitable accuracy has probably been reached on the
present system.

VII.2   Electrolytic Cell

The electrolytic cell used for oxygen evolution in ordinary electrolyte
is shown in Figure 1.   It is of the usual three-compartment type, with the
facility to monitor the potential of the working electrode (W) via the reference
electrode (R) in the third compartment which is attached by a Luggin capillary.
A purge gas can be introduced into the cell via the glass frit at the base
of the working electrode (I).

This cell was designed to have as little dead space as possible.   For
this reason the probe to the mass spectrometer (P) was placed in the path of

Fig. 1: The electrochemical cell. For description see text.

the outgoing gases, just above the surface of the electrolyte.   Calcium

chloride placed in this probe, reduced its volume and also removed water

vapour, but had little effect on reducing the inlet time for the gases

(Fig. 2).   The arrangement shown allows the majority of gases to pass out

through an air-lock (II);   only a small fraction were diverted into the mass

spectrometer, via a leak valve (L).

For the enrichment procedure, an ordinary two-armed cell was used.

VII.3   Electrodes

High surface area electrodes were required for this technique, as at

the limits of sensitivity at least 10^{18} surface atoms available to participate

in the oxygen evolution reaction were necessary.   The electrodes were

cylindrical in shape, so as to present a maximum surface area to the given

volume of the cell.   The methods of preparation of the various electrodes

are given in Chapter V.   Each electrode was sealed into a glass holder,

again to reduce dead space in the cell.

In the experiments performed in alkaline electrolyte, a larger nickel

mesh was used as the counter electrode;   a high surface area platinised

platinum electrode being used in acid electrolyte.

The potential of the working electrode was monitored by means of a

dynamic hydrogen electrode which had itself been standardised against a

standard hydrogen electrode.   No account of the ohmic drop in solution

was taken.

VII.4   Electrolyte

All reagents were of Analar grade.   The acid electrolyte was 1 mol

dm^{-3} sulphuric acid and the alkaline electrolyte was 5 mol dm^{-3} potassium

Fig. 2:   Inlet system to the mass spectrometer

Relative height of argon peak

Probe	Valve setting
× empty	100
○ $CaCl_2$	100
□ $CaCl_2$	120

Time / min
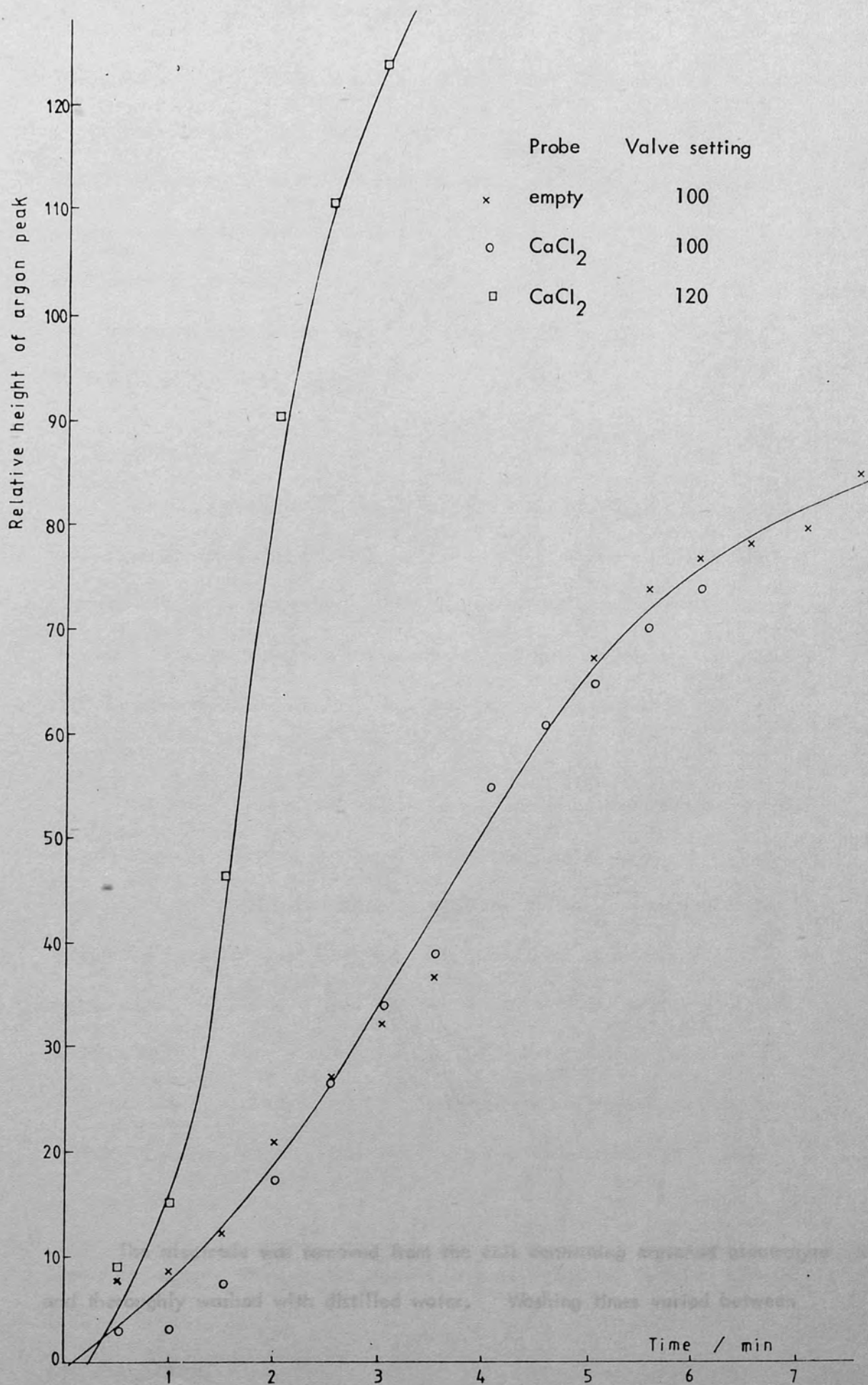
hydroxide.

Enrichment of the electrolyte was achieved by addition of a calculated amount of 20% ^{18}O H_2O (B.D.H.) to a stock solution of appropriate concentration of either the acid or the alkali, to give an enrichment of between 3-5%. The isotopic content of the electrolyte was determined by evolving oxygen in it and measuring the ratio of m/e 32 and 34 at the steady state.

VII.5   Method

Prior to enrichment of an electrode it was first ensured that any oxides present on the surface had been reduced.   In the case of platinum this was effectively achieved by evolution of hydrogen at 0.5A for five minutes.   The enrichment was then carried out in a cooled two-compartment cell, by reversal of the current, thus enabling oxygen evolution for a set period of time.

The time period of this procedure was varied between fifteen minutes and six hours to ascertain the length of time required to achieve maximum enrichment.   A rough calculation demonstrates that at a current of 0.5A, enough charge would have been passed in 30 minutes to oxidise 3×10^{21} oxygen atoms, which is at least ten-fold in excess of the number of actual surface sites available for this process.   Little difference in degree of enrichment was noted when the time period of the run ranged from six hours to those of shorter periods;   thus in general the time spent in enrichment was thirty minutes.

The electrode was removed from the cell containing enriched electrolyte and thoroughly washed with distilled water.   Washing times varied between

nought to five minutes, and additionally for extended periods of one hour. Little variation was found for the time range of one-five minutes, but for the extended times, no enrichment was subsequently determined. The main danger in the use of longer washing times lay in the fact that the greater time lapse, allowed at this stage, gives the higher oxide species formed on the electrode more time to disappear. With no washing, significantly higher enrichment values were found, as is shown in Figure 3. Presumably enriched $H_2^{18}O$ trapped on the surface, which would ordinarily be removed by the washing routine, remains on transfer from enriched to ordinary electrolyte, and is then strategically placed at the electrode surface to participate first in the evolution reaction.

After washing, the electrode was introduced into the cell containing ordinary electrolyte. This cell was continually purged with nitrogen, initially at a high rate so that any air entering the cell with the electrode is quickly removed, and subsequently at a steady rate to increase the speed at which the evolved gases travel to the probe of the mass spectrometer. The nitrogen purging rate was approximately five times the rate of oxygen evolution.

When the m/e 34 peak had fallen to an acceptably low value (usually less than 1% of the normal background) a constant current was passed through the cell by means of a Weir constant current supply. The quadrupole mass spectrometer (Vacuum Generators Anavac 2) operating at $10^{-6} - 10^{-5}$ mb continuously monitored m/e 34 which was displayed on a Y-t recorder. The peak reached a steady value corresponding to the normal background value in ten minutes or less. This run will be referred to as an enriched run.

Fig. 3: Variation in amount of enrichment detected with pretreatment of a $NiCo_2O_4$ electrode.

	Enrichment current A	Washing time S
×	0.250	120
□	0.500	120
○	0	120
•	0	0
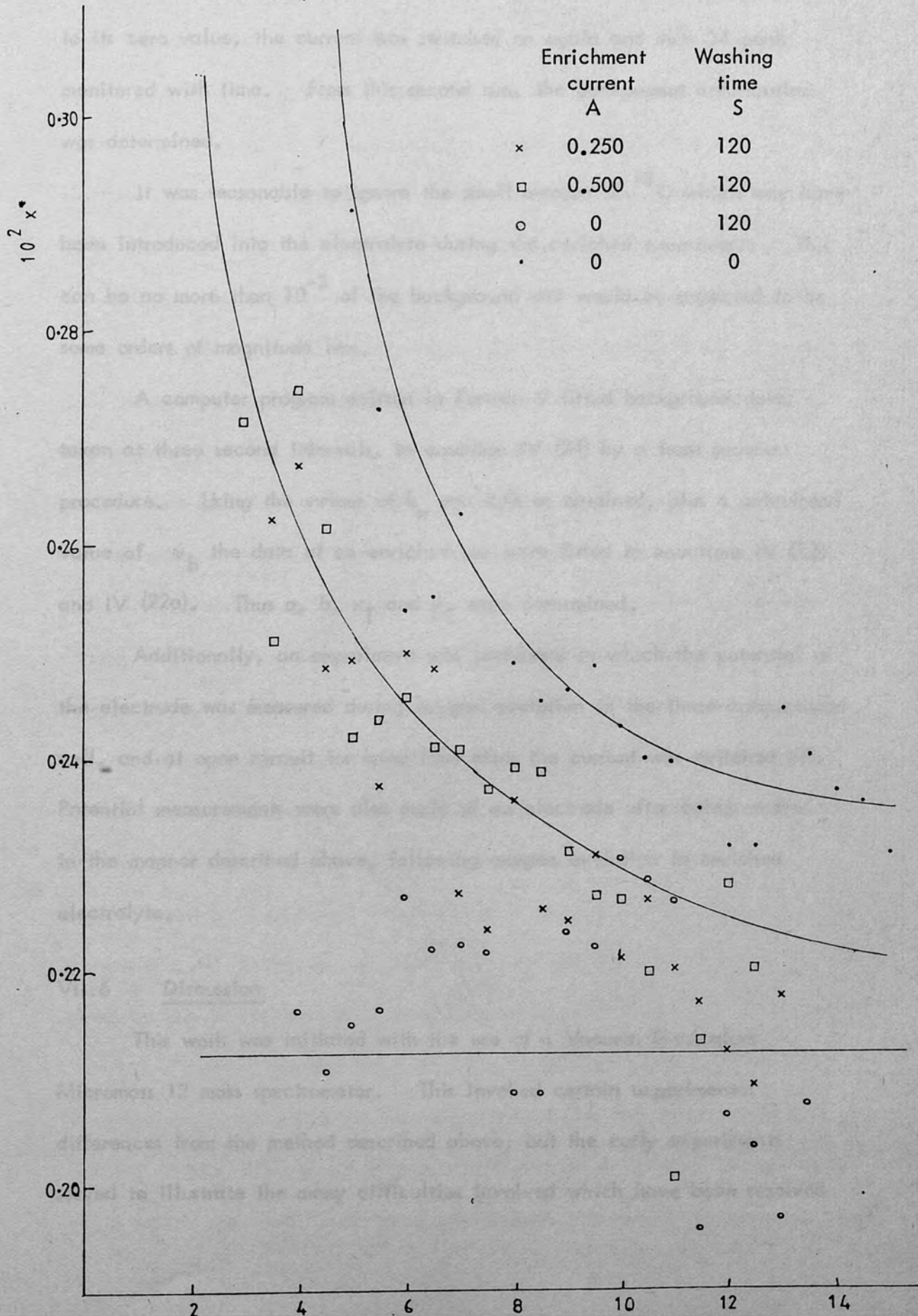
The current was switched off, but the nitrogen purging was continued through the cell at the same rate. When the peak height had fallen back to its zero value, the current was switched on again and m/e 34 peak monitored with time. From this second run, the background contribution was determined.

It was reasonable to ignore the small amount of ^{18}O which may have been introduced into the electrolyte during the enriched experiment. This can be no more than 10^{-3} of the background and would be expected to be some orders of magnitude less.

A computer program written in Fortran V fitted background data, taken at three second intervals, to equation IV (24) by a least squares procedure. Using the values of k_n and k/n as obtained, plus a calculated value of v_b the data of an enriched run were fitted to equations IV (22) and IV (22a). Thus a, b, x_T and y_T were determined.

Additionally, an experiment was performed in which the potential of the electrode was measured during oxygen evolution in the three-compartment cell, and at open circuit for some time after the current was switched off. Potential measurements were also made of an electrode after being washed in the manner described above, following oxygen evolution in enriched electrolyte.

VII.6   Discussion

This work was initiated with the use of a Vacuum Generators Micromass 12 mass spectrometer. This invoked certain experimental differences from the method described above, but the early experiments served to illustrate the many difficulties involved which have been resolved

to a large extent by modifications during the course of this project.

Initially, the transfer of the evolved gas to the mass spectrometer probe was achieved only by self-diffusion through the electrolyte as no constant purge gas was used. This also involved setting the mass spectrometer inlet valve to accept an exactly corresponding flow of gas as no overflow airlock was utilized. An argon purge gas was used for the first sixty seconds of each run, because during this period the rate of oxygen evolution was not sufficient to match the sucking rate of the mass spectrometer. Argon was used in this case as the purge gas, due to the nitrogen peak already being monitored to calculate the amount of background $^{34}O_2$. The advantage of this approach lay purely in the fact that all the enriched gas that was evolved was detected, there being no dilution by a purge gas; but two major drawbacks, namely the time period taken for the gas to leave the electrode surface and be detected and the requirement for the correct setting of the inlet valve, which was found to fluctuate even during one run, rather overshadowed this advantage. All detection time delays were found to arise in the cell-part of the apparatus, the actual response time of the mass spectrometer being only 2-3 seconds. The time taken for the evolved gas to reach the mass spectrometer probe could be decreased to a certain extent by increase of the evolution current, Fig. 4. This did not produce the reduction of time required and also proved to be less successful due to the method of peak measurement.

This method required the monitoring of the four peaks, m/e 28, 32, 34 and 40 as explained in the theoretical chapter on this work. The scanning of four peaks whose magnitude differed by a factor of 10^3 obviously led to difficulties, and the fastest possible cycle rate was a thirty second

Fig. 4: Variation in detection time with evolution current on a $NiCo_2O_4$ electrode in 5M KOH

○ 0.6A
× 0.4A
□ 0.2A
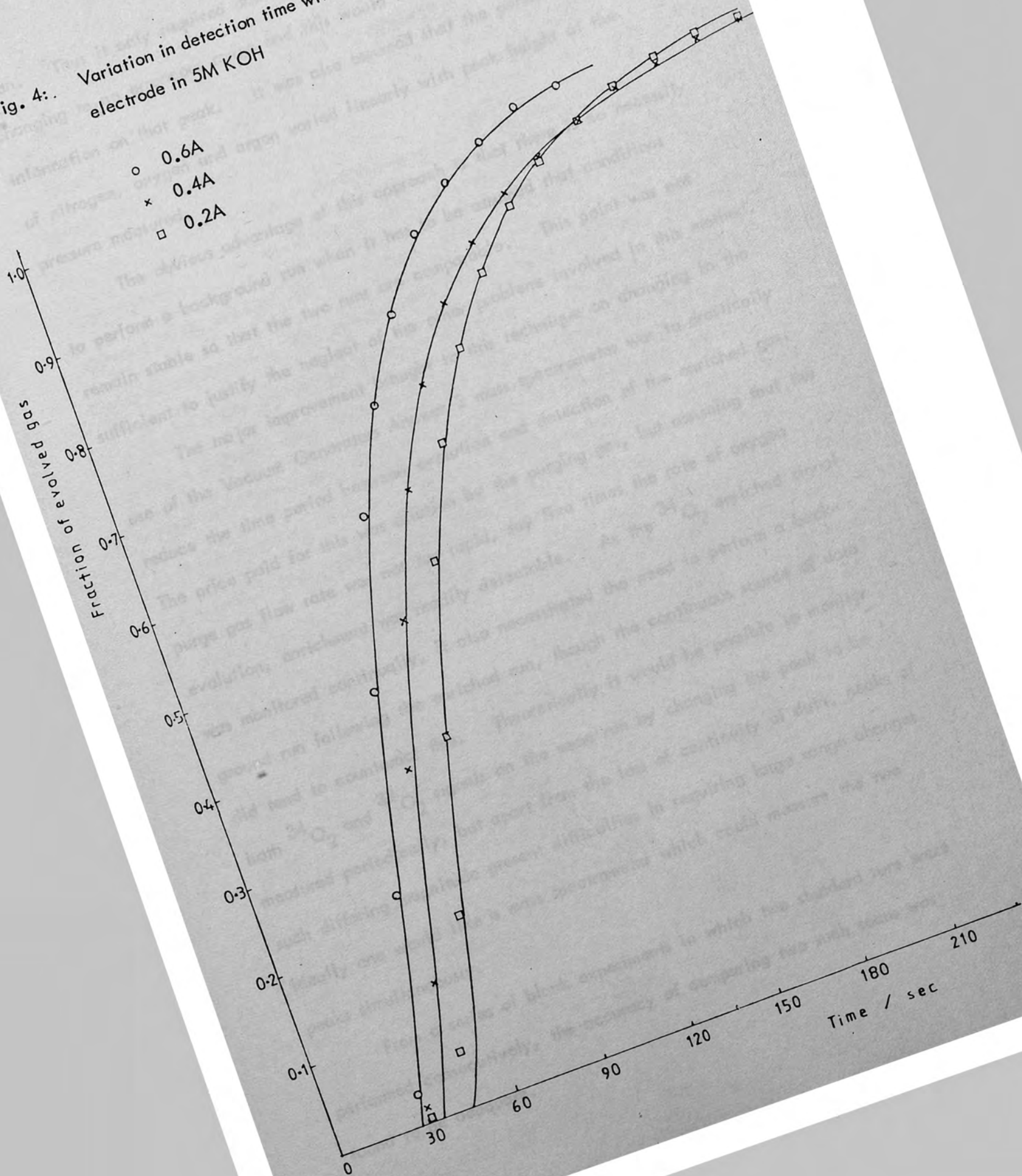
scan.   Thus it only required one reading to be missed, for instance by changing to an erroneous range and this would lead to one minute without information on that peak.   It was also assumed that the partial pressures of nitrogen, oxygen and argon varied linearly with peak height at the pressure measured.

The obvious advantage of this approach is that there is no necessity to perform a background run when it has to be assumed that conditions remain stable so that the two runs are comparable.   This point was not sufficient to justify the neglect of the other problems involved in this method.

The major improvement brought to this technique on changing to the use of the Vacuum Generators Anavac 2 mass spectrometer was to drastically reduce the time period between evolution and detection of the enriched gas. The price paid for this was dilution by the purging gas, but assuming that the purge gas flow rate was not too rapid, say five times the rate of oxygen evolution, enrichment was readily detectable.   As the $^{34}O_2$ enriched signal was monitored continually, it also necessitated the need to perform a background run following the enriched run, though the continuous source of data did tend to counteract this.   Theoretically it would be possible to monitor both $^{34}O_2$ and $^{32}O_2$ signals on the same run by changing the peak to be measured periodically, but apart from the loss of continuity of data, peaks of such differing magnitude present difficulties in requiring large range changes. Ideally one would like a mass spectrometer which could measure the two peaks simultaneously.

From a series of blank experiments in which two standard runs were performed consecutively, the accuracy of comparing two such scans was found to be adequate.

Oxygen was first considered as a purge gas so that the excess enrichment of $^{34}O_2$ peak would be measured above a steady state background of oxygen and thus the extra $^{32}O_2$ formed by the current flow would be negligible in comparison and thus need not be considered. In practice the huge $^{32}O_2$ peak formed tended to swamp the $^{34}O_2$ peak under consideration. Argon could not be used as a purge gas either due to the presence of its isotope ^{36}Ar which tends to obscure the $^{34}O_2$ peak under consideration. Thus nitrogen was chosen as the most likely candidate.

To ensure that it was actual oxides formed on the electrode surface during enrichment which were giving rise to the enrichment being detected, several experiments were performed, in which the electrode was just soaked in the enriched electrolyte, prior to being washed and the routine continued as normal. No enrichment was detected on such runs.

PART 3

RESULTS AND DISCUSSION OF THE ^{18}O ISOTOPIC EXPERIMENTS

CHAPTER VIII

Results and Discussion of the ^{18}O isotopic experiments

VIII.1   Results considering the formation of one higher oxide species

A typical set of results for one run, using a Vacuum Generators

micromass 12 mass spectrometer for analysis, depicting both the decrease in

enrichment (x*) and the variation of log (x* - x_o) with time is shown in

figure 1.   Error bars on the enrichment curve show the uncertainty in the

measurements.   The data obtained using this mass spectrometer for platinum

in acid solution (0.5M H_2SO_4) and $NiCo_2O_4$ electrodes in alkaline solution

(5M KOH) are shown in Tables I and II.   Values of the initial enrichment

and total number of sites available on the surface were calculated considering

the formation of only one higher oxide species.

VIII.1i   Platinum electrodes

On platinum a close agreement was obtained between the number of

sites used in the oxygen evolution reaction, found to be (2.15 $\pm$ 0.14) x 10^{20}

by this isotopic technique and (1.70 $\pm$ 0.27) x 10^{20} as determined by the

surface area measurement technique of oxygen charging.   As these two values

are effectively measured by the same process, that is the formation of an oxide

layer on the surface, their compatibility was very encouraging in the confir-

mation of the basic principles of this isotopic technique.

Of greater interest in these results was the decay of the initial amount

of surface oxide species with time.   The data showed that on platinum this

species was comparatively stable and long-lived, as enrichment above the

background level was detected at time periods longer than one hour after

removal of the electrode from enriched electrolyte.   The decay of the initial

Fig 1: Decrease in enrichment and variation of $\log(x^*-x_o)$ with time on a platinised platinum electrode in 0.5M H_2SO_4
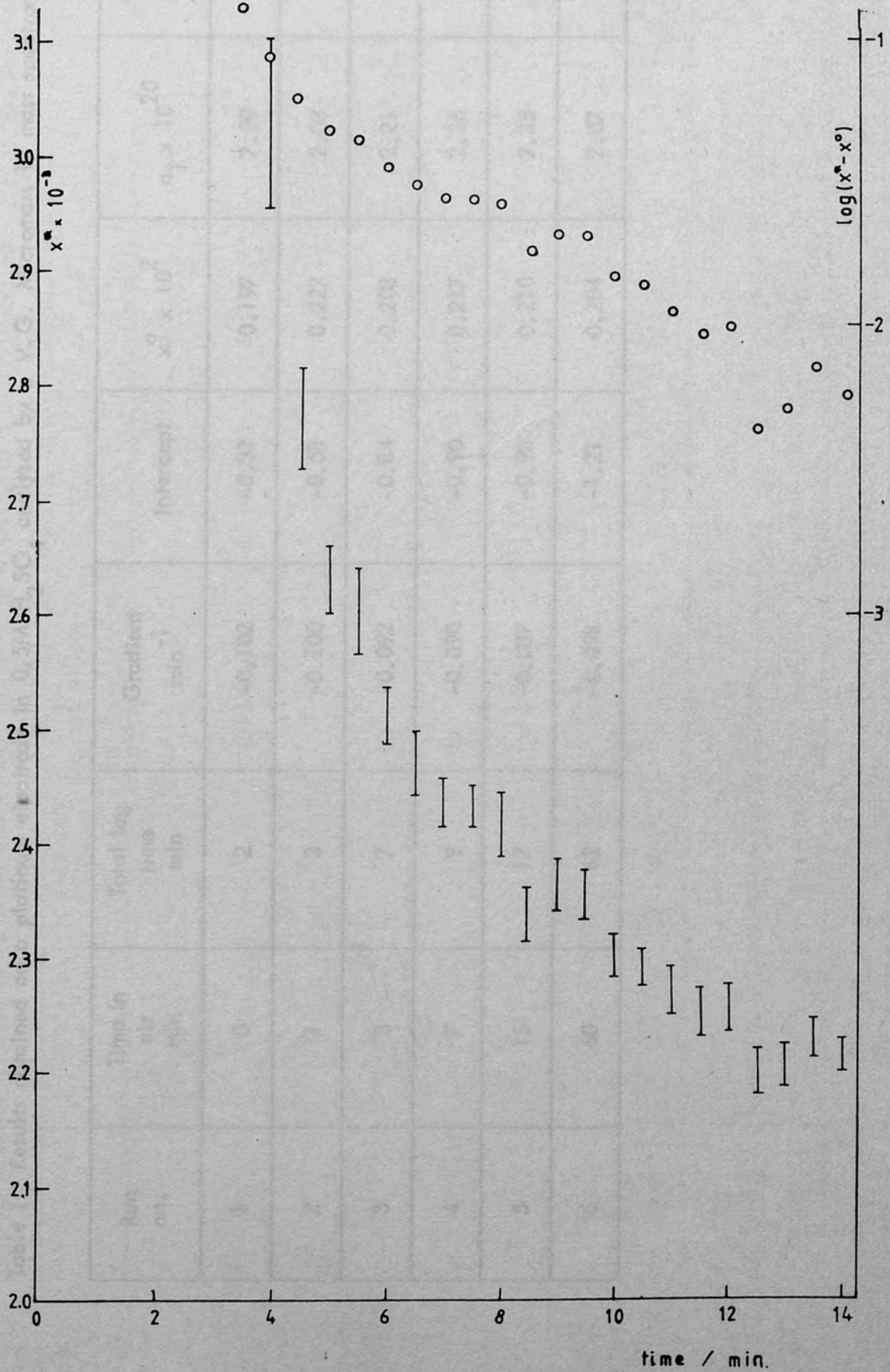
Table I: Results obtained on a platinum electrode in 0.5M H_2SO_4 analysed by a V.G. Micromass 12 mass spectrometer

Run no.	Time in air min	Total lag time min	Gradient min^{-1}	Intercept	$x^o \times 10^2$	$n_T \times 10^{20}$	$x^*_o \times 10^2$
1	0	2	-0.102	-0.33	0.197	7.99	0.67
2	1	3	-0.100	-0.58	0.227	2.03	0.49
3	5	7	-0.092	-0.84	0.203	2.21	0.35
4	7	9	-0.090	-0.90	0.217	2.26	0.34
5	15	17	-0.087	-0.93	0.210	2.35	0.33
6	60	62	-0.098	-1.21	0.204	2.07	0.27

Table II: Results obtained on a platinum electrode in 5M KOH analysed by a V.G. micromass 12 mass spectrometer

Run no.	Time in air min	Total lag time min	Gradient min^{-1}	Intercept	$x^o_o \times 10^2$	$n_T \times 10^{20}$	$x^*_o \times 10^2$
1a	0	2	-0.135	-0.78	0.205	1.506	0.371
1b	1	3	-0.123	-0.76	0.225	1.653	0.399
1c	1	3	-0.133	-0.74	0.203	1.528	0.377
1d	2	4	-0.138	-0.84	0.221	1.473	0.365
1e	3	5	-0.126	-0.84	0.206	1.613	0.351
1f	3	5	-0.134	-0.96	0.207	1.517	0.317
1g	4	6	-0.120	-0.84	0.214	1.694	0.359
1h	5	7	-0.133	-1.28	0.205	1.528	0.257
1i	7	9	-0.158	-1.16	0.207	1.287	0.276
1j	10	12	-0.087	-1.22	0.206	2.336	0.260

amount of this species, as determined from the intercept of the $\log (x^* - x_o)$ graphs at time $t = 0$, basically took the form of an exponential curve (figure 2).

VIII.1ii   Nickel Cobalt Oxide electrodes

However, with $NiCo_2O_4$ electrodes after resting periods of one hour prior to the second period of evolution of oxygen, no enrichment could then be detected.   Additionally the amount of enrichment monitored at brief resting periods was less than that determined on platinum for the same time lag, indicating a faster breakdown of the oxide surface species.

If we consider the reaction which causes the breakdown of the oxide species,

$$2MO \underset{}{\overset{v_3}{\rightleftharpoons}} 2M + O_2 \tag{1}$$
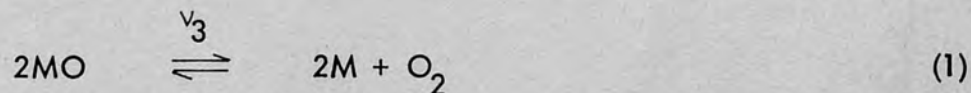
then, $$v_3 = k_2 [MO]^2 \tag{2}$$

where k_2 is a second order rate constant.   We have assumed for the evolution process driven by the current that

$$v_3 = k^1 [M^{18}O] \tag{3}$$

where $k^1 = k_2 M^{16}O$

As current is passed, $M^{16}O$ is consumed from the surface as oxygen is evolved, but is continuously replaced by the preceding reactions, and thus its concentration on the surface may be regarded as constant.

When the electrode is held in air after enrichment, the kinetics of the breakdown of the oxide species would be expected to change as this

Fig. 2: Decrease in initial enrichment with time for a platinised platinum electrode in 0.5M H_2SO_4

141
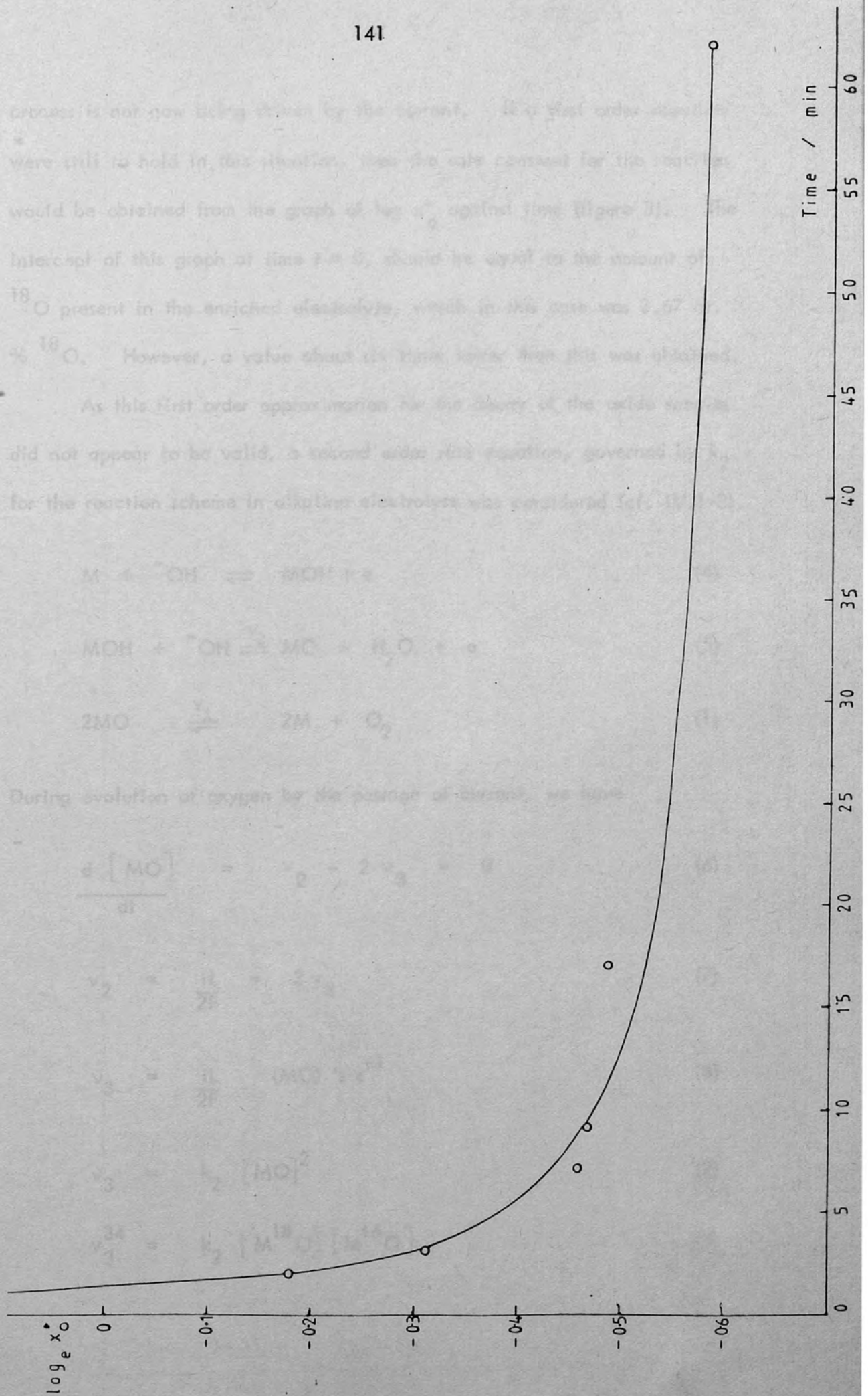
process is not now being driven by the current. If a first order reaction were still to hold in this situation, then the rate constant for the reaction would be obtained from the graph of log x_o^* against time (figure 3). The intercept of this graph at time $t = 0$, should be equal to the amount of ^{18}O present in the enriched electrolyte, which in this case was 3.67 at. % ^{18}O. However, a value about six times lower than this was obtained.

As this first order approximation for the decay of the oxide species did not appear to be valid, a second order rate equation, governed by k_2 for the reaction scheme in alkaline electrolyte was considered (cf. IV.1-3).

$$M + {}^-OH \rightleftharpoons MOH + e \qquad (4)$$

$$MOH + {}^-OH \overset{v_2}{\rightleftharpoons} MO + H_2O + e \qquad (5)$$

$$2MO \overset{v_3}{\rightleftharpoons} 2M + O_2 \qquad (1)$$
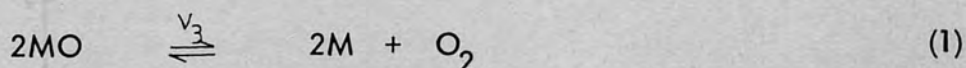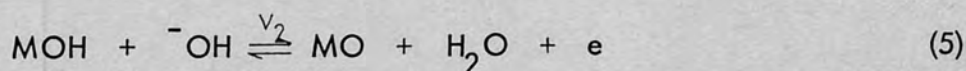
During evolution of oxygen by the passage of current, we have

$$\frac{d\,[MO]}{dt} = v_2 - 2\,v_3 = 0 \qquad (6)$$

$$v_2 = \frac{iL}{2F} = 2\,v_3 \qquad (7)$$

$$v_3 = \frac{iL}{2F} \quad (MO)\text{'s s}^{-1} \qquad (8)$$

$$v_3 = k_2\,[MO]^2 \qquad (2)$$

$$v_3^{34} = k_2\,[M^{18}O]\,[M^{16}O] \qquad (9)$$

Fig. 3: Decrease in initial enrichment with time for a $NiCo_2O_4$ electrode in 5M KOH
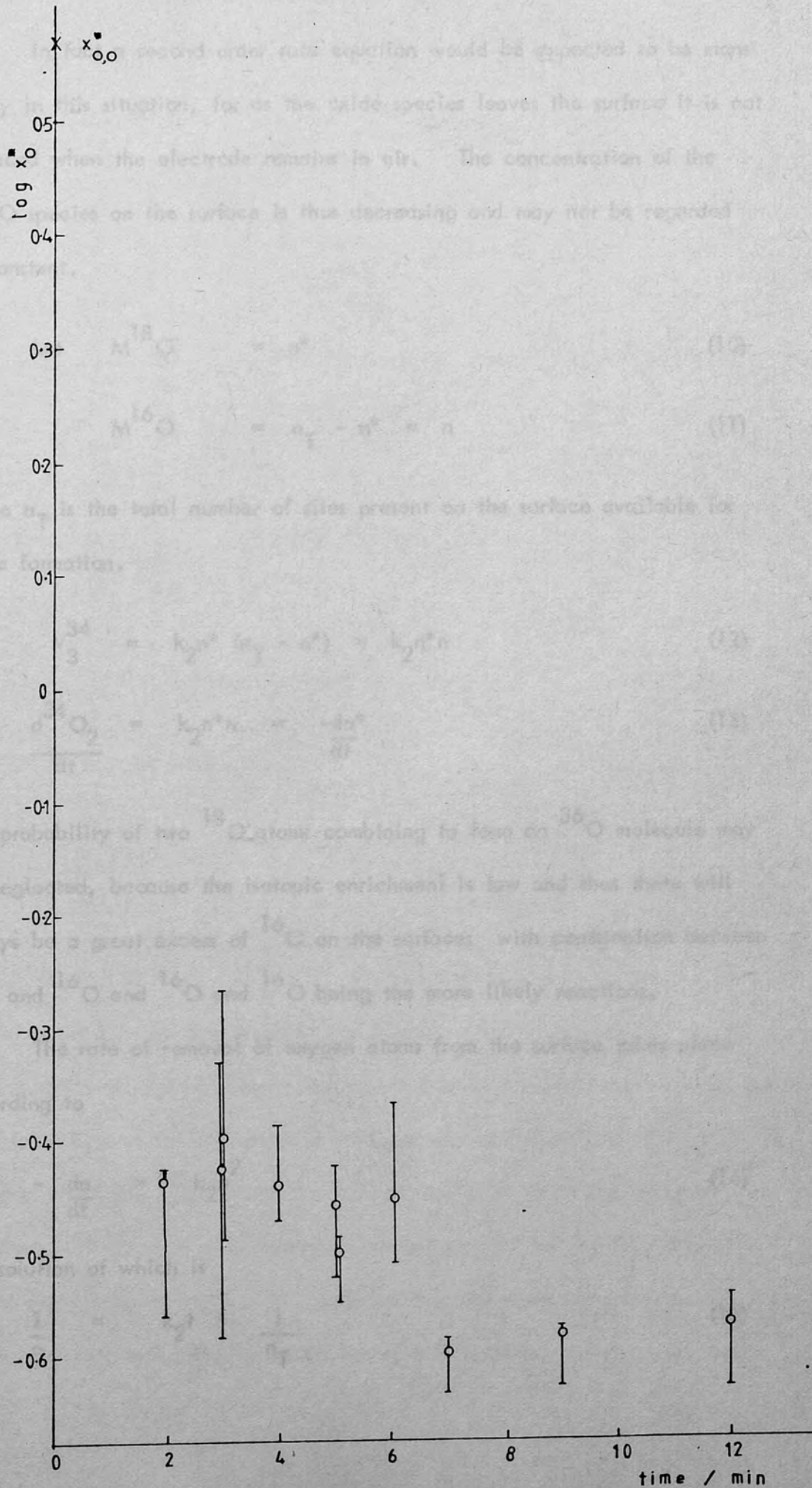
In fact a second order rate equation would be expected to be more likely in this situation, for as the oxide species leaves the surface it is not replaced when the electrode remains in air. The concentration of the $M^{16}O$ species on the surface is thus decreasing and may not be regarded as constant.

$$\text{Let} \quad M^{18}O \quad = n^* \tag{10}$$

$$M^{16}O \quad = n_T - n^* = n \tag{11}$$

where n_T is the total number of sites present on the surface available for oxide formation.

$$v_3^{34} = k_2 n^* (n_T - n^*) = k_2 n^* n \tag{12}$$

$$\frac{d^{34}O_2}{dt} = k_2 n^* n = \frac{-dn^*}{dt} \tag{13}$$

The probability of two ^{18}O atoms combining to form an ^{36}O molecule may be neglected, because the isotopic enrichment is low and thus there will always be a great excess of ^{16}O on the surface; with combination between ^{18}O and ^{16}O and ^{16}O and ^{16}O being the more likely reactions.

The rate of removal of oxygen atoms from the surface takes place according to

$$- \frac{dn}{dt} = k_2 n^2 \tag{14}$$

the solution of which is

$$\frac{1}{n} = k_2 t + \frac{1}{n_T} \tag{15}$$

Thus if we consider the removal of oxygen atoms which are ^{18}O enriched, equation (13) leads to

$$- \frac{dn^*}{dt} = \frac{k_2 n^*}{k_2 t + 1/n_T} = \frac{k_2 n^* n_T}{k_2 t n_T + 1} \qquad (16)$$

$$- \int_{n^*_{o,o}}^{n^*_o} \frac{dn^*}{n^*} = \int_0^t \frac{k_2 n_T}{k_2 t n_T + 1} \, dt \qquad (17)$$

$$- \log \frac{n^*_o}{n^*_{o,o}} = \log (k_2 t n_T + 1) \qquad (18)$$

where $n^*_{o,o}$ is the initial enrichment.

As $x^* = n^*/n_T$, we have

$$\frac{x^*_{o,o}}{x^*_o} - 1 = k_2 n_T t \qquad (19)$$

A graph of $\left[x^*_{o,o}/x^*_o - 1 \right]$ against time should be a straight line plot of slope $k_2 n_T$ passing through the origin. At time $t = 0$, $x^*_{o,o} = x^*_o$, because although only a certain fraction of adsorbed oxygen atoms are bound strongly enough to the surface to remain adhered after washing, the percentage of these which are ^{18}O enriched should be the same as in the enriched solution. If we were only observing the removal of the 'already formed' higher oxide species it would be expected that the ratio $x^*_{o,o}/x^*_o$ would remain constant with time. As an increase is observed, as shown in figure

Fig 4:   Variation of the quantity $(x^*_{o,o}/x^*_o -1)$ with time for a
$NiCo_2O_4$ electrode in 5M KOH
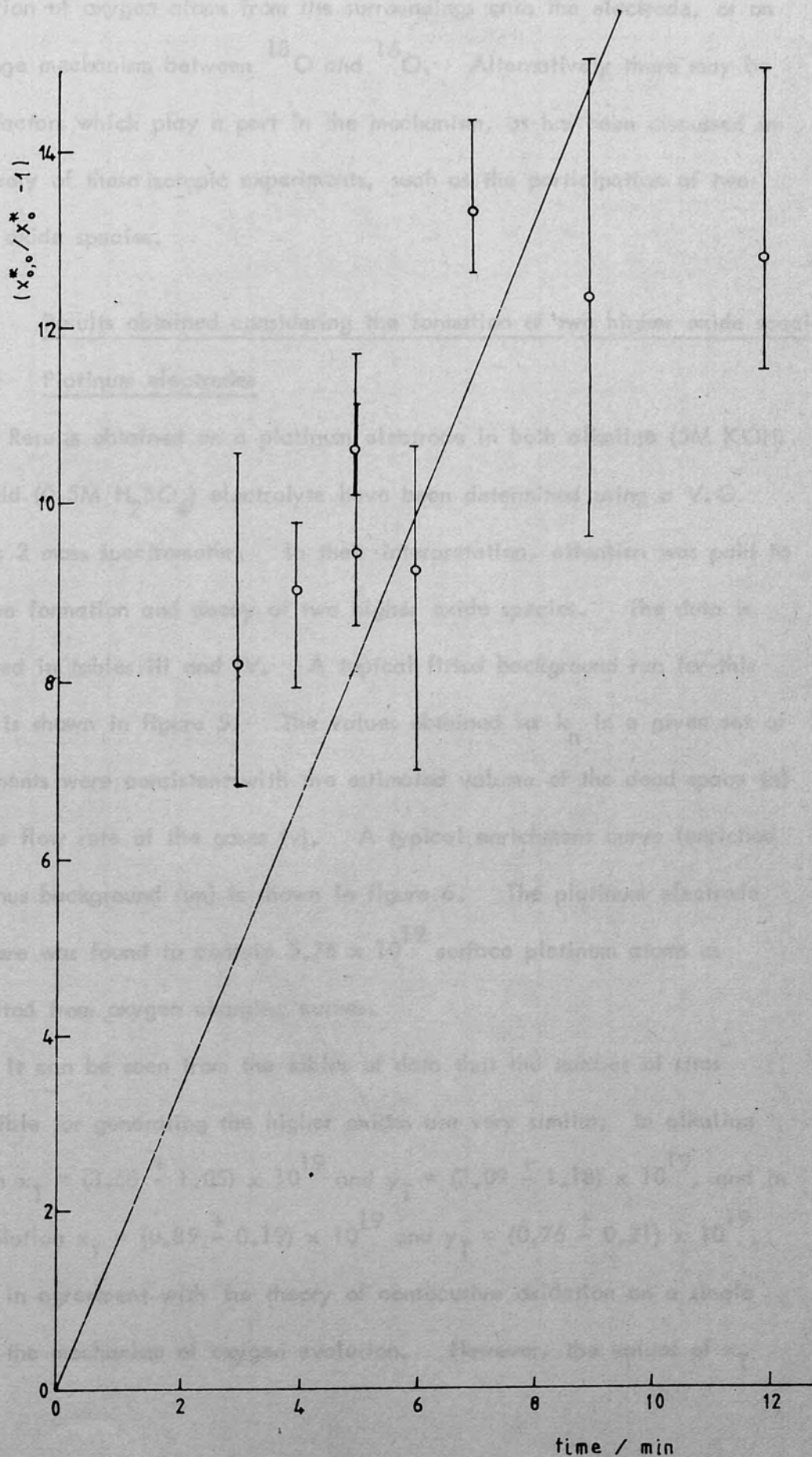
4, it suggests that some form of mechanism might be in operation for the adsorption of oxygen atoms from the surroundings onto the electrode, or an exchange mechanism between ^{18}O and ^{16}O. Alternatively there may be other factors which play a part in the mechanism, as has been discussed in the theory of these isotopic experiments, such as the participation of two higher oxide species.

VIII.2   Results obtained considering the formation of two higher oxide species

VIII.2i   Platinum electrodes

Results obtained on a platinum electrode in both alkaline (5M KOH) and acid (0.5M H_2SO_4) electrolyte have been determined using a V.G. Anavac 2 mass spectrometer. In their interpretation, attention was paid to both the formation and decay of two higher oxide species. The data is presented in tables III and IV. A typical fitted background run for this system is shown in figure 5. The values obtained for k_n in a given set of experiments were consistent with the estimated volume of the dead space (n) and the flow rate of the gases (v). A typical enrichment curve (enriched run minus background run) is shown in figure 6. The platinum electrode used here was found to contain 5.76×10^{19} surface platinum atoms as calculated from oxygen charging curves.

It can be seen from the tables of data that the number of sites responsible for generating the higher oxides are very similar; in alkaline solution $x_T = (3.58 \pm 1.05) \times 10^{19}$ and $y_T = (3.09 \pm 1.18) \times 10^{19}$, and in acid solution $x_T = (0.89 \pm 0.19) \times 10^{19}$ and $y_T = (0.76 \pm 0.21) \times 10^{19}$. This is in agreement with the theory of consecutive oxidation on a single site in the mechanism of oxygen evolution. However, the values of x_T

Table III: Results obtained on a platinum electrode in 5M KOH analysed by a V.G. Anavac 2 mass spectrometer

Run no.	Time in air S	Total lag time S	I A	Background			Cell lag time S	$x_T \times 10^{19}$	Enriched		
				Max. Signal	$k_n \times 10^{-2}$	Cell lag time S			$y_T \times 10^{19}$	$a \times 10^{16}$	$b \times 10^{13}$
A	0	150	0.25	1.06	1.68	25.0	28.0	2.67	2.58	1.43	3.01
B	0	150	0.25	1.11	1.50	19.4	34.7	3.02	2.9	1.01	3.01
C	0	150	0.25	1.14	1.28	28.0	30.0	3.39	2.40	1.05	3.01
D	0	210	0.25	1.37	0.37	90.0	61.9	4.64	4.4	1.30	3.01
E	0	210	0.25	1.23	0.34	126.0	17.4	4.94	4.04	2.37	3.01
F	300	450	0.25	1.03	0.20	31.7	24.0	4.80	4.66	1.14	0.60
G	3600	3750	0.25	1.11	0.19	30.7	61.4	2.37	1.19	0.55	3.01
S	0	150	0.25	1.13	0.12	114.6	13.5	2.84	2.60	0.63	0.01

Table IV: Results obtained on a platinum electrode in 0.5M H_2SO_4 analysed by a V.G. Anavac 2 mass spectrometer

Run no.	Time in air S	Total lag time S	I A	Background				Enriched			
				Max. Signal	$k_n \times 10^{-2}$	Cell lag time S	Cell lag time S	$x_T \times 10^{19}$	$y_T \times 10^{19}$	$a \times 10^{16}$	$b \times 10^{13}$
A1	0	210	0.25	1.08	0.42	137.3	316.2	1.11	1.00	2.17	0.60
B1	0	75	0.4	1.14	1.79	28.1	55.4	0.74	0.65	1.61	0.60
C1	0	60	0.4	1.08	2.17	25.0	50.5	0.84	0.62	1.34	0.60

Fig. 5:   Fitted background curve to oxygen evolution data on a platinised
          platinum electrode in 5M KOH.
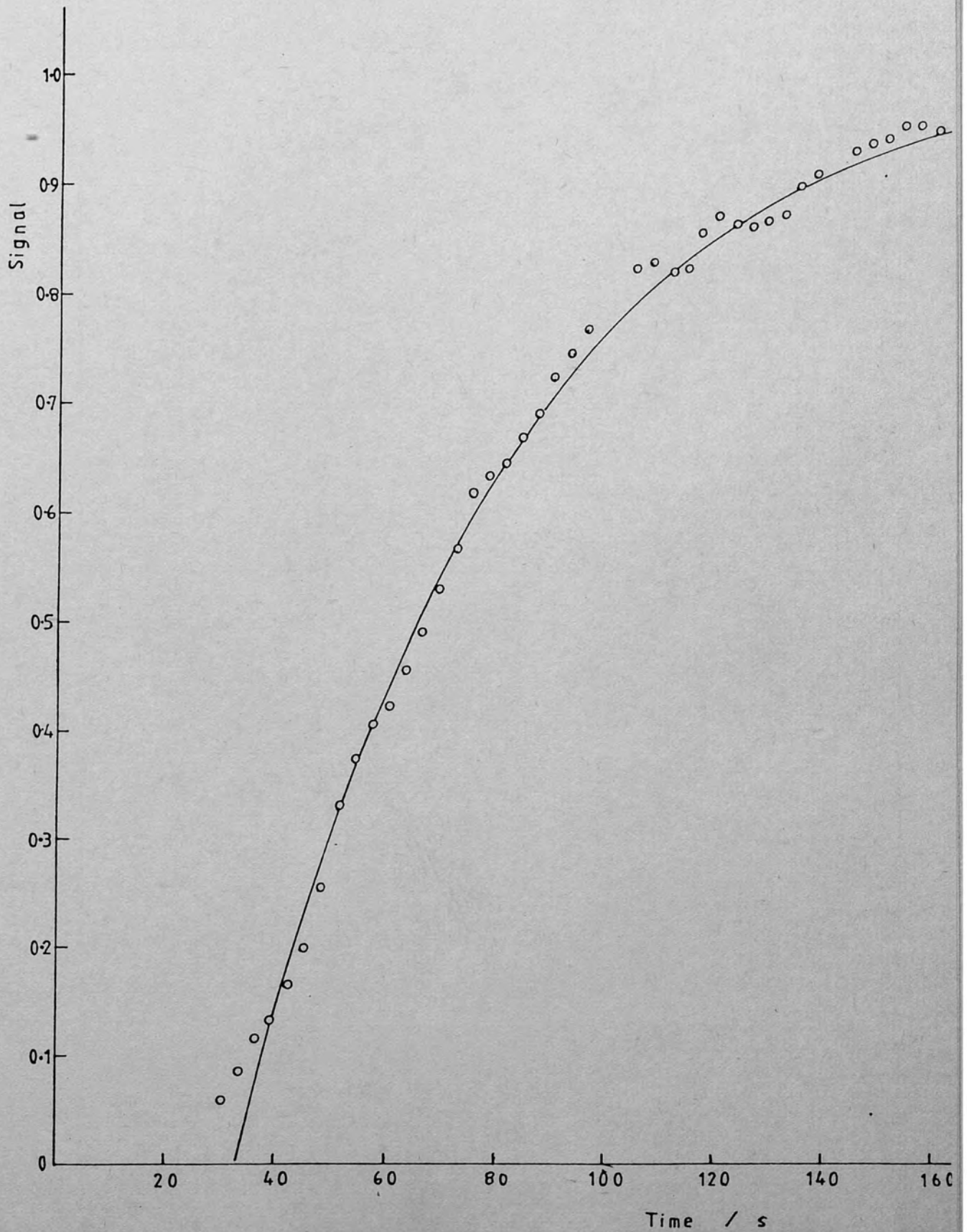
Fig. 6:   Difference between m/e 34 signal for oxygen evolution on a
platinised platinum electrode enriched with ^{18}O and the
background experiment.

Fig. 6

Signal

6

5

4

3

2

1

0

0   20   40   60   80   100   120   140   Time / s
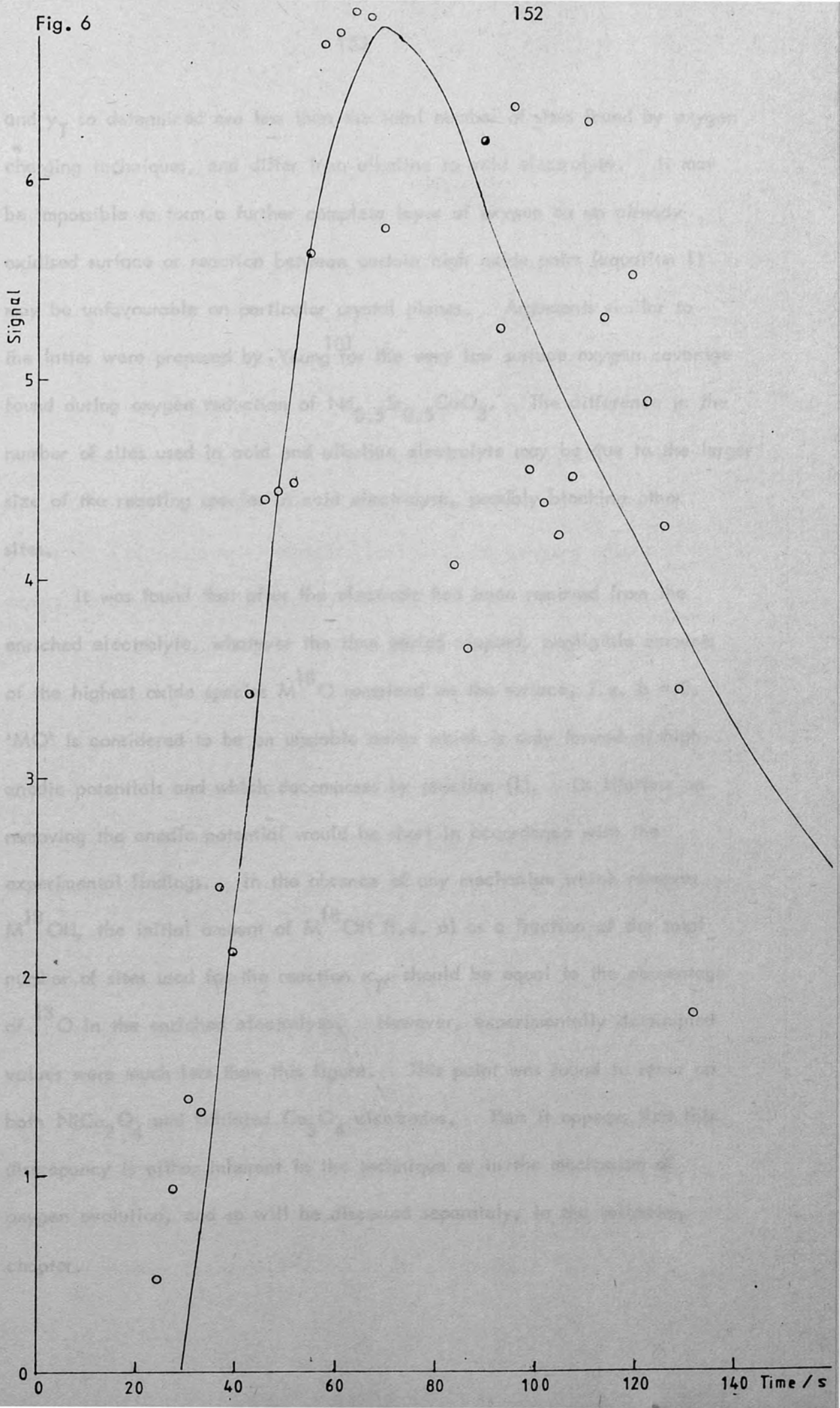
and y_T so determined are less than the total number of sites found by oxygen charging techniques, and differ from alkaline to acid electrolyte. It may be impossible to form a further complete layer of oxygen on an already oxidised surface or reaction between certain high oxide pairs (equation 1) may be unfavourable on particular crystal planes. Arguments similar to the latter were proposed by Yeung[101] for the very low surface oxygen coverage found during oxygen reduction of $Nd_{0.5}Sr_{0.5}CoO_3$. The difference in the number of sites used in acid and alkaline electrolyte may be due to the larger size of the reacting species in acid electrolyte, possibly blocking other sites.

It was found that after the electrode had been removed from the enriched electrolyte, whatever the time period elapsed, negligible amounts of the highest oxide species $M^{18}O$ remained on the surface, i.e. b = 0. 'MO' is considered to be an unstable oxide which is only formed at high anodic potentials and which decomposes by reaction (1). Its lifetime on removing the anodic potential would be short in accordance with the experimental findings. In the absence of any mechanism which removes $M^{18}OH$, the initial amount of $M^{18}OH$ (i.e. a) as a fraction of the total number of sites used for the reaction x_T, should be equal to the percentage of ^{18}O in the enriched electrolyte. However, experimentally determined values were much less than this figure. This point was found to recur on both $NiCo_2O_4$ and lithiated Co_3O_4 electrodes. Thus it appears that this discrepancy is either inherent in the technique or in the mechanism of oxygen evolution, and so will be discussed separately, in the following chapter.

VIII.2ii   Nickel Cobalt Oxide Electrodes

Results which assume the formation of two higher oxide species obtained on $NiCo_2O_4$ electrodes are presented in tables V and VI.   This data emphasises several important features, apart from points mentioned previously, such as the rate of decay of the surface oxide species and lower amounts of enrichment detected than would be anticipated.

It is interesting to note the decrease in activity of the electro-catalyst with use.   This feature has already been mentioned regarding $NiCo_2O_4$ electrodes by King and Tseung.[70] They found no change in performance of a sample of catalyst which had been stored dry for two years, but another portion stored under 5M KOH for eight weeks lost its activity during this time.   The loss of activity cannot be reversed by washing and drying the electrode nor by heat treatment.   As shown in the section discussing cyclic voltammetry in this work, polarisation of the electrode at a reducing potential could not restore it to its original state. Although the spinel phase is still present in the deactivated state, King and Tseung suggested that the loss of activity was caused by hydroxide ions being formed within the lattice during exposure to the electrolyte.   The decrease in activity with use is displayed graphically for the first $NiCo_2O_4$ electrode in figure 7.   These experiments would be equivalent to about ten hours use of the electrode.

Run N14 (Table V) was performed without the washing stage after the electrode had been enriched, excess electrolyte droplets only being removed by agitation.   Although the value of a determined is higher than would be expected after this amount of use of the electrode, it does not differ

Table V: Results obtained on a NiCo$_2$O$_4$ electrode (I) in 5M KOH analysed by a V.G. Anavac 2 mass spectrometer

Run no.	Wash Time S	Total lag Time S	I A	Max. Signal	Background				Enriched		
					$k_n \times 10^{-2}$	Cell lag Time S	Cell lag Time S	$x_T \times 10^{19}$	$y_T \times 10^{19}$	$a \times 10^{16}$	$b \times 10^{13}$
N1	30	90	0.3	1.002	1.93	33.0	22.0	4.26	3.45	15.66	6.02
N2	30	90	0.3	1.009	2.01	36.3	25.13	2.98	2.88	9.14	6.38
N3	30	90	0.3	1.008	1.97	32.7	24.0	3.74	3.6	10.06	6.02
N4	30	90	0.3	1.002	1.8	32.9	25.0	2.84	2.75	7.95	7.23
N5	30	90	0.25	1.006	3.35	23.9	31.0	2.89	2.69	4.99	12.05
N6	30	90	0.2	1.009	2.79	23.8	15.23	2.62	2.5	5.45	3.08
N7	30	90	0.4	1.006	3.18	24.3	13.43	4.74	3.68	5.77	6.02
N8	30	90	0.2	1.009	2.82	28.2	20.0	2.49	2.08	6.81	6.02
N9	30	120	0.3	1.014	2.13	48.6	47.42	3.57	3.42	3.13	1.58
N10	30	120	0.35	1.050	1.35	51.7	33.32	3.71	3.02	2.59	3.01
N11	90	180	0.3	1.043	1.85	38.0	27.94	0.9	0.89	0.49	3.01
N12	150	210	0.3	1.056	2.49	37.3	21.11	2.46	2.44	0.52	2.91
N13	210	300	0.3	1.035	2.42	36.4	21.29	1.29	0.89	0.27	3.01
N14	0	65	0.3	1.078	1.76	41.6	16.68	1.9	1.56	3.22	3.01

Table VI: Results obtained on a NiCo$_2$O$_4$ electrode (2) in 5M KOH analysed by a V.G. Anavac 2 mass spectrometer

Run no.	Wash Time S	Total lag Time S	I A	Background			Cell lag Time S	Enriched			
				Max. Signal	$k_n \times 10^{-2}$	Cell lag Time S		$x_T \times 10^{19}$	$y_T \times 10^{19}$	$a \times 10^{16}$	$b \times 10^{13}$
N15	30	90	0.3	1.012	2.16	32.0	25.94	5.34	3.15	5.78	0.96
N16	30	120	0.3	1.066	1.55	41.9	25.31	1.77	1.70	1.57	22.82
N17	30	150	0.3	1.037	1.55	47.7	18.35	1.94	1.79	1.35	1.21
N18	30	150	0.3	1.124	1.59	36.4	22.19	1.58	1.53	1.59	60.89
N19	30	90	0.5	1.022	1.74	37.7	30.87	3.95	3.89	2.86	1.81
N20	30	90	0.75	1.02	1.77	34.0	19.35	4.13	4.06	2.84	1.21

Fig. 7: Decrease in activity of a NiCo₂O₄ electrode in 5M KOH with oxygen evolution
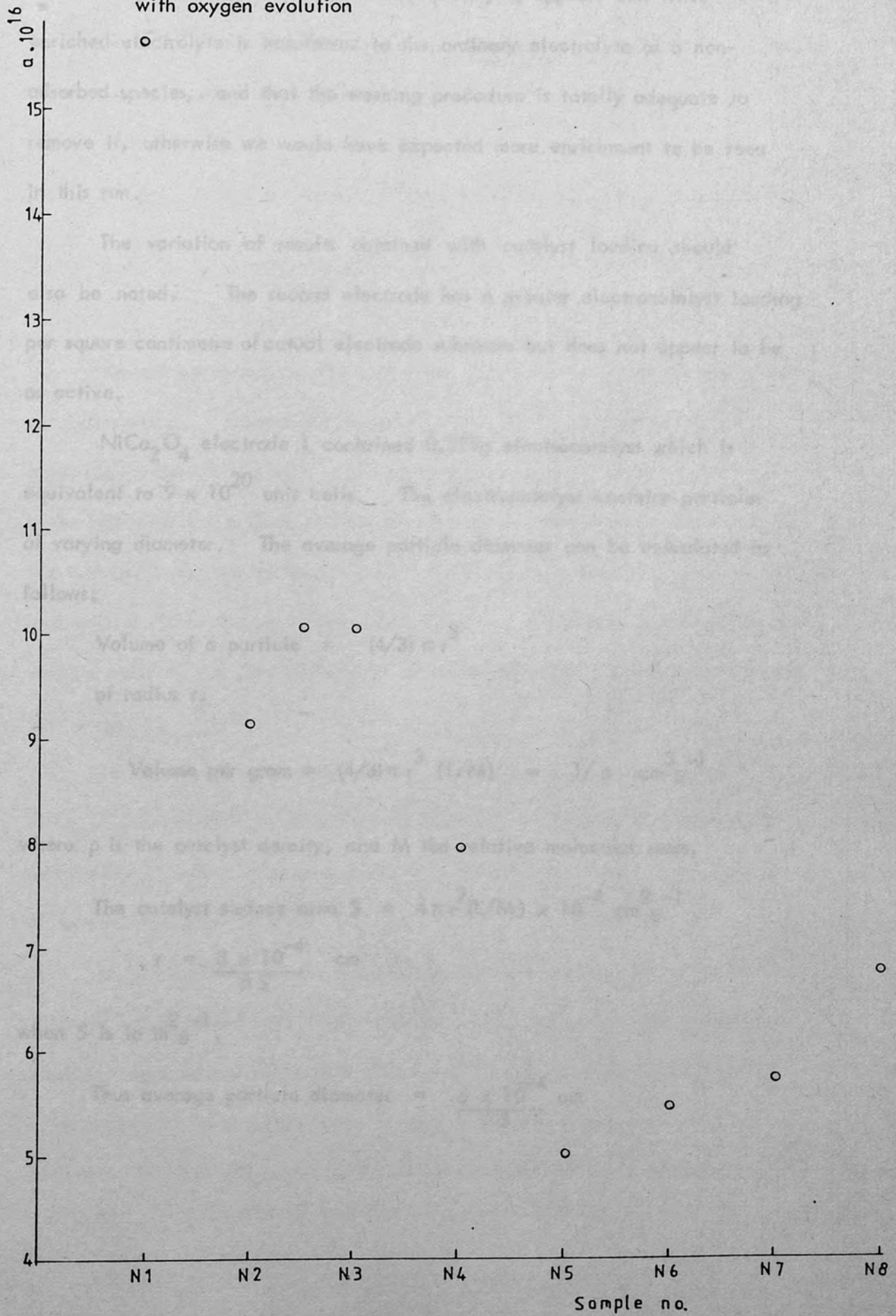
significantly from other values.   Consequently it appears that little

enriched electrolyte is transferred to the ordinary electrolyte as a non-

adsorbed species; and that the washing procedure is totally adequate to

remove it, otherwise we would have expected more enrichment to be seen

in this run.

The variation of results obtained with catalyst loading should

also be noted.   The second electrode has a greater electrocatalyst loading

per square centimetre of actual electrode substrate but does not appear to be

as active.

$NiCo_2O_4$ electrode 1 contained 0.379g electrocatalyst which is

equivalent to 9×10^{20} unit cells.   The electrocatalyst contains particles

of varying diameter.   The average particle diameter can be calculated as

follows:

Volume of a particle = $(4/3) \, \pi \, r^3$

of radius r.

Volume per gram = $(4/3) \pi \, r^3 \, (L/M)$ = $1/\rho \quad cm^3 g^{-1}$

where ρ is the catalyst density, and M the relative molecular mass.

The catalyst surface area S = $4 \pi \, r^2 (L/M) \times 10^{-4} \quad cm^2 g^{-1}$

$$r = \frac{3 \times 10^{-4}}{\rho \, S} \quad cm$$

when S is in $m^2 g^{-1}$.

Thus average particle diameter = $\dfrac{6 \times 10^{-4}}{\rho \, S} \, cm$

The $NiCo_2O_4$ electrocatalyst had a density of 6 g cm^{-3} and a surface area of 80m^2 g^{-1} determined on a powder sample by the BET method. This leads to an average particle diameter of 125 x 10^{-8} cm.

$NiCo_2O_4$ has the spinel structure with a cell edge of length 5.5 x 10^{-8} cm. Thus the fraction of unit cells at the surface of a particle,

$$f = 1 - \left[\frac{125 - 5.5}{125} \right] = 0.044$$

Hence approximately 4.4% of these unit cells are found at the electrocatalyst surface. Electrode 1 containing 9 x 10^{20} unit cells would be expected to have 3.9 x 10^{19} of these at the surface, which is in fairly good agreement with the number of sites used for oxide formation; determined by the isotopic technique as being (2.89 ± 1.08) x 10^{19}, assuming one site per unit cell. Surface area measurements detecting the charge passed during a voltage pulse in the potential region of oxide formation gave 2 x 10^{19} surface unit cells.

However, with a higher loading of electrocatalyst, in the case of $NiCo_2O_4$ electrode 2 which contained 0.5546g, a decrease in performance was noted. Surface area measurements gave this electrode a total number of surface sites of 0.94 x 10^{19}.

It can be seen that at lower electrocatalyst loadings the nickel mesh, although being coated with electrocatalyst, still retains the greater surface area of a mesh as compared to a planar surface. However as the loading is increased the holes in the mesh become filled and a denser coating is achieved, thus the utilisation of the electrocatalyst surface is lower at increased loading.

The coverage of the highest valent oxide (i.e. b) was consistently of the order of 10^{-6} of the number of sites for each electrode; in other words by the time the experiment was performed virtually none of the highest oxide remained. The average coverage of the intermediate oxide (i.e. a) was of the order of 0.1% of the number of sites. Assuming a simple first order process for the decrease in a with lag time before evolution of oxygen in the ordinary electrolyte, a graph of $\log (a/x_T)$ against lag time should be linear. (a/x_T) is the fractional coverage of this oxide. The relationship is shown in Fig. 8, from which a rate consistant for the decomposition of $0.005 \ s^{-1}$ is obtained. Extrapolating this line to zero time gives the initial coverage of $M^{18}OH$ in this case to be 0.005 of the total number of sites. The consequences of this low coverage in terms of reaction mechanism will be discussed in the next chapter in conjunction with the electrochemically determined parameters.

VIII.2.iii Lithiated cobalt oxide electrodes

The isotopic experiments were similarly performed on lithium doped cobalt oxide electrodes, of five different dopant levels. The results obtained on this group of electrodes are shown in tables VII, VIII and IX. On first viewing there seems to be little variation between the data in respect of the changing lithium content. However, this may well have been expected as the addition of lithium up to about 10% increases the conductivity of the catalyst and leads to a reduction in the oxygen overpotential. Thus having performed these experiments galvanostatically, one might anticipate similar results amongst these electrodes. Experiments performed potentiostatically may emphasise the differences amongst lithium dopant levels to a greater extent.

Fig 8: Graph of the variation in fractional coverage of the intermediate oxide (MOH) on a $NiCo_2O_4$ electrode with time lapsed at OCV, plotted as a first order process
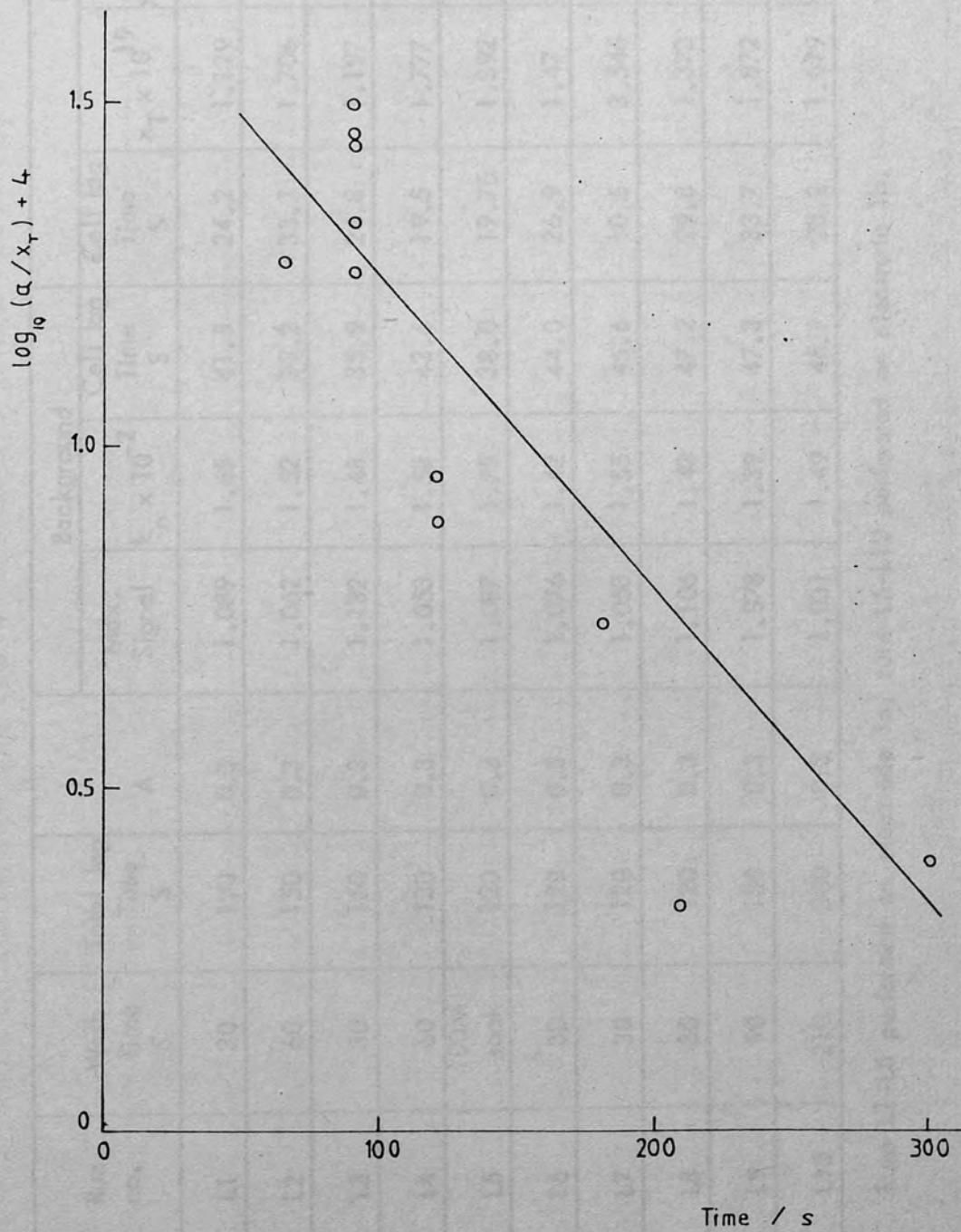
Table VII: Results obtained on a lithiated Co_3O_4 electrode (1) in 5M KOH analysed by a V.G. Anavac 2 mass spectrometer

Run no.	Wash Time S	Total lag Time S	I A	Background		Cell lag Time S	Cell lag Time S	Enriched			
				Max. Signal	$k_n \times 10^{-2}$			$x_T \times 10^{19}$	$y_T \times 10^{19}$	$a \times 10^{16}$	$b \times 10^{13}$
L1	30	120	0.3	1.089	1.65	41.5	24.2	1.129	1.031	1.41	6.023
L2	60	150	0.3	1.062	1.52	39.2	33.7	1.706	1.639	1.935	6.023
L3	30	150	0.3	1.132	1.48	35.9	24.8	1.197	1.149	1.429	6.023
L4	60	180	0.3	1.053	1.53	43.6	19.5	1.777	1.764	1.906	6.023
L5	100M soak	120	0.3	1.087	1.75	38.0	19.75	1.392	0.984	0.635	6.023
L6	30	120	0.3	1.076	1.42	44.0	26.9	1.47	1.407	1.56	12.17
L7	30	120	0.3	1.058	1.55	45.6	10.5	3.546	2.986	1.448	6.023
L8	30	120	0.3	1.106	1.43	47.2	29.8	1.373	1.263	1.043	19.58
L9	90	180	0.3	1.078	1.39	47.3	33.7	1.872	1.702	0.994	1.807
L10	210	300	0.3	1.031	1.49	46.7	28.2	1.019	0.715	0.624	6.023

Runs L1–L5 performed on electrode 1a, runs L6–L10 performed on electrode 1b.

Table VIII: Results obtained on a lithiated Co_3O_4 electrode (2) in 5M KOH analysed by a V.G. Anavac 2 mass spectrometer

Run no.	Wash Time S	Total lag Time S	I A	Background			Enriched				
				Max. Signal	$k_n \times 10^{-2}$	Cell lag Time S	Cell lag Time S	$x_T \times 10^{19}$	$y_T \times 10^{19}$	$a \times 10^{16}$	$b \times 10^{13}$
L11	30	90	0.3	1.031	2.27	37.8	15.9	1.825	1.694	0.784	6.023
L12	30	105	0.3	1.061	1.92	36.9	31.8	1.611	1.326	1.181	6.023
L13	30	120	0.3	1.149	1.29	42.4	25.5	1.259	1.174	1.740	6.023
L14	60	120	0.3	1.060	1.41	47.8	33.8	1.142	1.008	1.173	6.023
L15	30	125	0.3	1.061	1.93	42.2	25.0	1.040	0.9855	0.964	1.807
L16	180	270	0.3	1.075	1.42	44.6	26.4	2.658	2.420	0.670	6.023
L17	30	120	0.3	1.084	1.34	41.1	18.6	1.738	1.719	1.310	6.023
L18	90	210	0.3	1.052	1.37	44.1	32.0	2.505	2.134	1.438	6.023
L19	30	120	0.3	1.124	1.54	58.0	38.9	1.343	0.726	1.278	6.023
L20	60	180	0.3	1.049	1.40	56.0	25.9	1.828	1.459	0.712	6.023
L21	90	210	0.3	1.061	1.42	54.5	34.3	2.614	1.622	0.599	1.205

Runs L11–L16 performed on electrode 2a, runs L17–L21 performed on electrode 2b.

Table IX: Results obtained on a lithiated Co_3O_4 electrode (3) in 5M KOH analysed by a V.G. Anavac 2 mass spectrometer

Run no.	Wash Time S	Total lag Time S	I A	Background			Enriched				
				Max. Signal	$k_n \times 10^{-2}$	Cell lag Time S	Cell lag Time S	$x_T \times 10^{19}$	$y_T \times 10^{19}$	$a \times 10^{16}$	$b \times 10^{13}$
L22	30	120	0.3	1.085	1.51	44.0	25.1	1.863	1.653	1.826	6.023
L23	30	120	0.3	1.103	1.39	50.7	27.5	1.406	1.406	1.193	6.023
L24	30	120	0.3	1.092	1.41	43.2	38.0	0.936	0.9	0.934	6.023
L25	90	180	0.3	1.057	1.56	42.0	30.0	1.8	1.56	0.783	6.023
L26	30	210	0.3	1.057	1.56	44.2	27.7	1.389	1.200	1.308	6.023

The disappearance of the enriched surface species with delay time, prior to evolution of oxygen in the ordinary electrolyte, was noted. Similarly to results obtained on $NiCo_2O_4$ electrodes, virtually none of the highest oxide species remained by the time the experiment was performed after the washing procedure. Table X lists the range of values determined for x_T and y_T, the number of surface cells calculated from controlled potential coulometry experiments, n_T, the electrocatalyst loading and the percentage of lithium present in each electrode.

The latter was determined on an atomic absorption spectrometer operating in the emission mode. The lithium in these electrodes can be present in the form of free or bound lithium. The free lithium is soluble in dilute acetic acid at $60^\circ C$ and thus can be readily removed before dissolution of the bound lithium in concentrated nitric acid.

It was found that by increasing the temperature of the acetic acid, higher lithium concentrations were determined. It is possible that lithium contained in the lattice may start dissolving in addition to the free lithium. Whilst this was not found in the case of Li-doped nickel oxide,[76] it may well be that nickel oxide has a stronger lattice than Co_3O_4 and thus the effect may alter. If the effect of temperature on the amount of lithium determined in acetic acid were investigated more thoroughly, a point of inflexion in this curve may well occur at the point when the lattice starts to dissolve. This would indicate the temperature at which the analysis may be run without incurring dissolution of bound lithium also.

From Table X it appears that not every surface unit cell is active for higher oxide formation under these conditions. It will now be left

Table X   Data from ^{18}O enrichment experiments on lithiated Co_3O_4 electrodes

Electrode	Number of surface cells, $n_T \times 10^{19}$	Number of experiments	Number of intermediate oxide sites	
			$x_T \times 10^{19}$	$y_T \times 10^{19}$
1.5% Li/Co_3O_4 (3)	9.1	5	1.5 ± 0.3	1.3 ± 0.3
3.5% Li/Co_3O_4 (1a)	6.7	5	1.4 ± 0.3	1.3 ± 0.3
4.3% Li/Co_3O_4 (2a)	6.2	6	1.6 ± 0.5	1.4 ± 0.5
5.0% Li/Co_3O_4 (2b)	5.6	5	2.0 ± 0.5	1.5 ± 0.5
8.0% Li/Co_3O_4 (1b)	3.5	5	1.9 ± 0.9	1.6 ± 0.8

until the next chapter to consider these results in more detail with regard

to the oxygen evolution mechanism.

VIII.3.   Voltage measurements

VIII.3.i.   Nature and stability of the oxides on platinum

The potentials associated with the formation of the oxides of platinum,

measured against a hydrogen electrode in the same solution are, PtO 0.98V,

PtO_2 1.05V, and PtO_3 $2.0V^{32}$.   The stable form of the oxide in the

presence of oxygen is PtO_2.   There is some doubt about the exact potential

of the formation of PtO_3[32,103]   but it is known to decompose to PtO_2 and

oxygen.

Figure 9 shows the fall in open circuit potential with time on a platinised

platinum electrode in 0.5M H_2SO_4 at 25°C.   Pretreatment of this electrode

consisted of a five minute period of cathodic reduction at 250 mA, followed

by fifteen minutes of oxygen evolution at 25°C.   The fall in potential with

time was recorded on cessation of the current in two situations.   Firstly,

the electrode was removed and washed according to the usual procedure of the

isotopic experiments, before reinsertion in the electrolytic cell and the potential

decay monitored;   secondly, with the electrode remaining in the cell after the

current had been switched off.   Little difference was noted between the two

potential decay curves.   After 105 minutes the potential had only fallen

to 1.229V which is still above the potential for the formation of PtO_2.   This

voltage decrease presumably follows the decay of the species $PtO_2.OH$,

decomposing to PtO_2.   The very fact of the extended time period required

for this decomposition suggests that the species is comparatively stable.

Perhaps we should also consider the form of the highest oxide species,

Fig 9: Potential (vs DHE) of the platinum electrode in 5M KOH. Fall in open circuit potential of cell purged with nitrogen (dashed line). The continuous line shows effect of removal of electrode from the cell for 90s and washing in distilled water.

Time / s

Potential / V
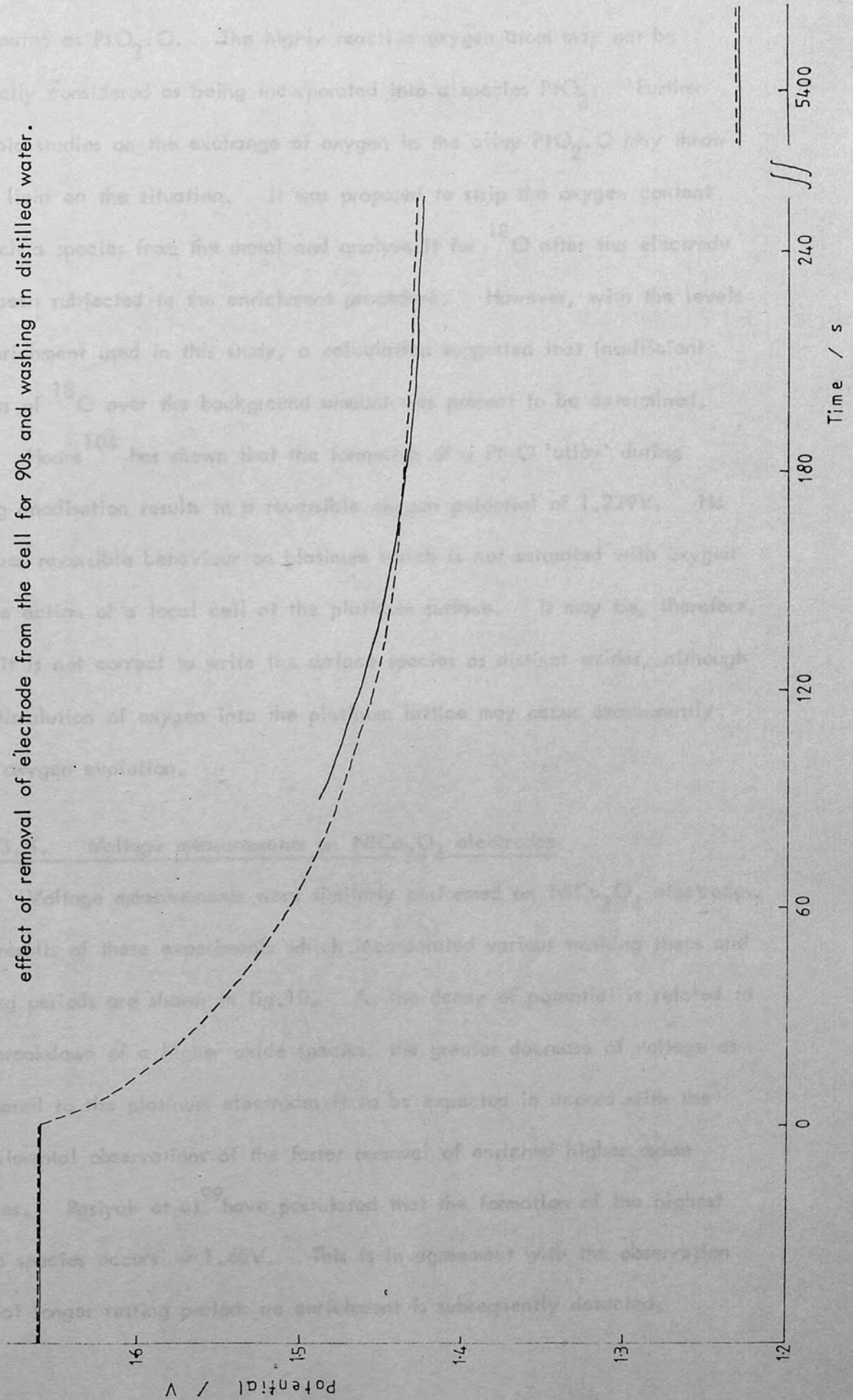
designated as $PtO_2.O$.   The highly reactive oxygen atom may not be

correctly considered as being incorporated into a species PtO_3.   Further

isotopic studies on the exchange of oxygen in the alloy $PtO_2.O$ may throw

more light on the situation.   It was proposed to strip the oxygen content

of such a species from the metal and analyse it for ^{18}O after the electrode

had been subjected to the enrichment procedure.   However, with the levels

of enrichment used in this study, a calculation suggested that insufficient

excess of ^{18}O over the background amount was present to be determined.

Hoare[104] has shown that the formation of a Pt-O 'alloy' during

strong anodisation results in a reversible oxygen potential of 1.229V.   He

ascribes reversible behaviour on platinum which is not saturated with oxygen

to the action of a local cell at the platinum surface.   It may be, therefore,

that it is not correct to write the surface species as distinct oxides, although

the dissolution of oxygen into the platinum lattice may occur concurrently

with oxygen evolution.

VIII.3.ii.   Voltage measurements on $NiCo_2O_4$ electrodes

Voltage measurements were similarly performed on $NiCo_2O_4$ electrodes.

The results of these experiments which incorporated various washing times and

resting periods are shown in fig.10.   As the decay of potential is related to

the breakdown of a higher oxide species, the greater decrease of voltage as

compared to the platinum electrodes is to be expected in accord with the

experimental observations of the faster removal of enriched higher oxide

species.   Rasiyah et al.[99] have postulated that the formation of the highest

oxide species occurs $\backsim$ 1.45V.   This is in agreement with the observation

that at longer resting periods no enrichment is subsequently detected.

VIII.5.III.   Voltage measurements on Lithiated Co₃O₄ electrodes

These electrodes showed a similar trend to the NiCo₂O₄ electrodes,
with a much more rapid decay in potential on open circuit than was noted
for the platinum electrodes.

Fig 10: Potential (vs DHE) of NiCo₂O₄ electrode in 5M KOH.   Continuous line shows open circuit
potential of electrode in cell purged with nitrogen prior to current pulse of 250mA after 90s.
(– – –) shows effect of removing the electrode from cell for 30 s.   (–·––·–) shows effect of
removing electrode from cell for 90s, followed by 60s immersion prior to current pulse.
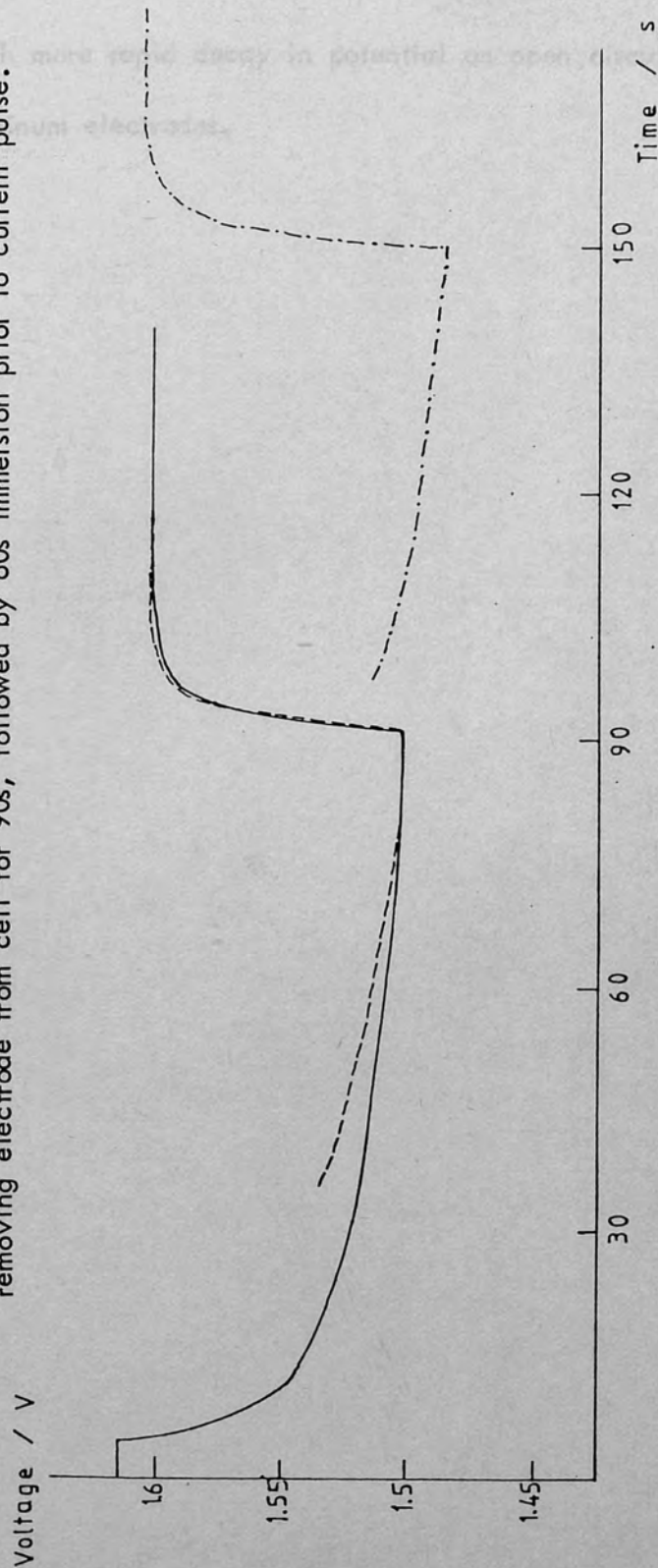
VIII.3.iii.   Voltage measurements on lithiated Co_3O_4 electrodes

These electrodes showed a similar trend to the $NiCo_2O_4$ electrodes, with a much more rapid decay in potential on open circuit than was noted for the platinum electrodes.

CHAPTER IX

Further discussion of the results of the oxygen isotopic experiments

The results obtained from the oxygen isotopic experiments on various electrode materials have been presented in the previous chapter and discussed individually.   It is the purpose of this chapter to consider some points that were applicable to all substrates utilised and to look at the relevance of these results to current theories of oxygen evolution.

IX.1   Residual ^{18}O in the surface

It was found that in all cases, on each type of electrode, after the electrode had been removed from the enriched electrolyte, whatever the time period elapsed (practically this was not less than three minutes), no higher oxide species ($M^{18}O$) remained in the surface, i.e. b=0.   Such an oxide is considered to be an unstable species which is only formed at high anodic potentials and decomposes by the reaction
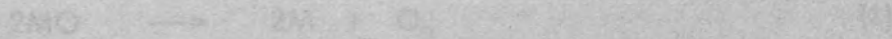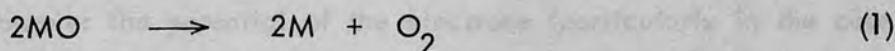
$$2MO \longrightarrow 2M + O_2 \qquad (1)$$

Its lifetime on removing the anodic potential would be short, in accordance with the experimental findings.

In the absence of any mechanism which removes $M^{18}OH$, the initial amount of this species in the surface (i.e. a) should be equal to the level of enrichment of the enriched electrolyte.   The values for a found in experiments throughout this work were many times less than this figure. This loss of $M^{18}OH$ may be postulated as being due to one or more of several mechanisms.

1.   Many workers[59] believe that the first water discharge step is rate determining and thus all subsequent steps can only proceed at the rate of

this step.   It thus seems possible that as soon as the adsorbed hydroxyl

species is formed by water discharge, the subsequent processes, namely the

highest oxide species formation and ultimately decomposition of two of these

highest oxide species to evolve oxygen would then take place so rapidly,

that effectively as soon as the lower oxide (MOH) species is formed it is

removed by further reactions.

It should also be considered that the very fact of there being such

a lack of an enriched oxide surface species may confirm a rate determining

step that occurs early in the process.

2.   A chemical decomposition step for the removal of $M^{18}OH$ may also

be considered such as:

$$2MOH \longrightarrow MO + M + H_2O \tag{2}$$

$$2MO \longrightarrow 2M + O_2 \tag{1}$$
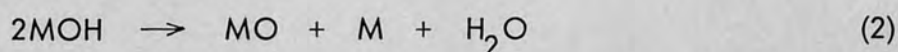
However the potential of the electrode (particularly in the case of

platinum) some minutes after the cessation of evolution of oxygen and in a

nitrogen purged solution is well above the ultimate steady state potential.

Thus the chemical decomposition of the intermediate oxide, MOH, is

relatively slow and would not cause the observed loss of $M^{18}OH$.

3.   Exchange of ^{18}O with an underlying oxide layer may be facile but

if the evolution of oxygen takes place on a metal surface, any oxide formed

should have the isotopic content of the enriched solution.

4.   Exchange of ^{18}O with the electrolyte may be possible.   Reaction

between the intermediate oxide, MOH, and adsorbed water by proton hopping,

$$M^{18}OH + M^{16}OH_2 \longrightarrow M^{18}OH_2 + M^{16}OH \tag{3}$$
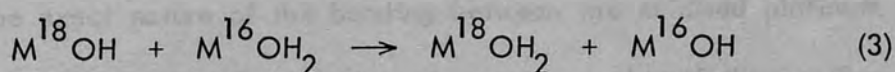
would diminish adsorbed $M^{18}OH$.

5.   It is possible, as Laitenen and Enke[105] have suggested, that evolution of oxygen, whilst being preceded by oxide formation as a necessary requirement, occurs via unstable adsorbed intermediates on the strongly bound oxide layer.   The former mechanism that they suggest regarding oxygen evolution on a bare platinum surface would seem unlikely to contribute to the oxygen evolution reaction as above about 1.0V, PtO must be present at the surface.   However the latter mechanism which takes this into account may be summarised as follows.

The formation of a surface oxide layer on platinum takes place by

$$Pt + H_2O \rightleftharpoons Pt \ldots OH + H^+ + e \qquad (4)$$
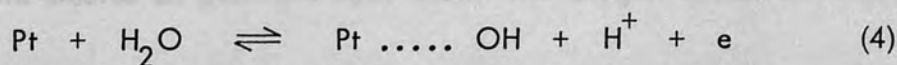
this species being converted to a surface oxygen atom which is more firmly held by,

$$Pt \ldots OH \longrightarrow PtO + H^+ + e \qquad (5)$$
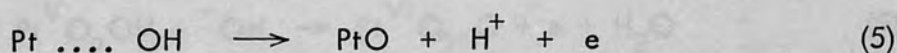
The formation of an oxygen evolution intermediate adsorbed on a PtO surface, at which the PtO bonds are not disrupted then occurs by

$$PtO + H_2O \longrightarrow Pt^0 \ldots OH + H^+ + e \qquad (6)$$
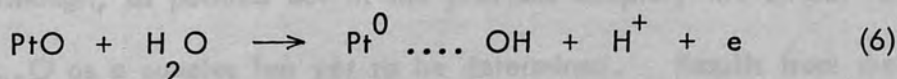
where Pt^0 represents the platinum oxide surface.

This is followed by,

$$Pt^0 \ldots OH + H_2O \rightarrow Pt^0 \ldots OOH + 2H^+ + 2e \qquad (7)$$

$$Pt^0 \ldots OOH \longrightarrow PtO + H^+ + e + O_2 \qquad (8)$$
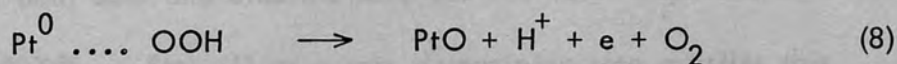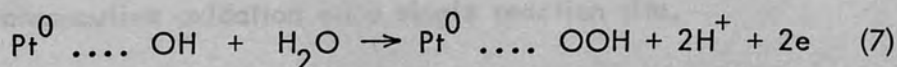
Thus further oxidation of the platinum surface only occurs when oxygen is being evolved concurrently.

The exact nature of the bonding between the oxidised platinum surface and the adsorbed intermediates is not clear, but if the bonding is

such that the platinum atom changes its valence state, then the mechanism that has been postulated in this work is followed.

6.   It is conceivable that more than one mechanism may operate in the process of oxygen evolution.   It has been fairly conclusively proved that formation of the highest oxide species is required, but a second mechanism could occur using this surface as a substrate.

IX.2   Mechanism of oxygen evolution on platinum

In agreement with the mechanism postulated by Iwakura et al,[102] the isotopic studies on platinum have shown the oxygen evolution reaction to follow

$$Pt^{IV}O_2 + {}^-OH \longrightarrow Pt^{V}O_2OH + e \tag{8}$$

$$Pt^{V}O_2OH + {}^-OH \rightarrow Pt^{VI}O_2.O + e + H_2O \tag{9}$$

$$2Pt^{VI}O_2.O \longrightarrow 2Pt^{IV}O_2 + O_2 \tag{10}$$
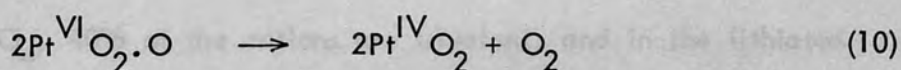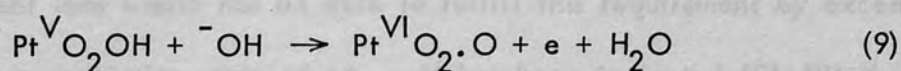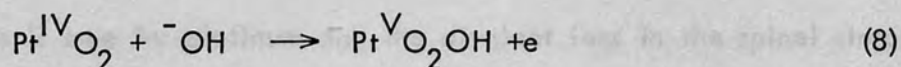
Although, as pointed out in the previous chapter, the actual form of $Pt^{VI}O_2.O$ as a species has yet to be determined.   Results from the isotopic experiments have shown that the number of sites generating the higher oxides $Pt^{V}O_2OH$ and $Pt^{VI}O_2O$ were the same, which is consistent with the consecutive oxidation on a single reaction site.

In both acid and alkaline solutions the Tafel slope has been found to equal $2RT/F$.   Step (1) as a rate determining step satisfies this requirement, which is also in agreement with the lack of detection of a higher oxide species, as discussed in section IX.1.

IX.3.   Mechanism of oxygen evolution on spinels

The situation in this case is more complicated than that found for platinum.   The results of the isotopic experiments show similarly that the oxygen evolution reaction follows a stepwise mechanism.

$$M^N + {}^-OH \longrightarrow M^{N+1}OH + e \tag{11}$$

$$M^{N+1}OH + {}^-OH \longrightarrow M^{N+2}O + H_2O + e \tag{12}$$

$$2M^{N+2}O \longrightarrow 2M^N + O_2 \tag{13}$$
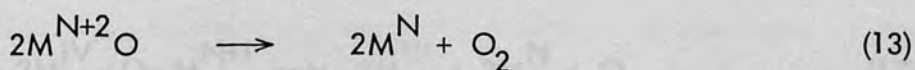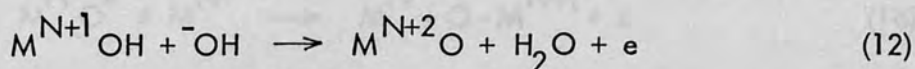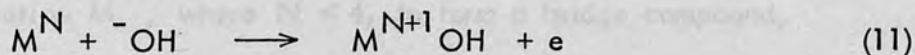
Here the mechanism is based on the assumption that the initial valence state of the metal may be increased by two during the reaction. Whilst this is true for platinum and the divalent ions in the spinel structure, the trivalent ions would not be able to fulfill this requirement by exceeding the maximum oxidation state of +4.   It has been indicated (Ch III) that in $NiCo_2O_4$, 40% of the cations are trivalent, and in the lithiated cobalt oxides, the proportion of trivalent cations may vary between 67 and 83%, assuming that all the lithium dopant enters the tetrahedral sites.[129] The tetrahedral site preference of the lithium ion is justified by,

1.   the ionisation potential of Co^{3+} (53 eV) being greater than that of Co^{2+} (33.5 eV).

2. Co_2O_3 being resistant to lithium doping: the resistivity of Co_2O_3 was not lowered on sintering with 10 at % lithium in the form of lithium hydroxide.

A mechanism involving a bridge structure has been postulated by Tseung and Rasiyah[130] as a means of oxygen evolution on a trivalent cation site, M^{III}.   Thus,

$$M^{III} + OH^- \longrightarrow M^{IV}OH + e \tag{14}$$

$$M^{IV}OH + {}^-OH \longrightarrow M^{IV}O^- + H_2O \tag{15}$$
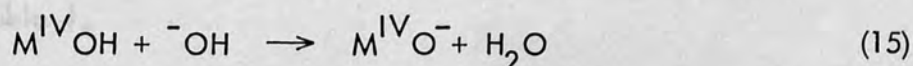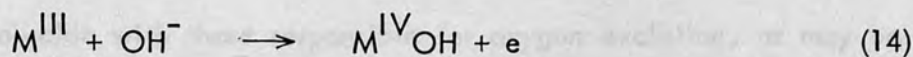
For the reaction to continue, the species $M^{IV}O^-$ may react with another cation M^N, where $N < 4$, to form a bridge compound,

$$M^{IV}O^- + M^N \longrightarrow M^{IV} - O - M^{N+1} + e \tag{16}$$
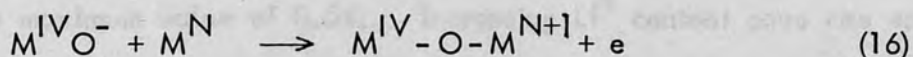
with subsequent oxygen evolution, according to

$$2M^{IV} - O - M^{N+1} \longrightarrow 2M^{III} + 2M^N + O_2 \tag{17}$$
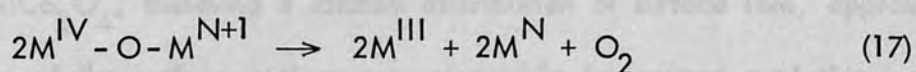
If the formation of the bridge intermediate is the rate determining step (16), an experimental Tafel stage of 40 mV decade^{-1} would be expected at low coverage of $M^{IV}O^-$. This was found to be the case at low over-potentials on $NiCo_2O_4$ electrodes. At higher potentials ($>1.6v$) the greater Tafel slope observed may be explained by equation (14) being rate determining. This implies a low coverage of MOH, in agreement with the observed initial coverage of MOH (a), which was found to be around 0.5% of the total number of sites.

On lithiated Co_3O_4 electrodes the Tafel slope found is consistent with the bridge mechanism if equation (15) is rate determining at low coverage. The kinetic analysis of the isotopic enrichment experiments does still hold for the mechanism of equations (14) to (17) if the coverage of intermediates is low, when the values of x_T and y_T represent the number of sites producing $M^{IV}OH$ and $M^{IV}O^-$ respectively. Experimentally, equality of x_T and y_T is found, in agreement with this mechanism.

On these materials, it was found that the number of surface cells which may be oxidised, as determined by controlled potential coulometry,

did not coincide with those responsible for oxygen evolution, as may be seen in table 1.

The fraction of oxygen evolution sites per formula unit at the surface for two $NiCo_2O_4$ electrodes was 1.5 and 2.8. However for the five lithiated Co_3O_4 electrodes the fraction was a function of the Li^+ content and had a maximum value of 0.54. Increasing Li^+ content gave rise to an increasing utilization of surface cells for oxygen evolution. In the case of $NiCo_2O_4$, assuming a random distribution of surface ions, approximately two of the surface cations are responsible for oxygen evolution. These could be two cobalt ions or two octahedrally coordinated ions. In either case a divalent ion takes part in the reaction. On lithiated Co_3O_4 the increasing fraction of sites responsible for oxygen evolution with increasing Li^+ doping shows the importance of tetrahedrally coordinated Co^{3+}, which fraction is increased by Li^+ doping. In the spinel lattice the tetrahedral ions lie at the surface and are available to interact with other species.

IX.4   Sensitivity of technique

In this work on platinum electrodes, an enrichment of $\sim 10^{16}$ atoms was determined. The lower level for the enrichment, (a), was found experimentally to be approximately 10% of the normal abundance of ^{18}O of the total number of sites, (x_T). For $x_T = 3.58 \times 10^{19}$ sites, the limit would be 7.30×10^{15} atoms. If the evolution of oxygen occurred from an electrolyte containing no ^{18}O, several orders of magnitude would be added to the sensitivity.

Table I   Data from the ^{18}O enrichment experiments on spinels

Electrode	no. of surface cells $n_T \times 10^{19}$	no. of intermediate oxide sites, $x_T \times 10^{19}$	x_T/n_T
$NiCo_2O_4$ (1)	2.0	2.9 ± 1.0	1.5
$NiCo_2O_4$ (2)	0.9	3.1 ± 1.4	2.8
1.5% Li/Co_3O_4	9.1	1.5 ± 0.3	0.16
3.5% Li/Co_3O_4	6.7	1.4 ± 0.3	0.21
4.3% Li/Co_3O_4	6.2	1.6 ± 0.5	0.26
5.0% Li/Co_3O_4	5.6	2.0 ± 0.5	0.36
8.0% Li/Co_3O_4	3.5	1.9 ± 0.9	0.54

PART 4

APPLICATION OF THE ISOTOPIC TECHNIQUE TO OTHER SYSTEMS

CHAPTER X

Isotopic Experiments in the hydrogen-deuterium system

X.1 Introduction

This chapter gives a brief background to the hydrogen evolution reaction and discusses the synergistic effect exhibited by platinized hydrogen tungsten bronzes. The kinetic equations are derived and an experimental method for following hydrogen evolution by means of a deuterium tracer is described. Results for hydrogen evolution on both platinum and platinized hydrogen tungsten bronze electrodes are discussed.

X.2 Theory of the hydrogen evolution reaction

This reaction has been the most thoroughly investigated of all the electrodic processes but the mechanism has still not been totally clarified. The reaction is influenced by many factors, but in the majority of cases the only intermediate is the adsorbed hydrogen atom on the metal surface.

The first step in the evolution of hydrogen must be the neutralisation of the hydrogen ion, represented by

$$H^+ + e \rightleftharpoons H \tag{1}$$

In fact, H^+ does not exist in aqueous solution and in reality is present as the hydroxonium ion. These are only present in sufficient quantities in acidic solution, the reaction taking place being

$$H_3O^+ + e + M \rightleftharpoons M\ldots H + H_2O \tag{2}$$
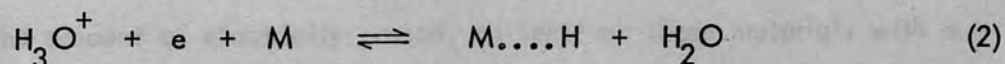
In neutral or alkaline solutions water is the available source of protons, the discharge of water molecules yielding adsorbed hydrogen ions,

$$H_2O + e + M \rightleftharpoons M\ldots H + {}^-OH \tag{3}$$

This step is proposed to be rate determining by Erdey-Gruz and Volmer.[106] They concluded that due to large differences between calculated and experimental Tafel slope values, hydrogen atoms can only accumulate on the electrode to a very small extent during hydrogen evolution. In this case the rate is limited by charge transfer from the metal to ions in solution. Hydrogen ions carried by the current do not undergo immediate neutralisation, but are first localised in the double layer on the side closer to the metal surface. Therefore they increase the charge on the double layer and the potential across it, giving rise to the overvoltage.

Whether the hydrogen potential is due to adsorbed hydrogen atoms or hydrogen ions awaiting neutralisation in the double layer can be determined experimentally by measuring the variation in overpotential as a function of the amount of electricity taken by the electrode immediately after switching the current on. If hydrogen atoms are the cause of overpotential, then the overpotential should increase logarithmically with hydrogen atom concentration as predicted by Nernst. If, however, it is due to hydrogen ions, increasing the charge on the double layer should cause the overpotential to vary linearly with the amount of electricity passed. Bowden and Rideal,[107] and Erdey-Gruz and Kromocy[108] have shown by oscillographic measurements that the overpotential varies linearly with the amount of electricity passed, at least on those materials with a Tafel slope of approximately 0.12V. Thus Erdey-Gruz and Volmer[106] concluded that this neutralisation step was rate determining.

Horiuti and Okamoto[109] stated that in certain cases, for instance on mercury and platinum electrodes, the primary product of electron transfer may be an H_2^+ ion,

$$2H_3O^+ + e \longrightarrow H_2^+ + 2H_2O \tag{4}$$
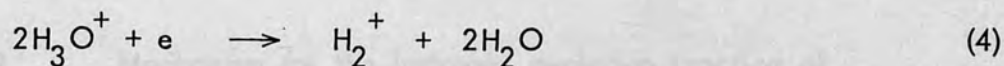
The activated complex is formed by the adsorption of hydrogen atoms on the surface, and its properties depend on the nature of the metal and the state of the surface. This adsorption step is fast and thus does not influence the overall rate; it is usually incorporated into the electron transfer step in mechanistic analyses.

Hydrogen molecules are finally formed by either direct combination of adsorbed hydrogen atoms

$$2M\ldots H \longrightarrow H_2 + 2M \tag{5}$$

or by electrochemical desorption.

$$M\ldots H + H_3O^+ + e \longrightarrow M + H_2 + H_2O \tag{6}$$
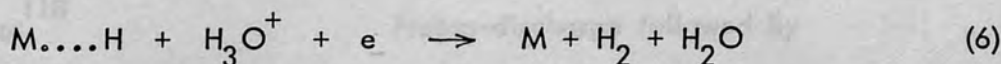
According to Tafel[110] the former step, equation (5), is rate-determining. The latter, equation (6), is thought to be rate controlling by Heyrovsky[111]. However, both these theories lead to calculated Tafel slopes which differ from the experimental results.

It has been found by experiment that none of the above alternatives is universally true, but that the mechanism and rate determining step are functions of the nature of the metal, surface conditions, bond strength of hydrogen on the substrate, etc. Even the removal of molecular hydrogen from the electrode surface by diffusion has been suggested to be rate determining by Hull and Lewis,[112] if the catalytic activity of the electrode is high. Today the point has come when the mechanism of hydrogen evolution on several substrates can be stated with a high degree of confidence, particularly in acidic solution. Some examples are given in Table 1.

Table 1   Mechanism for the hydrogen evolution reaction of

various metals in acidic solution

Metal	Mechanism
Mercury[113]	Proton-discharge rate determining
Lead[114]	followed by electrodic desorption
Nickel[115]	Proton-discharge followed by
Silver[116]	rate-determining electrodic desorption
Gold[117]	
Platinum[118]	Proton-discharge followed by
Palladium[119]	rate-determining chemical desorption

X.3   Synergism in hydrogen evolution on platinized tungsten trioxide

Platinum supported on tungsten trioxide has been shown to exhibit

a synergistic effect in the electrochemical oxidation of hydrogen by Hobbs

and Tseung.[120,121,122]   Abbaro, Tseung and Hibbert[123] have also

studied hydrogen evolution on platinized tungsten trioxide in acid medium,

and their results show the existence of a synergistic effect.   They

postulate a simple reaction scheme to exhibit this effect.   Normal gaseous

hydrogen evolution occurs via

$$Pt + H^+ + e \longrightarrow PtH \qquad\qquad (7)$$

$$2PtH \longrightarrow 2Pt + H_2 \qquad\qquad (8)$$
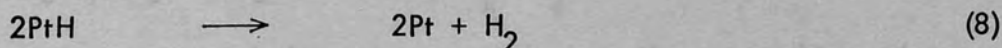
A route via the platinized hydrogen tungsten bronze follows

$$xPtH + WO_3 \longrightarrow xPt + H_xWO_3 \tag{9}$$

$$H_xWO_3 \longrightarrow {}^x/_2 H_2 + WO_3 \tag{10}$$
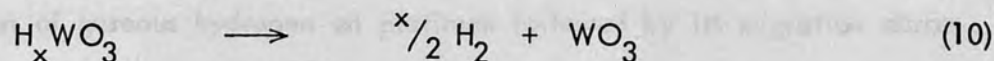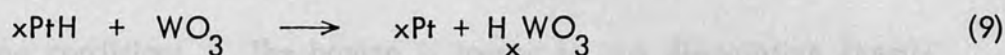
The tungsten bronze may decompose via reaction (10) or act as an

hydrogen evolution catalyst itself.

However, Vertes and Horanyi[124,125] disagree with these theories,

and claim that tungsten trioxide is an inactive support for the hydrogenation

of p-nitrophenol on platinum. They feel that if the support is to play

an active role, the rates of reactions (9) and (10) must at least be comparable

with those of the parallel processes (7) and (8). They consider this unlikely

due to the slowness of the diffusion of hydrogen through the solid phase and

the establishment of an effectively reversible redox equilibrium in reaction

(10). This equilibrium would be required to have an exchange current

several orders of magnitude higher than that of hydrogen evolution on

platinum for the rate of reaction (10) to exceed that of reaction (8). It

was hoped that the application of the isotopic technique to this system

may provide conclusive evidence one way or the other, as regards this

effect.

Tungsten trioxide is postulated[123] as functioning as an active support

due to reaction between hydrogen atoms and tungsten trioxide, giving a

conducting hydrogen tungsten bronze, H_xWO_3 ($0 < x < 1$).

Such compounds belong to a general class of non-stoichiometric

mixed oxides of the general formula $A_xM_yO_z$, M being a transition metal

and M_yO_z its highest binary oxide. A represents another metal or

hydrogen, and x is within the limits of zero and one. Blue H_xWO_3 bronzes are usually formed whenever tungsten trioxide is exposed to reducing conditions. The bronze is formed by the dissociative chemi-sorption of gaseous hydrogen on platinum followed by its migration across the metal/oxide interface.[126] The migration is aided by the presence of an adsorbed water layer when an exchange mechanism operates. Bronze oxide characteristics include chemical inertness and metallic conduction of electricity.[127] The hydrogen compounds are typical members of this class of compounds, except that they are sensitive towards oxidising conditions which reconvert them to the parent oxide. It has recently been shown[128] that the rate of adsorption of gaseous hydrogen by tungsten trioxide to form non-stoichiometric bronzes is promoted by the presence of platinum.

X.4 Theory of the isotopic experiments applied to the hydrogen evolution reaction

X.4i Hydrogen evolution on a platinum surface

Hydrogen evolution on platinum occurs by the chemical recombination of adsorbed hydrogen atoms. Thus in the enriched electrolyte (i.e. deuterated solution) for the process of hydrogen evolution we have,

$$D_3O^+ + e + Pt \underset{}{\overset{k_1^1}{\rightleftharpoons}} Pt....D + D_2O \qquad (11)$$
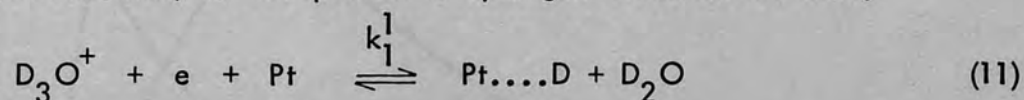
and in ordinary solution,

$$H_3O^+ + e + Pt \underset{}{\overset{k_2^1}{\rightleftharpoons}} Pt....H + H_2O \qquad (3)$$
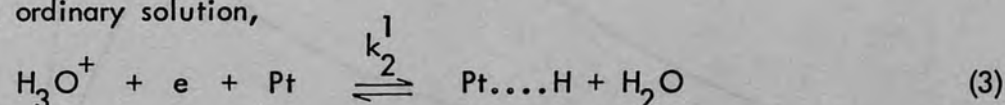
Due to the availability of 100% deuterated solution, this process has the advantage that no hydrogen atoms should be adsorbed on the electrode surface during enrichment in D_2O. Additionally, because of the very

low levels of D_2O present in ordinary water, there is a negligible background composition. Therefore when an electrode containing a surface coverage of a M....D species, generated by deuterium evolution from a deuterated solution, is introduced into a cell containing ordinary electrolyte, the three possible reactions for cathodic gas evolution on passage of current are,

$$Pt....D + Pt....D \xrightarrow{k_D} 2Pt + D_2 \qquad (12)$$

$$Pt....D + Pt....H \xrightarrow{k_{HD}} 2Pt + HD \qquad (13)$$

$$Pt....H + Pt....H \xrightarrow{k_H} 2Pt + H_2 \qquad (14)$$
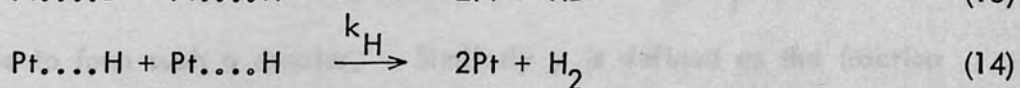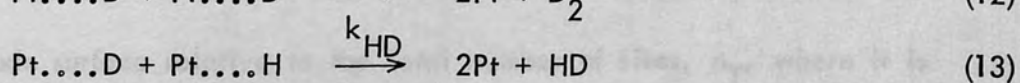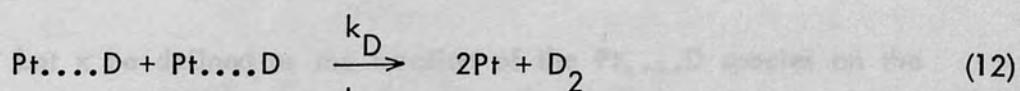
Obviously there is only a finite amount of the Pt....D species on the electrode surface, so a profile of the gas evolved on passage of current would appear as follows:
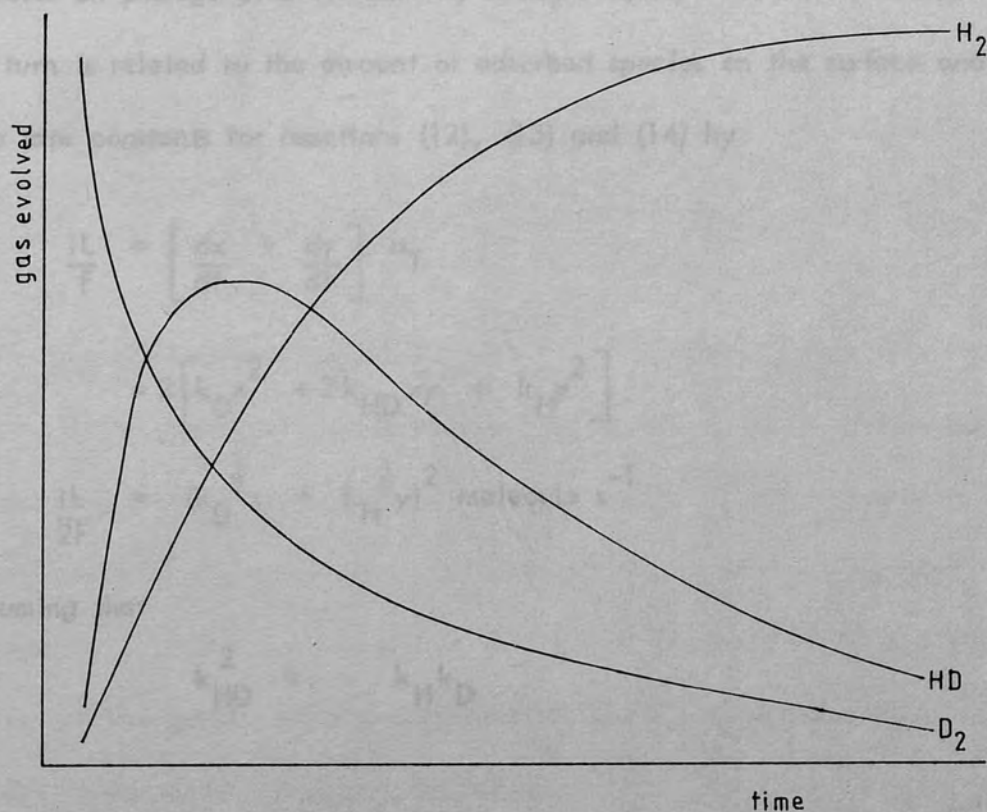
The D_2 species would disappear fairly quickly as hydrogen atoms replace deuterium atoms on the electrode surface, and deuterium atoms would become more likely to combine with hydrogen atoms to form HD as the fraction of hydrogen atoms increases. In time though, as all the deuterium atoms are removed, hydrogen evolution becomes the dominant process.

Let x be defined as the fraction of the Pt....D species on the electrode surface relative to the total number of sites, n_T, where it is possible to form such a species. Similarly y is defined as the fraction of Pt....H species on the surface relative to the total number of sites. As these quantities both represent fractional numbers, they are therefore dimensionless.

According to Faraday's Law, the rate of formation of gaseous species on passage of a current iA, is equal to iL/F atom s^{-1}. This in turn is related to the amount of adsorbed species on the surface and the rate constants for reactions (12), (13) and (14) by

$$\frac{iL}{F} = \left[\frac{dx}{dt} + \frac{dy}{dt} \right] n_T \tag{15}$$

$$= 2 \left[k_D x^2 + 2 k_{HD} xy + k_H y^2 \right] \tag{16}$$

$$\frac{iL}{2F} = (k_D^{\frac{1}{2}} x + k_H^{\frac{1}{2}} y)^2 \text{ molecule } s^{-1} \tag{17}$$

assuming that

$$k_{HD}^2 = k_H k_D \tag{18}$$

Hence,

$$y = \frac{(iL/2F)^{\frac{1}{2}} - k_D^{\frac{1}{2}}x}{k_H^{\frac{1}{2}}} \qquad (19)$$

The rate of removal of adsorbed deuterium is $-n_T(dx/dt)$ atom s^{-1}.

Therefore,

$$n_T\frac{dx}{dt} = -2k_Dx^2 - k_{HD}xy - k_{-1}x \qquad (20)$$

$$= -2k_Dx^2 - k_{-1}x - k_{HD}x\left[\frac{(iL/2F)^{\frac{1}{2}} - k_D^{\frac{1}{2}}x}{k_H^{\frac{1}{2}}}\right] \qquad (21)$$

$$= -k_Dx^2 - k_{-1}x - (iLk_D/2F)^{\frac{1}{2}}x \qquad (22)$$

Hence,

$$\frac{dx}{dt} = -\frac{k_Dx^2}{n_T} - \frac{x}{n_T}(k_{-1} + (iLk_D/2F)^{\frac{1}{2}}) \qquad (23)$$

Solution of this equation (Appendix AIII) gives

$$x = B/\left[(A + B/a)e^{Bt} - A\right] \qquad (24)$$

Where $A = \dfrac{k_D}{n_T}$ $\qquad B = \dfrac{\sqrt{\dfrac{iLk_D}{2F} + k_{-1}}}{n_T}$

and a is the value of x at t = 0.

   In an experiment, the gases evolved at the electrode surface cannot be detected at this point, but some distance away, to where they may have been carried by a purging gas.   Experimentally the m/e = 4 signal (equivalent to D_2) was monitored in the manner discussed in the experimental section of the oxygen isotope work (Section VII.5).   The m/e signal was related to the surface coverage as follows.

If the evolved gas and a purge gas expand into a fixed volume which

may accommodata n moles of an ideal gas at a total rate of v mole s^{-1},

the rate at which D_2 is evolved is equal to the rate of evolution of gases

multiplied by the square of the fraction of the Pt....D species on the

surface.   The rate at which it is removed is equal to the rate at which

all gases flow through (v) multiplied by the fraction which is deuterium

(n_D/n) where n_D is the number of deuterium atoms.   Thus,

$$\frac{dn_D}{dt} = \frac{k_D x^2}{L} - \frac{n_D}{n} v \quad s^{-1} \tag{25}$$

where x is given by equation (24).   This becomes

$$\frac{dn_D}{dt} = \frac{k_D a^2 B^2}{L((Aa + B) \exp (Bt) - aA)^2} - \frac{v}{n} n_D \tag{26}$$

If the rate of the back reactions are negligible compared to the rate

of the forward reactions which are driven by the current, and if $(Aa + B)^2$

$>> (aA)^2$, equation (26) becomes

$$\frac{dn_D}{dt} = \frac{k_D a^2 B^2}{L(Aa + B)^2 \exp (2Bt)} - \frac{v}{n} n_D \tag{27}$$

which has the solution (see Appendix AIV)

$$n_D = \frac{k_D a^2 B^2 \left[\exp(-2Bt) - \exp(-vt/n)\right]}{L(Aa + B)^2 (v/n - 2B)} \tag{28}$$

The mass spectrometer signal of m/e = 4 (D) is proportional to the fraction

of deuterium in the volume at constant pressure

$$D = \frac{K(n_D)}{n} \tag{29}$$

where K is the constant of proportionality.

X.4.ii   Relative volumes of deuterium evolved

In addition, an alternative method of determining relative volumes of
deuterium evolved was employed.   This used the m/e = 4 signal output directly
from the mass spectrometer.   The area under such a graph as a function of time
was proportional to the volume of deuterium evolved.   For quantitative data,
calibration of the system would be required, i.e. known volumes of deuterium
would have to be detected by the mass spectrometer.   Such calibration was
not performed, but values of relative volumes of deuterium evolved were
determined for the various electrode compositions.   Results obtained in this
manner will be considered later in this chapter.

X.5   Experimental Technique

X.5i.   Electrodes

Platinized platinum electrodes supported on a platinum mesh and Teflon bonded platinized hydrogen tungsten bronze electrodes supported on lead were prepared as described in Chapter V.   Lead was chosen as the substrate for the latter type of electrodes due to its high hydrogen over-potential.[114]   The platinum composition in the tungsten bronze electrodes ranged from 0-0.75%, giving a total electrocatalyst loading of 0.06g cm^{-2}.

X.5ii.   Electrolyte

The electrolyte was composed of a 0.5M solution of anhydrous sodium sulphate (May and Baker) in doubly distilled water to form the ordinary electrolyte and in D_2O (99.9%) for the enriched electrolyte.

X.5iii.   Method

The experimental apparatus used was the same as that described in Chapter VII.2 for the oxygen isotope experiments.   A very similar experimental technique was used for this study.   Deuterium was evolved on the electrode in a cooled two compartment cell at constant current (usually 0.4A) for a fixed period of time.   This cell contained the deuterated electrolyte.   The electrode was removed, washed in distilled water for varying periods of time and introduced into the three compartment cell described previously, at open circuit voltage.   Nitrogen purging was maintained at a constant rate throughout the experiment.   When the m/e = 4 peak had reached a steady level, a constant current was passed through the cell (150-300 mA) by a Weir constant current supply.   The V.G.

Anavac-2 quadrupole mass spectrometer operating at 10^{-5}-10^{-6} mbar

continuously monitored the m/e = 4 signal, which was displayed on a

Y-t recorder.

A subsequent run was then performed on the electrode by reapplication

of the constant current, but on no occasion was any deuterium detectable.

This was an equivalent procedure to the background run performed in the

oxygen electrode experiments.

Experiments were also performed in which the "enrichment" was

carried out in ordinary electrolyte, prior to the electrode being washed

and introduced into the experimental cell connected to the mass spectro-

meter which also contained ordinary electrolyte.   On passage then of a

cathodic current, no deuterium could be detected.

After each run, the value of the m/e = 2 signal was determined.

This is the steady state value for hydrogen evolution under the particular

conditions, and was used as a normalising factor for the deuterium data.

A computer programme written in Fortran V fitted experimental data

to equation (29) by a least squares procedure, allowing calculation of the

unknown variables.

The surface area of the platinized platinum electrodes was determined

by the oxygen charging curve method;   those of the platinized hydrogen

tungsten bronze electrodes were estimated from the B.E.T. surface area

measurements of the respective electrocatalyst powders.

X.6   Results and Discussion

X.6i.   Platinized platinum electrodes

A fitted curve of a typical $m/e = 4$ signal from the mass spectrometer for a deuterium enriched platinized platinum electrode is shown in fig. 1, fitted to equations (28) and (29).   Each run was normalised to the background hydrogen signal ($m/e = 2$) to allow comparison of different experiments.   Figure 2 shows a curve for the background amount of deuterium, alongside an enriched deuterium curve for comparison.   The slight continued decrease in signal for this background run was probably caused by insufficient time being allowed for the enriched run to completely finish, and thus conditions had not quite reached the steady state.   The background run was determined as soon as possible after the enriched run to ensure that conditions were as similar as possible.

The variables for the system obtained from analysis of the output curves by the computer fitting routine are presented in Table 11.   The number of sites active for the process ($n_T = (5.2 \pm 2.8) \times 10^{19}$) was found to agree well with the value obtained by the surface area measurement technique (5.8×10^{19}).   The correspondance between these two values shows that for the low current densities used here, no extra sites become available for hydrogen evolution than exist at open circuit.

For a washing time of 30s after evolution in deuterated electrolyte a value for (v/n) of $0.023 \pm 0.003 \ s^{-1}$ was found from three experiments. A value of $0.009 \pm 0.003 \ s^{-1}$ was determined for the background evolution of hydrogen.   This figure is approximately half that determined for deuterium evolution, as would be predicted if the rate of diffusion to the mass spectrometer inlet depended on the square root of the molecular mass.

Fig. 1: Mass spectrometer signal for m/e 4 after the start of deuterium evolution on a platinised platinum electrode.
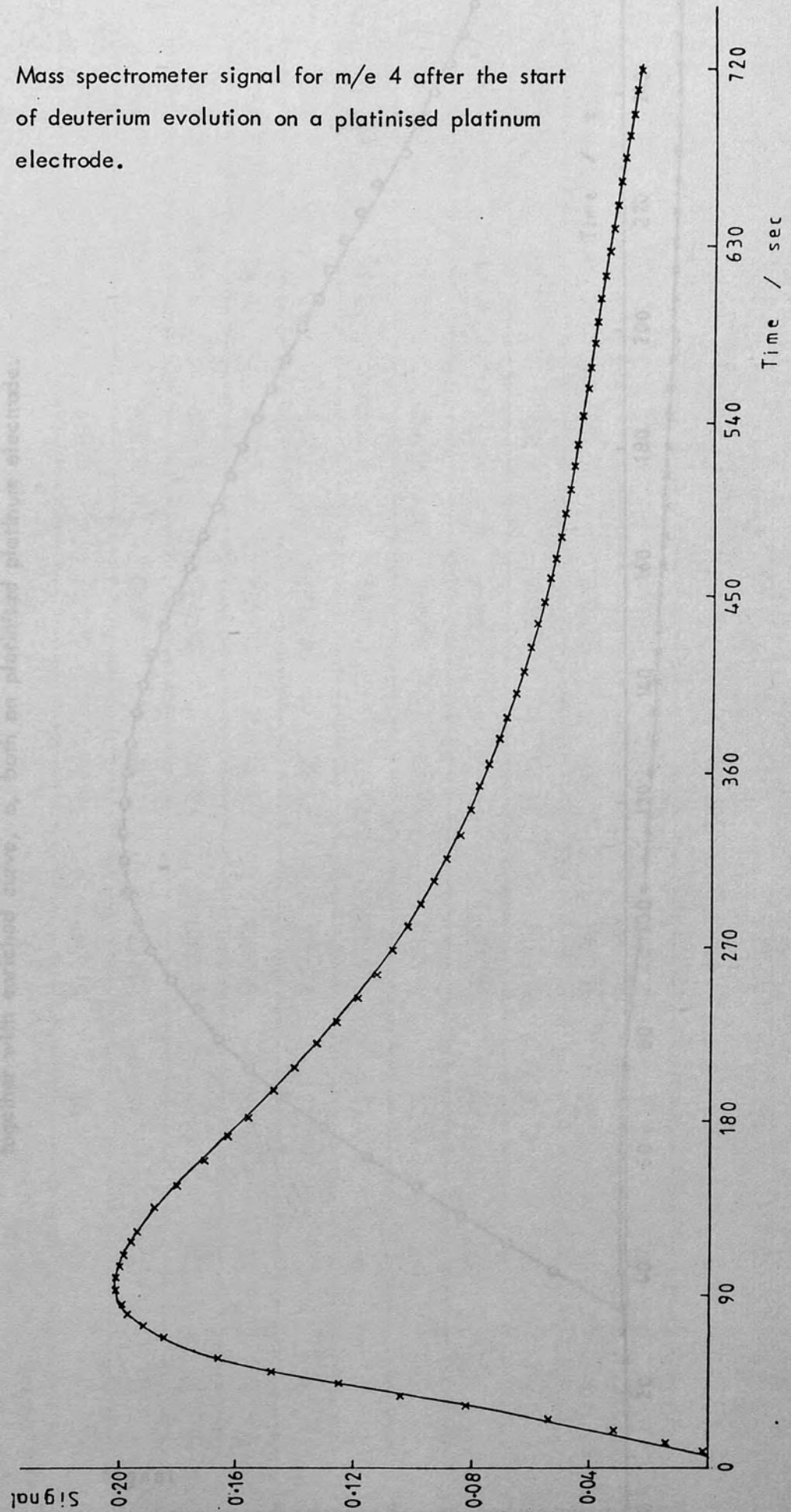
Fig 2: Mass spectrometer signal for m/e 4 for background component of deuterium, x, together with enriched curve, o, both on platinised platinum electrode.
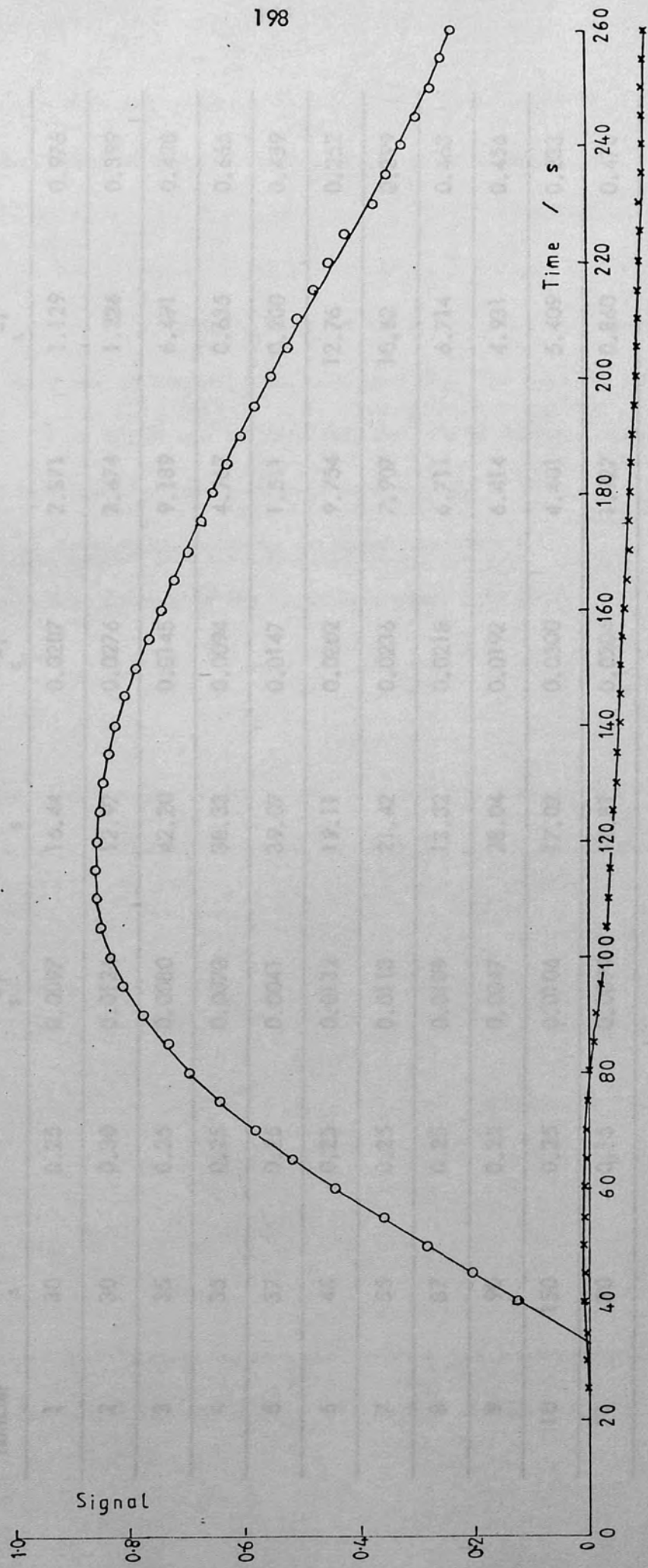
Table II   Deuterium evolution on a platinised platinum electrode

Electrode run number	Time lag after washing s	Current A	Background k_n s^{-1}	Time lag after current on s	Enriched k_n s^{-1}	$n_T \times 10^{19}$	$k_D \times 10^{17}$ atoms s^{-1}	a
1	30	0.25	0.0097	16.44	0.0207	2.871	1.129	0.976
2	30	0.30	0.0126	12.97	0.0276	2.474	1.226	0.399
3	35	0.25	0.0080	42.20	0.0145	9.189	6.491	0.428
4	35	0.25	0.0073	38.33	0.0094	4.767	0.635	0.665
5	37	0.25	0.0041	39.07	0.0147	1.511	0.200	0.459
6	45	0.25	0.0132	19.11	0.0202	9.754	12.76	0.252
7	55	0.25	0.0113	21.42	0.0236	7.907	10.62	0.399
8	87	0.25	0.0109	13.32	0.0218	6.711	6.714	0.463
9	90	0.25	0.0047	28.04	0.0192	6.414	4.931	0.456
10	150	0.25	0.0106	17.02	0.0300	4.401	5.409	0.233
11	30	0.15	0.0099	12.81	0.0204	1.927	0.860	0.470

The output data was additionally analysed by the alternative procedure, which assumed that the volume of deuterium detected was porportional to the area under the output trace (Fig. 1). Each curve was normalised to the background hydrogen signal (m/e = 2) to enable different runs to be compared. This data is listed in Table III, and Fig. 3 shows the decrease in amount of deuterium detected with lag time from the data of this table. From this it can be seen that the rate of disappearance of the deuterium from the electrode surface is fairly rapid.

Determination of the reaction order for deuterium evolution

Assuming that the rate of the reaction depends only on the concentration of deuterium, then

$$\frac{-dC}{dt} = kC^x \tag{30}$$

where C is the concentration of deuterium, k is the rate constant and x is the reaction order. With the condition that $C = C_0$ at $t = 0$, it follows that

$$\int_0^t k\,dt = -\int_{C_0}^{C} C^{-x}\,dC \tag{31}$$

Hence,

$$kt = \log_e(C_0/C) \quad \text{if } x = 1 \tag{32}$$

or

$$kt = \frac{(C_0^{-(x-1)} - C^{-(x-1)})}{x - 1} \quad \text{if } x \neq 1 \tag{33}$$

The time taken for half the reaction to occur can be measured as a function of the initial concentration. Thus equations (32) and (33) lead to

Table III Comparison of volume of deuterium evolved (by weight of area under deuterium evolution curve) with fitted values of initial amount of deuterium on the surface of the platinised platinum electrode

Electrode run number	Time lag after washing s	Current A	Volume of D_2 by area	Initial amount of D_2
1	30	0.25	0.478	0.976
2	30	0.30	0.383	0.399
3	35	0.25	0.526	0.428
4	35	0.25	0.569	0.665
5	37	0.25	0.916	0.459;
6	45	0.25	0.399	0.252
7	55	0.25	0.339	0.399
8	87	0.25	0.394	0.463
9	90	0.25	0.356	0.456
10	150	0.25	0.169	0.233
11	30	0.15		0.470
12	70	0.25	0.256	
13	120	0.25	0.245	
14	30	0.30	0.389	
15	35	0.25	0.498	
16	40	0.25	0.369	

Fig. 3: Decrease in amount of deuterium detected with lag time after washing on a platinised platinum electrode.
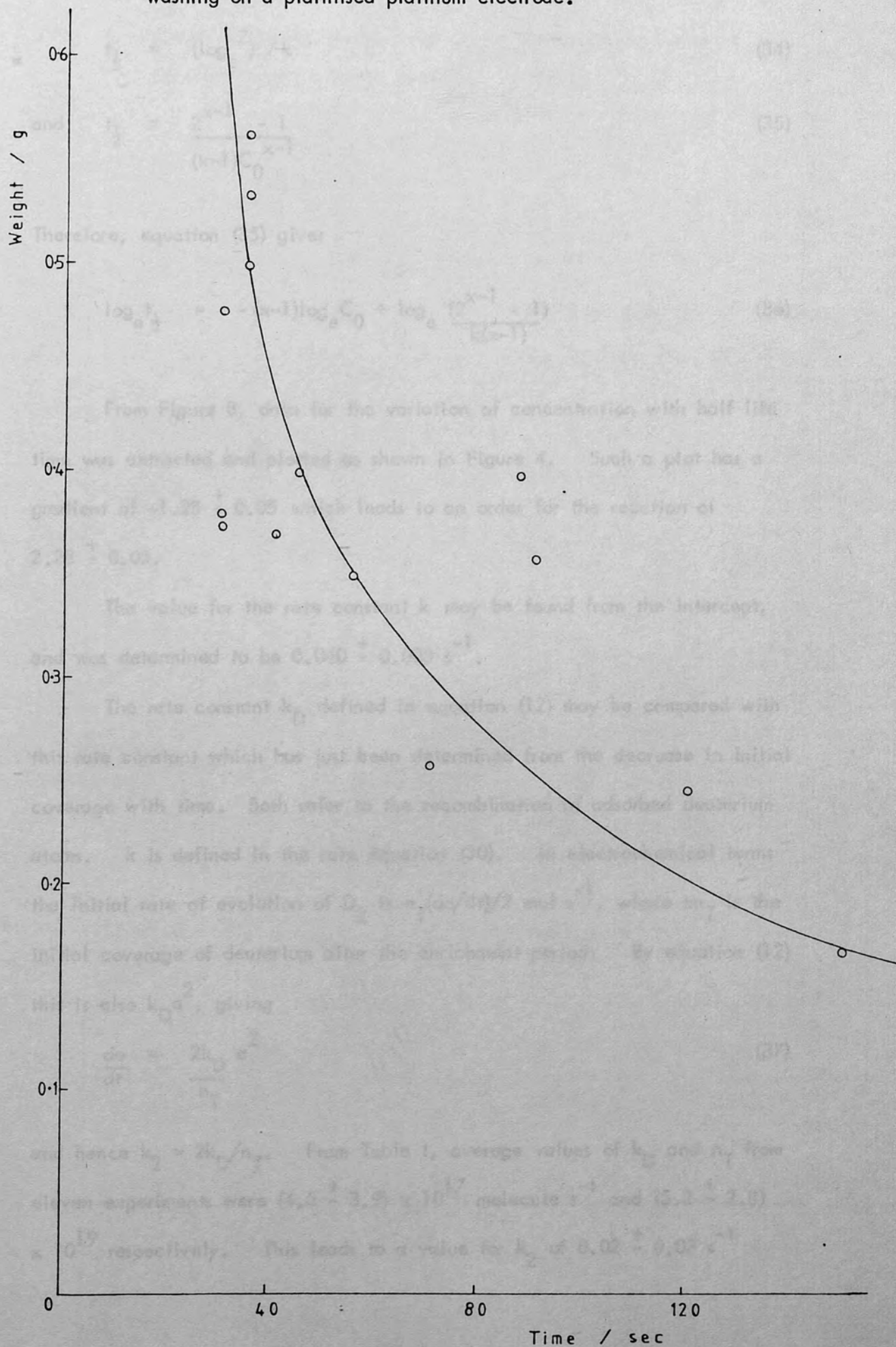
$$t_{\frac{1}{2}} = (\log_e 2)/k \tag{34}$$

$$\text{and} \quad t_{\frac{1}{2}} = \frac{2^{x-1} - 1}{(x-1)C_0^{x-1}} \tag{35}$$

Therefore, equation (35) gives

$$\log_e t_{\frac{1}{2}} = -(x-1)\log_e C_0 + \log_e \frac{(2^{x-1} - 1)}{k(x-1)} \tag{36}$$

From Figure 3, data for the variation of concentration with half life time was extracted and plotted as shown in Figure 4. Such a plot has a gradient of -1.28 ± 0.05 which leads to an order for the reaction of 2.28 ± 0.05.

The value for the rate constant k may be found from the intercept, and was determined to be $0.040 \pm 0.003 \ s^{-1}$.

The rate constant k_D defined in equation (12) may be compared with this rate constant which has just been determined from the decrease in initial coverage with time. Both refer to the recombination of adsorbed deuterium atoms. k is defined in the rate equation (30). In electrochemical terms the initial rate of evolution of D_2 is $n_T(da/dt)/2 \ mol \ s^{-1}$, where an_T is the initial coverage of deuterium after the enrichment period. By equation (12) this is also $k_D a^2$, giving

$$\frac{da}{dt} = \frac{2k_D a^2}{n_T} \tag{37}$$

and hence $k_2 = 2k_D/n_T$. From Table I, average values of k_D and n_T from eleven experiments were $(4.5 \pm 3.9) \times 10^{17}$ molecule s^{-1} and $(5.2 \pm 2.8) \times 10^{19}$ respectively. This leads to a value for k_2 of $0.02 \pm 0.02 \ s^{-1}$

Fig. 4:   Graph to determine the order of the deuterium evolution
reaction on a platinised platinum electrode.
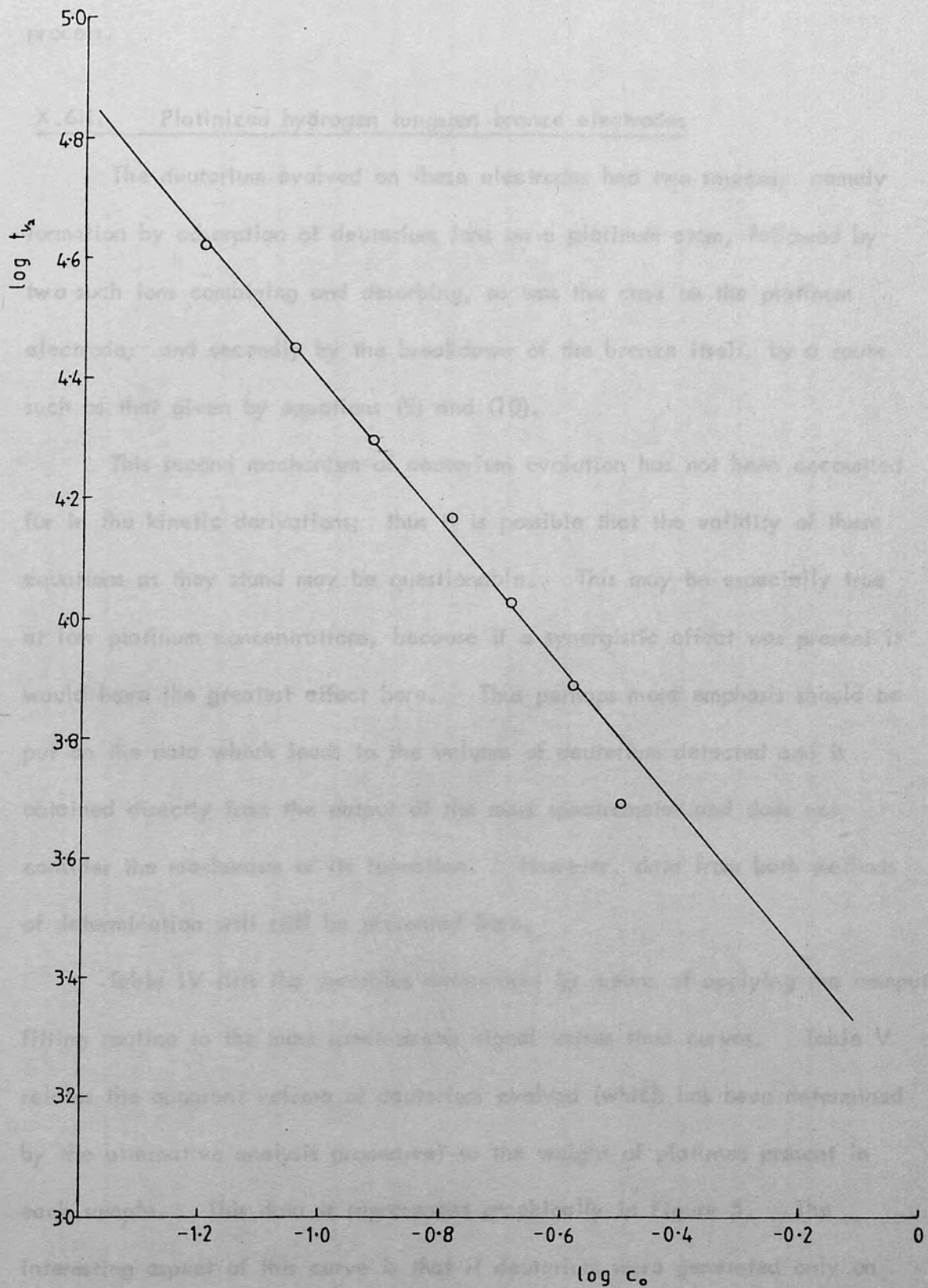
which includes the measured value of $0.04 \pm 0.003 \text{s}^{-1}$. These results

give two independent methods of determining the rate of recombination of

deuterium atoms at a metal surface in the course of an electrochemical

process.

X.6ii.   Platinized hydrogen tungsten bronze electrodes

The deuterium evolved on these electrodes had two sources; namely

formation by adsorption of deuterium ions on a platinum atom, followed by

two such ions combining and desorbing, as was the case on the platinum

electrode; and secondly by the breakdown of the bronze itself, by a route

such as that given by equations (9) and (10).

This second mechanism of deuterium evolution has not been accounted

for in the kinetic derivations; thus it is possible that the validity of these

equations as they stand may be questionable. This may be especially true

at low platinum concentrations, because if a synergistic effect was present it

would have the greatest effect here. Thus perhaps more emphasis should be

put on the data which leads to the volume of deuterium detected and is

obtained directly from the output of the mass spectrometer and does not

consider the mechanism of its formation. However, data from both methods

of determination will still be presented here.

Table IV lists the variables determined by means of applying the computer-

fitting routine to the mass spectrometer signal versus time curves. Table V

relates the apparent volume of deuterium evolved (which has been determined

by the alternative analysis procedure) to the weight of platinum present in

each sample. This data is represented graphically in Figure 5. The

interesting aspect of this curve is that if deuterium were generated only on

Table IV   Deuterium evolution on platinised hydrogen tungsten bronze electrodes

Electrode number	Time lag after washing s	Current A	Time lag after current on s	$k_n \times 10^{-3}$ s⁻¹	$n_T \times 10^{19}$	$k_D \times 10^{17}$ atoms s⁻¹	a	% platinum in electrode
W1	45	0.3	15.79	3.365	7.214	13.59	0.50	0.09
W2(1)	45	0.3	14.82	4.283	4.675	20.45	0.290	0.13
W2(2)	45	0.3	8.84	3.755	6.161	18.61	0.371	0.13
W3	45	0.3	17.44	3.735	4.017	5.03	0.221	0.25
W4	45	0.3	37.5	5.16	4.035	6.78	0.299	0.32
W5	45	0.3	18.54	8.085	6.513	2.12	0.207	0.40
W6(1)	45	0.3	16.1	3.83	7.329	13.66	0.264	0.56
W6(2)	45	0.3	25.1	2.96	4.84	3.66	0.291	0.56
W7	45	0.3	24.8	4.762	6.353	1.42	0.209	0.75
W8	45	0.3	19.6	5.35	4.60	24.23	0.299	0

Table V   Relationship between volume of deuterium evolved (by weight of area under deuterium evolution curve) to the weight of platinum present in each platinised hydrogen tungsten bronze electrode

Electrode number	Run number	% Platinum in electrode	Weight of platinum in electrode $g \times 10^{-2}$	Volume of D_2 evolved (by weight, g)	Volume of D_2 evolved per gram Pt
W1	1	0.093	0.0362	0.671	18.53
	2	0.093	0.0362	0.658	18.20
W2	1	0.127	0.0677	0.885	13.08
	2	0.127	0.0677	0.837	12.36
W3	1	0.25	0.1443	0.9039	6.26
W4	1	0.32	0.133	0.613	4.61
	2	0.32	0.133	0.549	4.12
W5	1	0.40	0.0806	0.399	4.95
	2	0.40	0.0806	0.502	6.23
W6	1	0.56	0.165	0.659	3.99
	2	0.56	0.165	0.876	5.30
	3	0.56	0.165	0.795	4.80
W7	1	0.75	0.308	0.641	2.08

Fig. 5:   Graph of the relationship between the volume of deuterium
evolved per gram of platinum present in the platinised
hydrogen tungsten bronze electrodes
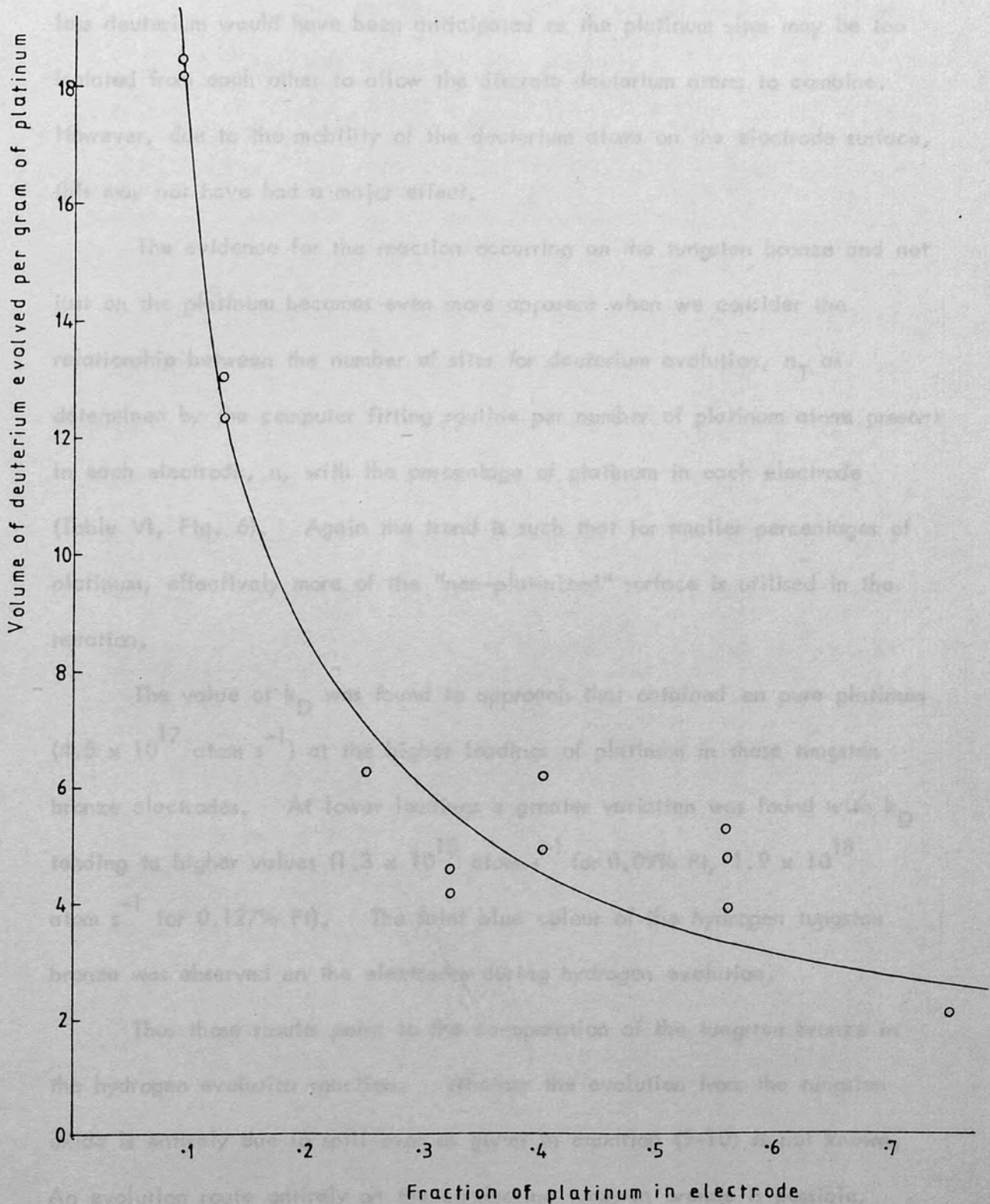
the platinum metal sites in the electrode, a linear relationship between the weight of platinum present and the apparent volume of deuterium evolved would have been expected. Additionally, at low concentrations of platinum perhaps less deuterium would have been anticipated as the platinum sites may be too isolated from each other to allow the discrete deuterium atoms to combine. However, due to the mobility of the deuterium atoms on the electrode surface, this may not have had a major effect.

The evidence for the reaction occurring on the tungsten bronze and not just on the platinum becomes even more apparent when we consider the relationship between the number of sites for deuterium evolution, n_T as determined by the computer fitting routine per number of platinum atoms present in each electrode, n, with the percentage of platinum in each electrode (Table VI, Fig. 6). Again the trend is such that for smaller percentages of platinum, effectively more of the "non-platinized" surface is utilised in the reaction.

The value of k_D was found to approach that obtained on pure platinum (4.5×10^{17} atom s^{-1}) at the higher loadings of platinum in these tungsten bronze electrodes. At lower loadings a greater variation was found with k_D tending to higher values (1.3×10^{18} atom s^{-1} for 0.09% Pt, 1.9×10^{18} atom s^{-1} for 0.127% Pt). The faint blue colour of the hydrogen tungsten bronze was observed on the electrodes during hydrogen evolution.

Thus these results point to the co-operation of the tungsten bronze in the hydrogen evolution reaction. Whether the evolution from the tungsten oxide is entirely due to spill-over as given in equation (9-10) is not known. An evolution route entirely on the conducting tungsten bronze is possible,

Table VI   Relationship between the number of sites for deuterium evolution, n_T determined using the computer fitting routine, per weight of platinum present in each platinised hydrogen tungsten bronze electrode

Electrode number	% platinum in electrode	Weight of platinum in electrode $g \times 10^{-2}$	Number Pt atoms in electrode $n \times 10^{18}$	$n_T \times 10^{19}$	n_T / n
W1	0.09	0.036	1.19	7.214	60.62
W2	0.13	0.067	2.09	5.418	25.92
W3	0.25	0.144	4.45	4.017	9.03
W4	0.32	0.133	4.11	4.035	9.82
W5	0.40	0.081	2.49	6.513	26.16
W6	0.56	0.165	5.09	6.085	11.95
W7	0.75	0.308	9.50	6.363	6.69

Fig. 6: Graph of the relationship between the number of sites for deuterium evolution per number of platinum atoms in the electrode, with percentage of platinum in the platinised hydrogen tungsten bronze electrodes.

$$e + H^+ + H_xWO_3 \longrightarrow H.H_xWO_3 \tag{38}$$

$$2H.H_xWO_3 \longrightarrow H_2 + 2H_xWO_3 \tag{39}$$
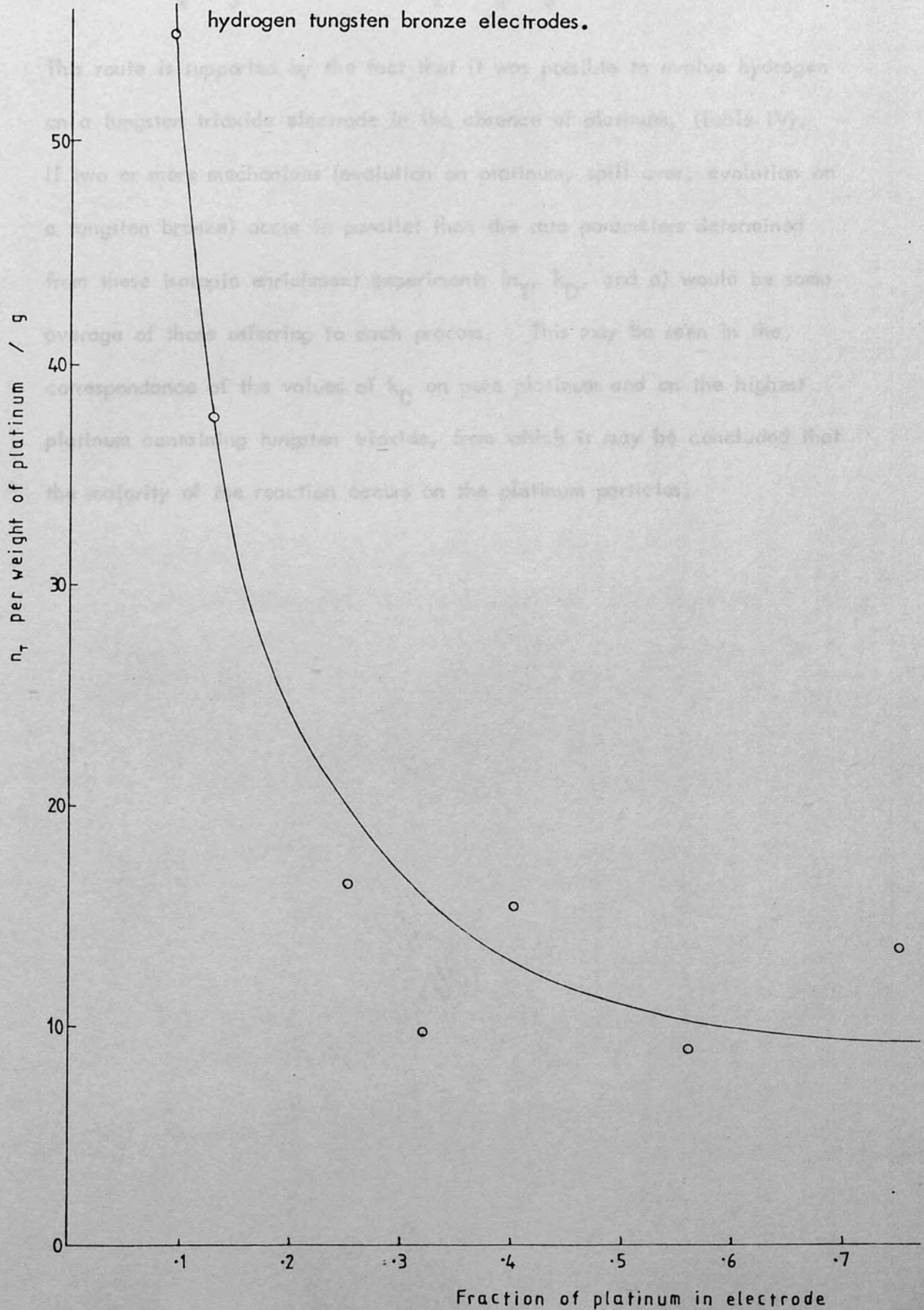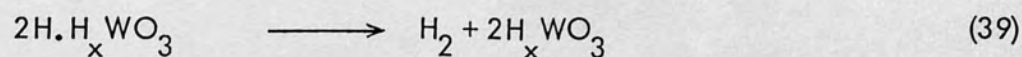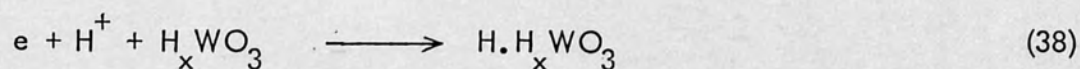
This route is supported by the fact that it was possible to evolve hydrogen on a tungsten trioxide electrode in the absence of platinum, (Table IV). If two or more mechanisms (evolution on platinum, spill over, evolution on a tungsten bronze) occur in parallel then the rate parameters determined from these isotopic enrichment experiments (n_T, k_D, and a) would be some average of those referring to each process. This may be seen in the correspondance of the values of k_D on pure platinum and on the highest platinum containing tungsten trioxide, from which it may be concluded that the majority of the reaction occurs on the platinum particles.

PART 5

CONCLUSIONS AND SUGGESTIONS FOR FURTHER WORK

214

CHAPTER XI

Conclusions and Suggestions for Further Work

XI.1   Conclusions

This work has developed a method to study the kinetics of the electrochemical evolution of gases; both the oxygen and hydrogen evolution reactions have been considered.   The oxygen evolution reaction is of particular importance in secondary metal air batteries and water electrolysis plants.   The electrodic evolution of hydrogen is a standard method of producing the gas, but it is an important reaction in many other respects. It is an unusual reaction in as much as the gas can be evolved upon many metals.   In the industrial production of D_2O, the process is based on the principle that hydrogen gas is evolved faster at the cathode than deuterium gas, which leaves a D_2O enriched solution.   The hydrogen evolution reaction plays an important part in the theory of the corrosion of metals in acidic solutions.   The rate of hydrogen evolution often determines the extent of corrosion of a metal, and thefore the stability of the metal surface.

For both the oxygen and hydrogen evolution reactions, the isotopic technique was first studied using a platinum electrode, as the majority of previous studies and hence, available data in the literature, referred to this substrate.   This work was then extended to more novel systems so as to gain an understanding of the mechanism of gas evolution on them.

The results have been discussed in some detail in the previous chapters, but it would seem worthwhile to mention the major facts revealed.

Firstly, for oxygen evolution on platinum the kinetics of the system in both acid and alkaline electrolyte were consistent with a mechanism '

which involved successive oxidations on a single platinum atom. The total number of platinum sites responsible for oxygen evolution was less than the total number of atoms at the surface but this may be explained by either the inability to form a further complete layer of oxygen on an already oxidised surface or that reaction between certain high oxide pairs may be unfavourable on certain crystal planes.

Oxygen evolution on the mixed oxide spinels followed either a multistep reaction at a single site or reaction via a bridged structure. The number of sites responsible for oxygen evolution increased with increasing Li^+ content in $Li_xCo_{3-x}O_4$, reaching a fraction of 0.53 of the total number of surface sites, confirming the importance of tetrahedrally co-ordinated Co^{3+} which was formed by Li^+ doping. Increasing the level of dopant not only improves the electrical conductivity of the electrocatalyst but also increases the number of trivalent cobalt cations present. In comparison, on $NiCo_2O_4$ approximately two of the surface cations per unit cell are responsible for oxygen evolution, and this must therefore include reaction involving a divalent ion.

An interesting aspect of the experiments on $NiCo_2O_4$ electrodes was the apparent decrease in activity of the electrodes with use. Coupled with this information we have the observation of the change in the cyclic voltammogram of a $NiCo_2O_4$ electrode on repeated cycling. The peak which eventually disappears from the cyclic voltammogram has been ascribed to a $M^{2+} \longrightarrow M^{3+}$ transition. On prolonged anodic polarisation oxygen penetration into the bulk may occur, leading to ordering in the lattice structure. The ionic distribution of $NiCo_2O_4$ has been shown to be[60]

$Co_{0.9}^{2+} Co_{0.1}^{3+} (Ni_{0.9}^{2+} Ni_{0.1}^{3+} Co^{3+}) O_{3.2}^{2-} O_{0.8}^{-}$. Thus on prolonged oxidation it may well be possible to effect a $Ni^{2+} \longrightarrow Ni^{3+}$ transition at the surface which is not readily reversible, by inclusion of oxygen ions within the lattice. This may also lead to a reduction in conductivity of the material, as this property is thought to depend on electron hopping between Ni^{2+} and Ni^{3+} sites.

In the deuterium evolution reactions, the number of sites responsible for this process on platinum was in agreement with those found from surface area measurements. The participation of tungsten trioxide as an active support for platinum allowing spill-over of hydrogen was confirmed from measurements of the number of sites and volume of deuterium evolved found for a series of platinum-tungsten trioxide electrodes.

Although the isotopic experiments following both oxygen and hydrogen evolution used a similar approach, there were several differences between the two systems. Practically, in many ways, the deuterium experiments were easier to perform than the oxygen experiments. Firstly, due to the lack of hydrogen in the air, the insertion of the electrode into the electrochemical cell connected to the mass spectrometer, did not introduce a background component to the signal. As the natural abundance of deuterium is low (0.015%) a background run was not necessary; in fact several background runs were performed, but a horizontal trace was recorded in all cases, as has been reported earlier. Thus the output signal for the enriched run could be interpreted as it appeared, without any necessary corrections having to be applied. Hence this alleviated the need to assume that conditions for the enriched and background runs were the same, as was necessary for the oxygen evolution experiments.

However, one disadvantage of the deuterium experiments was the rapid removal of deuterium species from the surface with washing time, prior to gas evolution in ordinary electrolyte. As would be expected, the surface species formed which could not be detected after five minutes washing, were found to be much less stable than their oxygen counterparts, which, particularly on platinum electrodes could still be detected after an hour had elapsed.

The kinetics of the deuterium system were also complicated by the fact that two enriched species, D_2 and HD, had to be considered, whereas because the concentration of ^{18}O used as $H_2^{18}O$ was low, the amount of $^{18}O^{18}O$ in the generated gas was considered to be negligible.

Additionally in the case of deuterium evolution on a platinised tungsten trioxide electrode, the kinetics were not adapted to consider the effect of deuterium generated by the breakdown of the bronze itself which would be necessary for a truly vigorous interpretation of the results. However the results obtained considering only the volume of deuterium detected clearly showed the existence of a synergistic effect. If deuterium were generated only on the platinum metal sites in the electrode, a linear relationship would be expected between the weight of platinum present and the volume of deuterium evolved. However a strong non-linear dependence was found, the effect being particularly marked at low concentration of platinum. Similar results were obtained by comparing the number of active sites present with the percentage of platinum in each electrode. It appeared that on the highest platinum containing tungsten trioxide electrode, the majority of the reaction occurs on the platinum particles. A similar use of tungsten trioxide as a support for iron

sulphide has been found to enhance the activity of the latter for hydrogen evolution in neutral solution.[131]

XI.2   Suggestions for further work

This work has developed an isotopic technique to study the oxygen evolution reaction and has presented many results of importance for elucidation of the mechanism.   There are, however, several ways in which the technique could be extended to generate extra useful information.

The use of potentiostatic rather than galvanostatic control would be enlightening.   This would lead to detailed information on the potential of formation of the relevant oxide species which participate in the oxygen evolution reaction.   It would be interesting, for instance, to hold the electrode in an enriched solution at a potential where the only anodic reaction is oxide formation.   Subsequent transfer of the electrode after washing to an ordinary electrolytic solution, whereupon a potential would be applied to it such that oxygen was evolved.   Monitoring of the gas formed would show the participation of the underlying oxide surface to oxygen evolution.

Although this isotopic technique has only been described for oxygen and hydrogen evolution, it could easily be extended to consider other gas evolution reactions.   For instance, we may consider chlorine evolution.   This reaction is the main industrial electrochemical process; the huge production of this gas today being caused by demand for alkyl chloride and in particular poly vinyl chloride.

Thermodynamically, oxygen evolution is favoured energetically rather than chlorine evolution, but the latter is favoured kinetically and

thus chlorine is obtained electrolytically.

On platinum, the mechanism is thought to be,[132]

$$Cl^-(aq) \longrightarrow Cl_{ads} + e \qquad (1)$$

$$2Cl_{ads} \longrightarrow Cl_2 \qquad (2)$$
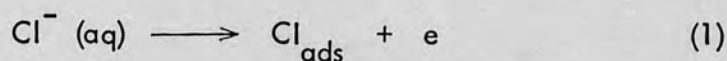
A detailed picture of the mechanism is not yet possible as the rate determining step is uncertain. It is thought that step (1) is rate determining at potentials greater than $1.42V$[133], with step (2) rate determining at lower potentials.[134]

However on other metals, such as iridium, step (3) may also occur,[133]

$$Cl_{ads} + Cl^-(aq) \longrightarrow Cl_2(aq) + e \qquad (3)$$
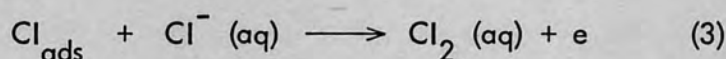
Cyclic voltammetric studies[135] have shown oxygen adsorption to be more and more hindered by increasing concentration of Cl^-. The reaction mechanism appears to change on increasing potential because of strongly varying coverage by adsorbed oxygen. At potentials above 2V, the reaction is likely to take place at a completely oxidised surface.[136]

If step (3) is important this could easily be demonstrated by forming an adsorbed layer of chloride ions of one isotope on the electrode, transferring this to an electrolyte containing chloride ions of another isotope, and monitoring the gas evolved on application of a current. No chlorine molecules in which both atoms consist of the "enriched" isotope should be detected if this step is important. Obviously the life of such a chloride intermediate would have to be considered before any set of experiments, but the system should lend itself to a kinetic analysis such as that described here for the oxygen and hydrogen evolution reactions.

To show that $y = \exp(-k_2 t)\left[\left(\dfrac{k_1 a}{k_2-k_1}\right)(\exp(k_2-k_1)t - 1) + b\right]$ (1)

is a solution of $dy/dt = k_1 x - k_2 y$ (2)

Rearranging equation (1) we have:

$y = \dfrac{k_1 a}{k_2-k_1} \cdot \exp(-k_1 t) - \dfrac{k_1 a}{k_2-k_1} \cdot \exp(-k_2 t) + b\exp(-k_2 t)$ (3)

Differentiating this equation with respect to time, leads to:

$\dfrac{dy}{dt} = \dfrac{-k_1^2 a}{k_2-k_1}\exp(-k_1 t) + \dfrac{k_1 k_2 a}{k_2-k_1}\exp(-k_2 t) - bk_2 \exp(-k_2 t)$ (4)

APPENDIXES

Now, with $x = a\exp(-k_1 t)$ (5)

$k_1 x - k_2 y = ak_1 \exp(-k_1 t) - \dfrac{k_1 k_2 a}{k_2-k_1}\exp(-k_1 t) + \dfrac{k_1 k_2 a}{k_2-k_1}\exp(-k_2 t)$

$\qquad - bk_2 \exp(-k_2 t)$ (6)

$= ak_1\left[1 - \dfrac{k_2}{k_2-k_1}\right]\exp(-k_1 t) + \dfrac{k_1 k_2 a}{k_2-k_1}\exp(-k_2 t) - bk_2 \exp(-k_2 t)$ (7)

$= \dfrac{-ak_1^2}{k_2-k_1}\exp(-k_1 t) + \dfrac{k_1 k_2 a}{k_2-k_1}\exp(-k_2 t) - bk_2 \exp(-k_2 t)$ (8)

$= \dfrac{dy}{dt}$ as equation (4)

Appendix AI

To show that $y = \exp(-k_2 t)\left[\left(\dfrac{k_1 a}{k_2 - k_1}\right) \cdot (\exp(k_2 - k_1)t - 1) + b\right]$ (1)

is a solution of $dy/dt = k_1 x - k_2 y$ (2)

Rearranging equation (1) we have,

$$y = \frac{k_1 a}{k_2 - k_1} \cdot \exp(-k_1 t) - \frac{k_1 a}{k_2 - k_1} \cdot \exp(-k_2 t) + b \exp(-k_2 t) \tag{3}$$

Differentiating this equation with respect to time, leads to,

$$\frac{dy}{dt} = \frac{-k_1^2 a}{k_2 - k_1} \exp(-k_1 t) + \frac{k_1 k_2 a}{k_2 - k_1} \cdot \exp(-k_2 t) - b k_2 \exp(-k_2 t) \tag{4}$$

Now, with $x = a \exp(-k_1 t)$ (5)

$$k_1 x - k_2 y = a k_1 \exp(-k_1 t) - \frac{k_1 k_2 a}{k_2 - k_1} \exp(-k_1 t) + \frac{k_1 k_2 a}{k_2 - k_1} \exp(-k_2 t)$$

$$- b k_2 \exp(-k_2 t) \tag{6}$$

$$= a k_1 \left[1 - \frac{k_2}{k_2 - k_1}\right] \exp(-k_1 t) + \frac{k_1 k_2 a}{k_2 - k_1} \exp(-k_2 t) - b k_2 \exp(-k_2 t) \tag{7}$$

$$= \frac{-a k_1^2 \exp(-k_1 t) + k_1 k_2 a \exp(-k_2 t) - b k_2 \exp(-k_2 t)}{k_2 - k_1} \tag{8}$$

$$= \frac{dy}{dt} \quad \text{as equation (4)}$$

Appendix AII

Case i

Solution of $dn_{18}/dt = k_2y + v_b - (n_{18}/n)V$ (1)

for $k_1 \neq k_2$

It has been shown previously (Chapter IV) that,

$$k_2y = k_2 \exp.(-k_2t)\left[\frac{k_1a \;(\exp\;(k_2-k_1)t - 1) + b}{k_2-k_1}\right] \quad (2)$$

Let $\quad A = \dfrac{k_2k_1a}{k_2-k_1} \quad$ and $\quad B = k_2\left[\dfrac{bk_2 - bk_1 - ak_1}{k_2 - k_1}\right]$

Then,

$$k_2y = k_2\left[\frac{k_1a}{k_2-k_1}\;\exp(-k_1t) - \frac{k_1a}{k_2-k_1}\;\exp(-k_2t) + b\;\exp(-k_2t)\right] \quad (3)$$

$$k_2y = A\;\exp\;(-k_1t) + B\;\exp\;(-k_2t) \quad (4)$$

Thus the differential equation (i) becomes,

$$dn_{18}/dt = A\;\exp(-k_1t) + B\;\exp(-k_2t) + v_b - (n_{18}/n)V \quad (5)$$

The integrating factor $= (V/n)t = k_nt$ (6)

Thus,

$$n_{18}\;\exp(k_nt) = \int\left[A\;\exp(k_n-k_1)t + B\;\exp(k_n-k_2)t + v_b\;\exp(k_nt)\right]dt \quad (7)$$

$$= \frac{A\;\exp\;(k_n-k_1)t}{k_n-k_1} + \frac{B\;\exp\;(k_n-k_2)t}{k_n-k_2} + \frac{v_b}{kn}\;\exp\;(k_nt) + C \quad (8)$$

where C is the constant of integration. It may be determined using the

condition that $n_{18} = 0$ when $t = 0$. Thus,

$$0 = \frac{v_b}{k_n} + \frac{A}{k_n-k_1} + \frac{B}{k_n-k_2} + C \qquad (9)$$

Hence,

$$n_{18} = \exp(-k_n t)\left[\frac{A \exp(k_n-k_1)t}{k_n-k_1} + \frac{B \exp(k_n-k_2)t}{k_n-k_2} + \frac{v_b \exp(k_n t)}{k_n} \right.$$

$$\left. - \frac{v_b}{k_n} - \frac{A}{k_n-k_1} - \frac{B}{k_n-k_2} \right] \qquad (10)$$

$$n_{18} = \exp(-k_n t)\left[\frac{v_b}{k_n}(\exp(k_n t) - 1) + \frac{A}{k_n-k_1}(\exp(k_n-k_1)t - 1) \right.$$

$$\left. + \frac{B}{k_n-k_2}(\exp(k_n-k_2) - 1) \right] \qquad (11)$$

$$n_{18} = \frac{v_b}{k_n}(1 - \exp(-k_n t)) + \frac{A}{k_n-k_1}(\exp(-k_1 t) - \exp(-k_n t))$$

$$+ \frac{B}{k_n-k_2}(\exp(-k_2 t) - \exp(-k_n t)) \qquad (12)$$

Thus,

$$n_{18} = \frac{v_b}{k_n}(1 - \exp(-k_n t)) + \frac{k_2 k_1 a}{k_2-k_1}\left[\frac{\exp(-k_1 t) - \exp(-k_n t)}{k_n-k_1} \right]$$

$$+ \frac{k_2}{k_n-k_2}\left[b - \frac{ak_1}{k_2-k_1} \right](\exp(-k_2 t) - \exp(-k_1 t)) \qquad (13)$$

as required

Case ii

Solution of equation (1) for $k_1 = k_2 = k$. We have (from Chapter IV)

$$ky = k(kat + b)\exp(-kt) \tag{14}$$

Again the integrating factor $= k_n t$.

Thus,

$$n_{18}\exp(k_n t) = \int\left[k^2 at\exp(k_n - k)t + bk\exp(k_n - k)t + v_b\exp(k_n t)\right]dt \tag{15}$$

$$= \left[\frac{k^2 at\exp(k_n - k)t}{k_n - k} - \frac{k^2 a\exp(k_n - k)t}{(k_n - k)^2} + \frac{bk\exp(k_n - k)t}{k_n - k} + \frac{v_b\exp(k_n t)}{k_n}\right.$$

$$\left. + D\right] \tag{16}$$

where D is the constant of integration. Using the condition that $n_{18} = 0$
at $t = 0$,

$$0 = -\frac{k^2 a}{(k_n - k)^2} + \frac{bk}{k_n - k} + \frac{v_b}{k_n} + D \tag{17}$$

Hence,

$$n_{18} = \exp(-k_n t)\left[\frac{k^2 at\exp(k_n - k)t}{k_n - k} - \frac{k^2 a\exp(k_n - k)t}{(k_n - k)^2} + \frac{bk\exp(k_n - k)t}{k_n - k}\right.$$

$$\left. + \frac{v_b\exp(k_n t)}{k_n} + \frac{k^2 a}{(k_n - k)^2} - \frac{bk}{k_n - k} - \frac{v_b}{k_n}\right] \tag{18}$$

$$n_{18} = \exp(-k_n t)\left[\frac{v_b}{k_n}(\exp(k_n t) - 1) + \frac{k\exp(k_n - k)t}{k_n - k}\left[kat - \frac{ka}{k_n - k} + b\right]\right.$$

$$\left. + \frac{k}{k_n - k}\left[\frac{ka}{k_n - k} - b\right]\right] \tag{19}$$

Thus,

$$n_{18} = \frac{v_b}{k_n} (1 - \exp(-k_n t)) + \frac{k}{k_n - k} \exp(-kt) \left[kat - \frac{ka}{k_n - k} + b \right]$$

$$+ \frac{k}{k_n - k} \exp(-k_n t) \left[\frac{ka}{k_n - k} - b \right] \tag{20}$$

as required.

Appendix AIII

Solution of the equation

$$\frac{dx}{dt} = - \frac{k_D}{n_T} x^2 - \frac{x}{n_T} \left[\sqrt{\frac{iLk_D}{2F}} + k_{-1} \right] \tag{1}$$

Let $\quad A = \frac{k_D}{n_T}, \quad B = \frac{1}{n_T} \left[\sqrt{\frac{iLk_D}{2F}} + k_{-1} \right] \tag{2}$

Equation (1) then becomes

$$\frac{dx}{dt} = -Ax^2 - Bx \tag{3}$$

or $\quad \int dt = \int \frac{dx}{-Ax^2 - Bx} \tag{4}$

$$\int dt = \int \left[- \frac{1}{Bx} + \frac{A}{B(Ax + B)} \right] dx \tag{5}$$

$$t = \frac{-1}{B} \log x + \frac{1}{B} \log (Ax + B) + \text{constant} \tag{6}$$

At $t = 0$, $x = a$, and therefore

$$\text{constant} = \frac{-1}{B} \log \left[\frac{Aa + B}{a} \right] \tag{7}$$

Hence,

$$t = \frac{1}{B} \left[\log \left[\frac{Ax + B}{x} \right] - \log \left[\frac{Aa + B}{a} \right] \right] \tag{8}$$

$$e^{Bt} = \left[\frac{Ax + B}{x} \right] \left[\frac{a}{Aa + B} \right] \tag{9}$$

$$\left[\frac{Aa + B}{a} \right] e^{Bt} = \frac{Ax + B}{x} = A + \frac{B}{x} \tag{10}$$

$$x = \frac{B}{\left[(A + B/a) \exp (Bt) - A \right]} \tag{11}$$

On resubstitution for A and B, equation (11) becomes

$$x = \frac{\left[(iLk_D/2F)^{\frac{1}{2}} + k_{-1}) / n_T \right]}{(k_D/n_T + ((iLk_D/2F)^{\frac{1}{2}} + k_{-1})/n_T a \,) \exp \left[\left[(iLk_D/2F)^{\frac{1}{2}} + k_{-1} \right] t/n_T \right] - k_D/n_T} \tag{12}$$

Then,

$$x = \frac{(iLk_D/2F)^{\frac{1}{2}} + k_{-1}}{(k_D + \left[(iLk_D/2F)^{\frac{1}{2}} + k_{-1} \right] /a) \exp \left[(iLk_D/2F)^{\frac{1}{2}} + k_{-1} \right] t - k_D} \tag{13}$$

as required

Appendix AIV

Solution of the equation

$$\frac{dn_D}{dt} = \frac{k_D x^2}{L} = \frac{v}{n} n_D \tag{1}$$

where $x = B/\left[(A + B/a) \exp (Bt) - A\right]$

$$\frac{dn_D}{dt} = \frac{k_D a^2 b^2}{L\left[(aA + B) \exp (Bt) - aA\right]^2} - \frac{v}{n} n_D \tag{2}$$

Integration factor $= \int_0^t (v/n) \, dt = vt/n \tag{3}$

Therefore,

$$n_D \exp (vt/n) = \int \frac{k_D a^2 B^2 \exp (vt/n)}{L\left[(aA + B) \exp (Bt) - aA\right]^2} \, dt \tag{4}$$

If $(aA + B)^2 \gg (aA)^2$ then equation (4) becomes

$$n_D \exp (vt/n) = \int \frac{k_D a^2 B^2 \exp (vt/n)}{L(aA + B)^2 \exp (2Bt)} \, dt \tag{5}$$

$$= \int \frac{k_D a^2 B^2}{L(aA + B)^2} \exp (v/n - 2B)t \, dt \tag{6}$$

$$= \frac{k_D a^2 B^2}{L(aA + B)^2 (v/n - 2B)} \exp (v/n - 2B)t + \text{constant} \tag{7}$$

Now $n_D = 0$ when $t = 0$, and thus,

$$\text{constant} = - \frac{k_D a^2 B^2}{L(aA + B)^2 (v/n - 2B)} \tag{8}$$

$$n_D \exp(vt/n) = \frac{k_D a^2 B^2}{L(aA + B)^2(v/n - 2B)}\left[\exp(v/n - 2B)t - 1\right] \qquad (9)$$

And thus,

$$n_D = \frac{k_D a^2 B^2}{L(aA + B)^2(v/n - 2B)}\left[\exp(-2Bt) - \exp(-vt/n)\right] \qquad (10)$$

as required.

Appendix BI

Computer programme to fit experimental results from oxygen evolution experiments to theoretical equation*

```
      PROGRAM FITVOL
C
C                  fits data on O18 fraction to
C                  f0 = k0/k (1 - exp(-k/n {t-t'} ))
C
C         k0   is rate of oxygen inflow
C         k    is total rate of outflow
C         n    is the total number of moles in the system
C
C         k0/k is one variable   VAR(1)
C         k/n  is another        VAR(2)
C         t'   is the third      VAR(3)
C
C                  The second part of the program fits the enriched
C                  run to the theoretical expression containing the
C                  rate constants of evolution and the already determined
C                  background constants VAR(1) and VAR(2).
C
C                  the five variables in X(5) are:        default
C                  x(1)  [lag time in seconds] *0.1          3
C                  x(2)  [rate constant for OH /s] *100.     4
C                  x(3)  [rate constant for O /s] *100.      4
C                  x(4)  [initial OH18 /mol   ] *1e8         2
C                  x(5)  [initial O18  /mol   ] *1e8         .1
C
C
C                  -        This version fits the difference data (21/7/81)
C
C
C                  the data is in the form:
C
C                          title              on first card
C                          ITITLE (A80)
C
C                          current,background o18  on second card
C                          CUR         X0          (2E10.4)
C
C                          number of data points on third card
C                          N                       (I3)
C
C                          data : time + difference + background
C                                  T(I)    DIFF(I)     BACK(I)  (3E10.4)
C
C
C
C         The output is to the screen (FOR006)
C                  to file OUT.LIS        (FOR007)
C         and to file O.LIS              (FOR008)
C
C                          OUT contains a record of the fitted data and
C                          variables put to the screen, plus a graph of
C                          the fitted function produced by PRGRAF.
C
C                          O   contains three graphs from VDUGRAF, one of
C                          the fitted background, one of the fitted
C                          function including background, and one of the
C                          difference data and fitted curve.
C                          These are  suitable for viewing on the VT100
C                          with width 132.
C
```

*Programme written by D.B. Hibbert

```
        COMMON /B1/ T(200),ENRICH(200),BACK(200),DIFF(200),N
        COMMON /B2/ CONCUR, X0, VAR(3), ALPHN, VK,VBACK
        COMMON /B3/ Q(5),IQ(5)
        COMMON /FITS/ TT(200), ZZ(200), NN
        DIMENSION XX2(10,200),YY2(10,200)
        DIMENSION XX(10,200),YY(10,200),NUM(3)
        DIMENSION W(50),X(5),B(5)
        EXTERNAL MON ,FV
        CHARACTER *3 FIX,FIXVAR(5),INFILE*20
        CHARACTER *80 ITITLE
        PARAMETER (CON=1./(2.*96500.),FIX='FIX',AVAGADR=6.023E23)
          WRITE(6,'(//10X,''Data in which file? '',$)')
          READ(*,'(A20)')INFILE
        OPEN(7,STATUS='NEW',RECL=132,FILE='OUT2.LIS')
          OPEN(4,STATUS='OLD',RECL=80,FILE=INFILE)
          OPEN(8,STATUS='NEW',FILE='O2.LIS',RECL=200)
        READ(4,100)ITITLE,CUR,X0
 100    FORMAT(A80/2E10.4)
        CONCUR=CON*CUR
        READ(4,99) N, (T(I), DIFF(I), BACK(I),I=1,N)
                              DO 9 I=1,N
   9                          ENRICH(I) = BACK(I) + DIFF(I)

  99    FORMAT(I3/(3E10.4))
        WRITE(*,'(10X,''Guesses for background variables'')')
        READ(*,*)VAR
        IF( VAR(1) .GE. 0.)THEN
        NVAR = 3
C
C                               set up common block for background determination
C
        NN = N
        DO 11 I=1,N
        TT(I) = T(I)
        ZZ(I) = BACK(I)
  11    CONTINUE
C
C                               general subroutine to fit function in FUN to exptl
C                               points.
C
        CALL FITSIM(VAR,NVAR)
        ENDIF
        VAR(1) = ABS(VAR(1))
        VBACK = X0 * CONCUR
        ALPHN = VAR(1) * VAR(2) / VBACK
C
C                               Main part of program dealing with the enriched
C                               signal.
C
        WRITE(6,'(//10X,''Guess values of variables for enrichment'')')
        READ(*,*) (X(I),FIXVAR(I), I=1,5)
C
C               look for zero values and set the default values
C
        IF(X(1) .LE. 0.) X(1)=3.
        IF(X(2) .LE. 0.) X(2)=4.
        IF(X(3) .LE. 0.) X(3)=4.
        IF(X(4) .LE. 0.) X(4)=2.
        IF(X(5) .LE. 0.) X(5)=.1
        STEP =(X(1)+X(2)+X(3)+X(4)+X(5))/100.
      WRITE(6,1000)ITITLE, CUR,X0
      WRITE(6,1001)(T(I),ENRICH(I),I=1,N)
      WRITE(6,1002)(X(I),FIXVAR(I),I=1,5)
```

```fortran
C
C                 set up correct number of variables which are not
C                 'fixed'
C
      J=0
      DO 1 I=1,5
      Q(I)=X(I)
      IF(FIXVAR(I) .EQ. FIX)GOTO1
      J=J+1
      IQ(J)=I
      B(J)=X(I)
  1   CONTINUE
      IF (J .EQ. 0)THEN
            WRITE(6,'('' All values fixed'')')
            WRITE(7,'('' All values fixed'')')
            J = 5
            DO 12 I=1,5
 12         IQ(I) = I
      ELSE
C
C
C                    MINIMISE !!!!!!!!!!!!!!!!!
C
C
            CALL SIMPLEX(B,J,FV,STEP,MON,W,50)
      ENDIF
      write(6,'('' concur and x0 '',2e10.4)')concur,x0
      F=FV(Q,J)
      X(1) = Q(1)*10.
      X(2) = Q(2)*0.01
      X(3) = Q(3)*0.01
      X(4) = Q(4)*1.E-8
      X(5) = Q(5)*1.E-8
C
C                 open output file on unit 7 for data to line printer
C
      WRITE(7,1000)ITITLE,CUR,X0
      WRITE(7,1007) VAR, VBACK, ALPHN
      WRITE(6,1007) VAR, VBACK, ALPHN
      WRITE(7,1003)X,F
      WRITE(6,1003)X,F
      TM180H = CON*AVAGADR/X(2)
      TM180  = CON*AVAGADR/X(3)
      XM180H = AVAGADR*X(4)
      XM180  = AVAGADR*X(5)
      WRITE(7,1004)X(1),TM180H,TM180,XM180H,XM180
      WRITE(6,1004)X(1),TM180H,TM180,XM180H,XM180
       WRITE(7,1005)
       WRITE(6,1005)
      DO 2 I=1,N
      YCALC=QFUNCT(X,T(I))
      DIF=YCALC-DIFF(I)
      WRITE(7,1006)T(I),DIFF(I),YCALC,DIF
  2   WRITE(6,1006)T(I),DIFF(I),YCALC,DIF
C
C                 set up variables for graph
C
      DIF=T(N)/200.
      TIME=0.
      YH2 = 0.
      YH = 0.
      DO 10 I=1,200
```

```
            TIME=TIME+DIF
            XX(2,I)=TIME
            XX(1,I)=TIME
            XX2(1,I) = TIME
            YY(1,I) = FUN(VAR,3,TIME)
            YY(2,I)=QFUNCT(X,TIME) + YY(1,I)
            YY2(1,I) = YY(2,I) - YY(1,I)
            IF(YY(1,I) .GT. YH) YH = YY(1,I)
            IF(YY(2,I) .GT. YH) YH = YY(2,I)
            IF(YY2(1,I) .GT. YH2) YH2 = YY2(1,I)
   10       CONTINUE
            DO 21 I=1,N
            XX(3,I)=T(I)
            YY(3,I)=ENRICH(I)
            XX2(2,I) = T(I)
            YY2(2,I) = MAX(0.,DIFF(I))
            IF(YY(3,I) .GT. YH) YH = YY(3,I)
            IF(YY2(2,I) .GT. YH2) YH2 = YY2(2,I)
   21       CONTINUE
            NUM(1)=200
            NUM(2)=200
            NUM(3)=N
            CALL PRGRAF(XX,YY,3,200,NUM,T(N),0.,YH,0.,7)
            CALL VDUGRAF(XX,YY,3,200,NUM,T(N),0.,YH,0.,8)
            NUM(2) = N
            CALL VDUGRAF(XX2,YY2,2,200,NUM,T(N),0.,YH2,0.,8)
            STOP
 1000 FORMAT(1X,A80//' CURRENT= ',1PE10.3/' BACKGROUND FRACTION 180 ',
      1 E10.3)
 1001 FORMAT(//5X,'INPUT DATA TIME     Y'/50(15X,F6.1,3X,F7.4/))
 1002 FORMAT(//5X,'GUESS VALUES FOR UNKNOWNS'/5(2X,E10.4,A3/))
 1003 FORMAT(//5X,'MINIMISATION ROUTINE  /VALUES/ ',5(2X,E10.4),
      1/5X,'FUNCTION= ',E10.4)
 1004 FORMAT(//5X,'TO ',1PE10.3,2X,'TOTAL OH',E10.3,2X,'TOTAL O ',E10.3
      1,2X, 'INITIAL 180H ',E10.3,' INITIAL 180 ',E10.3)
 1005 FORMAT(///10X,'TIME',10X,'Y',10X,'YCALC',10X,'DIF'/)
 1006 FORMAT(7X,1PE10.3,3X,E10.3,3X,E10.3,4X,E10.3)
 1007 FORMAT(/10X,'Variables from background fit'/10x,'Maximum signal fr
      1om mass spectrometer = ',G12.6/10X,'Rate constant Kv  = ',G12.6/
      210x,'Las time  = ',F5.1//10X,'Rate background evolution  = ',G12.6
      3/10X, 'Alpha / N = ',G12.6)
            END
            FUNCTION FV(X,N)
C
C              fv calculates the function to be minimized for simplex
C              routine. it is the square of the difference between the
C              calculated and experimental values of the function.
C
C              this is for the enriched sample
C
      COMMON /B1/T(200),ENRICH(200),BACK(200),Y(200),L
      COMMON /B3/ Q(5),IQ(5)
      DIMENSION X(N),B(5)
C
C                      if any of the variables are negative fv is set to
C                      a large value and the calculation terminated
C
      FV=1.E8
      DO 2 I=1,N
      J=IQ(I)
      Q(J)=X(I)
      IF(X(I) .LT. 0.)RETURN
   2  CONTINUE
```

```
C
C                              the true values of the variables are in B
C
      B(1)=Q(1)*10.
      B(2)=Q(2)*0.01
      B(3)=Q(3)*0.01
      B(4)=Q(4)*1.E-8
      B(5)=Q(5)*1.E-8
      S=0.
      DO 8 I=1,L
      YC= QFUNCT(B,T(I))
      S=S+(YC-Y(I))**2
   8  CONTINUE
      FV=S
      RETURN
      END
      FUNCTION QFUNCT(W,R)
C
C              QFUNCT CALCULATES THE HEIGHT OF THE MASS34 PEAK
C              AT X = W(1)-R, OVER THE BACKGROUND, NORMALISED TO 1.
C
      COMMON /B2/ CONCUR, X0, VAR(3), ALPHN, VK,VBACK
      DIMENSION W(5)
      REAL K2,K3,KV
      QFUNCT=0.
      X=R-W(1)
      IF(X .LT. 1.E-10)RETURN
      KV = VAR(2)
      K2 = W(2)
      K3 = W(3)
      A  = W(4)
      B  = W(5)
      QQ=ABS(K2 -K3)
      IF(QQ .GT. 1.E-10)THEN
C
C                      k2 not equal to k3
C
             BIGA = K2 * K3 * A/ QQ
             BIGB = K3 * B - BIGA
             EXP2 = EXPON(-K2*X)
             EXP3 = EXPON(-K3*X)
             EXPV = EXPON(-KV*X)
             TERM1 = BIGA * (EXP2-EXPV) / (KV-K2)
             TERM2 = BIGB * (EXP3-EXPV) / (KV-K3)
      ELSE
C
C                      k2 equal to k3
C
             AK2 = A*K2
             AK2ON = AK2 / (KV-K2)
             BIGC = AK2 / (KV-K2)
             EXP2 = EXPON(-K2*X)
             EXPV = EXPON(-KV*X)
             TERM1 = BIGC * EXP2 * (AK2*X + B - AK2ON)
             TERM2 = BIGC * EXPV * (AK2ON - B)
      ENDIF
      ZED  = TERM1 + TERM2
      QFUNCT = ALPHN * ZED
      RETURN
      END
      FUNCTION FUN(V,NV,X)
      DIMENSION V(NV)
      FUN = 0.
```

```
          IF (X .LT. V(3)) RETURN
          Q = X-V(3)
          FUN = V(1) * (1.-EXPON(-V(2)*Q))
          RETURN
          END
          FUNCTION EXPON(X)
          IF (X .LT. -50.)THEN
                  EXPON = 0.
                  RETURN
          ELSE
                  EXPON = EXP(X)
                  RETURN
          ENDIF
          END
          SUBROUTINE FITSIM(VAR,NVAR)
C
C                      calculates best fit function given N experimental
c                      points (X,Y) and generating function FUN.
c                      NVAR is the number of variables.
C
          DIMENSION XGRAF(10,200),YGRAF(10,200)
          DIMENSION VAR(NVAR)
          DIMENSION W(2000),NUM(10)
          COMMON /FITS/ X(200),Y(200),N
          EXTERNAL SIMFUN,MON
C
C                      Calculate step size
C
          SV = 0.
          DO 1 I=1,NVAR
   1      SV = SV + VAR(I)
          STEP = SV/(FLOAT(NVAR)*5.)
C
C                      Minimise using SIMPLEX
C
          CALL SIMPLEX(VAR,NVAR,SIMFUN,STEP,MON,W,2000)
          F = SIMFUN(VAR,NVAR)
          WRITE(6,'(//10X,''Simplex has converged''/2x,''Function= '',
   1          G10.4/(2X,''Variable('',I2,'') = '',G10.4))')F,
   2                     (I,VAR(I),I=1,NVAR)
          WRITE(6,'(///5X,''X'',10X,''Y'',9X,''Calc'',8X,''Difference'')')
          DO 2 I=1,N
          CALC = FUN(VAR,NVAR,X(I))
          DIF = Y(I) - CALC
          WRITE(6,'(4(2X,G10.4))')X(I),Y(I),CALC,DIF
   2      CONTINUE
C
C                      set up graphing function
C
          YM = 0.
          DO 3 I=1,N
          XGRAF(1,I) = X(I)
          YGRAF(1,I) = Y(I)
          IF (YGRAF(1,I) .GT. YM) YM=YGRAF(1,I)
   3      CONTINUE
          NUM(1) = N
          NUM(2) = 100
          DIFX = (X(N) - X(1))/100.
          DO 4 I=1,100
          XGRAF(2,I) = X(1) + DIFX*FLOAT(I-1)
          YGRAF(2,I) = FUN(VAR,NVAR,XGRAF(2,I))
          IF (YGRAF(2,I) .GT. YM) YM = YGRAF(2,I)
   4      CONTINUE
```

```
            CALL VDUGRAF(XGRAF,YGRAF,2,200,NUM,X(N),X(1),YM,0.,8)
            RETURN
            END
            FUNCTION SIMFUN(V,NV)
C
C                          subroutine for SIMPLEX calculates the square of
C                          the difference between the calculated and experimental
C                          values of Y at N points X.
C
C
            COMMON /FITS/ X(200),Y(200),N
            DIMENSION V(NV)
            S = 0.
            SIMFUN = 1.E8
            DO 2 I=1,NV
            IF ( V(I) .LT. 0.)RETURN
  2         CONTINUE
            DO 1 I=1,N
            CALC = FUN(V,NV,X(I))
            DIF = Y(I) - CALC
            S = S + DIF*DIF
  1         CONTINUE
            SIMFUN = S
            RETURN
            END
            FUNCTION MON(I,FH,FL)
C
C           :::::::::::::::::::::::::::::::::::::::::::::::::::::::::::::::::::
C                      THIS IS A DUMMY CALLED BY E04CCF
C
C
            CHARACTER *20 ISTR,ISTR1,ISTR2,ISTR3
            PARAMETER(ISTR='CALCULATING SIMPLEX ')
            IQ = OTS$CVT_L_TI(I,ISTR1)
            IQ= FOR$CVT_D_TE(FH,ISTR2,%VAL(5))
            IQ =FOR$CVT_D_TE(FL,ISTR3,%VAL(5))
            IQ = LIB$PUT_SCREEN(ISTR//ISTR1//ISTR2//ISTR3,24,1)
            MON=0
            RETURN
            END
```

239

Appendix BII

Computer programme to fit experimental results from hydrogen evolution experiments to theoretical equation

```
      PROGRAM FITVOL
C
C
C                              fits data on D2 fraction to
C                              nH = (i/2F)(y**2)(n/k)(1-e[(-k/n)(t-x)])
C
C          nH  is the signal due to hydrogen
C          k   is total rate of outflow
C          n   is the total number of moles in the system
C          x   is the lag time
C
C          y**2  is one variable    VAR(1)
C          k/n   is another         VAR(2)
C          t'    is the third       VAR(3)
C
C                  The second part of the program fits the enriched
C                  run to the theoretical expression containing the
C                  rate constants of evolution and the already determined
C                  background constants VAR(1) and VAR(2).
C
C                  the five variables in X(6) are:       default
C                  x(1)  [lag time in seconds] *0.1           3
C                  x(2)  [k/n from background /s] *100        2
C                  x(3)  [total no. sites] *1E-19             2
C                  x(4)  [rate constant kD atom/s] *1E-16     3
C                  x(5)  [initial coverage] *10               2
C                  x(6)  [multiplying factor] *1E5            1
C
C                          This version fits the difference data (3/2/82)
C
C
C                  the data is in the form:
C
C                          title                on first card
C                          ITITLE (A80)
C
C                          current on second card
C                          CUR         (E10.4)
C
C                          number of data points on third card
C                          N                        (I3)
C
C                          data : time + signal + background
C                          T(I)   ENRICH(I)  BACK(I)   (3E10.4)
C
C
C                  The output is to the screen (FOR006)
C                      to file OUT.LIS        (FOR007)
C                  and to file O.LIS          (FOR008)
C
C                          OUT contains a record of the fitted data and
C                          variables put to the screen, plus a graph of
C                          the fitted function produced by PRGRAF.
C
C                          O   contains three graphs from VDUGRAF, one of
C                          the fitted background, one of the fitted
C                          function including background, and one of the
C                          difference data and fitted curve.
C                          These are  suitable for viewing on the VT100
C                          with width 132.
C
```

```
C
      COMMON /B1/ T(200),ENRICH(200),BACK(200),N
      COMMON /B2/ CONCUR, VAR(3), FF
      COMMON /B3/ Q(6),IQ(6)
      COMMON /FITS/ TT(200), ZZ(200), NN
      DIMENSION XX2(10,200),YY2(10,200)
      DIMENSION XX(10,200),YY(10,200),NUM(3)
      DIMENSION W(50),X(6),B(6)
      EXTERNAL MON ,FV
      CHARACTER *3 FIX,FIXVAR(5),INFILE*20
      CHARACTER *80 ITITLE
      PARAMETER (CON=1./(2.*96500.),FIX='FIX',AVAGADR=6.023E23)
        WRITE(6,'(//10X,''Data in which file? '',$)')
        READ(*,'(A20)')INFILE
      OPEN(7,STATUS='NEW',RECL=132,FILE='OUT2.LIS')
        OPEN(4,STATUS='OLD',RECL=80,FILE=INFILE)
        OPEN(8,STATUS='NEW',FILE='O2.LIS',RECL=200)
      READ(4,100)ITITLE,CUR
  100 FORMAT(A80/E10.4)
      CONCUR=CON*CUR
      READ(4,99) N, (T(I), ENRICH(I),BACK(I),I=1,N)
   99  FORMAT(I3/(3E10.4))
        WRITE(*,'(10X,''Guesses for background variables'')')
        READ(*,*)VAR
        IF( VAR(1) .GE. 0.)THEN
        NVAR = 3
C
C
C                         set up common block for background determinatio
C
        NN = N
        DO 11 I=1,N
        TT(I) = T(I)
        ZZ(I) = BACK(I)
   11   CONTINUE
C
C                         general subroutine to fit function in FUN to exptl
C                         points.
C
      CALL FITSIM(VAR,NVAR)
      ENDIF
      VAR(1) = ABS(VAR(1))
C
C                         Main part of program dealing with the enriched
C                         signal.
C
      WRITE(6,'(//10X,''Guess value for FF'')')
      READ(*,*) FF
      WRITE(6,'(//10X,''Guess values of variables for enrichment'')')
      READ(*,*) (X(I),FIXVAR(I), I=1,6)
C
C           look for zero values and set the default values
C
      IF(X(1) .LE. 0.) X(1)=3.
      IF(X(2) .LE. 0.) X(2)=2.
      IF(X(3) .LE. 0.) X(3)=2.
      IF(X(4) .LE. 0.) X(4)=3.
      IF(X(5) .LE. 0.) X(5)=2
      IF(X(6) .LE. 0.) X(6)=1
      STEP =(X(1)+X(2)+X(3)+X(4)+X(5)+X(6))/100.
      WRITE(6,1000)ITITLE, CUR
      WRITE(6,1001)(T(I),ENRICH(I),I=1,N)
      WRITE(6,1002)(X(I),FIXVAR(I),I=1,6)
C
```

```
C                    set up correct number of variables which are not
C                    'fixed'
C
        J=0
        DO 1 I=1,6
        Q(I)=X(I)
        IF(FIXVAR(I) .EQ. FIX)GOTO1
        J=J+1
        IQ(J)=I
        B(J)=X(I)
    1   CONTINUE
        IF (J .EQ. 0)THEN
                WRITE(6,'('' All values fixed'')')
                WRITE(7,'('' All values fixed'')')
                J = 6
                DO 12 I=1,6
    12          IQ(I) = I
        ELSE
C
C
C                    MINIMISE !!!!!!!!!!!!!!!!!!
C
C
                CALL SIMPLEX(B,J,FV,STEP,MON,W,50)
        ENDIF
        write(6,'('' concur '',e10.4)')concur
        F=FV(Q,J)
        X(1) = Q(1)*10.
        X(2) = Q(2)*0.01
        X(3) = Q(3)*1.E+19
        X(4) = Q(4)*1.E+16
        X(5) = Q(5)*0.1
        X(6) = Q(6)*1.E+5
C
C                    open output file on unit 7 for data to line printer
C
        WRITE(7,1000)ITITLE,CUR
        WRITE(7,1007) VAR
        WRITE(6,1007) VAR
        WRITE(7,1003)X,F
        WRITE(6,1003)X,F
        WRITE(7,1004)X(1),X(2),X(3),X(4),X(5)
        WRITE(6,1004)X(1),X(2),X(3),X(4),X(5)
        WRITE(7,1005)
        WRITE(6,1005)
        DO 2 I=1,N
        YCALC=QFUNCT(X,T(I))
        DIF=YCALC-ENRICH(I)
        WRITE(7,1006)T(I),ENRICH(I),YCALC,DIF
    2   WRITE(6,1006)T(I),ENRICH(I),YCALC,DIF
C
C                    set up variables for graph
C
        DIF=T(N)/200.
        TIME=0.
        YH2 = 0.
        YH = 0.
        DO 10 I=1,200
        TIME=TIME+DIF
        XX(2,I)=TIME
        XX(1,I)=TIME
        XX2(1,I) = TIME
```

```
          YY(1,I) = FUN(VAR,3,TIME)
          YY(2,I)=QFUNCT(X,TIME)
          YY2(1,I) = YY(2,I)
          IF(YY(1,I) .GT. YH) YH = YY(1,I)
          IF(YY2(1,I) .GT. YH2) YH2 = YY2(1,I)
   10     CONTINUE
          DO 21 I=1,N
          XX(3,I)=T(I)
          YY(3,I)=ENRICH(I)
          XX2(2,I) = T(I)
          YY2(2,I) = BACK(I)
          IF(YY(3,I) .GT. YH2) YH2  = YY(3,I)
          IF(YY2(2,I) .GT. YH) YH = YY2(2,I)
   21     CONTINUE
          NUM(1)=200
          NUM(2)=200
          NUM(3)=N
          CALL PRGRAF(XX,YY,3,200,NUM,T(N),0.,YH2,0.,7)
          CALL VDUGRAF(XX,YY,3,200,NUM,T(N),0.,YH2,0.,8)
          NUM(2) = N
          CALL VDUGRAF(XX2,YY2,2,200,NUM,T(N),0.,YH,0.,8)
        STOP
 1000 FORMAT(1X,A80//' CURRENT= ',1PE10.3/)
 1001 FORMAT(//5X,'INPUT DATA TIME      Y'/50(15X,F6.1,3X,F7.4/))
 1002 FORMAT(//5X,'GUESS VALUES FOR UNKNOWNS'/6(2X,E10.4,A3/))
 1003 FORMAT(//5X,'MINIMISATION ROUTINE  /VALUES/ ',6(2X,E10.4),
     1/5X,'FUNCTION= ',E10.4)
 1004 FORMAT(//5X,'T0 ',1PE10.3,2X,'k/n ',E10.3,2X,'nT ',E10.3
     1,2X, 'kD ',E10.3,' INITIAL COVERAGE,a ',E10.3,'X(6) ',E10.3)
 1005  FORMAT(///10X,'TIME',10X,'Y',10X,'YCALC',10X,'DIF'/)
 1006 FORMAT(7X,1PE10.3,3X,E10.3,3X,E10.3,4X,E10.3)
 1007 FORMAT(/10X,'Variables from background fit'/10x,'Maximum signal fr
     1om mass spectrometer = ',G12.6/10X,'Rate constant Kv  = ',G12.6/
     210x,'Las time  = ',F5.1//)
      END
      FUNCTION FV(X,N)
C
C                   fv calculates the function to be minimized for simplex
C                   routine. it is the square of the difference between the
C                   calculated and experimental values of the function.
C
C                   this is for the enriched sample
C
      COMMON /B1/T(200),ENRICH(200),BACK(200),L
      COMMON /B3/ Q(6),IQ(6)
      DIMENSION X(N),B(6)
C
C                   if any of the variables are negative fv is set to
C                   a large value and the calculation terminated
C
      FV=1.E8
      DO 2 I=1,N
      J=IQ(I)
      Q(J)=X(I)
      IF(X(I) .LT. 0.)RETURN
    2 CONTINUE
C
C                   the true values of the variables are in B
C
      B(1)=Q(1)*10.
      B(2)=Q(2)*0.01
      B(3)=Q(3)*1.E+19
      B(4)=Q(4)*1.E+16
```

```fortran
      B(5)=Q(5)*0.1
      B(6)=Q(6)*1.E+5
      S=0.
      DO 8 I=1,L
      YC= QFUNCT(B,T(I))
      S=S+(YC-ENRICH(I))**2
   8  CONTINUE
      FV=S
      RETURN
      END
      FUNCTION QFUNCT(W,R)
C
C              QFUNCT CALCULATES THE HEIGHT OF THE D2 PEAK
C              AT X = W(1)-R, NORMALISED TO 1.
C
      COMMON /B2/ CONCUR, VAR(3), FF
      DIMENSION W(6)
      REAL KN,NT,KD,ND
      AVAGADR=6.023E23
      QFUNCT=0.
      X=R-W(1)
      IF(X .LT. 1.E-10)RETURN
        KN = W(2)
        NT = W(3)
        KD = W(4)
        A = W(5)
        Z = W(6)
        B=SQRT((4*(CONCUR*AVAGADR*KD)))/NT
        AA=KD/NT
        EXPB=EXPON(-2*B*X)
        EXPK=EXPON(-KN*X)
        QF=Z*((CONCUR*(A**2)*(B**2))/((((A*AA)-B)**2)*(KN-2*B)))*(EXPB-EXPK)
        QFUNCT=QF*FF
        RETURN
      END
      FUNCTION FUN(V,NV,X)
      DIMENSION V(NV)
      COMMON /B2/ CONCUR
      FUN = 0.
      IF (X .LT. V(3)) RETURN
      Q = X-V(3)
      FUN = CONCUR*(V(1)/V(2))*(1.-EXPON(-V(2)*Q))
      RETURN
      END
      FUNCTION EXPON(X)
      IF (X .LT. -50.)THEN
             EXPON = 0.
             RETURN
      ELSE
             EXPON = EXP(X)
             RETURN
      ENDIF
      END
      SUBROUTINE FITSIM(VAR,NVAR)
C
C               calculates best fit function given N experimental
C               points (X,Y) and generating function FUN.
C               NVAR is the number of variables.
C
      DIMENSION XGRAF(10,200),YGRAF(10,200)
      DIMENSION VAR(NVAR)
      DIMENSION W(2000),NUM(10)
      COMMON /FITS/ X(200),Y(200),N
```

```
        EXTERNAL SIMFUN,MON
C
C                      Calculate step size
C
        SV = 0.
        DO 1 I=1,NVAR
1       SV = SV + VAR(I)
        STEP = SV/(FLOAT(NVAR)*5.)
C
C                      Minimise using SIMPLEX
C
        CALL SIMPLEX(VAR,NVAR,SIMFUN,STEP,MON,W,2000)
        F = SIMFUN(VAR,NVAR)
        WRITE(6,'(//10X,''Simplex has converged''/2X,''Function= '',
     1         G10.4/(2X,''Variable('',I2,'') = '',G10.4))')F,
     2         (I,VAR(I),I=1,NVAR)
        WRITE(6,'(///5X,''X'',10X,''Y'',9X,''Calc'',8X,''Difference'')')
        DO 2 I=1,N
        CALC = FUN(VAR,NVAR,X(I))
        DIF = Y(I) - CALC
        WRITE(6,'(4(2X,G10.4))')X(I),Y(I),CALC,DIF
2       CONTINUE
C
C                      set up graphing function
C
        YM = 0.
        DO 3 I=1,N
        XGRAF(1,I) = X(I)
        YGRAF(1,I) = Y(I)
        IF (YGRAF(1,I) .GT. YM) YM=YGRAF(1,I)
3       CONTINUE
        NUM(1) = N
        NUM(2) = 100
        DIFX = (X(N) - X(1))/100.
        DO 4 I=1,100
        XGRAF(2,I) = X(1) + DIFX*FLOAT(I-1)
        YGRAF(2,I) = FUN(VAR,NVAR,XGRAF(2,I))
        IF (YGRAF(2,I) .GT. YM) YM = YGRAF(2,I)
4       CONTINUE
        CALL VDUGRAF(XGRAF,YGRAF,2,200,NUM,X(N),X(1),YM,0.,8)
        RETURN
        END
        FUNCTION SIMFUN(V,NV)
C
C                      subroutine for SIMPLEX calculates the square of
C                      the difference between the calculated and experimental
C                      values of Y at N points X.
C
C
        COMMON /FITS/ X(200),Y(200),N
        DIMENSION V(NV)
        S = 0.
        SIMFUN = 1.E8
        DO 2 I=1,NV
        IF ( V(I) .LT. 0.)RETURN
2       CONTINUE
        DO 1 I=1,N
        CALC = FUN(V,NV,X(I))
        DIF = Y(I) - CALC
        S = S + DIF*DIF
1       CONTINUE
        SIMFUN = S
        RETURN
```

```
      END
      FUNCTION MON(I,FH,FL)
C
C     :::::::::::::::::::::::::::::::::::::::::::::::::::::::::::::::::::::::
C                 THIS IS A DUMMY CALLED BY E04CCF
C
C
      CHARACTER *20 ISTR,ISTR1,ISTR2,ISTR3
      PARAMETER(ISTR='CALCULATING SIMPLEX ')
      IQ = OTS$CVT_L_TI(I,ISTR1)
      IQ= FOR$CVT_D_TE(FH,ISTR2,%VAL(5))
      IQ =FOR$CVT_D_TE(FL,ISTR3,%VAL(5))
      IQ = LIB$PUT_SCREEN(ISTR//ISTR1//ISTR2//ISTR3,24,1)
      MON=0
      RETURN
      END
```

REFERENCES

References

1. W.M. Latimer, Oxidation Potentials (Prentice Hall, N.J., 1952).

2. D.P. Gregory, Electrochemistry and the Hydrogen Economy, Ch. 5, in Modern Aspects of Electrochemistry, No. 10 (Plenum Press, N.Y., 1975).

3. J.A.V. Butler, Trans. Far. Soc., 19, 659, (1924).

4. J.A.V. Butler, Trans. Far. Soc., 19, 729, 735, (1924).

5. A. Damjanovic, A. Dey and J. O'M. Bockris, Electrochim. Acta, 11, 791, (1966).

6. T. Erdey-Grúz, Kinetics of Electrode Processes, (Adam Hilger Ltd., 1972).

7. N.I. Rosental and V.I. Veselovskiy, Doklady Akad. Nauk., SSSR, 111, 637, (1956).

8. T.P. Hoar, Proc. Roy. Soc., 142, 628, (1933).

9. J. O'M. Bockris and A.K.M.S. Huq, Proc. Roy. Soc., A237, 277, (1956).

10. W.R. Grove, Proc. Roy. Soc., 4, 463, (1843).

11. J.O'M. Bockris and L.F. Oldfield, Trans. Far. Soc., 51, 249, (1955).

12. J. Giner, Z. Elektrokhim, 63, 386, (1959).

13. J.P. Hoare, J. Electrochem. Soc., 109, 858, (1962).

14. N. Watanabe and M.A.V. Devanathan, J. Electrochem. Soc., 111, 615, (1964).

15. S. Shuldiner, T.B. Warner and B.J. Piersma, J. Electrochem. Soc., 114, 343, (1967).

16.   M.L.B. Rao, A. Damjanovic and J. O'M. Bockris, J. Phys. Chem.,

       67, 2508, (1963).

17.   L.D. Burke and A. Moyniham, Trans. Far. Soc., 67, 3550 (1971).

18.   F.P. Bowden, Proc. Roy. Soc., 125, 446, (1929).

19.   J.A.V. Butler and G. Armstrong, Proc. Roy. Soc., 137, 604, (1932).

20.   G. Armstrong, F.R. Himsworth and J.A.V. Butler, Proc. Roy. Soc.,

       143, 89, (1933).

21.   J.P. Hoare, The Electrochemistry of Oxygen, (Wiley-Interscience,

       N.Y., 1968).

22.   J. O'M. Bockris, J. Chem. Phys., 48, 671, (1968).

23.   A. Damjanovic, Mechanistic Analysis of Oxygen electrode Reactions,

       Ch. 5 in Modern Aspects of Electrochemistry, No. 5 (Plenum Press,

       1969).

24.   B.E. Conway, H. Angerstein-Kozlowska and W.B.A. Sharp, J.

       Electroanal. Chem., 43, 9, (1973).

25.   K. Vetter and J. Schultze, J. Electroanal. Chem., 34, 131, 141

       (1972).

26.   M.A.H. Lanyon and B .M.W. Trapnell, Proc. Roy. Soc., A227,

       387, (1955).

27.   P. Ruetschi and P. Delahay, J. Chem. Phys., 23, 556, (1955).

28.   A. Hickling and S. Hill, Disc. Far. Soc., 1, 236, (1947).

29.   S.E.S. El Wakkad and S.H. Emara, J. Chem. Soc., 461, (1952).

30.   F.C. Anson and J.J. Lingane, J. Am. Chem. Soc., 79, 4901 (1957).

31.   M.W. Brieter and J.L. Weininger, J. Electrochem. Soc., 109,

       1135, (1962).

32.   M. Pourbaix, Atlas of Electrochemical Equilibria in Aqueous
       Solutions, (Pergamon Press, London 1966).

33.   K.J. Vetter, Electrochemical Kinetics, (Academic Press, London,
       1967).

34.   J.P. Hoare, J. Electrochem. Soc., 112, 602 (1965).

35.   T. Biegler, D.A.J. Rand and R. Woods, J. Electroanal. Chem.,
       29, 269, (1971).

36.   R. Thacker and J.P. Hoare, J. Electroanal. Chem., 30, 1, (1971).

37.   A. Damjanovic and A.T. Ward, Electrochemistry – The Past 30 Years
       and the next 30 years, (Ed. H. Bloom and F. Gutmann, Plenum
       Press, London, 1977).

38.   A. Damjanovic, J.F. Wolf and L-S. R. Yeh, Electrochim. Acta,
       26, 81, (1981).

39.   W. Visscher and M. Blijlevens, Electrochim. Acta, 19, 387, (1974).

40.   J.O'M. Bockris, A.K.N. Reddy and M.A. Genshaw, J. Chem.
       Phys., 48, 671, (1968).

41.   H. Dietz and H. Göhr, Electrochim. Acta, 8, 343, (1963).

42.   S.W. Feldberg, C.G. Enke and C.E. Bricker, J. Electrochem.
       Soc., 110, 826, (1963).

43.   H.A. Laitinen and C.G. Enke, J. Electrochem. Soc., 107, 773,
       (1960).

44.   J.D. Pearson and J.A.V. Butler, Trans. Far. Soc., 34, 1163, (1938).

45.   S. Schuldiner and T.B. Warner, J. Electrochem. Soc., 112, 212, (1965).

46.   D.C. Johnson, D.T. Napp and S. Bruckerstein, Electrochim. Acta,
       15, 1493, (1970).

47. S. Schuldiner, T.B. Warner and B.J. Piersma, J. Electrochem.Soc., 113, 573, (1966).

48. J.P. Hoare, J. Phys. Chem., 79, 2175, (1975).

49. J.P. Hoare, J. Electrochem. Soc., 121, 872 (1974).

50. J.P. Hoare, J. Electrochem. Soc., 112, 849, (1965).

51. J. O'M. Bockris, J. Chem. Phys., 24, 817, (1956).

52. P.C. Milner, J. Electrochem. Soc., 111, 438, (1964).

53. A. Hickling and S. Hill, Trans. Far. Soc., 46, 550, 557, (1950).

54. F.P. Bowden, Proc. Roy. Soc., A126, 107, (1930).

55. T.P. Hoar, Proc. C.I.T.C.E., 8, 439, (1958).

56. H.P. Stout, Disc. Far. Soc., 1, 246, (1947).

57. J.A.V. Butler and W.M. Leslie, Trans. Far. Soc., 32, 427, 435, (1936).

58. A.C. Riddiford, Electrochim. Acta., 4, 170, (1961).

59. A.I. Krasil'shchikov, Z. Fiz. Khim., 37, 531, (1963).

60. R. Parsons, Trans. Far. Soc., 47, 1332, (1951).

61. A.C.C. Tseung and S. Jasem, Electrochim. Acta., 22, 31, (1977).

62. A.C.C. Tseung and S. Jasem, Proc-Electrochem. Soc., 1977, 77-6, 414 (Proc. Symp. Electrode Materials, Processes Energy Convers. Storage).

63. W.D. Johnstone, R.C. Miller and R. Magelsky, J. Phys. Chem., 63, 198, (1959).

64. A.C.C. Tseung and W.J. King, Electrochim. Acta, 19, 485 (1974).

65. F. Lutgering, Philips Res. Dep., 11, 337.

66. P. Cossee, J. Inorg. Nucl. Chem., 8, 483, (1958).

67. A.C.C. Tseung and P. Rasiyah, 159th Meeting of the Electrochemical Society, Minneapolis, 1981, Extended Abstracts No. 529.

68. V.V. Shalaginov, I.D. Belova, Yu. E. Roginskaya and D.M. Shub, Elektrokhimiya, 14, 1707, (1978).

69. D.S. McClure, J. Physics. Chem. Solid, 3, 311, (1957).

70. A.C.C. Tseung and W.J. King, Electrochim. Acta, 19, 493, (1974).

71. H. Lord and R. Parker, Nature, 188, 929, (1960).

72. D.M. Shub, A.N. Chemodanov and V.V. Shalaginor, Elektrokhimiya, 14, 595, (1978).

73. A.C.C. Tseung and R. Rasiyah, 159th Meeting of the Electrochemical Society, Minneapolis, 1981, Extended Abstracts No. 530.

74. D.B. Hibbert, J.C.S. Chem. Comm., 203, (1980).

75. C. Iwakura, A. Honji and U. Tarnura, Electrochim. Acta., 26, 1319, (1981).

76. A.C.C. Tseung and H.L. Bevan, J. Mat. Sci., 5, 604, (1970).

77. D.B. Hibbert and A.C.C. Tseung, J. Mat. Sci., 14, 2665, (1979).

78. D.B. Hibbert, J. Kelly and A.C.C. Tseung, J. Mat. Sci., 13, 1053, (1978).

79. D.B. Hibbert, N. Thomas and A.C.C. Tseung, J.C.S. Chem. Comm., 193, (1977)

80. A.C.C. Tseung, N.P. Rasiyah and D.B. Hibbert, Brit. Patent Appl., 81-03750.

81. A. Tantrum and A.C.C. Tseung, Nature, 221, 167, (1969).

82. G.A. El-Shobaky and N. SH. Petro, Surf. Tech., 13, 197, (1981).

83. A.C.C. Tseung and P.R. Vassie, Electrochim. Acta, 21, 315, (1976), 20, 759, 763, (1975).

84.   A.C.C. Tseung, M.N. Mahmood, S. Jasem and M. Man, EEC
        Contract, 311, 77, 11 EH.

85.   A.C.C. Tseung, P. Rasiyah, M.C.M. Man and K.L.K. Yeung,
        Comm. Eur. Communities (Rep) EUR 1980, Eur. 6783,
        Hydrogen energy vector, 240.

86.   K.R. Williams, An Introduction to Fuel Cells, (Elsevier, 1966).

87.   J. Giner, J. Electrochem. Soc., 111, 376, (1964).

88.   D.J.G. Ives and G.J. Janz, Reference Electrodes, Theory and
        Practice (Academic Press, Inc., N.Y., 1961).

89.   G.J. Hill and D.J.G. Ives, Nature, 48, 997 (1949).

90.   R. Fricke and P. Ackermann, Z. Anorg. Chem., 211, 233, (1933).

91.   G.N. Lewis and M. Randall, Thermodynamics, (McGraw-Hill,
        N.Y., 1923).

92.   J.N. Brönsted, Z. Physik. Chem., 65, 84, 744, (1909).

93.   F.G. Donnan and A.J. Allmann, J. Chem. Soc., 99, 845, (1911).

94.   S. Brunauer, P.H. Emmett and E. Teller, J. Am. Chem. Soc.,
        60, 309, (1938).

95.   J.P. Hoare, J. Electroanal. Chem., 12, 260, (1966).

96.   J.A.V. Butler and G. Armstrong, Proc. Roy. Soc., A137, 604, (1932).

97.   T.A. Dorling, C.J. Burlace and R.L. Moss, J. Catalysis,
        4, 704, (1965).

98.   A. Damjanovic, 159th Meeting of the Electrochemical Society,
        Minneapolis, 1981, Extended Abstracts No. 43.

99.   P. Rasiyah, A.C.C. Tseung and D.B. Hibbert, J. Electrochem.
        Soc., 129, 1734, (1982).

100.   R.C. Weast, Editor, Handbook of Chemistry and Physics, 53rd
        Edition, (The Chemical Rubber Co., Florida, 1973).

101.   K.Y.Y. Yeung, Ph.D. Thesis, (The City University, 1979).

102.   C. Iwakura, K. Fukunda and T. Tamura, Electrochim. Acta, 21, 501, (1976).

103.   C. Marie, C.R. Acad. Sci., 145, 117 (1907).

104.   J.P. Hoare, J. Electrochem. Soc., 125, 1768 (1978).

105.   H.A. Laitenen and C.G. Enke, J. Electrochem. Soc., 107, 773, (1960).

106.   T. Erdey-Gruz and M. Volmer, Z. Phys. Chem., 150A, 203 (1930).

107.   F.P. Bowden and E.K. Rideal, Proc. Roy. Soc., A120, 59, (1928).

108.   T. Erdey-Gruz and G.G. Kromocy, Z. Phys. Chem., A157, 213, (1931).

109.   J. Horiuti and G. Okamoto, Sci. Papers Inst. Phys. Chem. Res. (Tokyo), 28, 231, (1936).

110.   J. Tafel, Z. Phys. Chem., 34, 187 (1900).

111.   J. Heyrovsky, Rec. Trav. Chem. Pays-Bas, 46, 582, (1927).

112.   M.N. Hull and F.A. Lewis, Trans. Far. Soc., 64, 2463, 2469, (1968).

113.   J. O'M Bockris and R. Parsons, Trans. Far.Soc., 45, 916, (1948).

114.   Ya. M. Kolotyrkin, J. Phys. Chem. Moscow, 20, 667, (1946).

115.   J. O'M. Bockris and E.C. Potter, J. Chem. Phys., 20, 614, (1952).

116.   J. O'M. Bockris and B.E. Conway, Trans. Far. Soc., 47, 914, (1951).

117.   N. Pentland, J. O'M Bockris and E. Sheldon, J. Electrochem. Soc., 104, 182, (1957).

118.   J. O'M. Bockris and A.M. Assam, Trans. Far. Soc., 48, 145, (1952).

119. A.N. Frumkin and Y. Aladjolova, Acta. Physiochem., 19, 1, (1944).

120. B.S. Hobbs and A.C.C. Tseung, J. Electrochem. Soc., 119, 580, (1972).

121. B.S. Hobbs and A.C.C. Tseung, J. Electrochem. Soc., 120, 766, (1973).

122. B.S. Hobbs and A.C.C. Tseung, J. Electrochem. Soc., 122, 1174, (1975).

123. S.A. Abbara, A.C.C. Tseung and D.B. Hibbert, J. Electrochem. Soc., 127, 1106, (1980).

124. G. Vertes and G. Horanyi, Acad. Chim. Acad. Sci. Hung., 83, 135, (1974).

125. G. Vertes and G. Horanyi, Acad. Chim. Acad. Sci. Hung., 83, 265, (1974).

126. J.E. Benson, H.W. Kohn and M. Bondart, J. Catal., 307, (1966)

127. P.G. Dickens and M.S. Whittingham, Quart. Rev. 30, (1968).

128. P.A. Sermon and A.R. Bergins, Met. Hydrogen Syst., Proc. Miami Int. Symp., 1981, (Pub 1982), 451-7, (Eng.).

129. J.P. Suchet, Chem. Phys. of Semiconductors, D. Van Nostrand, 85, (1965).

130. P. Rasiyah and A.C.C. Tseung, J. Electrochem. Soc., 130, 2384, (1983).

131. A.I. Onuchukwu, J. Electrochem. Soc., 130, 1077, (1983).

132. G.A. Tedoradse, Z. Fiz. Khim., 33, 129, (1959).

133. T. Yokoyama and M. Enyo, Electrochim. Acta, 15, 1921, (1970).

134.   G. Faiti, G. Fiori and A. Nidola, J. Electrochem. Soc., <u>117</u>, 1333, (1970).

135.   M.W. Breiter, Electrochim. Acta, <u>8</u>, 925, (1963).

136.   E.L. Littauer and L.L. Shreir, Electrochim. Acta., <u>11</u>, 527, (1966).

137.   E.J.W. Verwey and E.L. Heilmann, J. Chem. Phys., <u>15</u>, 174, (1947).

Kinetics of the Electrochemical Evolution of Isotopically Enriched Gases

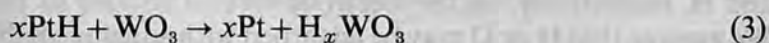## Part 3.—Hydrogen and Deuterium Evolution on Platinum and Platinised Tungsten Trioxide

By D. Brynn Hibbert* and Christine R. Churchill

Department of Chemistry, Bedford and Royal Holloway Colleges,
Egham Hill, Surrey TW20 0EX

The kinetics of the electrochemical evolution of deuterium from solutions of sodium sulphate on platinised platinum electrodes enriched with adsorbed deuterons have been fitted to a theoretical model which yielded values for the coverage of deuterium and the total number of surface sites responsible for the reaction. The number of sites agreed with that determined from hydrogen stripping. The kinetics of the removal of adsorbed deuterium on allowing the electrode to stand in air at open-circuit voltage (OCV) were consistent with a second-order recombination with $k_2 = 0.02$ s^{-1} for $da/dt = k_2 a^2$, where a is the fractional coverage of deuterium at the electrode. The numbers of sites and the volume of deuterium evolved measured for a series of platinised tungsten trioxide electrodes showed spillover of hydrogen from platinum to tungsten trioxide, in agreement with earlier theories.
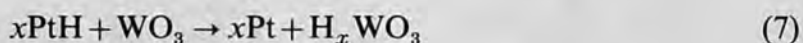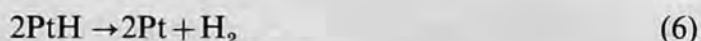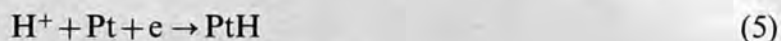

The measurement of the rate of evolution of an isotopically enriched gas from a surface containing a heavy isotope has been shown[1–3] to allow calculation of the number of surface atoms involved in the reaction. The evolution of oxygen (as $^{18}O^{16}O$) was used to investigate the mechanism of oxygen evolution on platinum,[2] nickel cobalt oxide[1,3] and lithiated cobalt oxide,[3] the results being consistent with a model of successive oxidations at a single site. In this paper we report the use of the method when applied to the hydrogen-evolution reaction on platinum and platinised tungsten trioxide. In the case of platinum the kinetics and mechanism of the electrochemical evolution of hydrogen are well known[4] and work has been done on the isotope effects of the evolution of deuterium and tritium.[5] This system is therefore a useful test of the method adopted here. Spillover of hydrogen atoms from platinum to tungsten trioxide was first demonstrated for the electrochemical reduction of hydrogen by Hobbs and Tseung:[6–8]

$$H_2 + 2Pt \rightarrow 2PtH \tag{1}$$

$$PtH \rightarrow Pt + H^+ + e \tag{2}$$

$$xPtH + WO_3 \rightarrow xPt + H_xWO_3 \tag{3}$$

$$H_xWO_3 \rightarrow \tfrac{x}{2}H_2 + WO_3 \tag{4}$$

where Pt is a surface platinum atom. Step (1) only occurs on platinum, but if spillover of hydrogen atoms on to tungsten trioxide [reaction (3)] and the subsequent oxidation is fast with respect to the normal oxidation route [reaction (2)], then a rate of oxidation is seen which is greater than that expected from platinum alone. Vertes and

Horanyi[9] have criticised these conclusions and claim that tungsten trioxide is an inert support, as the spillover reaction [reaction (3)] may be expected to be slow compared with the direct reaction at platinum. However, Hobbs and Tseung have stressed the need to maintain constant platinum crystallite size when preparing supported catalysts for comparison, and suggest this experimental origin for the apparently contrary results. More recently spillover of hydrogen from platinum to tungsten trioxide has been observed in the hydrogenation of nitrophenol[10] and in the electrochemical evolution of hydrogen.[11] The normal and spillover routes for the evolution of hydrogen may be written as

$$H^+ + Pt + e \rightarrow PtH \tag{5}$$

$$2PtH \rightarrow 2Pt + H_2 \tag{6}$$

$$xPtH + WO_3 \rightarrow xPt + H_x WO_3 \tag{7}$$

$$H_x WO_3 \rightarrow \frac{x}{2} H_2 + WO_3. \tag{8}$$

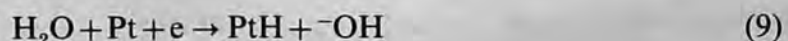In terms of the isotopic experiments, if the number of sites responsible for gas evolution includes a contribution from WO_3 then the above mechanism would be supported.

THEORY

We shall derive an expression for the change in the $m/e\,4$ signal during the electrochemical evolution of H_2, HD and D_2 in an electrolyte containing only H_2O, from an electrode having preadsorbed deuterons. The derivation differs from that of the evolution of $^{18}O^{16}O$ discussed in earlier papers[1-3] in three respects. First, the atomic weight of the heavy isotope cannot be disregarded. Thus separate rate constants for the evolution of H_2, HD and D_2 must be used, although they may be related. Secondly, the complexity of the mechanism of oxygen evolution, involving two intermediate surface oxides, required the experiments to be performed with a low enrichment of ^{18}O, which allowed terms involving the concentration of $^{18}O_2$ to be ignored. Here, in order to improve the accuracy and sensitivity of the method, we have used pure D_2O to produce a surface layer containing, initially, only D. Finally, the evolution of background D_2 is sufficiently small to be disregarded.

The equations which describe the evolution of gas in neutral electrolyte containing adsorbed D (PtD) are

$$H_2O + Pt + e \rightarrow PtH + {}^-OH \tag{9}$$

$$2PtH \rightarrow 2Pt + H_2 \tag{10}$$

$$PtH + PtD \rightarrow 2Pt + HD \tag{11}$$

$$2PtD \rightarrow 2Pt + D_2 \tag{12}$$

if the evolution occurs in normal water. Let x and y be the fraction of adsorbed D and H, respectively, on the electrode surface relative to the total number of sites n_T. We assume that H or D may be adsorbed with equal probability at a site. By Faraday's laws the rate of formation of gaseous species on passage of current iA is iN/F atom s^{-1}, where N is Avagadro's number and F is the Faraday constant. This rate in terms of the change in concentration of adsorbed species at the electrode surface is

$$iN/F = (\mathrm{d}x/\mathrm{d}t + \mathrm{d}y/\mathrm{d}t)\, n_T \tag{13}$$

$$= 2(k_D x^2 + 2k_{HD} xy + k_H y^2) \tag{14}$$

where k_H, k_D and k_{HD} (in molecule s^{-1}) are second-order rate constants for reactions (10)–(12) in terms of the fractional coverages. We now make the simplifying assumption that these constants are related by $k_{HD}^2 = k_H k_D$. Therefore

$$iN/2F = (k_D^{\frac{1}{2}} x + k_H^{\frac{1}{2}} y)^2 \tag{15}$$

or

$$y = [(iN/2F)^{\frac{1}{2}} - k_D^{\frac{1}{2}} x]/k_H^{\frac{1}{2}}. \tag{16}$$

The rate of removal of adsorbed deuterium is $-n_T(dx/dt)$ atom s^{-1}, where

$$n_T(dx/dt) = -2k_D x^2 - k_{HD} xy - k_{-1} x \tag{17}$$

therefore

$$dx/dt = -k_D x^2/n_T - [(iNk_D/2F)^{\frac{1}{2}} + k_{-1}] x/n_T \tag{18}$$

which has the solution

$$x = B/[(A + B/a) \exp(Bt) - A] \tag{19}$$

where $B = [(iNk_D/2F)^{\frac{1}{2}} + k_{-1}]/n_T$, $A = k_D/n_T$ and a is the value of x when $t = 0$. In an experiment the composition of the evolved gas cannot be determined at the electrode surface but some distance away, where it is diluted by the purging gas. The signal of m/e 4 (D_2) measured by the mass spectrometer may be related to the fraction of deuterium at the electrode surface by considering the fate of a gas expanding into a fixed volume which may accommodate n mol of an ideal gas at a total rate of v mol s^{-1}. The rate at which D_2 is evolved is given by the relevant part of the expression for the total evolution rate, $viz.$ $k_D x^2$. The rate at which the gas is removed from the volume is the rate at which all gases flow through (v) multiplied by the fraction which is deuterium (n_D/n), where n_D is the number of deuterium atoms. Therefore

$$dn_D/dt = k_D x^2/N - v(n_D/n). \tag{20}$$

$v/n (= k_n)$ is a first-order rate constant which determines the response of the mass spectrometer to changes in deuterium at the electrode surface. x is given as a function of time by eqn (19). Eqn (20) becomes

$$dn_D/dt = k_D a^2 B^2/\{N[(Aa + B) \exp(Bt) - aA]^2\} - k_n n_D. \tag{21}$$

If the rate of the back reaction may be neglected and if $(Aa + B)^2 \gg (aA)^2$, eqn (21) becomes

$$dn_D/dt + k_n n_D = k_D a^2 B^2/[N(Aa + B)^2 \exp(2Bt)] \tag{22}$$

which has the solution

$$n_D = k_D a^2 B^2[\exp(-2Bt) - \exp(-k_n t)]/N(Aa + B)^2 (k_n - 2B)]. \tag{23}$$

The mass-spectrometer signal of m/e 4(S) is proportional to the fraction of D_2 in the volume at constant pressure:

$$S = K(n_D/n) \tag{24}$$

where K is the constant of proportionality. Plots of mass-spectrometer signal against time may be fitted to eqn (23) and (24) and values for the unknowns K, k_n, n, n_T, k_D and a found. Of particular interest are the values of n_T (the total number of sites at the surface) and a (the initial coverage).

EXPERIMENTAL

MATERIALS

Platinum-black electrodes on 80 gauge platinum mesh screens were prepared by electrolysis of a solution of 5 g PtCl$_4$ in 0.1 dm^3 doubly distilled, deionised water. The electrodes were formed into cylinders to provide the maximum area in a given volume of cell. The surface areas of the platinum electrodes were measured by anodic stripping of adsorbed hydrogen atoms and from oxide charging curves. A stock sample of 1 wt % platinum on tungsten trioxide was prepared by freeze-drying chloroplatinic acid on tungsten trioxide followed by reduction in hydrogen (50 °C for 30 min, 90 °C for 3 h).[6] By this method the specific surface area of platinum has been shown to be 35 m^2 g^{-1}.[6] Loadings down to 0.09% platinum were prepared by mechanically mixing tungsten trioxide with the stock sample. It is of some importance to ensure that the morphology and specific surface area of the platinum remains constant;[10] for this reason each loading was not individually freeze-dried. Teflon-bonded electrodes were prepared by ultrasonically mixing a 50% PTFE dispersion (G.P.I. Plastic Coating Systems Ltd) with the freeze-dried catalyst in the ratio 3:10 by weight. This mixture was painted on a preweighed lead electrode, dried and cured at 300 °C for 10 h. Catalyst loadings were typically 10–15 mg cm^{-2}. The electrolyte was 0.5 mol dm^{-3} sodium sulphate in either H$_2$O or 99.9% D$_2$O.

APPARATUS

The three-compartment electrochemical cell with an outlet to the mass spectrometer has been described elsewhere.[2]

METHOD

Deuterium was evolved galvanostatically (400 mA) in a two-compartment cell for 10 min. The electrode was removed, washed in distilled water and introduced into the cell connected to the inlet of a quadrupole mass spectrometer (Vacuum Generators Anavac 2). Nitrogen purging was maintained at a constant rate throughout the experiment. After a given time at OCV (in order to conduct experiments on the stability of the adsorbed deuterium layer) a constant current (150–300 mA) was passed through the cell. A small fraction of the gases passing out of the cell was continuously admitted to the mass spectrometer operating between 10^{-5} and 10^{-6} mbar. The m/e 4 signal was plotted against time on a $Y-t$ recorder. Eqn (23) and (24) were fitted to these data by a least-squares method written as a computer program in FORTRAN 77.

RESULTS

DEUTERIUM ENRICHMENT ON PLATINUM

Fig. 1 shows the variation of a typical m/e 4 signal with time for a deuterium-enriched platinised platinum electrode, fitted to eqn (23) and (24). Each run was normalised to the background hydrogen signal (m/e 2) to allow comparison of different experiments. For a washing time of 30 s after evolution in deuterated electrolyte the following values were obtained from three experiments: $k_n = 0.023 \pm 0.003$ s^{-1}, $a = 0.6 \pm 0.2$. The fitted results for n_T and k_D over eleven experiments with evolution currents between 150 and 300 mA and washing times of 30–150 s gave $n_T = (5.2 \pm 2.8) \times 10^{19}$ and $k_D = (4.5 \pm 3.9) \times 10^{17}$ molecule s^{-1}. The number of platinum atoms determined by hydrogen stripping was 5.8×10^{19}, in good agreement with n_T. The deviations of the fitted values reflect the sensitivity of eqn (23) and (24) to small changes in the unknowns. Thus k_n may be determined to a greater accuracy than a or k_D. A value of 0.009 ± 0.003 s^{-1} was determined for the background evolution of hydrogen. This is roughly half that determined for deuterium evolution, as would be predicted if the rate of diffusion to the mass-spectrometer inlet depended on the square root of the molecular mass. The initial fractional coverage decreased with increasing washing time, until after 5 min no deuterium could be detected on
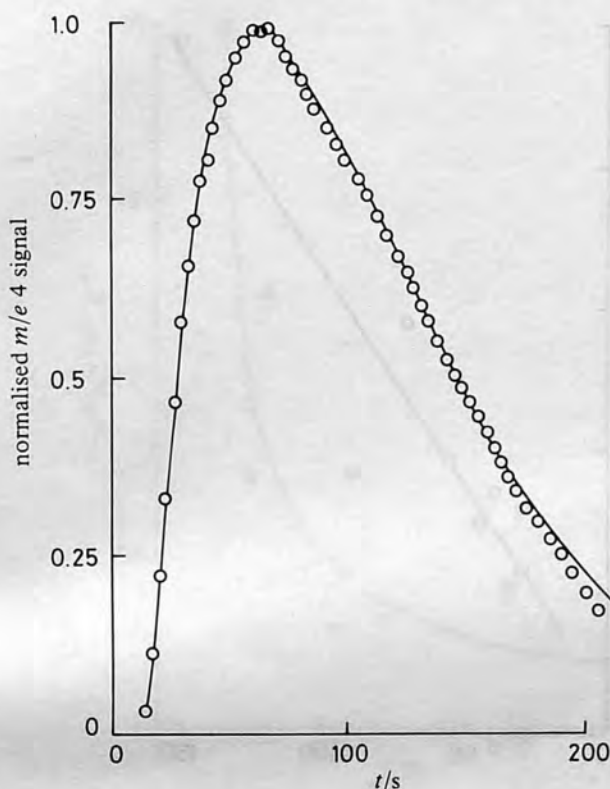
Fig. 1. Mass-spectrometer signal (circles) for $m/e\,4$ after the start of hydrogen evolution on a platinum electrode enriched with D. The continuous line is a fit to eqn (23) and (24). The total elapsed time between evolution in enriched and normal electrolyte was 30 s.

the electrode. The recombination of deuterium atoms on the surface followed a second-order rate law:

$$da/dt = k_2 a^2 \qquad (25)$$

where a is the fractional coverage determined from the total amount of deuterium evolved from an enriched electrode (fig. 2). k_2 was found to be 0.027 ± 0.003 s^{-1}.

### DEUTERIUM ENRICHMENT OF PLATINISED TUNGSTEN TRIOXIDE

Similar plots of mass spectrometer signal against time were obtained for a series of platinised tungsten electrodes. These data were fitted to eqn (23) and (24). Graphs of specific volume of deuterium and specific number of sites (per unit weight of platinum in the electrode) are plotted against the percentage of platinum in the electrode in fig. 3 and 4. For higher loadings of platinum the value of k_D approached the value on pure platinum (4.5×10^{17} atom s^{-1}). A greater variation was found at lower loadings, with k_D tending to higher values (1.3×10^{18} atom s^{-1} for 0.09% Pt, 1.9×10^{18} atom s^{-1} for 0.127% Pt).

DISCUSSION

NUMBER OF EMISSION SITES

The correspondance between n_T and the number of hydrogen atoms determined from hydrogen-stripping experiments shows that for the low current densities used here no extra sites become available for hydrogen evolution than exist at open circuit.
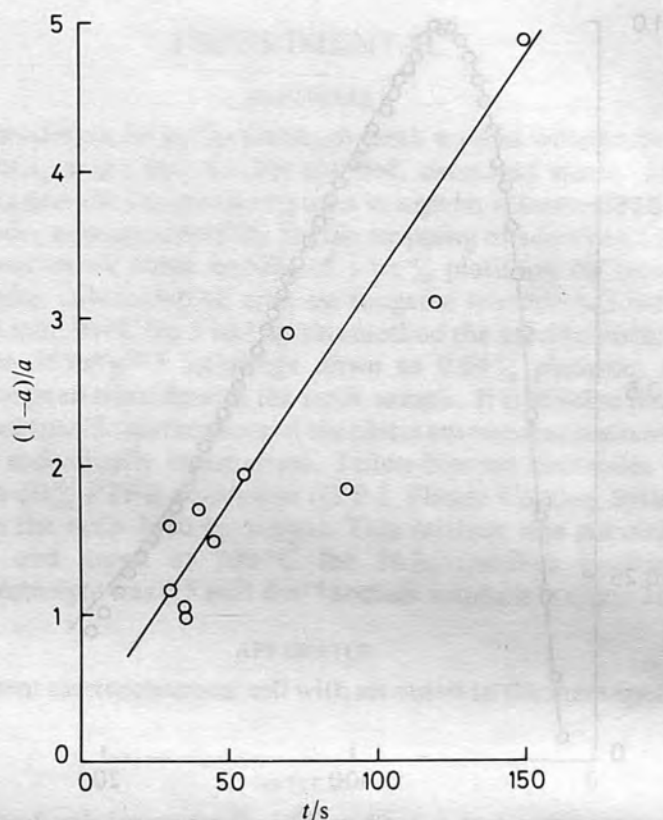
Fig. 2. Variation of the initial fractional coverage of deuterium (a) with the time lapse between evolution in enriched and normal electrolyte, plotted according to second-order kinetics.
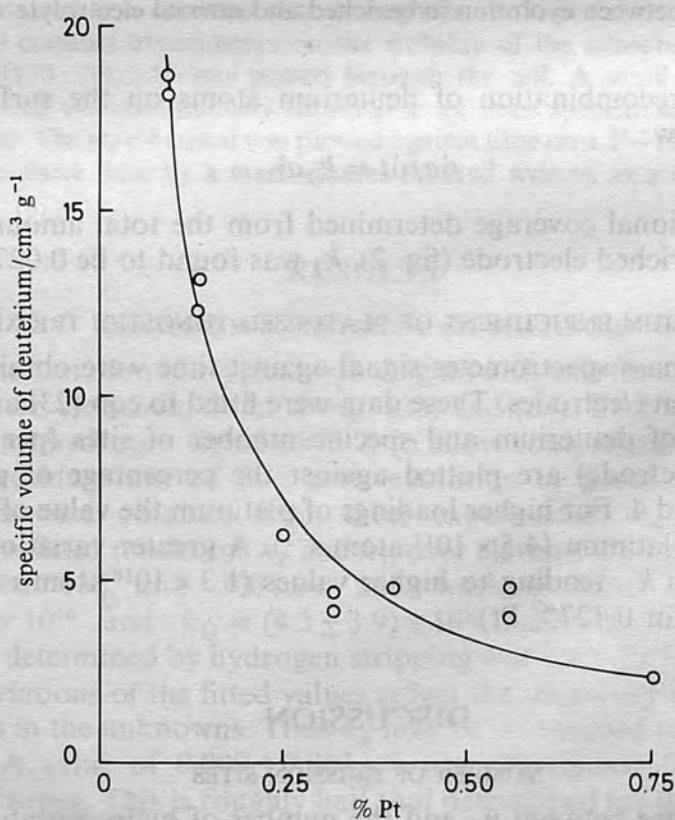
Fig. 3. Specific volume of deuterium (per weight of platinum in the electrode) evolved from deuterium-enriched platinised tungsten trioxide electrodes plotted as a function of platinum content.
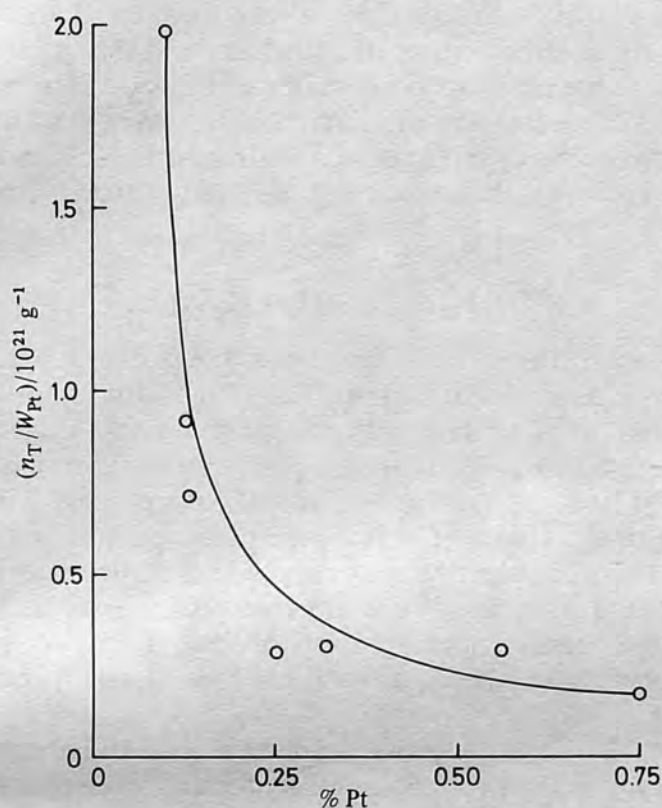
Fig. 4. Specific number of sites (per weight of platinum, W_{Pt}) determined from the evolution of deuterium from deuterium-enriched platinised tungsten trioxide electrodes plotted as a function of platinum content.

Platinum is known to adsorb hydrogen efficiently as atoms, but for metals for which this is not the case a variation of n_T with evolution current may be observed.

RECOMBINATION OF ADSORBED DEUTERIUM ATOMS

The rate constant k_D defined in eqn (14) may be compared with the second-order rate constant k_2 determined from the decrease in the initial coverage with time. Both refer to the recombination of adsorbed deuterium atoms. k_2 is defined in eqn (25). In electrochemical terms the initial rate of evolution of D_2 is $n_T(da/dt)/2$ molecule s^{-1}, where an_T is the initial coverage of deuterium after the enrichment experiment. By eqn (14) this is also $k_D a^2$, giving

$$da/dt = 2k_D/n_T a^2 \qquad (26)$$

and so $k_2 = 2k_D/n_T$. Taking the average values of k_D and n_T given above, $k_2 = 0.02 \pm 0.02$, which includes the measured value of 0.027 ± 0.003 s^{-1}. We have thus provided two independent methods of determining the rate of recombination of deuterium atoms at a metal surface in the course of an electrochemical process. The rate for hydrogen may be found by performing the experiments in normal electrolyte and the subsequent evolution in fully deuterated electrolyte.

HYDROGEN EVOLUTION ON PLATINISED TUNGSTEN TRIOXIDE

The experiments described here should provide a means of measuring the extent to which spillover catalysis occurs in this system. The evidence for reaction occurring on the tungsten bronze and not just on platinum is clear, a conclusion which is in

agreement with other work.[10, 11] This may be seen from fig. 3 and 4. For a reaction on platinum alone, the specific volume of deuterium and the specific number of sites would be constant with the platinum content of the electrode. Here we find an increase in these quantities with decreasing platinum loading. Whether the evolution from tungsten oxide is entirely due to spillover as given in reactions (7) and (8) is not known. An evolution route solely on the conducting tungsten bronze is possible:

$$H^+ + H_x WO_3 + e \rightarrow H \cdot H_x WO_3 \tag{27}$$

$$2H \cdot H_x WO_3 \rightarrow H_2 + H_x WO_3. \tag{28}$$
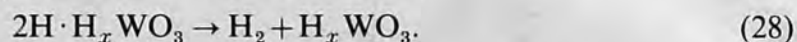
This route is supported by the fact that it was possible to evolve hydrogen at tungsten trioxide in the absence of platinum, although at a high overpotential. If two or more mechanisms (evolution at platinum, spillover, evolution on a tungsten bronze) occur in parallel, the rate parameters determined from the isotopic enrichment experiments (n_T, k_D and a) would be some average of those of each process. This may be seen in the correspondance of the values of k_D on pure platinum and on the highest-loaded platinised tungsten trioxide, when we may conclude that the majority of the reaction occurs on the platinum particles. Work is in progress to solve the kinetics of the schemes involving the bronze route. Analysis of data from the isotopic-enrichment experiments may show the relative contributions of reactions (7) and (8) and reactions (27) and (28).

The use of cheap, synergistically active supports such as tungsten trioxide may have some use in industry, *e.g.* the production of deuterium by electrolysis.

[1] D. B. Hibbert, *J. Chem. Soc., Chem. Commun.*, 1980, 202.
[2] C. R. Churchill and D. B. Hibbert, *J. Chem. Soc., Faraday Trans. 1*, 1982, **78**, 2937.
[3] D. B. Hibbert and C. R. Churchill, *J. Chem. Soc., Faraday Trans. 1*, 1984, **80**, 1965.
[4] J. O'M. Bockris and A. K. N. Reddy, *Modern Electrochemistry* (Plenum Press, New York, 1977), vol. 2, chap. 10.
[5] J. O'M. Bockris and S. Srinivasan, *J. Electrochem. Soc.*, 1964, **111**, 858.
[6] B. S. Hobbs and A. C. C. Tseung, *J. Electrochem. Soc.*, 1972, **119**, 580.
[7] B. S. Hobbs and A. C. C. Tseung, *J. Electrochem. Soc.*, 1973, **120**, 766.
[8] B. S. Hobbs and A. C. C. Tseung, *J. Electrochem. Soc.*, 1975, **122**, 1174.
[9] G. Vertes and G. Horanyi, *Acta Chim. Sci. Hung.*, 1974, **83**, 135.
[10] D. B. Hibbert, N. Thomas and A. C. C. Tseung, *J. Chem. Soc., Chem. Commun.*, 1977, 193.
[11] S. A. Abbaro, A. C. C. Tseung and D. B. Hibbert, *J. Electrochem. Soc.*, 1980, **127**, 1106.

Kinetics of the Electrochemical Evolution of Isotopically Enriched Gases

Part 1.—$^{18}O^{16}O$ Evolution on Platinum in Acid and Alkaline Solution

By Christine R. Churchill and D. Brynn Hibbert*

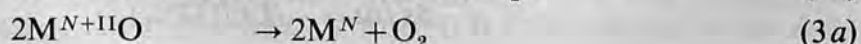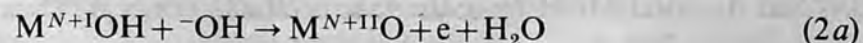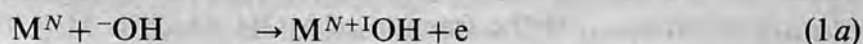Department of Chemistry, Bedford College, Regent's Park, London NW1 4NS

A method is described which follows, by mass spectrometry, the kinetics of $^{18}O^{16}O$ evolution from an electrode surface enriched with ^{18}O. The kinetics on a platinum surface in acid and alkaline electrolyte were consistent with a mechanism of oxygen evolution which involves successive oxidations on a single platinum atom. The total number of platinum sites responsible for oxygen evolution was less than the total number of atoms at the surface.

The electrochemical evolution of oxygen from metals occurs on an oxide-covered surface,[1-8] but the exact nature and participation of this surface in the reaction has yet to be fully interpreted. Rosenthal and Veselovski[9] first demonstrated the existence of surface oxides during oxygen evolution by means of an ^{18}O tracer. They showed that whilst surface oxygen compounds formed between 0.8 and 1.2 V (vs. SHE) do not take part in the process, higher oxides formed at potentials >1.4 V do participate. Several authors have postulated schemes involving reactions of higher oxides but no direct evidence has been forthcoming. Tseung and Jasem[10] have correlated, with some success, the potentials of the metal/metal-oxide couple or lower-metal-oxide/higher-metal-oxide couple with the onset of oxygen evolution. Further work on $NiCo_2O_4$[11] has confirmed that Ni^{3+} (possibly Ni^{4+}) and Co^{4+} are formed at potentials at which oxygen is evolved. The importance of this approach to electrolytic devices is obvious; no matter how efficiently oxygen is evolved on a particular surface, if the highest metal oxide is not formed until a potential is reached which is substantially above $E^{\ominus}$ for oxygen evolution (1.23 V at 25 °C), then a voltage loss is inevitable. In the case of platinum, Hoare[1] agreed that unless the platinum electrode is anodically polarised beyond the equilibrium potential of the PtO/PtO_2 couple, oxygen evolution cannot proceed. In an earlier work[12] the use of ^{18}O to observe the kinetics of evolution of oxygen on $NiCo_2O_4$ was demonstrated. Here, using an improved experimental technique and an extended kinetic interpretation which allows for two intermediate oxides, information is obtained regarding the total number of sites, the extent of higher oxide formation and the general mechanism.
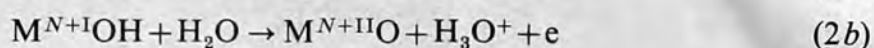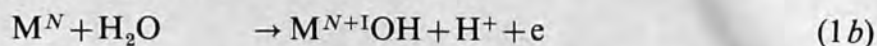
THEORY

FRACTION OF ^{18}O IN THE EVOLVED GAS AT THE SURFACE

A simple mechanism for oxygen evolution on a metal in oxidation state, N, M^N via higher oxidation states $N+I$, $N+II$ is

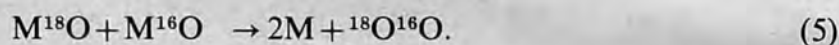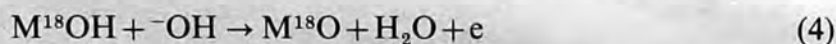$$M^N + {}^-OH \rightarrow M^{N+I}OH + e \qquad (1a)$$

$$M^{N+I}OH + {}^-OH \rightarrow M^{N+II}O + e + H_2O \qquad (2a)$$

$$2M^{N+II}O \rightarrow 2M^N + O_2 \qquad (3a)$$

for reactions in alkaline media, and

$$M^N + H_2O \quad\quad \rightarrow M^{N+I}OH + H^+ + e \tag{1b}$$

$$M^{N+I}OH + H_2O \rightarrow M^{N+II}O + H_3O^+ + e \tag{2b}$$

$$2M^{N+II}O \quad\quad \rightarrow 2M^N + O_2 \tag{3b}$$

for reactions in acid media. The initial oxidation state of the metal (N) may refer to a bare metal surface ($N = 0$), or to an oxide covered surface ($N > 0$). For example, on platinum PtO_2 (*i.e.* $N = 4$) is the stable oxide on which oxygen is evolved.

If the reactions are carried out in electrolyte containing a fraction f_0 of ^{18}O, in the steady state a fraction f_0 of $M^{18}OH$ and $M^{18}O$ will be found at the surface. Evolution of oxygen on such an enriched electrode in an electrolyte having a normal ^{18}O content leads to a progressive depletion of ^{18}O from the surface and the appearance of $^{18}O^{16}O$ and $^{18}O^{18}O$ in the gas phase by reactions such as

$$M^{18}OH + {}^-OH \rightarrow M^{18}O + H_2O + e \tag{4}$$

$$M^{18}O + M^{16}O \quad \rightarrow 2M + {}^{18}O^{16}O. \tag{5}$$

If the surface enrichment is small, reactions such as

$$2M^{18}O \rightarrow 2M + {}^{18}O^{18}O \tag{5'}$$

may be neglected. In addition, if the overpotential for oxygen evolution is high, the back reactions of (4) and (5) may be neglected. Thus the reaction scheme comprising reactions (4) and (5) is one of consecutive first-order processes giving rise to $^{18}O^{16}O$ in the gas phase. Let a and b be the initial enrichment of ^{18}O in the surface oxide layer as $M^{18}OH$ and $M^{18}O$, respectively, and let x, y and z be the enrichment of ^{18}O at time t as $M^{18}OH$, $M^{18}O$ and $^{18}O^{16}O$, respectively. The kinetic equations are thus

$$dx/dt = -k_4 x$$

$$dy/dt = k_4 x - k_5 y$$

$$dz/dt = k_5 y$$

where k_4 and k_5 are first-order rate constants for reactions (4) and (5). In this derivation no account is taken of kinetic isotope effects and single values of k_4 and k_5 are assumed. The solution for y is

$$y = \exp(-k_5 t)\,[k_4 a/(k_5 - k_4)]\,\{[\exp((k_5 - k_4)t) - 1] + b\} \tag{6}$$

for $k_4 \neq k_5$ and

$$y = (kat + b)\exp(-kt) \tag{7}$$

for $k_4 = k_5 = k$. The fraction of ^{18}O in the evolved oxygen (f_{18}) is the ratio of the rate of evolution of ^{18}O as $^{18}O^{16}O$ and the total rate of evolution of oxygen atoms. Thus

$$f_{18} = (dz/dt)/(Li/2F) = k_5 y/(Li/2F) \tag{8}$$

where i is the galvanostatic current, F is the Faraday constant and L is Avogadro's number. The rate constants k_4 and k_5 are dependent on the current flowing and the total number of sites at the electrode surface. The rate of reaction (4) for all oxygen atoms must be $iL/2F$ atom s^{-1} and therefore the rate of reaction of $M^{18}OH$ is $(iL/2F)$ (f_{MOH}), where f_{MOH} is the fraction of MOH which is $M^{18}OH$. In terms of $M^{18}OH$ (x) and the total MOH (x_T), the rate is $(iL/2F)(x/x_T)$. Thus

$$dx/dt = -iLx/(2Fx_T). \tag{9}$$

Comparison with the treatment above shows that $k_4 = iL/(2Fx_T)$. If y_T is the total MO, then by similar reasoning $k_5 = iL/(2Fy_T)$. Substituting values of k_5 into eqn (8) gives

$$f_{18} = y/y_T \tag{10}$$

where y is given by eqn (6) or (7).

FRACTION OF ^{18}O IN THE EVOLVED GAS AT THE MASS SPECTROMETER

In an experiment the fraction of ^{18}O in the evolved gas cannot be measured at the electrode surface but some distance away where it is diluted by a purging gas. It is possible to allow for this in the kinetic equations and obtain an expression for the experimental m/e 34 signal. Let the evolved oxygen and a purge gas expand into a volume which may accommodate n moles of an ideal gas at a total rate v mol s^{-1}. The rate at which all ^{18}O is introduced into the volume is $k_5 y$ [eqn (5)] plus a background component v_b. The natural abundance of ^{18}O is 0.002, so $v_b = (iL/2F) \times 0.002$ atom s^{-1}. The rate at which ^{18}O is removed from the volume is the rate at which all gas flows through (v) multiplied by the fraction of ^{18}O in the volume, which is n_{18}/n, if n_{18} is the total ^{18}O in the volume. Therefore

$$dn_{18}/dt = k_5 y + v_b - (n_{18}/n)v \tag{11}$$

where $v/n \; (= k_n)$ is a first-order rate constant which determines the rate at which the mass spectrometer 'sees' changes in ^{18}O at the electrode surface. Eqn (11) may be solved using the expression for y, eqn (6),

$$n_{18} = (v_b/k_n)[1 - \exp(-k_n t)] + [ak_4 k_5/(k_5 - k_4)][\exp(-k_4 t) - \exp(-k_n t)]/(k_n - k_4)$$
$$+ [k_5/(k_n - k_5)]\{b - [ak_4/(k_5 - k_4)]\}[\exp(-k_5 t) - \exp(-k_n t)] \tag{12}$$

for $k_4 \neq k_5$ and

$$n_{18} = (v_b/k_n)[1 - \exp(-k_n t)] + [k/(k_n - k)]\{akt - [ka/(k_n - k)] + b\}\exp(-kt)$$
$$+ [k/(k_n - k)][ka/(k_n - k) - b]\exp(-k_n t) \tag{12'}$$

for $k_4 = k_5 = k$. The mass spectrometer signal of m/e 34 (S) is proportional to the fraction of ^{18}O in the volume at constant pressure

$$S = K(n_{18}/n) \tag{13}$$

where K is the constant of proportionality. In a background experiment in which there is no enrichment (a and b both zero)

$$S = (K/n)(v_b/k_n)[1 - \exp(-k_n t)]. \tag{14}$$

Data from enriched and background experiments will thus allow calculation of the unknowns in eqn (12)-(14).

EXPERIMENTAL

MATERIALS

Platinum black electrodes on 80 gauge platinum mesh screens were prepared by electrolysis of a solution which contained 5 g PtCl$_4$ in 0.1 dm^3 water.[13] The electrodes were formed into a cylinder to provide the maximum area in a given volume of cell. The surface areas of the platinum electrodes were measured by hydrogen stripping[14] and oxygen charging curves.[15] All reagents were of AnalaR grade. The acid electrolyte was 1 mol dm^{-3} sulphuric acid and the alkaline electrolyte was 5 mol dm^{-3} potassium hydroxide, made up in doubly distilled, deionised water. Enrichment to $ca.$ 3% ^{18}O in alkaline electrolyte and 4% ^{18}O in acid electrolyte was accomplished by the addition of suitable amounts of 20% ^{18}O H$_2$O (B.D.H.) to a stock solution

of appropriate concentration of either the acid or the alkali. The isotopic content of the electrolyte was determined by evolving oxygen in the electrolyte and measuring the ratio of m/e 32 and 34 at the steady state.

APPARATUS

The enrichment of a surface with ^{18}O was performed in a thermostatted (20 ± 1 °C) two-compartment cell, continuously purged with nitrogen. The cell used to monitor the subsequent evolution of ^{18}O in normal electrolyte is shown in fig. 1. The aim of the experiment is to detect ^{18}O near to the electrode with as little dead space as possible. The probe to the mass spectrometer (P) was placed in the path of the outgoing gases just above the surface of the
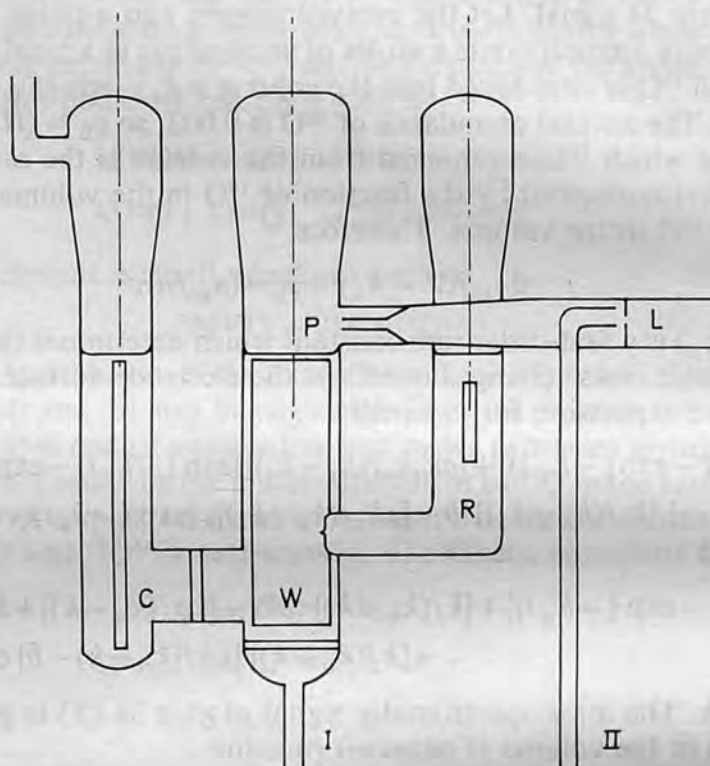

FIG. 1.—The electrochemical cell. For description see text.

electrolyte. Calcium chloride in the probe removed water vapour and also cut down the volume of the probe. Nitrogen was introduced into the working electrode compartment at (I). The arrangement shown allows the majority of the gases in the cell to pass out through an air-lock (II); only a small fraction was diverted into the mass spectrometer *via* a leak valve (L). The counter-electrode was a high-surface-area platinum electrode (C) and the potential of the working electrode (W) was measured against a dynamic hydrogen electrode (DHE) reference electrode (R) *via* a Luggin capillary. The DHE itself was standardised against a bubbling hydrogen electrode. No account was taken of the ohmic drop in the electrolyte.

METHOD

The platinum electrode was first reduced by evolving hydrogen on it at 0.5 A. The current was reversed and oxygen was then evolved in enriched electrolyte at constant current (usually 0.5 A) for periods of time between 15 min and 6 h. The electrode was removed, washed in distilled water for periods up to 1 h and introduced into the cell of fig. 1 at open-circuit voltage. Nitrogen purging was maintained at a constant rate (*ca.* 5 times the rate of oxygen evolution) throughout the experiment. When the m/e 34 peak had fallen to an acceptably low value ($< 1\%$ of the normal background), showing that the small amount of air introduced with the electrode

had been purged away, a constant current (0.25-0.75 A) was passed through the cell by a Weir constant current supply or a Thompson Associates potentiostat operating in a galvanostatic mode. The quadrupole mass spectrometer (Vacuum Generators Anavac 2) operating at 10^{-6} to 10^{-5} mbar continuously monitored m/e 34 which was displayed on a Y–t recorder. This procedure will be referred to as an enriched run. The peak reached a steady state corresponding to the normal background value in $\leqslant$ 10 min. The current was switched off and when the peak height had fallen back to its zero value the current was switched on again and m/e 34 monitored with time. From this second run the background $^{18}O^{16}O$ evolution was determined. It is possible to ignore the small amount of ^{18}O which can be introduced into the electrolyte during the enriched experiment. This can be no more than 10^{-3} of the background and would be expected to be some orders of magnitude less. During the experiment the potential of the working electrode was continually monitored. The accuracy of the method was tested by a series of blank experiments in which two background runs were performed consecutively, and others in which the electrode was simply soaked in enriched electrolyte before being washed *etc.* in the manner described above. A computer program written in FORTRAN V fitted background data, taken at 3 s intervals, to eqn (14) by a least-squares procedure. Using the values of k_n and K/n so obtained, plus a calculated value of v_b, the data of an enriched run were fitted to eqn (12) and (13). Thus a, b, x_T and y_T were determined. In addition, an experiment was performed in which the potential of the electrode was measured during oxygen evolution in the cell of fig. 1 and at open circuit for some time after the current was switched off. Potential measurements were also made for an electrode after it had been washed in the manner described above, following oxygen evolution in enriched electrolyte.

RESULTS

SURFACE AREA OF THE ELECTRODE

The surface area of the platinum electrode determined by hydrogen stripping and by oxygen charging curves agreed within 10%. A typical surface area of a 1 cm $\times$ 1 cm mesh determined by these methods was 2000 cm².

^{18}O ENRICHMENT

A typical fitted background run is given in fig. 2. k_n was of the order of 0.0142 s^{-1} for an evolution current of 0.25 A. The values obtained for k_n in a series of experiments were consistent with the estimated volume of the dead space (n) and the flow rate of the gases (v). A typical enrichment curve (enriched run minus background run) for evolution in alkali is given in fig. 3. The results obtained from acid and alkali solutions were of the same orders of magnitude. For the same 5.0 m² platinum electrode, values of the constants in eqn (6) were: in alkali, $x_T = (1.09 \pm 0.12) \times 10^{19}$, $y_T = (1.02 \pm 0.13) \times 10^{19}$, $a = (1.48 \pm 0.46) \times 10^{16}$ and $b = (1.42 \pm 1.26) \times 10^{13}$. The errors in these values represent the standard errors of six experiments. For experiments in acid the constants were $x_T = (0.99 \pm 0.08) \times 10^{19}$, $y_T = (0.80 \pm 0.03) \times 10^{19}$, $a = (1.48 \pm 0.19) \times 10^{16}$ and $b = 6.02 \times 10^{12}$. The number of platinum atoms on this electrode from oxygen charging experiments was 5.76×10^{19}. All blank experiments showed that no enrichment of ^{18}O could be imparted to an electrode by soaking in enriched electrolyte alone.

VOLTAGE MEASUREMENTS

Fig. 4 shows the potential of an electrode during oxygen evolution and at open circuit in the cell for up to 90 min. The continuous line shows the effect on the open circuit potential of removing the electrode from the cell and washing it for 90 s before re-introduction into the cell.
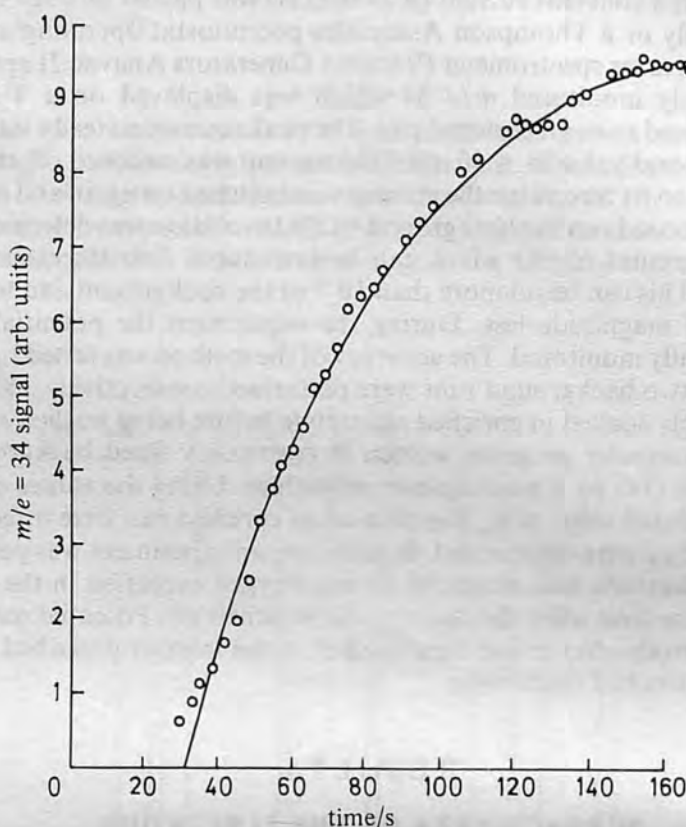
FIG. 2.—Mass spectrometer signal (circles) for m/e 34 after the start of oxygen evolution on the Pt electrode in normal alkaline electrolyte. The continuous line is a fit to eqn (14).

DISCUSSION

TOTAL NUMBER OF SITES

Two facts emerge from these experiments concerning the number of sites on the platinum surface responsible for evolution of oxygen in alkali. First, the numbers of sites generating the higher oxides MOH and MO [x_T and y_T of eqn (9) and (10)] are the same. This is consistent with consecutive oxidation on a single platinum atom. Secondly, the values of x_T and y_T are *ca.* $1/5$ of the value determined for the total number of sites by oxygen charging in alkaline solution. It may be impossible to form a further complete layer of oxygen on an already oxidised surface or reaction between certain high oxide pairs [reaction (3)] may be unfavourable on particular crystal planes. Arguments similar to the latter were proposed by Yeung for the very low surface oxygen coverage found during oxygen reduction on $Nd_{0.5}Sr_{0.5}CoO_3$.[16]

RESIDUAL ^{18}O IN THE SURFACE

It was found that after the electrode was taken out of the enriched electrolyte, whatever the period elapsed (practically this was not less than 3 min), no $M^{18}O$ remained in the surface, *i.e.* $b = 0$. 'MO' is considered to be an unstable oxide which is only formed at high anodic potentials and which decomposes by reaction (3). Its lifetime on removing the anodic potential would be short, in accordance with the experimental findings. In the absence of any mechanism which removes $M^{18}OH$, the initial $M^{18}OH$ [a of eqn (6), (7) *etc.*] should be *ca.* 3% of x_T in alkaline electrolyte and *ca.* 4% of x_T in acid electrolyte. The values for a found in experiments with both acid and alkaline electrolyte were twenty times less than this figure. The loss of $M^{18}O$
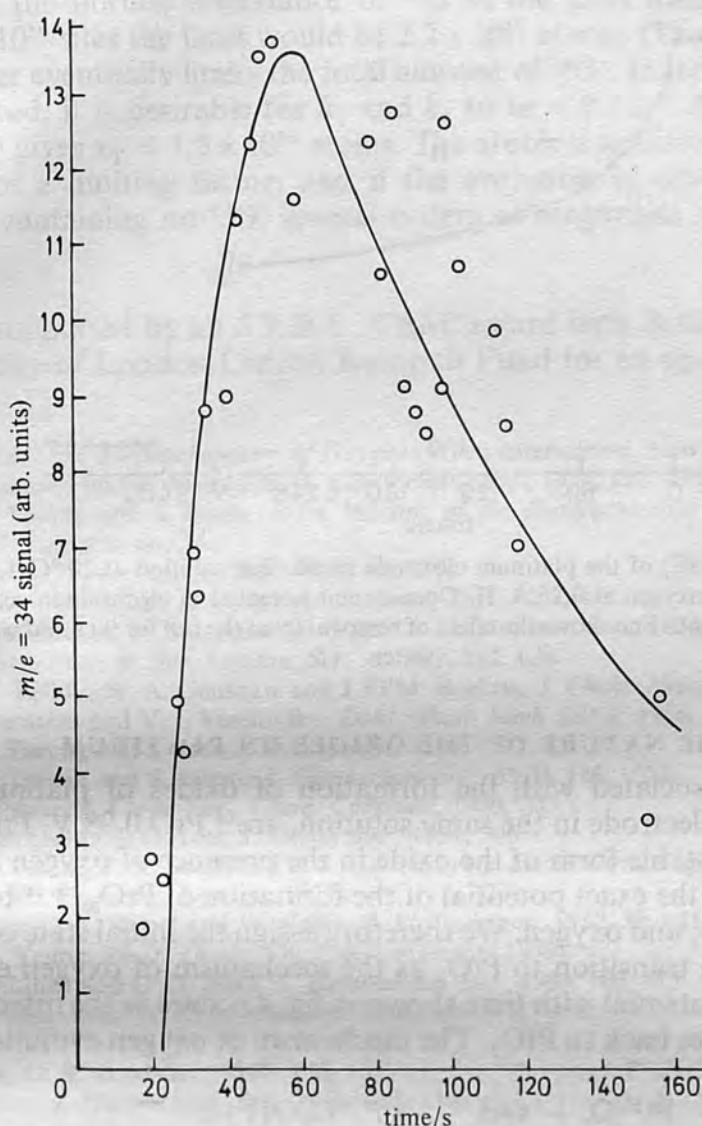
FIG. 3.—Difference between m/e 34 signal for oxygen evolution on the Pt electrode enriched with ^{18}O and the background experiment (circles). The continuous line is a fit to eqn (12) and (13). Washing time was 90 s. The total elapsed time between evoltution in enriched and normal electrolyte was 3 min.

may arise from chemical decomposition of MOH, exchange of ^{18}O with an underlying oxide layer or exchange of ^{18}O with the electrolyte. It is also possible, as Laitinen and Enke have suggested, that evolution of oxygen, whilst being preceded by oxide formation, occurs *via* unstable adsorbed intermediates on the strongly bound oxide layer.[17] The potential of the electrode some minutes after cessation of evolution of oxygen and in a nitrogen purged solution (fig. 4) is well above the ultimate steady-state potential. The chemical decomposition of the intermediate oxide MOH is thus relatively slow and would not cause the observed loss of $M^{18}OH$. Exchange with an underlying oxide layer may be facile, but if the evolution of oxygen takes place on a metal surface, any oxide formed would have the isotopic content of the enriched solution. Exchange of oxygen with the normal electrolyte offers the most likely explanation of the apparent loss of ^{18}O. Reaction between the intermediate oxide MOH and adsorbed water by proton hopping

$$M^{18}OH + M^{16}OH_2 \rightarrow M^{18}OH_2 + M^{16}OH \tag{15}$$
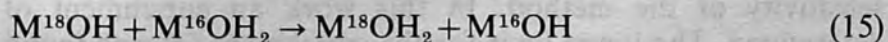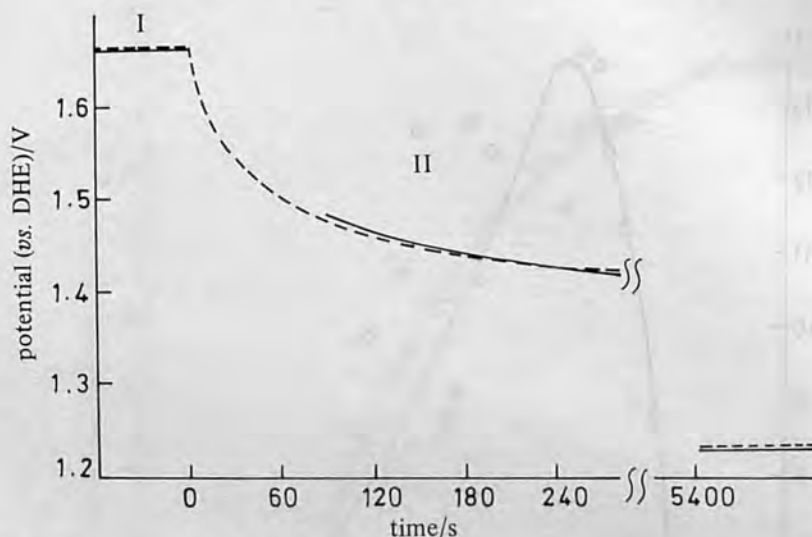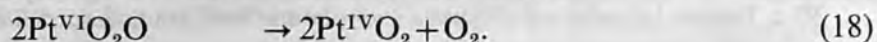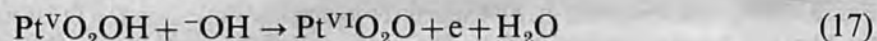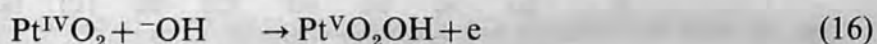
would diminish adsorbed $M^{18}OH$.

FIG. 4.—Potential (*vs.* DHE) of the platinum electrode in alkaline solution at 20 °C. I, Potential during steady-state evolution of oxygen at 0.25 A. II, Open-circuit potential of electrode in cell purged with N_2 (dashed line). The continuous line shows the effect of removal from the cell for 90 s and washing in distilled water.

THE NATURE OF THE OXIDES ON PLATINUM

The potentials associated with the formation of oxides of platinum, measured against a hydrogen electrode in the same solution, are[18] PtO 0.98 V, PtO_2 1.05 V and PtO_3 *ca.* 2.0 V. The stable form of the oxide in the presence of oxygen is PtO_2. There is some doubt about the exact potential of the formation of PtO_3,[18, 19] but it is known to decompose to PtO_2 and oxygen. We therefore assign the initial state of the platinum surface as PtO_2 with transition to PtO_3 as the mechanism of oxygen evolution. The fall in open-circuit potential with time shown in fig. 4 occurs as the intermediate oxide $PtO_2 \cdot OH$ decomposes back to PtO_2. The mechanism of oxygen evolution is therefore

$$Pt^{IV}O_2 + {}^-OH \quad \rightarrow Pt^VO_2OH + e \tag{16}$$

$$Pt^VO_2OH + {}^-OH \rightarrow Pt^{VI}O_2O + e + H_2O \tag{17}$$

$$2Pt^{VI}O_2O \quad \rightarrow 2Pt^{IV}O_2 + O_2. \tag{18}$$

Another question concerning this mechanism is to what extent is the reactive oxygen atom of eqn (18) part of a recognisable species PtO_3? A highly mobile adsorbed atom may not be correctly represented as PtO_3. Further isotopic studies on the exchange between the oxygen atoms in $PtO_2 \cdot O$ may give the answer. Hoare[20] has shown that the formation of a Pt—O 'alloy' during strong anodisation results in a reversible oxygen potential of 1.229 V. He ascribes irreversible behaviour on platinum which is not saturated with oxygen to the action of a local cell at the platinum surface. It may be, therefore, that it is not correct to write the surface species as distinct oxides, although the dissolution of oxygen into the platinum lattice may occur concurrently with oxygen evolution.

SENSITIVITY

The use of ^{18}O as a tracer for oxygen evolution studies reveals the exceptional sensitivity of the method. In this work an enrichment of *ca.* 10^{16} atoms was determined. The lower limit for the enrichment (a) was found experimentally to be

ca. 10% of the normal abundance of ^{18}O in the total number of sites (x_T). For $x_T = 1.1 \times 10^{19}$ sites the limit would be 2.2×10^{15} atoms. (The sensitivity of the mass spectrometer eventually limits the total amount of ^{18}O). In terms of the rate at which ^{18}O is evolved, it is desirable for k_4 and k_5 to be $< 0.2 \text{ s}^{-1}$. For a current of 0.1 A, $k_4 = 0.2 \text{ s}^{-1}$ gives $x_T = 1.5 \times 10^{18}$ atoms. The absolute sensitivity of the mass spectrometer is not a limiting factor, and if the evolution of oxygen occurred from an electrolyte containing no ^{18}O, several orders of magnitude would be added to the sensitivity.

[1] J. P. Hoare, *The Electrochemistry of Oxygen* (Wiley Interscience, New York, 1968).
[2] A. Damjanovic and B. Jovanovic, *J. Electrochem. Soc.*, 1976, **123**, 374.
[3] A. C. C. Tseung and S. Jasem, *151st Meeting of the Electrochemical Society*, Philadelphia, 1977, Extended Abstracts no. 351.
[4] A. Hickling, *Trans. Faraday Soc.*, 1945, **41**, 333.
[5] S. E. S. El Wakkad and S. H. Emara, *J. Chem. Soc.*, 1952, 461.
[6] A. Damjanovic, A. T. Ward and M. O'Jea, *J. Electrochem. Soc.*, 1974, **121**, 1186.
[7] T. R. Hoar, *Proc. R. Soc. London, Ser. A*, 1933, **142**, 628.
[8] A. K. N. Reddy, M. A. Genshaw and J. O'M. Bockris, *J. Chem. Phys.*, 1968, **48**, 671.
[9] N. I. Rosenthal and V. I. Veselovsky, *Dokl. Akad. Nauk SSSR*, 1956, **111**, 637.
[10] A. C. C. Tseung and S. Jasem, *Electrochim. Acta*, 1977, **22**, 31.
[11] A. C. C. Tseung and S. Jasem, *J. Electrochem.Soc.*, 1979, **126**, 1353.
[12] D. B. Hibbert, *J. Chem. Soc., Chem. Commun.*, 1980, 203.
[13] G. J. Hills and D. J. G. Ives, *J. Chem. Soc.*, 1951, 305.
[14] A. C. C. Tseung, P. R. Vassie and B. S. Hobbs, *Symp. Electrochem. Eng.*, ed. J. D. Thornton (Institute of Chemical Engineers, London, 1971), vol. 1, p. 123.
[15] M. Breiter, C. A. Knorr and W. Volkl, *Z. Elektrochem.*, 1955, **59**, 681.
[16] K. Y. Y. Yeung, *Ph.D. Thesis* (The City University, 1979).
[17] H. A. Laitinen and C. G. Enke, *J. Electrochem. Soc.*, 1960, **107**, 773.
[18] M. Pourbaix, *Atlas of Electrochemical Equilibria in Aqueous Solutions* (Pergamon Press, London, 1966).
[19] C. Marie, *C. R. Acad. Sci.*, 1907, **145**, 117.
[20] J. P. Hoare, *J. Electrochem. Soc.*, 1978, **125**, 1768.

(PAPER 1/1924)

Kinetics of the Electrochemical Evolution of Isotopically Enriched Gases

Part 2.—$^{18}O^{16}O$ Evolution on $NiCo_2O_4$ and $Li_xCo_{3-x}O_4$ in Alkaline Solution
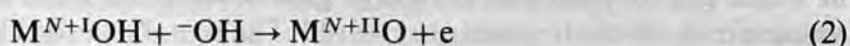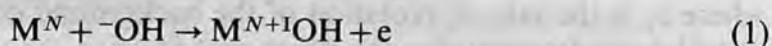
By D. Brynn Hibbert* and Christine R. Churchill

Department of Chemistry, Bedford and Royal Holloway Colleges,
Egham Hill, Surrey TW20 0EX

The kinetics of the electrochemical evolution of $^{18}O^{16}O$ from $NiCo_2O_4$ and $Li_xCo_{3-x}O_4$ ($0 < x < 1.5$) electrodes enriched with ^{18}O have been studied. The number of sites responsible for oxygen evolution is related to the lithium content of $Li_xCo_{3-x}O_4$, showing the importance of tetrahedrally coordinated Co^{3+}. $NiCo_2O_4$ has different Tafel parameters and a greater number of sites. In this case some participation of Ni^{2+} and Co^{2+} is indicated. The data are consistent with a multistep reaction on a single site, or reaction *via* a bridged structure.

The possible use of electrolytically generated hydrogen as a secondary energy vector has sustained interest in the oxygen-evolution reaction. For low-temperature alkaline electrolysis the use of transition-metal oxides as electrocatalysts has been studied.[1-4] In particular, $NiCo_2O_4$ and Li-doped Co_3O_4 have been shown to have high activity.[1-3] A correlation has been drawn between the potential of the highest metal oxide couple and the potential at which oxygen is evolved.[1] A simple scheme for this process may be written as follows:
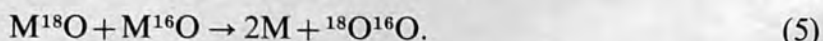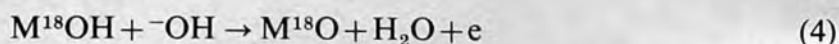
$$M^N + {}^-OH \rightarrow M^{N+I}OH + e \tag{1}$$

$$M^{N+I}OH + {}^-OH \rightarrow M^{N+II}O + e \tag{2}$$

$$2M^{N+II}O \rightarrow 2M^N + O_2 \tag{3}$$

where M^N is the metal surface atom in oxidation state N. For evolution at a metal N may be zero if the highest oxidation state is two. At platinum for example, oxygen evolution probably takes place on the stable oxide PtO_2 (*i.e.* $N = IV$) with the highest unstable oxide PtO_3 ultimately decomposing in reaction (3).[5] Rasiyah and Tseung[3] have pointed out that for ions already in high oxidation states a double transition may not be possible. For example, in $NiCo_2O_4$, for Ni^{3+} and Co^{3+} to be involved, transitions to the $+5$ state would be predicted. A scheme proposed by Rasiyah and Tseung[3] involving a bridged structure is discussed later in this paper.
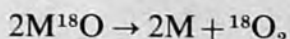
THEORY

The theory of the evolution of $^{18}O^{16}O$ from an electrode containing ^{18}O has been fully developed in a previous paper.[5] Here we shall briefly outline the theory and quote the final equation, which describes the variation of the mass spectrometer signal m/e 34 with time. The electrode surface is enriched with a small percentage of ^{18}O (typically 3%) by evolving oxygen in a solution containing that isotope. In a separate experiment, oxygen is evolved galvanostatically from the enriched surface but now

in electrolyte having normal isotopic content. As ^{18}O in the surface is displaced by ^{16}O an enrichment of ^{18}O in the gas (as $^{18}O^{16}O$) is observed. The rate at which the m/e 34 peak changes with time may be analysed in terms of the mechanism given by reactions (1)–(3). At a surface containing $M^{18}OH$ and $M^{18}O$, the reactions which result in $^{18}O^{16}O$ are

$$M^{18}OH + {}^-OH \rightarrow M^{18}O + H_2O + e \tag{4}$$

$$M^{18}O + M^{16}O \rightarrow 2M + {}^{18}O^{16}O. \tag{5}$$

If the surface enrichment is small, reactions such as

$$2M^{18}O \rightarrow 2M + {}^{18}O_2$$

may be neglected. If the enrichments of ^{18}O as $M^{18}OH$, $M^{18}O$ and $^{18}O^{16}O$ at time t are x, y and z, respectively, the kinetic equations are

$$dx/dt = -k_4 x \tag{6}$$

$$dy/dt = k_4 x - k_5 y \tag{7}$$

$$dz/dt = k_5 y \tag{8}$$

where k_4 and k_5 are first-order constants for reactions (4) and (5). k_4 and k_5 may be expressed in terms of the current density i and the total number of sites available to form $M^{18}OH$ (x_T) and $M^{18}O$ (y_T):[5]

$$k_4 = iN/2Fx_T, \quad k_5 = iN/2Fy_T$$

where N and F are Avagadro's number and the Faraday constant. Eqn (6)–(8) may be solved for y, which is related to the change in concentration of ^{18}O in the gas phase (n_{18}) as seen by the mass spectrometer:

$$dn_{18}/dt = k_5 y + v_b - (v/n)n_{18} \tag{9}$$

where v_b is the rate of evolution of the background component of ^{18}O, v is the rate at which gas (oxygen plus the purge gas) flows to the mass spectrometer and n is the volume into which the gases are evolved. The signal recorded by the mass spectrometer (S) is given by

$$S = K(n_{18}/n) \tag{10}$$

where K is a constant. For evolution of ^{18}O from an electrode having normal isotopic content, the m/e 34 signal varies with time according to

$$S = (K/n)(v_b/k_n)[1 - \exp(-k_n t)] \tag{11}$$

where $k_n = v/n$. The mass spectrometer signal for evolution from an enriched electrode is

$$\begin{aligned} S = {} &(K/n)(v_b/k_n)[1 - \exp(-k_n t)] \\ &+ [ak_4 k_5/(k_5 - k_4)][\exp(-k_4 t) - \exp(-k_n t)]/(k_n - k_4) \\ &+ [k_5/(k_n - k_5)]\{b - [ak_4/(k_5 - k_4)]\}[\exp(-k_5 t) - \exp(-k_n t)] \end{aligned} \tag{12}$$

for $k_4 \neq k_5$, and

$$\begin{aligned} S = {} &(K/n)(v_b/k_n)[1 - \exp(-k_n t)] \\ &+ [k/(k_n - k)]\{akt - [ka/(k_n - k)] + b\}\exp(-kt) \\ &+ [k/(k_n - k)][ka/(k_n - k) - b]\exp(-k_n t) \end{aligned} \tag{13}$$

for $k_4 = k_5 = k$. a and b are the fractional coverages of MOH and MO, respectively, at the start of the evolution of oxygen in the enriched run.

Data from enriched and background experiments allow calculation of the unknowns in eqn (11)–(13).

EXPERIMENTAL

MATERIALS

All chemicals were of AnalaR grade and used without further purification. $NiCo_2O_4$ was prepared by freeze-drying[6] a solution of nickel(II) nitrate and cobalt(II) nitrate in acetic acid, followed by decomposition *in vacuo* at 250 °C (1 h) and curing in air (10 h). Lithiated cobalt oxide was prepared by the slurry method.[4] $Co(OH)_2$ was precipitated from a solution of $CoCl_2$ with a KOH solution and filtered. The precipitate was washed with a saturated solution of LiOH, dried in air at 100 °C (5 h) and heated to 400 °C (5 h). Teflon-bonded electrodes were made by ultrasonically mixing the catalyst and a Teflon dispersion (G.P.I. Plastic Coating Systems Ltd) in the ratio of 10:3 by weight. The resulting slurry was painted on a 400 mesh nickel screen (Goodfellow Metals) and cured at 300 °C for 10 h. The final catalyst loading was $10-15$ mg cm^{-2}. Alternatively, $NiCo_2O_4$ electrodes were prepared by dipping a weighed nickel mesh into a solution of 0.5 mol dm^{-3} nickel(II) nitrate $+ 1$ mol dm^{-3} cobalt(II) nitrate and decomposing the adhering solution at 300 °C for 10 min. This was repeated until the required loading was achieved. Lithiated cobalt oxide electrodes were prepared in a similar manner from lithium nitrate and cobalt nitrate solutions. The compositions of the lithiated cobalt oxide electrodes were determined by atomic absorption and emission spectroscopy. A portion of each electrode was leached in dilute acetic acid at 60 °C and the solution analysed for lithium. The leached electrode material was then dissolved in hot concentrated nitric acid and analysed for lithium and cobalt. The initial leach in acetic acid removes free lithium oxide which has not been incorporated into the cobalt oxide lattice and which therefore does not contribute to the conductivity or electrochemical properties.[7] The structures of the catalysts were analysed by powder X-ray diffraction. Single-point B.E.T. surface-area measurements (Micromeritics 2200) were made on each catalyst. The alkaline electrolyte was 5 mol dm^{-3} KOH made up in doubly distilled deionised water. Enrichment to *ca.* 3% ^{18}O was by the addition of 20% $H_2^{18}O$ (B.D.H.) to a stock solution of appropriate concentration. The isotopic content of the enriched electrolyte was determined by evolving oxygen in the electrolyte and measuring the ratio of m/e 32 and 34 at the steady state.

APPARATUS

The isotope experiments were performed in a three-compartment cell which has been described elsewhere.[5] The counter-electrode was a platinum mesh and the reference electrode was a dynamic hydrogen electrode which had been standardised against a bubbling hydrogen electrode. The isotopic content of the gas was measured by a quadrupole mass spectrometer (V.G. Anavac 2) operating at 10^{-6} to 10^{-5} mbar. Electrochemical measurements were performed in the same cell using a Thompson Associates potentiostat and, for the cyclic voltammetry experiments, a ramp generator.

METHOD

The electrode was held at 1.0 V *vs* DHE for several minutes in the enriched electrolyte before oxygen was galvanostatically evolved at 0.5 A for periods of time between 15 min and 6 h. The electrode was removed, washed in distilled water for up to 5 min (after which no enrichment could be subsequently detected) and introduced into the cell connected to the mass spectrometer. Nitrogen purging was maintained at a constant rate (*ca.* 5 times the rate of oxygen evolution) throughout the experiment. When the m/e 34 peak had fallen to $< 1\%$ of the normal background a constant current (0.2–0.75 A) was passed through the cell and the m/e 34 signal recorded continuously. The peak reached a steady-state value corresponding to the background $^{18}O^{16}O$ in *ca.* 5 min. The current was switched off, and when the peak had fallen to its zero value the current was switched on again and m/e 34 measured with time. From the second run the background $^{18}O^{16}O$ evolution was determined. A computer program written in FORTRAN 77 fitted the background data taken at 3 s intervals to eqn (11) by a least-squares procedure, and values of k_n and K/n were determined. With a calculated value of v_b, a second least-squares

procedure fitted the data of the first run to eqn (12) and (13) giving values of x_T, y_T, a and b. For the cyclic-voltammetry experiments an electrode was cycled between 0.6 and 1.8 V vs DHE at scan rates of 8–80 mV s^{-1}. The number of surface ions was determined by controlled potential coulometry.[8] The potential of the electrode was maintaned at its rest potential (1.0 V) for 10 min to reduce all surface compounds. Pulsing to a more anodic potential (1.6 V) caused a current to flow which was recorded on a Y–t recorder. Integration of the current with respect to time gave the charge passed which may be related to the number of surface ions. Both methods were repeated for a nickel screen and the results have been corrected for the small component introduced by the screen.

After each electrode had been used for an enrichment experiment samples of the electrolyte were analysed by atomic absorption for nickel, cobalt and lithium.

RESULTS

CHARACTERISATION OF THE ELECTROCATALYST

The B.E.T. (Brunauer–Emmett–Teller) surface areas of the freeze-dried catalysts were 35 m^2 g^{-1} for $NiCo_2O_4$ and between 23 and 53 m^2 g^{-1} for the lithiated cobalt oxide catalysts. Powder X-ray patterns confirmed the spinel structure. The resistivity of the catalyst powders compressed in a Teflon die were $< 10 \, \Omega$ cm. Analysis of combined lithium in the lithiated cobalt oxide electrodes is given in table 1. Up to 50% of the lithium was in the free state. No corrosion of the electrodes was found, even after prolonged use.

TAFEL PARAMETERS

Fig. 1 shows a Tafel plot for a $NiCo_2O_4$ electrode and two $Li_xCo_{3-x}O_4$ ($x = 0.36$, 0.07) electrodes. The slopes of the two lines obtained from the $NiCo_2O_4$ electrode were 46 and 145 mV per decade, and the single slope from the lithiated electrodes was 70 mV per decade.
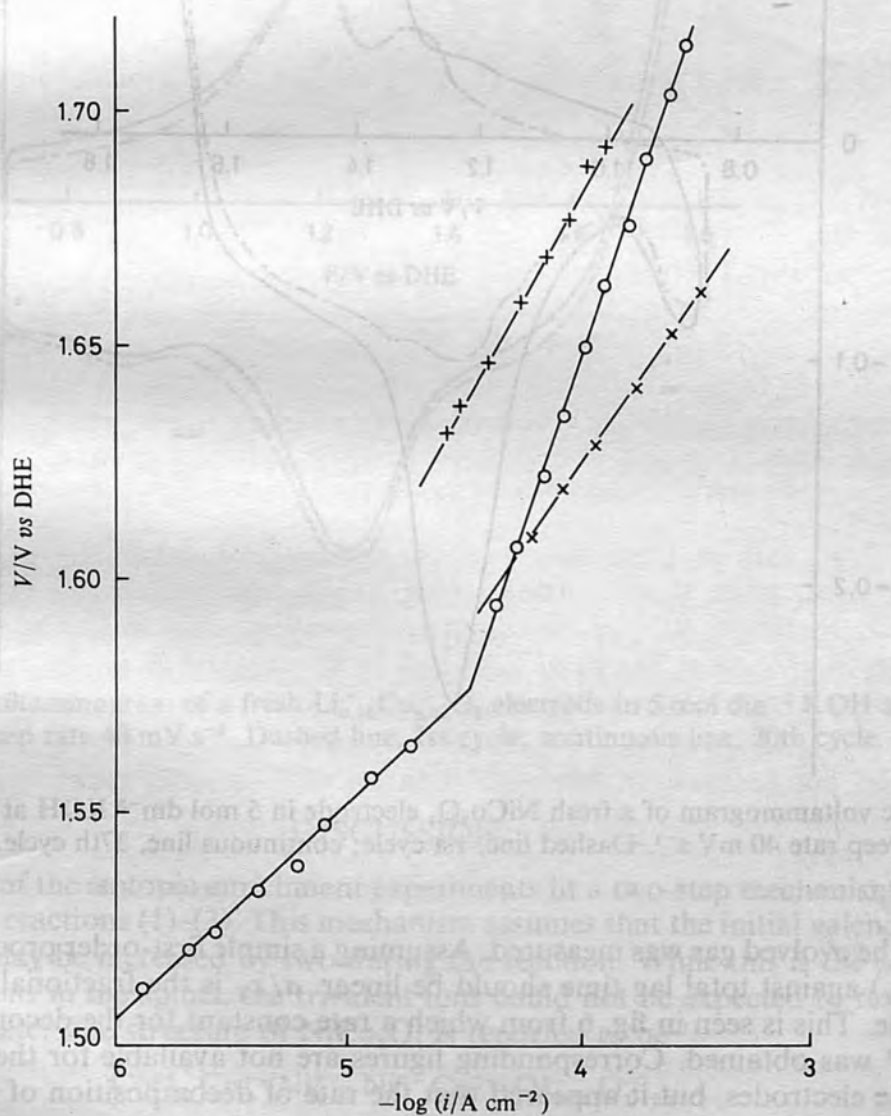
CYCLIC VOLTAMMETRY

A cyclic voltammogram of a fresh $NiCo_2O_4$ electrode showed two anodic peaks at 1.30 and 1.43 V which, after 40 cycles, merged into a single peak at 1.40 V (fig. 2). A 10% Li/Co_3O_4 electrode, however, consistently showed two peaks (fig. 3).

EVOLUTION OF $^{18}O^{16}O$

Fig. 4 shows a typical background run for the evolution of $^{18}O^{16}O$ on $NiCo_2O_4$. k_n was of the order of 0.02 s^{-1} for an evolution current of 0.3 A. Fig. 5 is of the enrichment (with the background subtracted) for evolution from the same electrode after enrichment with ^{18}O. The values of x_T and y_T from two $NiCo_2O_4$ electrodes and five $Li_xCo_{3-x}O_4$ electrodes are given in table 1, where they are compared with the number of surface ions calculated from constant-potential coulometry experiments. It has been shown[9, 10] that the charge passed in this experiment is sufficient to oxidise all surface ions in $NiCo_2O_4$ to the $+4$ state. A check on this calculation comes from surface-area measurements and a knowledge of the catalyst loading. Experiments repeated at different evolution currents gave values of the kinetic parameters that were independent of current, showing the validity of the expressions for k_4 and k_5. The coverage of the highest-valence oxide [b in eqn (12)] was consistently of the order of 10^{-6} of the number of sites for both catalysts; $i.e.$ by the time the experiment was performed virtually none of the highest oxide remained. Both catalysts showed a coverage of the intermediate oxide [a in eqn (12)] of $ca.$ 0.1% of the number of sites. The value of a fell with increasing washing time. For $NiCo_2O_4$ the variation of the initial coverage of M^{18}OH was studied with the time elapsed between evolution of oxygen in the enriched solution and the subsequent experiment in which the ^{18}O

Table 1. Data from ^{18}O enrichment experiments on $NiCo_2O_4$ and $Li_xCo_{3-x}O_4$ electrodes

electrode	no. of surface cells,[a] $u/10^{19}$	no. of experiments	no. of intermediate oxide sites		x_T/u
			$x_T/10^{19}$	$y_T/10^{19}$	
$NiCo_2O_4$	2.0	14	2.9 ± 1.0	2.6 ± 0.9	1.5
$NiCo_2O_4$	0.9	6	3.1 ± 1.4	2.7 ± 1.1	2.8
1.5% Li/Co_3O_4	9.1	5	1.5 ± 0.3	1.3 ± 0.3	0.16
3.5% Li/Co_3O_4	6.7	5	1.4 ± 0.3	1.3 ± 0.3	0.21
4.3% Li/Co_3O_4	6.2	6	1.6 ± 0.5	1.4 ± 0.5	0.26
5.0% Li/Co_3O_4	5.6	5	2.0 ± 0.5	1.5 ± 0.5	0.36
8.0% Li/Co_3O_4	3.5	5	1.9 ± 0.9	1.6 ± 0.8	0.53

[a] Calculated from oxide-charging experiments.

Fig. 1. Tafel plots for the evolution of oxygen on: $\bigcirc$, $NiCo_2O_4$; $\times$, $Li_{0.07}Co_{2.93}O_4$ and $+$, $Li_{0.36}Co_{2.64}O_4$ in 5 mol dm^{-3} KOH at 25 °C.
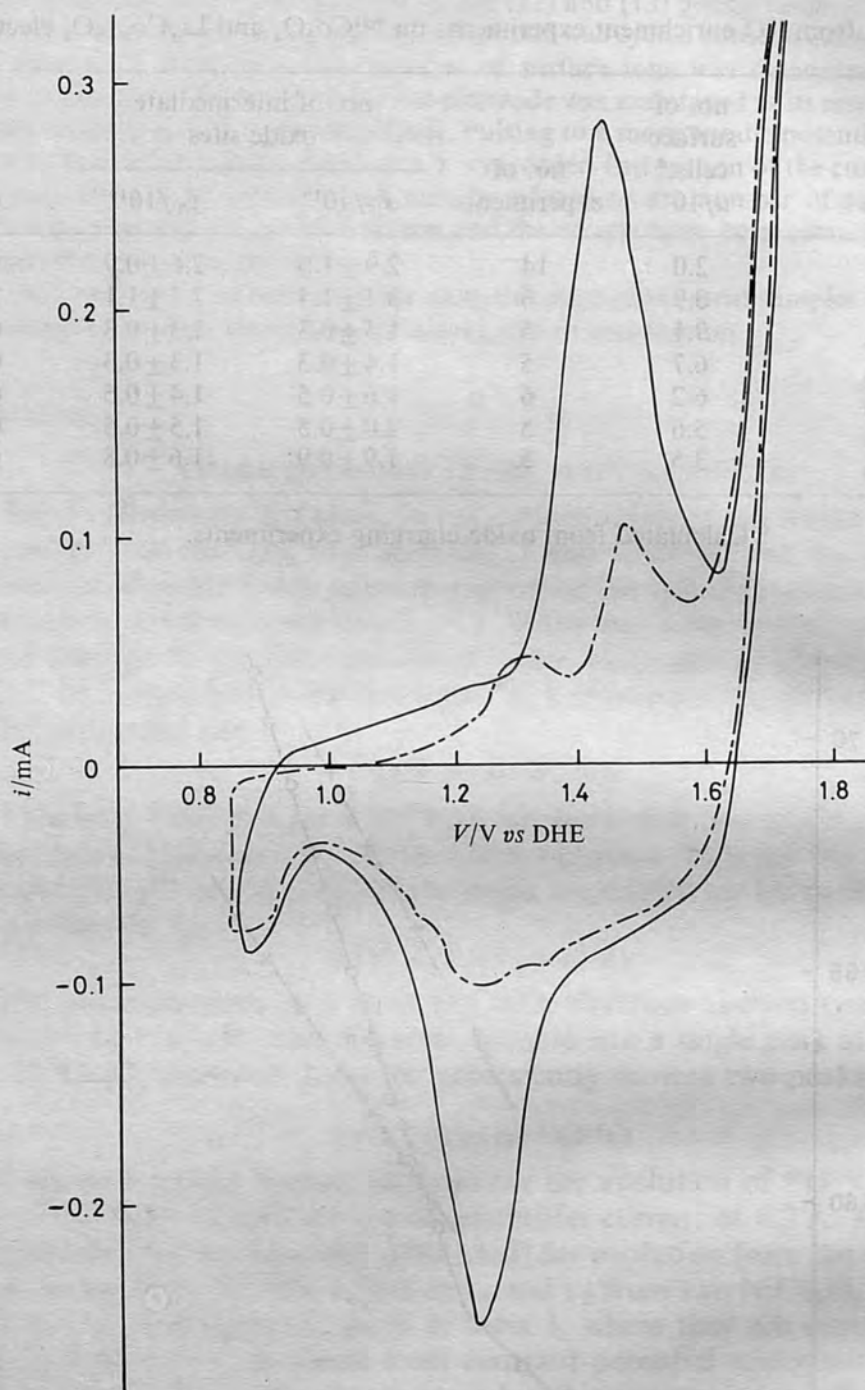
Fig. 2. Cyclic voltammogram of a fresh $NiCo_2O_4$ electrode in 5 mol dm^{-3} KOH at 25 °C and sweep rate 40 mV s^{-1}. Dashed line, 1st cycle; continuous line, 37th cycle.

content of the evolved gas was measured. Assuming a simple first-order process a plot of $\log(a/x_T)$ against total lag time should be linear. a/x_T is the fractional coverage of this oxide. This is seen in fig. 6 from which a rate constant for the decomposition of 0.005 s^{-1} was obtained. Corresponding figures are not available for the lithiated cobalt oxide electrodes, but it appeared that the rate of decomposition of the lower oxide was of the same order as for $NiCo_2O_4$.
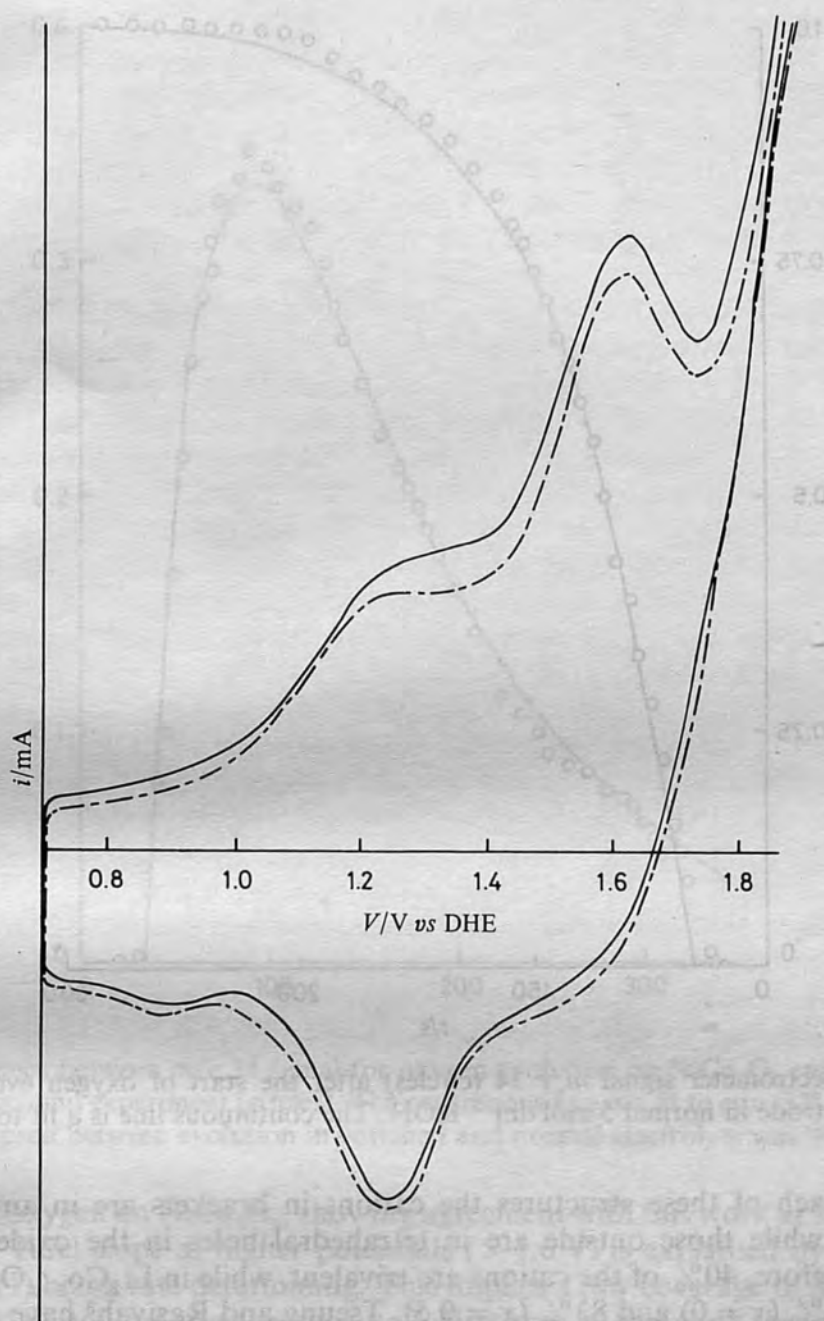
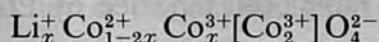**Fig. 3.** Cyclic voltammogram of a fresh $Li_{0.36}Co_{2.64}O_4$ electrode in 5 mol dm^{-3} KOH at 25 °C and sweep rate 40 mV s^{-1}. Dashed line, 1st cycle; continuous line, 20th cycle.

DISCUSSION

The results of the isotopic enrichment experiments fit a two-step mechanism of the form given by reactions (1)–(3). This mechanism assumes that the initial valence state of the metal may be increased by two during the reaction. While this is the case for the divalent ions in the spinel, the trivalent ions could not be expected to reach the pentavalent state. The structure of $NiCo_2O_4$ is reported to be[11]

$$Co_{1-a}^{2+} Co_a^{3+}[Ni_{1-a}^{2+} Ni_a^{3+} Co^{3+}] O_{3+2a}^{2-} O_{1-2a}^{-}$$
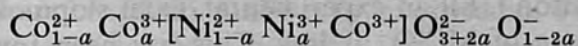
with $a \approx 0.1$, and for $Li_xCo_{3-x}O_4$

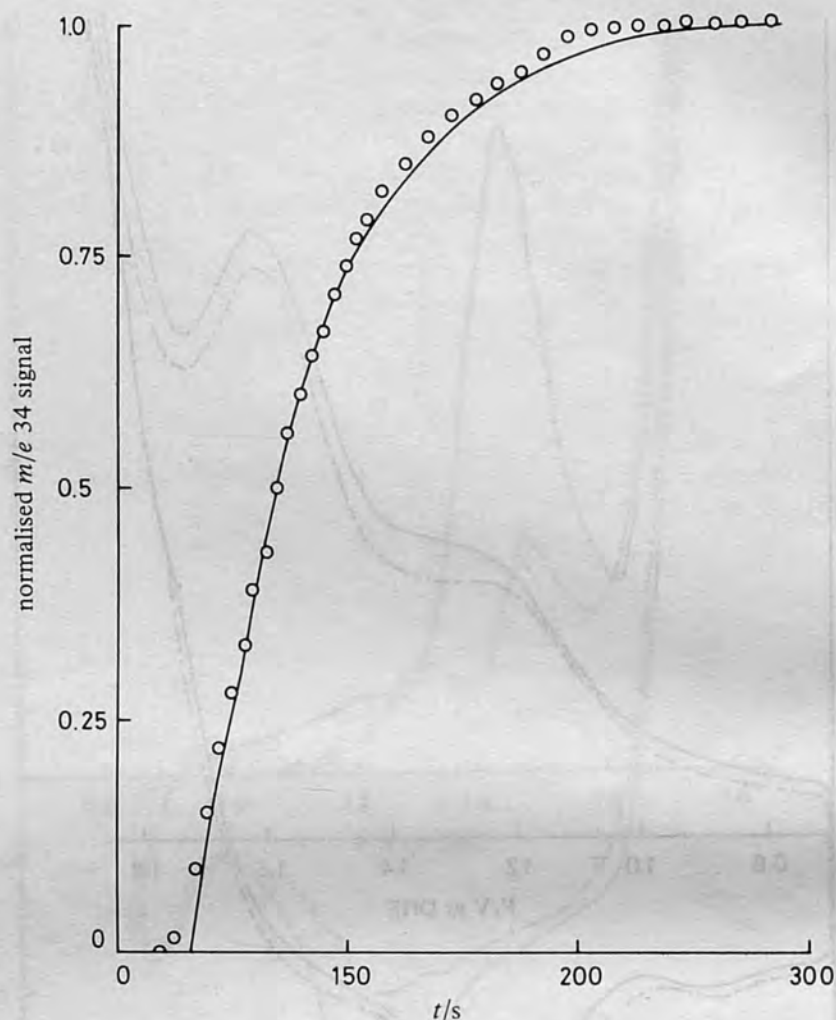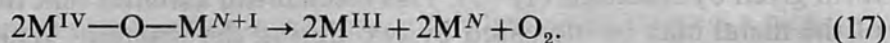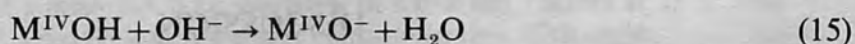$$Li_x^+ Co_{1-2x}^{2+} Co_x^{3+}[Co_2^{3+}] O_4^{2-}$$

Fig. 4. Mass-spectrometer signal m/e 34 (circles) after the start of oxygen evolution on a $NiCo_2O_4$ electrode in normal 5 mol dm^{-3} KOH. The continuous line is a fit to eqn (11).

[ref. (3)]. In each of these structures the cations in brackets are in an octahedral environment, while those outside are in tetrahedral holes in the oxide lattice. In $NiCo_2O_4$, therefore, 40% of the cations are trivalent, while in $Li_xCo_{3-x}O_4$ there may be between 67% ($x = 0$) and 83% ($x = 0.5$). Tseung and Rasiyah[3] have suggested a mechanism involving an initial trivalent state with a second site forming a bridge structure:

$$M^{III} + OH^- \rightarrow M^{IV}OH + e \tag{14}$$

$$M^{IV}OH + OH^- \rightarrow M^{IV}O^- + H_2O \tag{15}$$

$$M^{IV}O^- + M^N \rightarrow M^{IV}-O-M^{N+I} + e \tag{16}$$

$$2M^{IV}-O-M^{N+I} \rightarrow 2M^{III} + 2M^N + O_2. \tag{17}$$

An advantage of this mechanism is that if the formation of the bridge intermediate is rate determining [reaction (16)] an experimental Tafel slope of 40 mV per decade is expected if the coverage of $M^{IV}O^-$ is low. This has been found independently by Rasiyah and Tseung[12] and ourselves at low potentials for $NiCo_2O_4$. Two Tafel slopes of 50 and 90 mV per decade have been reported by Efremov and Zhukov[13] for the
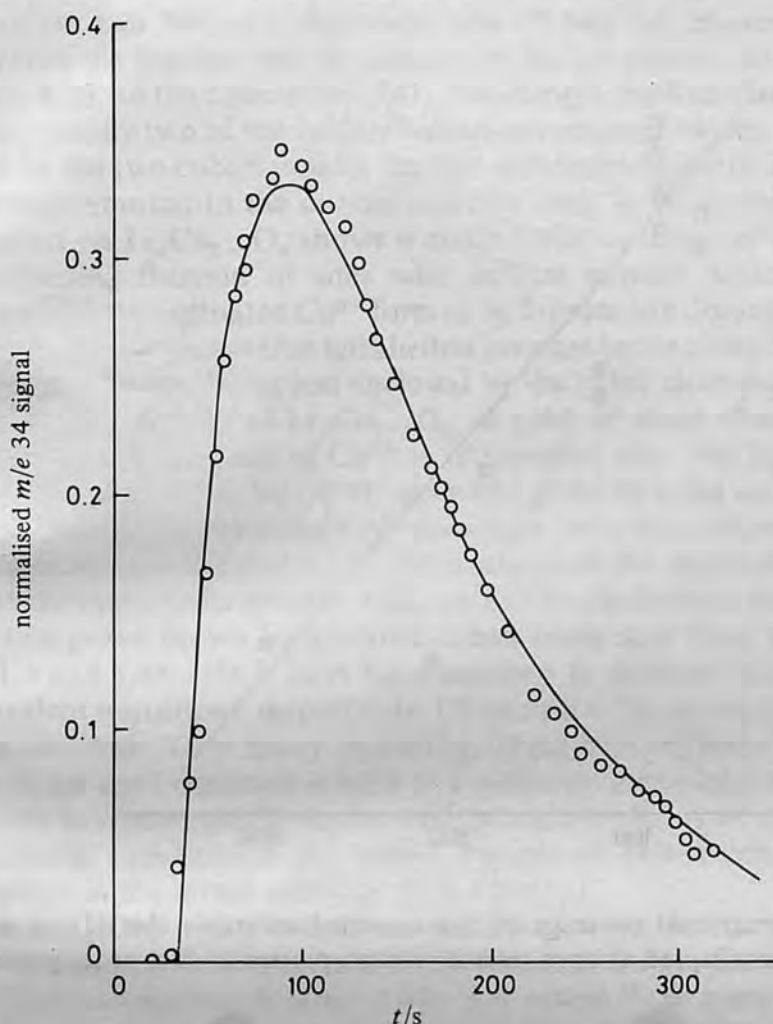
Fig. 5. Difference between m/e 34 signal for oxygen evolution on $NiCo_2O_4$ enriched with ^{18}O and the background experiment (circles). The continuous line is a fit to eqn (12) and (13). Time lapsed between evolution in enriched and normal electrolyte was 90 s.

evolution of oxygen on $NiCo_2O_4$, showing agreement with this work at low potentials. The greater Tafel slope at higher potentials (> 1.6 V) is explained by reaction (14) or reaction (1) being rate determining. This implies a low coverage of MOH, a result not indicated by coulometry experiments.[10] However, in this work the initial coverage of MOH [a in eqn (12)] found, in the case of $NiCo_2O_4$, by extrapolating the line of fig. 6 to zero time is 0.005 of the total number of sites. Although agreement is found between the Tafel slopes reported here and those reported by Rasiyah and Tseung[12] our data have not been corrected for ohmic losses from the resistance between the Luggin capillary and the working electrode. The Tafel slope for oxygen evolution on the lithiated cobalt oxide electrodes is consistent with the bridge mechanism if reaction (15) is rate limiting at low coverage. Note that the kinetic analysis of the isotopic enrichment experiments would still hold for the mechanism of reactions (14)–(17) if the coverage of the intermediates were low, when the values of x_T and y_T would be the number of sites producing $M^{IV}OH$ and $M^{IV}O^-$, respectively. If this were the case the equality of x_T and y_T found experimentally is to be expected. The difference between the evolution of oxygen on lithiated cobalt oxide and nickel cobalt oxide is seen in the values of x_T when compared with the total number of surface sites calculated from charging experiments. The fraction of oxygen evolution sites per formula unit at the
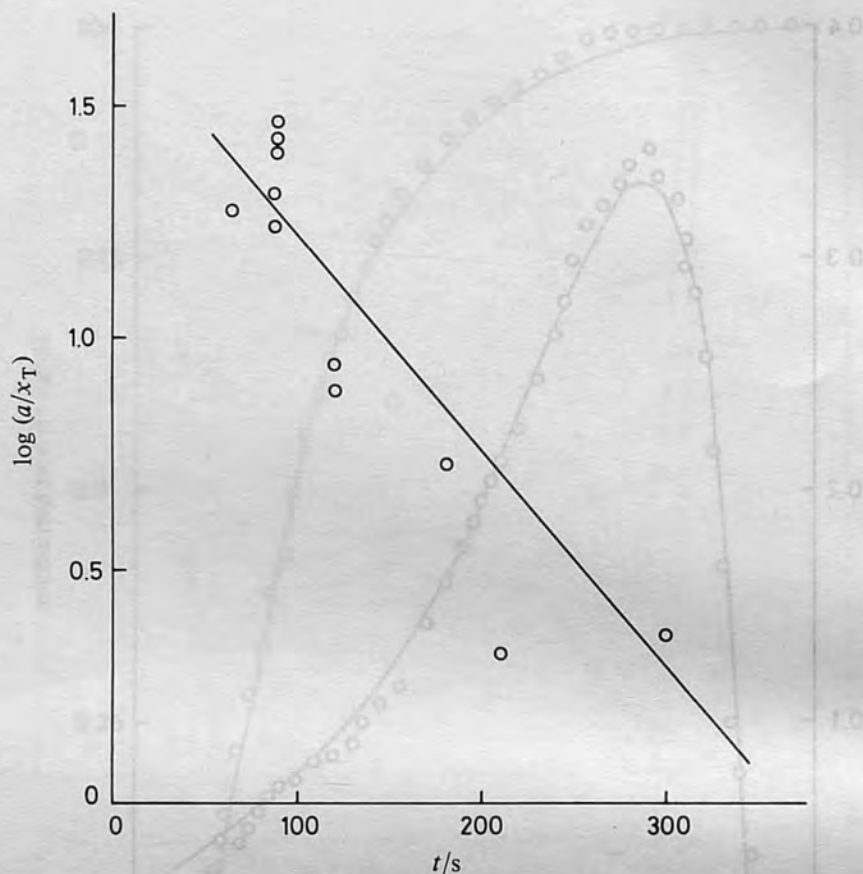
Fig. 6. Variation in fractional coverage of the intermediate oxide (MOH) on a $NiCo_2O_4$ electrode with time lapsed at open-circuit voltage, plotted as first-order process.
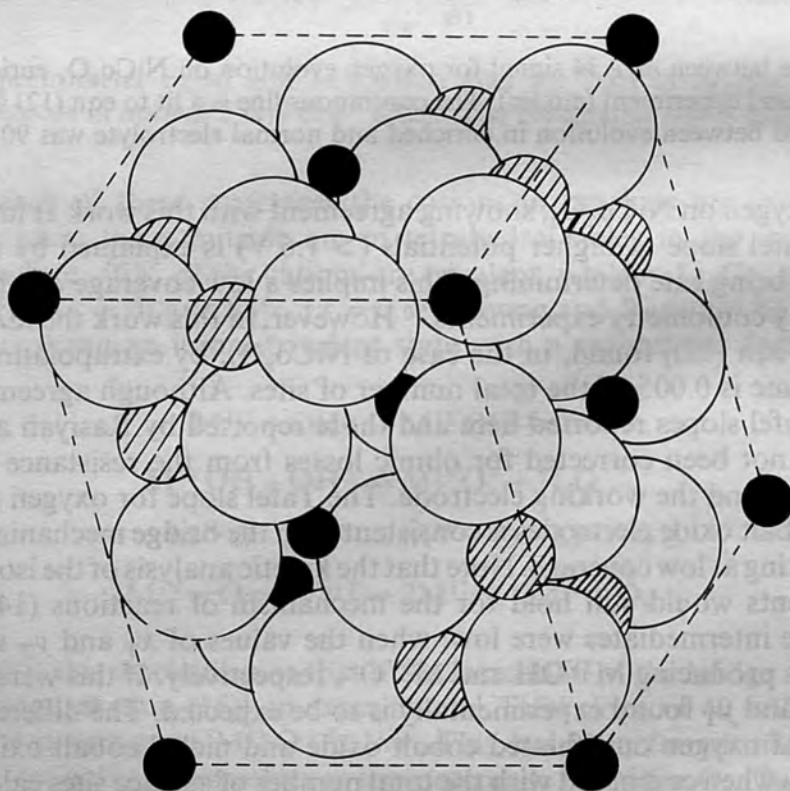

Fig. 7. Unit cell of a spinel oxide AB_2O_4. Filled circles are tetrahedrally coordinated cations (A), small hatched circles are octahedrally coordinated cations (B) and large unfilled circles are oxygen anions (O).

surface for two $NiCo_2O_4$ electrodes was 1.5 and 2.8. However, for five $Li_xCo_{3-x}O_4$ electrodes the fraction was dependent on the Li^+ content and had a maximum value of only 0.53. In the case of $NiCo_2O_4$, assuming a random distribution of surface ions, approximately two of the surface cations are responsible for oxygen evolution. These could be the two cobalt ions or the two octahedrally coordinated ions. In either case some contribution to the overall reaction must be made by a divalent ion. Oxygen evolution on $Li_xCo_{3-x}O_4$ shows a much lower coverage of sites, and here the trend of increasing fraction of sites with lithium content indicates the importance of tetrahedrally coordinated Co^{3+} formed by lithium-ion doping. Inspection of the spinel unit cell (fig. 7)[14] shows that tetrahedral ions are better placed at the surface to interact with other species, being less enclosed by the cubic close-packed lattice oxygen ions. The superior activity of $Li_xCo_{3-x}O_4$, in spite of fewer sites, may be thus explained in terms of the existence of Co^{3+} in tetrahedral sites. $NiCo_2O_4$ may have a structure nearer to $Co^{2+}[Ni^{2+}Co^{3+}]O_3^{2-}O^-$ than that given by King and Tseung,[11] when the lack of tetrahedrally coordinated Co^{3+} ions may force reaction *via* reactions (1)–(3), or by octahedrally coordinated Co^{3+}. An analysis of the oxidations occurring which give rise to the cyclic-voltammetry peaks on nickel cobalt oxide has been made elsewhere.[10] The two peaks shown by lithiated cobalt oxide and fresh nickel cobalt oxide at *ca.* 1.2–1.3 and 1.45–1.55 V have been ascribed to divalent to trivalent and trivalent to tetravalent transitions, respectively. Of interest is the ageing shown by the nickel cobalt oxide electrode. Over many cycles (fig. 2) the irreversibility of the lower oxidation is seen. If an aged electrode is held at a reducing potential for some time it is still not possible to regenerate the cyclic voltammogram of a fresh electrode. In the isotopic-enrichment experiments the ageing process of nickel cobalt oxide was seen as a reduction in the initial coverage [a in eqn (12)].

The use of the isotopic-enrichment method is seen here. The numbers of ions which may be oxidised, as determined by coulometry, are not the same as those responsible for oxygen evolution. Further study may reveal if the number of sites increases with current, as on both catalysts there would appear to be unused sites at the low current densities employed.

[1] A. C. C. Tseung and S. Jasem, *Electrochim. Acta*, 1977, **22**, 31.
[2] G. Fiori, C. Mandelli, C. M. Mari and P. V. Scolari, in *Hydrogen Energy Systems*, ed. T. N. Vizirogalu and W. Seifritz (Pergamon Press, Elmsford, N.Y., 1978), vol. 1, p. 193.
[3] P. Rasiyah and A. C. C. Tseung, *J. Electrochem. Soc.*, 1983, **130**, 365.
[4] P. Rasiyah, A. C. C. Tseung and D. B. Hibbert, *Provisional Brit. Patent*, 1980, *Prov. Appl.* 804,483.
[5] C. R. Churchill and D. B. Hibbert, *J. Chem. Soc., Faraday Trans. 1*, 1982, **78**, 2937.
[6] D. B. Hibbert and A. C. C. Tseung, *J. Electrochem. Soc.*, 1979, **14**, 2665.
[7] A. C. C. Tseung and H. L. Bevan, *J. Mater. Sci.*, 1979, **5**, 604.
[8] C. Iwakura, K. Fukunda and T. Tamura, *Electrochim. Acta*, 1976, **21**, 501.
[9] D. B. Hibbert, *J. Chem. Soc., Chem. Commun.*, 1980, 202.
[10] P. Rasiyah, A. C. C. Tseung and D. B. Hibbert, *J. Electrochem. Soc.*, 1982, **129**, 1724.
[11] W. J. King and A. C. C. Tseung, *Electrochim. Acta*, 1974, **19**, 492.
[12] P. Rasiyah and A. C. C. Tseung, *J. Electrochem. Soc.*, 1983, in press.
[13] B. N. Efremov and S. R. Zhukov, *2nd All-union Conference on Electrocatalysis* (Abstracts), Moscow, 1978, p. 39.
[14] E. J. W. Verwey and E. L. Heilmann, *J. Chem. Phys.*, 1947, **15**, 174.